Evaluation of Mechanical Properties of Fused Filament Fabrication 3D Printed Parts

Master Degree in Mechanical Engineering – Industrial Production

Catarina Cortez Bento

Leiria, September 2022

Evaluation of Mechanical Properties of Fused Filament Fabrication 3D Printed Parts

Master Degree in Mechanical Engineering – Industrial Production

Catarina Cortez Bento

Project under the supervision of Professor Joel Vasco, Professor Dino Freitas, and Professor Miranda Fateri.

Leiria, September 2022

Originality and Copyright

This project report is original, made only for this purpose, and all authors whose studies and publications were used to complete it are duly acknowledged.

Acknowledgments

I wish to show my appreciation to all the people and entities that made this project possible:

To the supervisors of this project, Professor Miranda Fateri, Professor Dino Freitas, and Professor Joel Vasco for all their help and availability throughout this project.

To all professionals and colleagues in the Aalen University laboratory for all the help and knowledge sharing.

To Aalen University, for making its facilities available and allowing this project to be carried out.

To my mother Paula Cortez, my aunt Elsa Silva, my grandmother Irene Silva, and my boyfriend Marcel Ribeiro for all their encouragement, support, and motivation throughout this journey.

Finally, to all my colleagues and friends who have accompanied me along this path.

Thank you all!

Abstract

This report was based on the project at Aalen University in the scope of the curricular subject of the thesis, inserted in the study program of the master's degree in Mechanical Engineering – Industrial Production. The project had a duration of six months.

The project goal was to study the manufacturing process of metal parts using Fused Filament Fabrication (FFF). The FFF is a technique in which a fused filament is deposited controlled over or adjoining previous deposited filaments, leading to the construction of a structural part.

To realize the evaluation of mechanical properties of FFF three dimensional (3D) printed parts it was performed in four main tasks: First, specimens were printed at 0º with three different infill patterns (gyroid, tri-hexagon, and quarter cubic) and two different infill densities (25% and 40%). The printing of these specimens was intended to perform density tests, tensile tests, and roughness tests. Secondly, small cubes with the same infill density (100%) were printed but with different infill patterns (gyroid, tri-hexagon, and quarter cubic) so that it was possible to compare the roughness on the different faces of the cube. These infill patterns and infill densities were chosen, to complement studies previously done by other colleagues. Third, 0°, 45°, and 90° specimens were printed with support structures to perform the charpy v test. However, performing these tests was impossible because the debinding and sintering company could not deliver the parts in time. At last, a cost analysis of the FFF process and the Selective Laser Melting (SLM) process in the production of a compressor turbine was made.

With the tests performed throughout this study, it was possible to conclude that the debinding and sintering process influences the weight of the specimens and the infill density and pattern have an influence on the mechanical behaviour of the specimens.

Keywords: 3D Printing, Additive Manufacturing, Fused Filament Fabrication, BASF Ultrafuse 316L, Sintering.

Contents

List of Figures

List of Tables

List of Abbreviations and Acronyms

3D	Three Dimensional
3DP	Three Dimensional Printing
ABS	Acrylonitrile Butadiene Styrene
AM	Additive Manufacturing
ASTM	American Society for Testing and Materials
BJ	Binder Jetting
CAD	Computer Aided Design
CAM	Computer Aided Manufacturing
CLIP	Continuous Liquid Interface Production
CNC	Computer Numeric Control
CPJ	ColorJet Printing
DED	Directed Energy Deposition
DfAM	Design for Additive Manufacturing
DIN	Deutsches Institut für Normung
DLP	Direct Light Processing
DMD	Direct Metal Deposition
DOD	Drop On Demand
DPP	Daylight Polymer Printing
EBAM	Electron Beam Additive Manufacturing
EBM	Electron Beam Melting
EN	European Norm
ESTG	*Escola Superior de Tecnologia e Gestão*
FDM	Fused Deposition Modeling
FFF	Fused Filament Fabrication
HIPS	High-Impact Polystyrene
ISO	International Standards Organization
LASER	Light Amplification by Stimulated Emission of Radiation
L-DED	Laser-Direct Energy Deposition
LDW	Laser Deposition Welding
LENS®	Laser Engineering Net Shape

LMD	Laser Metal Deposition
LOM	Laminated Object Manufacturing
MIM	Metal Injection Molding
MJP	Multi-Jet Printing
NPJ	Nano Particle Jetting
PBF	Powder Bed Fusion
PC	Polycarbonate
PLA	Polylactic Acid
PSDO	Partnership Standards Development Organization
RP	Rapid Prototyping
SDL	Selective Deposition Lamination
SLA	Stereolithography Apparatus
SLM	Selective Laser Melting
SLS	Selective Laser Sintering
SOUP	Solid Object Ultraviolet-Laser Plotting
STL	Standard Triangle Language
TCO	Total Cost of Operation
TPU	Thermoplastic Polyurethane
UC	Ultrasonic Consolidation
UV	Ultraviolet
WAAM	Wire Arc Additive Manufacturing

1. Introduction

This research work was based on the project at the University of Aalen in the scope of the curricular subject of the thesis, inserted in the study program of the master's degree in Mechanical Engineering – Industrial Production of the *Escola Superior de Tecnologia e Gestão* (ESTG) – *Politécnico de Leiria*. The project had a duration of six months.

The project aims to study the behaviour of FFF printed specimens with different infill densities and patterns. For this, several specimens were printed, and then these were subjected to roughness, tensile strength, and density tests and performed a cost comparison between FFF and SLM technology. With this project, it was possible to make the practical application of the knowledge and theoretical-practical skills acquired during the undergraduate of Engineering and Industrial Management and the master's thesis.

This report is structurally divided into four chapters.

This chapter is where a straightforward approach is made to the objective of this thesis. The second chapter presents the evolution of additive manufacturing (AM), the definition, process, advantages and limitations, application, and materials of AM. Also, in this chapter is presented and explains all the additive manufacturing process categories according to ISO/ASTM 529000, the additive manufacturing technology for metals are presented too. In the end, the support structures are explained to whom it works. The third chapter explains all the methodology used in the practical part and is presented the results and analysis of the results. Finally, the last chapter presents the conclusion of the studies derived from the FFF process.

2. Literature Review

2.1.Evolution of Additive Manufacturing

Rapid prototyping was born in 1980, providing the early stages for Additive Manufacturing. Hideo Kodama files the first 3D printing patent application, describing a rapid prototyping system using ultraviolet (UV) light to harden the photopolymer material. After that, in 1986, Charles Hull patented Stereolithography and founded 3D Systems. In 1988, Carl Deckard filed a patent for selective laser sintering (SLS). This patent was issued in 1989 and was later licensed to DTM Inc, which 3D Systems later acquired. Also, in the same year, the fused deposition modeling (FDM) technology was patented by Scott Crump. This technology applies materials in a series of additive layers by mathematically slicing and orienting models. Crump established Stratasys and filed a series of patents that protected the FDM technology till 1986 (Sculpteo 2022).

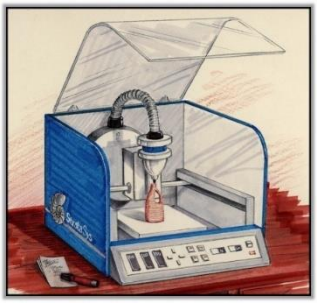

Figure 1 - Stratasys 3D Printer (Sam Davies 2020)

At the beginning of the 90s, Wilifried Vancraen founded Materialise, the First Rapid Prototyping Service Bureau, established in Belgium, focused on researching and developing solutions for the knowledge transfer to AM equipment. A year later, in 1991, was created laminated object manufacturing (LOM) was by Helisys. This process prints in 3D using unrolled paper and glued layer by layer. In 1994, Solidscape created the first 3D wax printer, ModelMaker. (Education Department at the Museum of Arts and Design 2022).

In 2000, Materialise launched the Mammoth Stereolithography AM machine, based on the Stereolithography process, which has a build area of more than two square meters. This enables the large-scale creation of 3D objects in one piece through the successive addition of liquid polymer hardened using a laser beam. Two years later, in 2002, Fast, High-Quality 3D Objects becomes available, and in 2003, Arcam launches the first commercial Electron

Beam Melting (EBM) system. This system melts metal powder together, layer by layer, using an electron beam in a high-temperature vacuum (Anon 2022b).

In 2006, EOS processed cobalt chrome, and stainless steel emerged as the first laser-melting AM equipment. After that, in 2007, Objet introduced the Connex series of 3D printers that enable users to combine two different materials in a single print job in various combinations that produce up to fourteen different levels of hardness, texture, and shading. Again, with no assembly, forms range from rigid to rubber, dense to hollow and translucent to opaque (Education Department at the Museum of Arts and Design 2022).

In 2009, 3D printing got its first standard reference guide. Seventy individuals from around the world meet at the American Society for Testing and Materials (ASTM) International to establish ASTM Committee F42 on Additive Manufacturing Technologies (Education Department at the Museum of Arts and Design 2022).

In 2011, ISO Technical Committee 261 was established after an initiative from German Institute for Standardization (DIN) based on VDI Guidelines on “Rapid Technologies”. After that, ISO and ASTM signed a Partnership Standards Development Organization (PSDO) agreement and published AM standards like EN ISO/ASTM52921-13 Standard Terminology for Additive Manufacturing-Coordinate Systems and Test Methodologies, EN ISO/ASTM 52900-15 Additive Manufacturing – General principles – Terminology, among others (Boivie 2022).

Later in 2012, Stratasys Ltd merged with Objet Geometries Ltd. This company manufactures 3D printers and materials for prototyping and production (Stratasys 2022b).

In 2014, NASA took a 3D printer into space and successfully used it on the International Space Station. Then in 2015, announcing the first commercial sale of “bioink” that allows the 3D printing of body tissue. This was quickly followed in 2016 with a Dublin lab announcing that they could print human bone and cartilage. In 2018, the first family moved into a fully 3D printed home, and in 2019, the world’s largest functional 3D printed building was completed (All3DP 2022c).

According to Statista, the global additive manufacturing market is expected to grow 17% through 2023, as the applications for the technology increases and metal additive becomes more and more viable (Autodesk 2021).

2.2.Additive Manufacturing

Additive manufacturing is defined by ISO/ASTM 52900:2015 as joining materials to make parts from 3D model data, usually layer upon layer, as opposed to subtractive manufacturing and formative manufacturing methodologies (ISO/ASTM 2015).

Additive manufacturing closes some of the gaps and limitations in conventional manufacturing. Through greater flexibility in the design of parts that can be complex and customizable, there is also a reduction in material waste, a lower risk of human error, and greater precision than in conventional processes. In short, the AM process are ideal to print small lots and complex parts (Praveena et al. 2022). Figure 2 shows the comparison between additive manufacturing and conventional manufacturing.

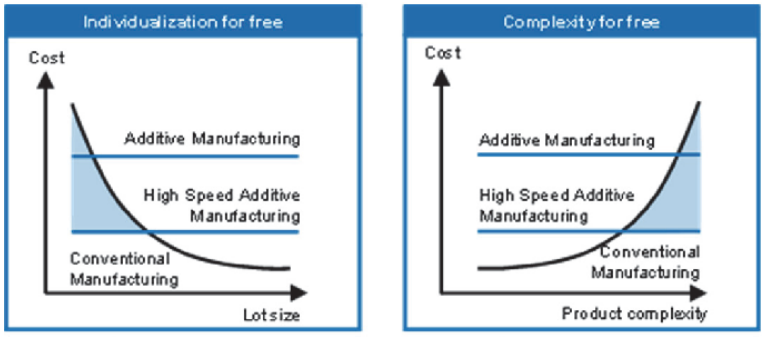

Figure 2 - Additive Manufacturing VS Conventional Manufacturing (Hinke 2017)

The evolution of computer modeling systems intrinsic to developing new prototyping technologies resulted in the reduction of model manufacturing by traditional means. Rapid Prototyping is generally used to describe the manufacture of physical models directly from a Computer Aided Design (CAD) model, based on the use of a set of technological processes and information technologies (Alves 2014).

2.2.1. 3D Printing Process

All technologies and processes that use additive manufacturing follow a similar workflow. First, the drawings are generated in appropriate software, then the files are converted, printing is done, and finally, if necessary, post-processing is performed. There are fundamental stages in the additive manufacturing process, shown in a diagram in Figure 3.

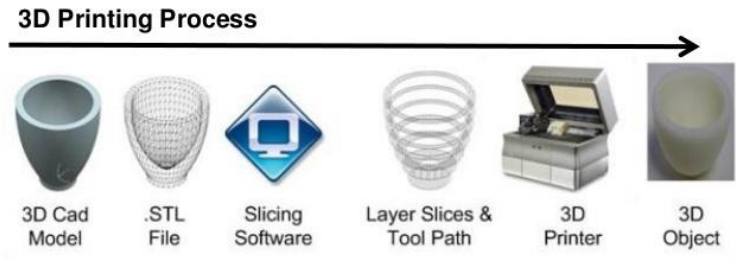

Figure 3 - 3D Printing Process (Anon 2022a)

The first step, the 3D model, is created in a CAD modeling system. New design prescriptions and standards are currently appearing, providing the designer with a way to mitigate the limitations of the technologies and increase the functional performance of the final fabricated parts, known as design for additive manufacturing (DfAM) (Nieto and Sánchez 2021). It is also necessary to consider the orientation of the parts, support for the parts, and structure of parts that are difficult to build, such as thin walls, small slots or holes, and protruding elements. In this step, the constraints associated with the production phase, such as dimensions, tolerances, material, and equipment, must be considered. Next, the 3D model built in the CAD modeling system is converted to Standard Triangle Language (STL) format. This file is a geometric description of the part volume through the triangles. After that, the STL file is transferred to the AM equipment. Soon after, the part is built, the material is deposited layer-by-layer to produce the desired product at this stage. Finally, some additive manufacturing techniques may require some form of post-processing, such as cleaning and polishing, among others (Marques 2020).

2.2.2. Advantages and Limitations of Additive Manufacturing

Like all other manufacturing processes, additive manufacturing also presents advantages and limitations, like:

The AM allows design parts to incorporate impossible complexity in complex geometries using other methods. Intricate features, such as conformal cooling passages, can be incorporated directly into a design. Parts that previously required assembly and welding or brazing of multiple pieces can now be grown as a single part, which makes for greater strength and durability. Designers are no longer restricted by the limitations of traditional machines, and they can create parts with greater design freedom. Time savings, when it is necessary to design and produce prototypes, parts are manufactured directly from a 3D CAD file, which eliminates the cost and lengthy process of having fixtures or dies created. Plus, changes can be made mid-stream with virtually no interruption. Weight savings, by

incorporating organic structures into designs, designers can eliminate substantial weight while maintaining the part's strength and integrity (General Electric 2022).

With a wide range of materials, unlike conventional manufacturing processes (subtractive), AM allows the application of materials that would be very difficult to work on using other types of processes. However, with size limitations, AM only allows manufacturing inside the building area, meaning that there are dimensional constraints for each AM process that cannot be exceeded (Marques 2020). Otherwise, it is necessary to use hybrid additive manufacturing, that requires to print the final part in several small parts and then use welding and machining processes to combine the individual parts in one.

In some cases, layer-by-layer deposition introduces precision errors, meaning that the final component needs to go through post-processing processes to improve surface quality (Marques 2020).

Depending on the part that needs to be produced, the production speed can be influenced by the process used, complexity, and size of the part, and the AM process can take from a few hours until a few days (Pratheesh Kumar et al. 2021).

Post-processing, AM certain level of post-processing is required, because surface finishes and dimensional accuracy can be of lower quality than other manufacturing methods. In addition, the layering and multiple interfaces of additive manufacturing can cause defects in the product, like poor layer deposition and superficial quality, whereby post-processing is needed to rectify any quality issues (Unleashed 2022).

2.2.3. Additive Manufacturing Applications

Additive manufacturing can have various applications, as its technologies and materials constantly evolve. In Figure 4, the sectors where AM can be applied are shown.

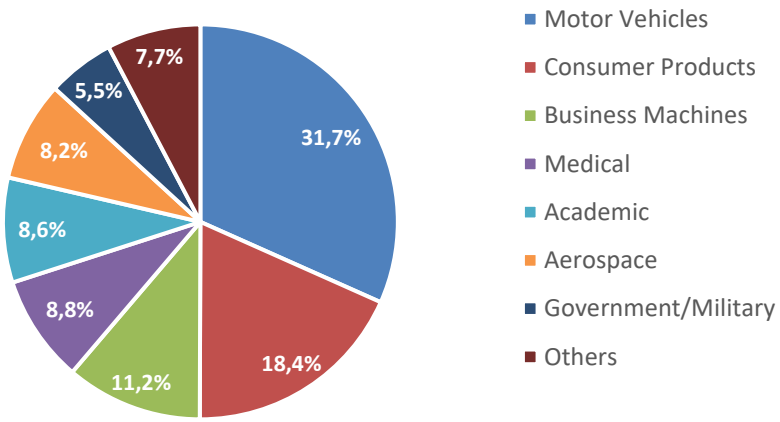

Figure 4 - Additive Manufacturing Applications (Adapted from Beyhan and Arslan Selçuk 2017)

Rapid tool manufacturing has emerged with the need to manufacture tools with high complexity. With this method, it is possible to obtain a tool in a short period of time, with fewer steps during its manufacturing process, which translates into cost and time savings (Junk and Tränkle 2011).

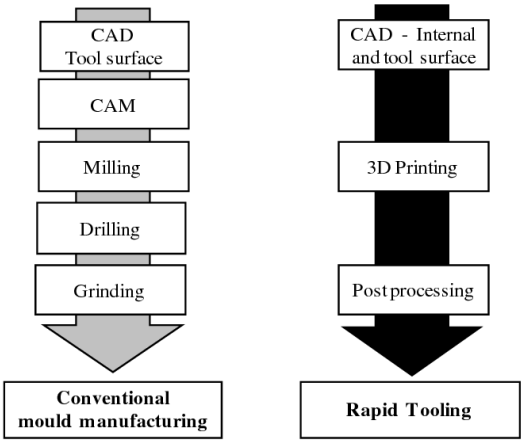

Figure 5 - Conventional Manufacturing VS Rapid Tooling (Junk and Tränkle 2011)

One example of this method is the manufacture of injection moulds with internal cooling channels, as presented in Figure 6.

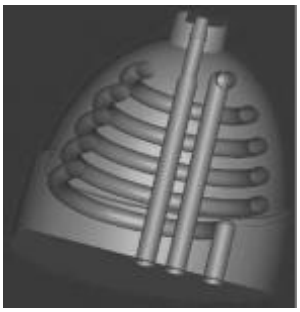

Figure 6 - Internal Cooling Channels (Gomes 2014)

Another application of additive manufacturing is the creation of prototypes. With the increase in the quality surface finish and dimensional accuracy, the manufacturing of prototypes simplifies the product development process, as shown in Figure 7.

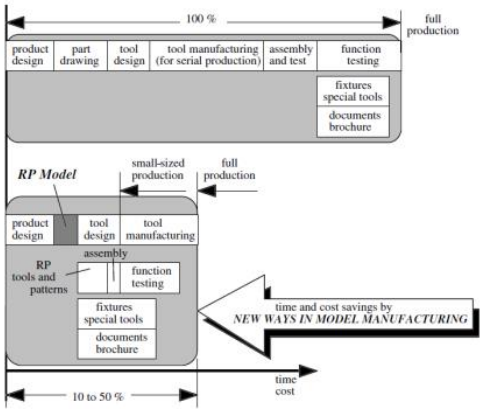

Figure 7 - Result of the integration of AM (Enoch Olalere 2022)

Additive manufacturing can be involved in a product's production phase, as presented in Figure 8.

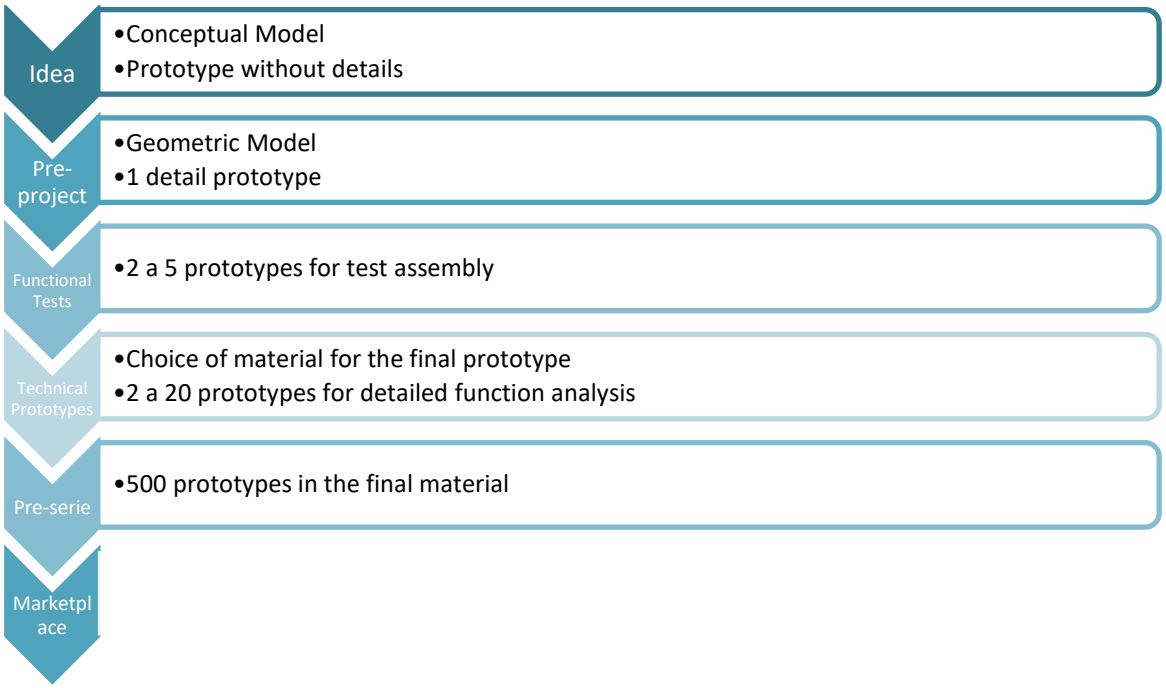

Figure 8 - Production Phase of a Product with AM (Adpated from Mário Correia 2021)

It is also possible to manufacture components for the automotive industry with additive manufacturing. Additive technology is genuinely becoming essential to the automotive value chain by disrupting traditional supply chains. From prototyping to mass production of engine, transmission, and chassis components, the automotive industry is ready to evaluate how additives can drive greater returns on investment (Gomes 2014). Figure 9 presents a highly alloyed tool steel gear hob manufactured by GE Additive.

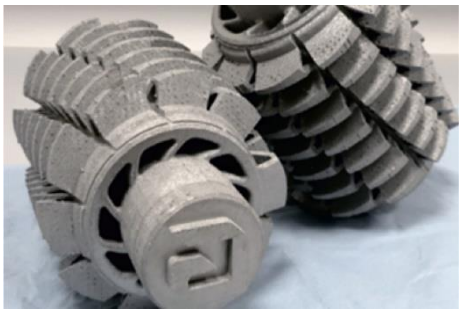

Figure 9 - Steel Gear Hob (GE Additive 2022a)

Another application of additive manufacturing is the medical industry to produce prosthetics or implants has evolved its industry, obtaining a customized component very quickly and at a lower cost which has driven the introduction of this technology (Gomes 2014). Figure 10 shows an orthopaedic implant.

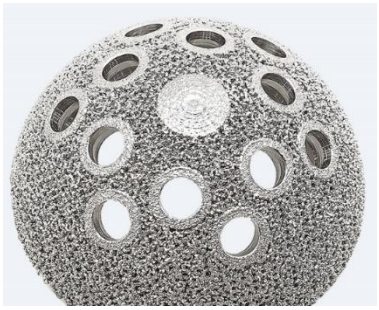

Figure 10 - Orthopedic Implants (GE Additive 2022a)

2.2.4. Conventional Manufacturing Materials VS Additive Manufacturing Materials

In this chapter, it is possible to compare the materials used in conventional manufacturing with the materials used in additive manufacturing. The materials that can be used in each conventional machining process are presented in Table 1.

Table 1 – Conventional Manufacturing Materials (Formlabs 2022)

Process	Materials
CNC machining (turning, drilling, boring, milling, reaming)	Hard thermoplastics, thermoset plastics, soft metals, hard metals
Electrical discharge machining	Hard metals
Laser cutting	Thermoplastics, wood, acrylic, fabric metals
Water jet cutting	Plastics, hard and soft metals, stone, glass, composites

Several types of materials can be used in additive manufacturing, ranging from polymers, ceramics, metals, composites, and natural materials (food). For example, metal additive manufacturing takes additive manufacturing and applies it to exclusively metals, and these advances allowed the creation of new objects with better properties and resistance. Table 2 are presented some materials that can be used in the AM process.

Table 2 – Additive Manufacturing Materials (Adpated from Bourell et al. 2017)

Processes	Materials
Vat Photopolymerization	Photo-sensitive resins, eventually filled with ceramic or metallic nanoparticles
Material Extrusion	Polymers and composites
Powder Bed Fusion	Polymers, metals, and ceramic powders
Material Jetting	Polymers and composites
Binder jetting	Polymers, metal, and ceramic powders
Sheet Lamination	Paper, metal, and polymers
Directed Energy Deposition	Metal, polymers, powders, and filaments

2.3.Process Categories of Additive Manufacturing

According to ISO/ASTM 529000, additive manufacturing can be divided into seven categories: vat photopolymerization, material jetting, binder jetting, material extrusion, powder bed fusion, sheet laminating, and direct energy deposition. Table 3 shows the categories and which technologies each one uses.

Table 3 – Categories of Additive Manufacturing

Category	Process	Technologies
1	Vat Photopolymerization	SLA, DLP, CLIP, DPP
2	Material Jetting	DOD, Polyjet, NPJ
3	Binder Jetting	CPJ
4	Material Extrusion	FDM, FFF
5	Powder Bed Fusion	SLS, SLM, EBM, MJF
6	Sheet Lamination	LOM, UC
7	Direct Energy Deposition	LENS, LDW, EBAM, WAAM

2.3.1. Category 1 – Vat photopolymerization

Vat photopolymerization is an AM process in which a photo-sensitive liquid in a vat is selectively cured by light-activated polymerization. Layer-by-layer, a 3D physical object is built until conclusion. (ISO/ASTM 2015).

The vat photopolymerization 3D printing technologies include the following:

- Stereo Lithography (SLA);
- Direct Light Processing (DLP);
- Continuous Liquid Interface Production (CLIP) by Carbon;
- Daylight Polymer Printing (DPP) by Photocentric.

In this process, the build platform is lowered downwards from the top of the resin vat by the layer thickness. A UV light cures the resin layer-by-layer, the platform continues to move downwards, and additional layers are built on top of the previous. After completion, the vat is drained of resin, and the object is removed (Loughborough University 2021c). In Figure 11 is illustrated the Vat Photopolymerization Process.

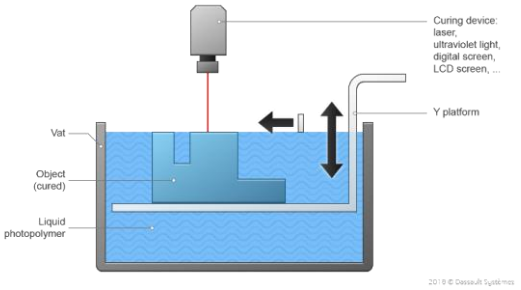

Figure 11 - Vat Photopolymerization Process (Make 2022a)

This process uses plastics, polymers, and resins as materials. This technology has excellent applicability in medical modeling, which enables the creation of accurate 3D models of various anatomical regions of a patient based on data from computer scans. The high resolution of this technique also makes it ideal for all types of prototyping and mass production. Vat polymerization processes are excellent at producing parts with fine details and a smooth surface finish. This makes them ideal for jewellery, investment casting and many dental and medical applications. Material developments have also allowed the printing of low-run injection moulds. The main limitations for vat polymerization are the build size and part strength (Make 2022c).

2.3.2. Category 2 – Material Jetting

Material jetting is an additive manufacturing process in which droplets of build material are selectively deposited (ISO/ASTM 2015). This technique ensures that the part is produced layer-by-layer by using photopolymers, metals, or waxes that solidify when exposed to light or heat. In addition, the material jetting manufacturing process allows different materials to be 3D printed within the same part (Make 2022d).

The material jetting printing technologies include the following:

- Drop On Demand (DOD);
- PolyJet by Objet;
- NanoParticle Jetting (NPJ) by Xjet.

Material jetting dispenses a photopolymer from hundreds of tiny nozzles in a printhead to build a part layer-by-layer. This allows material jetting operations to deposit build-material in a rapid line-wise fashion. As the droplets are deposited into the build platform, they are directly cured and solidified using UV light. Material jetting processes require support, often 3D printed simultaneously during the build from a dissolvable material. The support material is then removed during the post-processing step (Make 2022d). In Figure 12 is illustrated the Material Jetting Process.

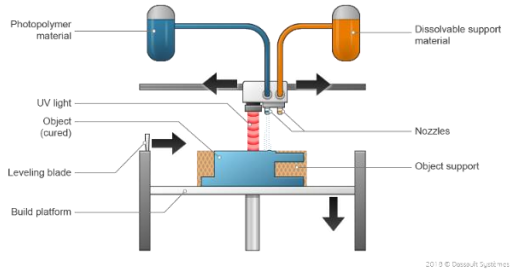

Figure 12 - Material Jetting Process (Make 2022a)

The material jetting process uses polymers, plastics, and metal. With the process, achieving an excellent level of detail, high precision, smooth surface finish, and low material waste is possible. In addition, it is possible to print parts in multiple colours. However, this technology has a high cost, and it uses UV-activated photopolymers means that the material loses its mechanical properties over time and can become brittle. In addition, support material is required (Make 2022d).

2.3.3. Category 3 – Binder Jetting

Binder jetting is an additive manufacturing process in which a liquid bonding agent is selectively deposited to join powder materials (ISO/ASTM 2015).

The binder jetting 3D printing process includes the following techniques:

- ColorJet Printing (CPJ) by 3D Systems

In the first step of this process, the powder material is spread on the build platform using a roller. After that, the printhead deposits the binder adhesive on top of the powder where needed, and the thickness of the model layer lowers the build platform. Next, another layer of powder is spread over the previous layer. Finally, the object is formed where the powder is bonded to the liquid (Loughborough University 2022a). Figure 13 shows the Binder Jetting Process.

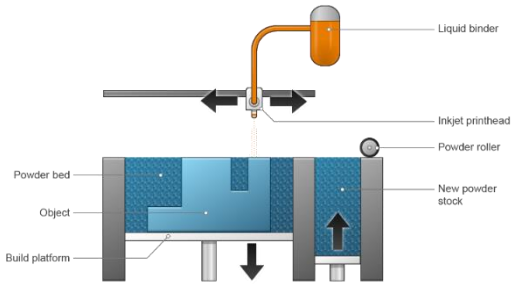

Figure 13 - Binder Jetting Process (Make 2022a)

The binder jetting process can work with various materials, including metals, sands, and ceramics. Some materials, like sand, require no additional processing. This technology can be used, in parts that require good aesthetics and form, such as architectural models, packaging, toys, and figurines (Make 2022a).

2.3.4. Category 4 – Material Extrusion

Material extrusion is an additive manufacturing process in which material is selectively dispensed through a nozzle or orifice (ISO/ASTM 2015).

The material extrusion 3D printing process includes the following techniques:

- Fused Deposition Modeling (FDM);
- Fused Filament Fabrication (FFF).

In this process, the filament is fed from a coil through a moving heated extruder head or extruder. The molten material is forced out of the extruder's nozzle and is deposited first onto the building platform, which can be heated, for extra adhesion. Then, the following layers are added on top of the previous layers, fused upon deposition of the material in its melted state (Make 2022b). In Figure 14 is illustrated the Material Extrusion Process.

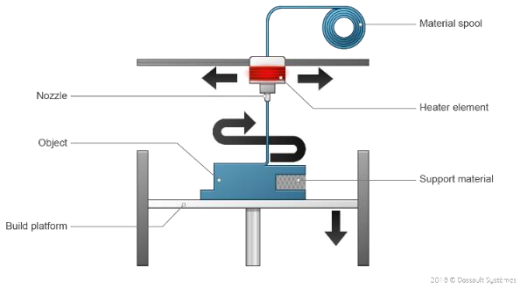

Figure 14 - Material Extrusion Process (Make 2022a)

A wide variety of materials can be extruded, for example, thermoplastics, such as Acrylonitrile Butadiene Styrene (ABS), PolyLactic Acid (PLA), High-Impact Polystyrene (HIPS), Thermoplastic PolyUrethane (TPU). Printing with metal and paste-like materials such as ceramics, concrete, and chocolate can be extruded using this 3D printing technique (Make 2022a).

2.3.5. Category 5 – Powder Bed Fusion

The powder bed fusion is an additive manufacturing process in which thermal energy selectively fuses regions of a powder bed (ISO/ASTM 2015). This 3D printing technique enables manufacturing a vast range of geometrically complex products using a heat source, mainly laser or electron beams, to fuse powder particles layer-by-layer, forming a solid part (Make 2022c).

The different Powder Bed Fusion methods includes:

- Selective Laser Sintering (SLS);
- Selective Laser Melting (SLM);
- Electron Beam Melting (EBM);
- Multi Jet Fusion (MJF) by HP.

The powder bed fusion process starts with a material layer spread over the build platform by a roller. Next, a laser fuses the model first layer or first cross selection, and a new layer

of powder is spread over the previous layer using a roller. Then, more distant layers are fused and added, and the process is repeated until the entire model is created (Loughborough University 2021a). In Figure 15 is presented the Powder Bed Fusion Process.

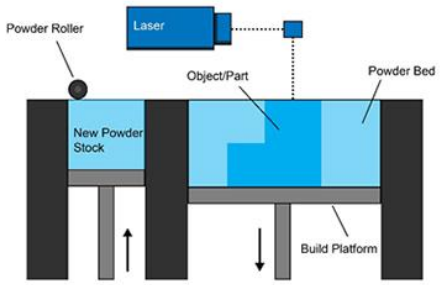

Figure 15 - Powder Bed Fusion Process (Make 2022a)

The powder bed fusion process uses powder-based materials, metals and polymers like nylon, steel, titanium, aluminium, and cobalt chrome, among others (Loughborough University 2022).

2.3.6. Category 6 – Sheet Lamination

Sheet lamination is an additive manufacturing process in which sheets of material are bonded to form a part (ISO/ASTM 2015). In this process, thin sheets of material are bonded layer-by-layer to form a single piece cut into a 3D object (Siemens Software 2022).

This process includes the following techniques:

- Laminated Object Manufacturing (LOM);
- Ultrasonic Consolidation (UC).

In this process, the material is first positioned on the cutting bed. Next, the material is bonded over the previous layer using adhesive. The required shape is then cut from the layer by laser or knife, and the process is repeated until the entire model is created (Loughborough University 2021b). In Figure 16 is illustrated the Sheet Lamination Process.

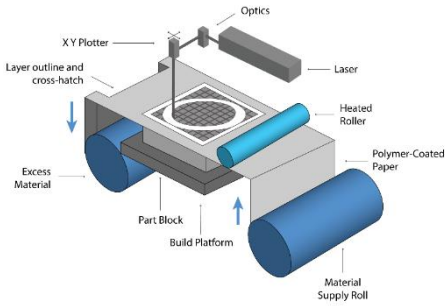

Figure 16 - Sheet Lamination Process (fabheads 2022)

This process is low cost and easy to handle material, but the strength and integrity of models are reliant on the adhesive used. Also, the cutting can be very fast due to the cutting route only being that of the shape outline, not the entire cross-sectional area. On the other hand, finishes can vary depending on paper or plastic material but may require post-processing to achieve the desired effect (Loughborough University 2021b).

2.3.7. Category 7 – Direct Energy Deposition

Direct energy deposition (DED) is an additive manufacturing process in which focused thermal energy is used to fuse materials by melting as they are being deposited (ISO/ASTM 2015). This technique makes it possible to manufacture a wide range of complex products by applying a heat source, such as a laser or electron beam, to fuse powder particles layer by layer.

This process includes the following techniques:

- Laser Engineering Net Shape (LENS®);
- Aerosol Jet Technology by Optomec;
- Laser Deposition Welding (LDW) and Hybrid Manufacturing by DMG MORI;
- Electron Beam Additive Manufacturing (EBAM).

DED uses a five-axis arm with a nozzle that moves around a fixed object, and the material is deposited onto an existing surface of the object. Then the material is melted using a laser, electron beam, or plasma arc upon deposition. Further material is added layer-by-layer and solidifies, creating or repairing new material features on the existing object (Loughborough University 2022). Figure 17 shows the Direct Energy Deposition Process.

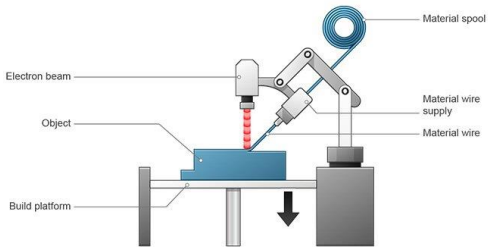

Figure 17 - Direct Energy Deposition Process (Make 2022a)

This technology uses metals such as aluminium, copper, titanium, stainless steel, tool steel, copper-nickel alloys, and several steel alloys (Make 2022c).

2.4. Additive Manufacturing for Metals Technologies

Five of the seven categories of AM presented in chapter 2.3 – material jetting, binder jetting, material extrusion, powder bed fusion, and direct energy deposition – can integrate processes that produce metal parts. Therefore, this chapter will present the workflow of these technologies processes and equipment.

Printing with metals brings some advantages, like high repeatability count on a printer architecture and workflow, the lowest oxygen exposure and content consistently below 25ppm results in high part quality, low Total Cost of Operation (TCO) through almost full material usage, low Argon consumption, robust material databases count on parameters thoroughly developed and tested and lowering the time needed to get your production up and running (3D Systems 2022a) .

2.4.1. Material Jetting

Nano Particle Jetting

The NanoParticle Jetting™ technology uses a liquid dispersion methodology. A liquid suspension containing selected build material solid nanoparticles is jetted onto the build tray to manufacture detailed parts additively. These liquid suspensions serve as the base materials for the Xjet AM process, unlike most existing ceramic and metal AM technologies that utilize hazardous and hard-to-handle powders. In addition, liquid dispersion makes it possible to simultaneously jet a unique soluble support material (XJET 2022). Figure 18 represents all the workflow of this process.

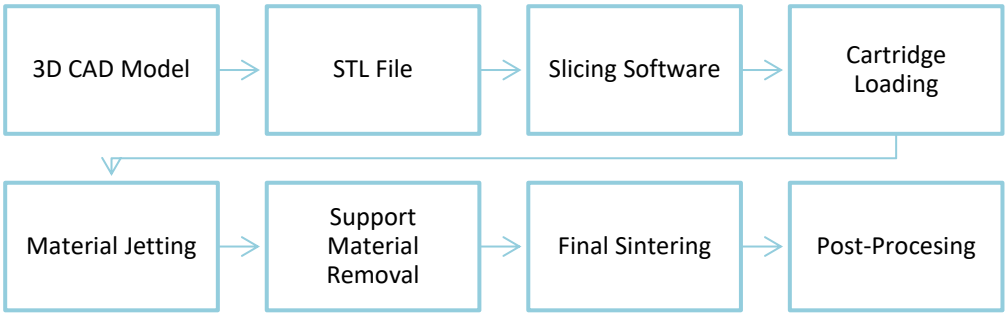

Figure 18 - Nano Particle Jetting Workflow

It is challenging to use metal in this technology to enable the metal to be deposited in a liquid form so it can be jetted from inkjet nozzles. To do this, nano-sized particles suspended within a liquid formula must be used, eliminating inefficient lasers. This metal liquid formula can be jetted from the printing heads. The metal materials are packaged within specially adapted cartridges that are easily loaded by hand into the X-jet system. After sending the STL file to the print, the printhead deposits a fine layer of metal liquid droplets and support material onto the system build tray at each printhead pass. The metal part builds up as the tray descends the metal liquid formula, and the support material forms thousands of printing nozzles simultaneously. The temperature of up 300ºC causes the liquid jacket (coating) around the metal nanoparticles to evaporate, allowing the stochastic metal particles to achieve virtually the same metallurgy and density as traditionally made metal parts. After printing, the support component, which is made of different material, is easily disintegrated, and removed to finalize the printed parts' process through sintering. Depending on the application of the part, this may still undergo post-processing (XJet 2019).

Materials

The NPJ enables the additive manufacturing of ceramic and metal parts, using materials like zirconia, alumina, stainless steel, and soluble supports (XJet 2022).

Advantages and Disadvantages

This technology has some advantages and disadvantages, which are presented in Table 4.

Table 4 – Advantages and Disadvantages of Nano Particle Jetting (Xjet 2022) (Manufactur3D 2022)

Advantages	Disadvantages
Good part quality (isotropic uniformity, good levels of detail and extremely low shrinkage).	New technology (It is a new technology and too early to use in part production).
Geometrical freedom (complex geometries, fine details, nearest net shapes and smooth surfaces).	Small material library (The material library is tiny for use in different applications).
Operational efficiency (automated support planning, hands-free support removal).	High cost (The technology has high costs associated with it).

Equipment

The Xjet Carmel 1400M (Figure 19) is an example of equipment used in NanoParticle Jetting™ technology. This machine uses patented NanoParticle Jetting technology to 3D print with ceramic and metal materials (Xjet 2022).

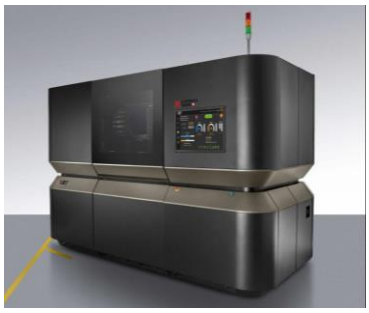

Figure 19 - Xjet Carmel 1400M (Aniwaa 2022)

This machine allows users to 3D print complex parts without worrying about support structures. Moreover, it avoids wasting material due to its technology only using the precise amount of material, among others (Aniwaa 2022). Table 5 presents some system specifications of The Xjet Carmel 1400M.

Table 5 – Xjet Carmel 1400M Specifications (Aniwaa 2022)

Xjet Carmel 1400M Specifications	
Build Tray	2 trays, 500 x 140 mm
Layer Thickness	8 microns
Building Speed	Up to 1.0 mm height per hour
Dimensions (w/h/d)	310 x 212 x 185 cm
Weight	3 tons
Operating Temperature	18ºC – 25ºC

Applications

The NanoParticle Jetting™ technology addresses many applications such as short-run production batches, on-demand production, and functional prototyping.

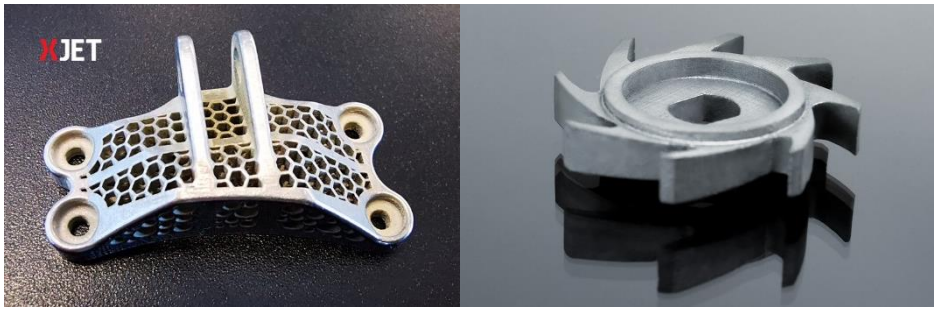

Figure 20 - NanoParticle Jetting Applications (Xjet 2022)

In Figure 20 are presented some parts that can be produced through the NPJ technology. With this technology, it is possible to produce metal AM parts with levels of detail, finish, and precision that by conventional manufacturing would not be possible.

2.4.2. Binder Jetting

Two examples of the binder jetting process are the desktop metal shop system and the desktop metal production system.

Desktop Metal Shop System

The shop system is the first metal binder jetting designed to bring metal 3D printing to machine shops. This system comprises a printer, a powder station, and a furnace. In Figure 21 is presented the metal shop system.

Figure 21 - Metal Shop System (Desktop Metal Inc 2022)

Process

The process is very similar to the Studio System, in the first step, the secure, web-based software creates build plans from STL or CAD files, automatically generating media and

control parameters based on the part geometry and material. After that, the file is sent to the printer, and for each layer, the printer spreads metal powder across the build bed and precisely jets a binding agent to bond loose powder and define part geometry. Layer-by-layer, metal powder and binder are deposited until the entire build volume is packed with bound parts and surrounding loose powder. The next step is the depowder, and once an entire build is complete, the build box is removed and placed in a powder station for bulk and fine depowering, with the help of a hand-held air pick. Next, loose powder is removed from the parts and recovered via a built-in powder recycling system with powder sieving. At last, occurs the sinter, where the depowered parts are placed onto trays in a shop-safe, high-throughput furnace for batch sintering (Desktop Metal Inc 2022).

Benefits

The shop system has a software that simulates the parts of complex forces experienced during sintering and automatically adjusts the geometries that, once printed, will sinter to the original, intended design specifications. This eliminates the problem of part shrinkage and distortion. This system also has a high-speed, single-pass print engine that produces high-quality metal parts at up to 10x the speed of laser powder bed fusion systems, so it is possible to print hundreds or thousands of metal parts daily (Desktop Metal Inc 2022).

Applications

With a desktop metal shop system, it is possible to manufacture products for the following areas: manufacturing, tooling, automotive, consumer, electronics, and oil & gas.

The gear shift knob (Figure 22) is an example of mass customization, and this textured gear shift knob can be printed to customer specifications. On-demand manufacturing of custom knobs is enabled with the Shop System – expanding design flexibility and avoiding warehousing costs. This system also allows for a dramatic cost reduction compared to traditional manufacturing methods (Desktop Metal Inc 2022).

Figure 22 - Gear Shift Knob (Desktop Metal Inc 2022)

Another example is a bulb nozzle (Figure 23), this part is a custom nozzle for use in chemical processing. Traditional manufacturing of this part would require casting followed by extensive secondary machining on a 5-axis CNC. Because only a few hundred of this nozzles needed to be manufactured, it was an excellent fit for the Shop System. By printing, the entire order of nozzles could be produced on the Shop System in less than a week, with only one secondary thread-tapping operation required (Desktop Metal Inc 2022).

Figure 23 - Bulb Nozzle (Desktop Metal Inc 2022)

Desktop Metal Production System

The production system is high-speed metal 3D printing for mass production. This has bidirectional printing, where all steps of the printing process, like powder deposition, spreading, compacting, ballistic suppression, and binder jet printing, are applied with each pass. In Figure 24 is presented the metal production system.

Figure 24 - Metal Production System (Desktop Metal 2022b)

Process

This system features a single-pass bi-directional jet. All steps of the printing process – powder deposition, spreading, compacting, ballistic suppression, and binder jetting – are applied with each pass over the build area. Layer-by-layer, metal powder and binder are deposited until the entire build volume is packed with bound parts and surrounding loose powder. When a build is complete, the build box is removed and replaced with a new box for the next build. The completed build box is moved to a depowdering station where the loose powder is removed, and parts are prepared for sintering. The depowdered parts and loaded into an industrial furnace where they are heated to temperatures near melting. The remaining binder is removed, causing the metal particles to fuse and the parts to densify (Desktop Metal 2022b).

Benefits

The production system is a binder jetting system with high-resolution printing. It can print parts with excellent surface finish and incredibly fine features, with a resolution of 1200x1200 dpi and layers heights of 50 µm (Desktop Metal 2022a).

This system also used the same low-cost powders used in the metal injection moulding (MIM) industry, allowing customers to access an established powder supply chain with the scale required to support volume production and a variety of readily usable alloys. In addition, as much as 99% or more of the loose powder recovered during the process can be recycled, driving further cost efficiencies while reducing waste (Desktop Metal 2022a).

Applications

With a desktop metal production system, it is possible to deliver the speed, quality, and cost-per-part needed for metal 3D printing to compete with traditional manufacturing.

The Parking Shift Bracket (Figure 25) is used in the parking brake assembly of a continuously variable transmission. This part would require a complex die and multiple secondary operations to be produced via traditional powder metallurgy techniques. The production system eliminates the need for tooling, dramatically reducing lead times, reducing part costs, and enabling the redesign of this part to consolidate an assembly into a single part (Desktop Metal 2022b).

Figure 25 - Parking Shift Bracket (Desktop Metal 2022b)

Ntopology Gear (Figure 26), this gear features a complex internal lattice structure only achievable via 3D printing. This part features a complex lattice structure used to lightweight the part while still providing strength. The production system allows manufacturing complex geometries that cannot be manufactured any other way (Desktop Metal 2022b).

Figure 26 - Ntopology Gear (Desktop Metal 2022b)

2.4.3. Powder Bed Fusion

Two examples of the powder bed fusion process are selective laser sintering and selective laser melting.

Selective Laser Sintering

Selective laser sintering is a powder-based layer-additive manufacturing process generally meant for rapid prototyping1 and rapid tooling (Kumar 2003). The typical SLS setup configuration involves a low-power laser source with a scanning mechanism, a computer control system, a platform to build the part, a roller to spread the feed material above the platform, and two powder feed chamber chambers build chamber. Figure 27 presents the workflow of the Selective Laser Sintering process.

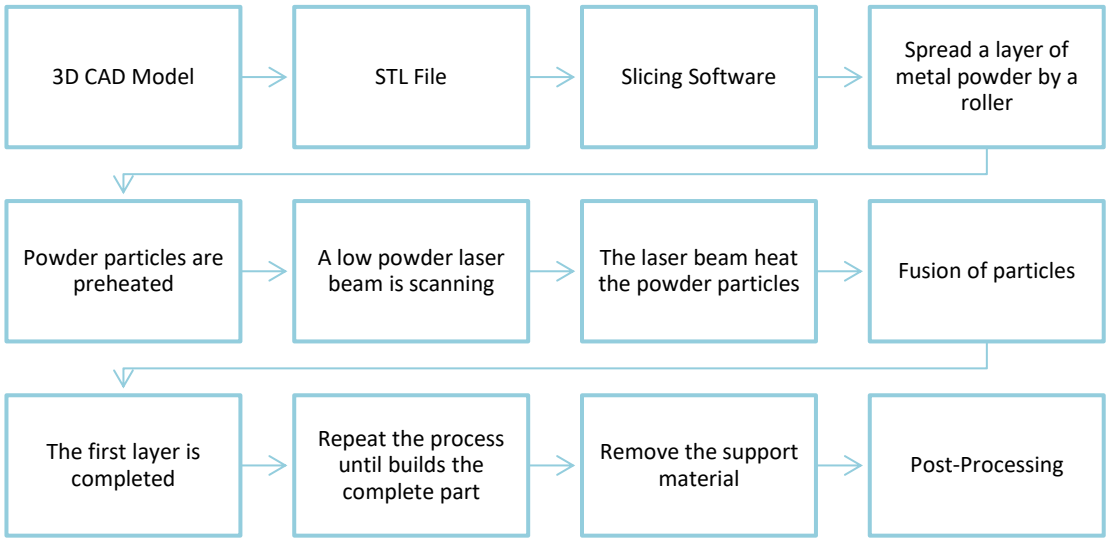

Figure 27 - Selective Laser Sintering Workflow

Like the other AM processes, the SLS also starts with making a CAD model of the part produced. The CAD model will then be stored in an STL format, and the model is then sliced into layers and sent to the SLS machine. After this, the SLS process begins, and a controlled quantity of powder is fed into the platform by raising the piston inside the powder feed chamber. The feed chamber is then spread evenly over the platform using a roller. Finally, the powder particles over the platform are preheated considerably below their melting temperature using heating mechanisms such as resistance, infrared, and feed cartridge heaters. Further, based on the CAD model's sliced data, a high-power laser beam is scanned through the cross-sectional area defined by the layer. The laser beam directed to the powder bead heats the powder particles. Hence, they melted wholly or partially, resulting in the fusion of particles. When the first layer is completed, the piston in the build chamber moves down to a height equal to the layer thickness. Simultaneously, the piston from the feed chamber moves up to the same height and feeds the material into the platform. The spreading mechanism then levels the feed powder through the platform. Therefore, a new layer of

powder deposition is obtained, and now the laser is scanned over the powders to create a second layer sintered to the underlying one. This process is repeated several times until the complete 3D component is built and the support material is removed. The un-sintered particles removed from the build chamber can be recycled (M. Bhuvanesh Kumar, P. Sathiya, and M. Varatharajulu, 2021).

Materials

A wide range of materials has been used in SLS. A number of those materials make SLS superior to other techniques for rapid prototyping when materials' characteristics depend on the type of process. The materials include wax, cermet, ceramics, nylon/glass composite, metal-polymer powders, metals, nylon, and carbonate (Kumar 2003).

Advantages and Disadvantages

The Selective Laser Sintering technology has advantages and disadvantages, as shown in Table 6.

Table 6 - Advantages and Disadvantages of Selective Laser Sintering (3D Systems 2022b)

Advantages	Disadvantages
Recycle material, reduce the material waste.	It is not possible to achieve the best quality in appearance with the best mechanical properties.
Geometric freedom complex geometries, such as monolithic designs, lightweight components, and mass-customized products.	Requires support structures.
Get superior accuracy, part resolution, edge definition, and surface finish with 3D Systems' SLS solutions.	SLS parts have a grainy surface finish and internal porosity that may require post-processing if a smooth surface or water tightness is required.

Equipment

The ProX™ 500 Plus is a cutting-edge Selective Laser Sintering production 3D printer from 3D Systems that create injection moulding-grade parts without expensive tooling, the ProX™ 500 Plus prints possible to use several materials in Figure 28 presents the machine.

Figure 28 - ProX™ 500 Plus (Protocom 2022)

Table 7 presents some specifications of The ProX™ 500 Plus.

Table 7 - ProX™ 500 Plus Specifications (Protocom 2022)

Machine Specifications	
Print Envelope Capacity	381 x 330 x 457 mm
Scanning speed	Fill: 12 m/s | Outline: 3.5 m/s
Volume build rate	2 l/h
Layer thickness	0.08 - 0.15 mm
Laser Power/Type	100 W / CO_2

Applications

The SLS technology is used in different industries to produce aerospace hardware, medical and healthcare, military hardware, and short-run end-use components.

The air seat buckles have been rethought to reduce the aeroplane's weight so that fuel consumption can be reduced. These still have the same design and geometry as a conventional seat buckle. However, they have been optimized to use new production processes for laser-synthesized metals to obtain a lighter product. Figure 29 is an example of a seat buckle.

Figure 29 - Air Seat Buckles (3DPrint.com 2019)

Selective Laser Melting

The SLM technology appeared in 1998 and used materials such as plastic, glass, and ceramics in its process, but with the evolution of technologies came SLM. The only difference between these processes is that SLM uses metal as a material because it has a laser with more power (GE Additive 2022e). Figure 30 presents the workflow process of the SLM technology.

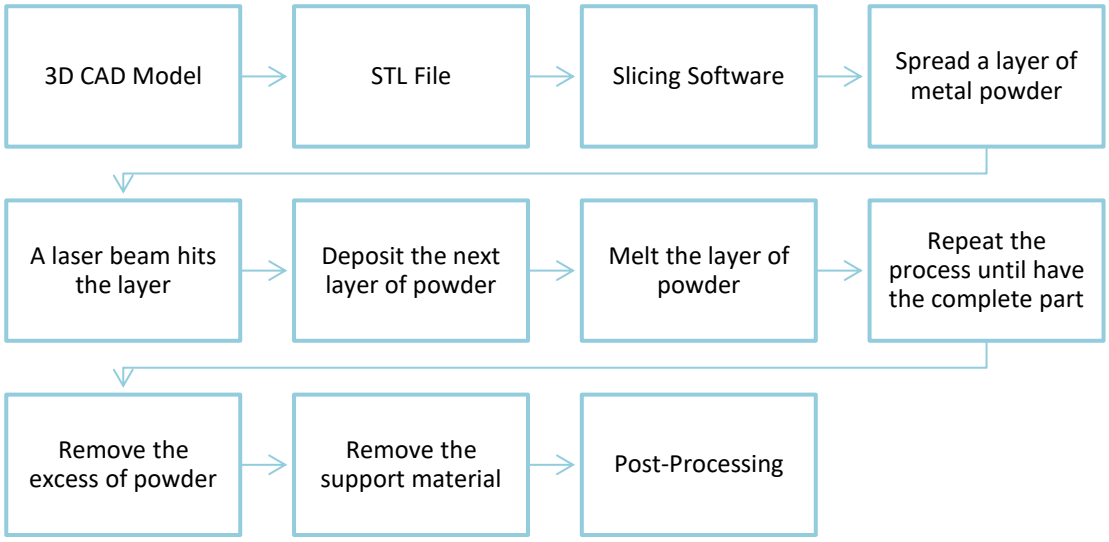

Figure 30 - Selective Laser Melting Workflow

The SLM is a powder bed fusion additive manufacturing process. This technology uses one or more lasers to melt ultra-thin layers of metal powder to build 3D parts. The parts are built from CAD files and converted into slice files, and these files are then uploaded to the SLM machine. During the SLM process, the recoated moves across the build platform, evenly spreading a thin layer of fine metal powder. Next, a cross-section of the part is melted based on a layer of a slice file. Finally, the build platform is lowered, and the next layer of powder is distributed and melted. Although in the case of multiple lasers, overlapping areas are stitched together to create a seamless part, the superior gas flow within the build chamber helps to keep a clean environment ensuring better part quality. When the part is completed, the platform is raised and removed from the build chamber, and the excess powder is removed from the finished part (GE Additive 2021).

The definition of parameters can influence the result of the final part. The optimization of these parameters has a direct influence on the characteristics of the manufactured part, such as surface finish, microstructure, and mechanical properties. In the SLM technique, it is necessary to take into consideration the following parameters: laser power (1), laser speed

(2), layer thickness (3), the distance between laser passes (4), the diameter of the laser beam (5) and processing path (6) (Bartolomeu 2015). In Figure 31, identify the parameters.

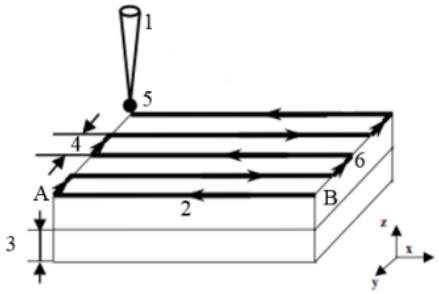

Figure 31 - SLM Parameters (Bartolomeu 2015)

Materials

With Selective Laser Melting, it is possible to use the following materials: stainless steel, aluminium-based alloys, nickel-based alloys, titanium-based alloys, and copper-based alloys, among others (SLM Solutions 2022b). Like other materials, processing aluminium in SLM technology causes an often-reactive atmosphere, so a controlled atmosphere is required for oxide reduction. In laser aluminium casting, a nitrogen atmosphere is usually used since the reaction of aluminium with nitrogen forms aluminium nitride, which contributes to good densification of the part. There are also studies on argon and helium atmospheres (Santos 2014).

Advantages and Disadvantages

In Table 8 are presented the advantages and disadvantages of the SLM process:

Table 8 - Advantages and Disadvantages of Selective Laser Melting (Matmatch 2022)

Advantages	Disadvantages
Quality metal parts using metal powders allows a homogeneous build-up of components.	High surface roughness and high residual stress.
Several materials can be used with this technology.	Deficiency of quality on-line control.
Allows the creation of complex and unique shapes.	It requires an inert gas supply, but when it is used, aluminium and titanium as a material require argon.
High recyclability of the raw material.	Difficulty in removing powder from small channels.

Equipment

The increased functionality given by metal processing by this technology has resulted in many applications and equipment needs that meet diverse target markets. Figure 32 shows an example of an SLM machine.

Figure 32 - SLM 500 (SLM Solutions 2022d)

The universally usable machine with high productivity from SLM Solutions is ideally suited for the series production of complex build parts. It is specifically designed for use in the production environment. It serves as the flagship AM system for high-volume metal additive manufacturing. In addition, the SLM 500 offers fully automated powder management (3D Natives n.d.). In Table 9 is presented the SLM 500 specifications.

Table 9 - SLM 500 Specifications (Solutions 2020)

Machine Specifications	
Build Envelope (L x W x H)	500 x 280 x 365 mm
Variable Layer Thickness	20 μm - 90 μm
Beam Focus Diameter	80 - 115 μm
Maximum Scan Speed	10 m/s
Machine Dimensions (L x W x H)	6080 x 2530 x 2620 mm

Applications

Selective Laser Melting technology has applications in the aerospace and defence industry, automotive industry, energy industry, healthcare industry, tooling industry, and research industry.

The manufacture of rocket components requires many criteria factors to be taken into consideration. Not only is consequent, lightweight construction essential, but materials must also be able to withstand exceptionally high stresses and temperatures. Additionally, the

manufacturing costs for their complex geometries are very high when limited to conventional manufacturing processes (SLM Soluctions 2022). An example of these applications is the monolithic thrust chamber, presented in Figure 33.

Figure 33 - Monolithic Thrust Chamber (SLM Soluctions 2022)

With the production of the Monolithic Thrust Chamber through additive manufacturing instead of conventional machining, it is possible to simplify manufacturing and minimal post-processing despite complex structure to avoid tooling wear when processing is too difficult to machine nickel-based alloy. Also, it is possible to directly integrate multiple parts and interior features, e.g. internal ducts (SLM Soluctions 2022).

Another example of an SLM technology application is a single-piece extrusion tool, shown in Figure 34. Technical hoses are used in many different industries. The production takes place with the help of an extruder, in which a screw conveyor transports material through a cylinder. The material is heated to a homogeneous mass and pressed through the tool at the end of the extruder. After the melt has the desired shape, the material is cooled (SLM Solutions 2022a).

Figure 34 - SLM Application (SLM Solutions 2022c)

Instead of using conventional manufacturing, this part was produced with additive manufacturing using the AM. As a result, it was possible to create an integrated, reduced assembly design, combining individual components into one. Also, the production efficiency

is considerably improved, thanks to the ability of this process to integrate interior features into a reduced assembly (SLM Solutions 2022a).

Electron Beam Melting

The EBM process utilizes a high-power electron beam that generates the energy needed for high melting capacity and high productivity. In addition, the hot process allows for the production of parts with no residual stress, and the vacuum ensures a clean and controlled environment (GE, 2022). Figure 35 represents all the workflow of this process.

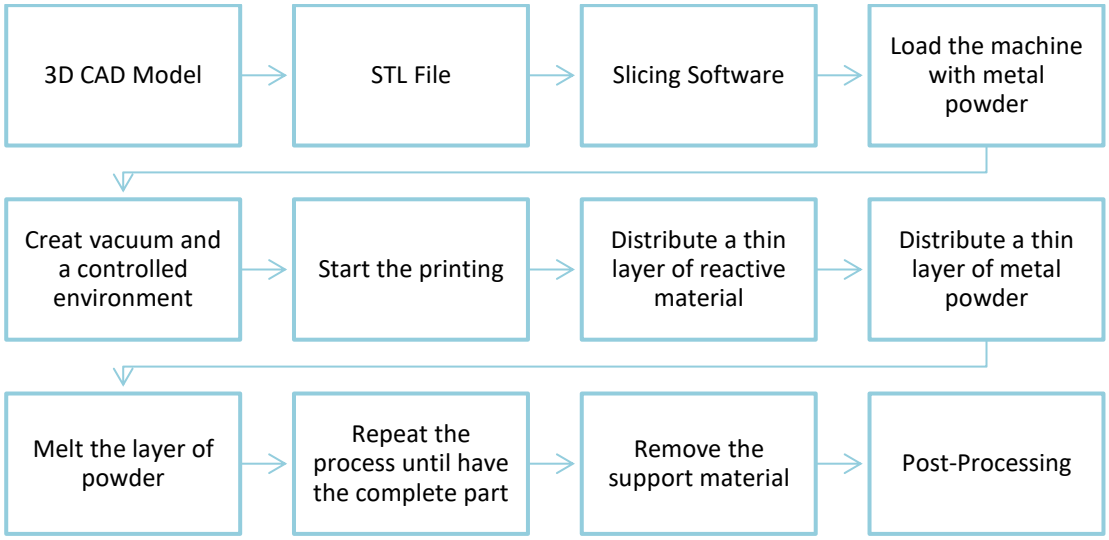

Figure 35 - Electron Beam Melting Workflow

An optimized build file is sliced and into the Arcam EBM system, following this, metal powder is loaded into the machine, the build chamber is then closed, and a vacuum is created to ensure a clean, controlled environment that allows, that allows for the processing of reactive material. Next, the Arcam EBM layering system evenly distributes a thin layer of powder on the build area. A powerful 6 KW electron beam heats the powder bed to the optimal ambient temperature and then proceeds to melt the powder, first contour melting and then hatch melting. The electron beam unit generating the beam contains no moving parts, allowing for extremely fast and accurate beam control. The built environment is kept hot, reaching temperatures exceeding 1000ºC, resulting in no residual stresses and allowing for the processing of crack pro materials. As each layer is completed, the build is lower, and the fresh layer of build powder is raked over it. This process repeats drawing the build one layer at a time. Finally, the tank is extracted when the build is complete, and the Arcam EBM machine is prepared for the next build (GE 2022).

Materials

The materials used in this technology are essentially alloys of titanium and chromium-cobalt, having as most important customer industry the area of implants and medical prostheses, in addition to all areas where the high performance of titanium is relevant (3Dnatives 2022b).

Advantages and Disadvantages

Table 10 shows some of the advantages and disadvantages of using the Electron Beam Melting technology.

Table 10 - Advantages and Disadvantages of Electron Beam Melting (All3DP 2022b) (3Dnatives 2022b)

Advantages	Disadvantages
Geometrical Freedom.	Precision. The electron beam is wider than the laser beam at the powder level, reducing accuracy.
Manufacturing speed. The electron beam can separate from heating the powder in several places simultaneously, which significantly speeds up production.	Small print volume (max. 350-mm diameter and 380-mm height).
Pre-heating the power before it melts limits the deformations and thus reduces the need for reinforcements and supports during manufacturing.	Expensive machines and materials.

Equipment

The Arcam EBM Q10plus (Figure 36) is GE Additive's electron beam melting machine explicitly designed for the cost-effective production of orthopaedic implants. In addition, the Q10plus is used to produce high-volume implants with advanced trabecular structures (GE Additive 2022d).

Figure 36 - Arcam EBM Q10plus (GE Additive 2022b)

The Q10 plus machine has a small machine footprint with a powder handling system to support the additive process. Table 11 presents the machine specifications.

Table 11 - Arcam EBM Q10plus Specifications (GE Additive 2022b)

Machine Specifications	
Max. build size (W x D x H)	200 x 200 x 200 mm
Max. beam power	3kW
Minimal part resolution	0.75mm (70um layer parameter set/theme)
He consumption, build process	1 liter / hour
He consumption, ventilation	50-75 liters / build
Size (W x D x H)	2112 x 1134 x 2758 mm
CAD interface	Standard: STL

The Arcam EBM A2X (Figure 37) machine was designed essentially to process materials at high temperatures, such as titanium, titanium aluminide, and refractory alloys.

Figure 37 - Arcam EBM A2X (GE Additive 2022c)

This machine is ideal for material studies because it operates in a vacuum, providing a clean and controlled environment and minimising the risk of contamination. In addition, this

machine uses electrons as energy carriers, provides deep energy penetration, and low reflection in the powder (GE Additive 2022c). Table 12 presents the machine specifications.

Table 12 - Arcam EBM A2X Specifications (GE Additive 2022c)

Machine Specifications	
Max. build size (W x D x H)	200 x 200 x 380 mm
Max. beam power	3kW
Max. EB translation speed	8,0 m/s
He consumption, build process	1 l/h
He consumption, ventilation	50 -75 liters / build
Size (W x D x H)	1,850 x 900 x 2,200 mm
CAD interface	Standard: STL

Applications

The EBM technology can be used to produce parts for the orthopaedic industry, as it offers significant freedom of design and higher build volume. In addition, thanks to part-stacking capability, this combination allows for manufacturing complex and detailed orthopaedic implants. Figure 38 shows an example of one acetabular cup.

Figure 38 - Acetabular Cup (GE Additive 2022f)

In the production of acetabular cups, the AM replaces traditional coatings with 3-Dimensional lattice structures, which improve initial fixation and allow for faster fusion and bone in-growth. With the production of acetabular cups in additive manufacturing, it was also possible: up to 58% improved time to market 14-22 weeks with EBM technology, compared to 26-38 weeks with traditional manufacturing and improved osseointegration, the optimal pore size is 650 µm, standard coating pore sizes are only 100-300 µm, with EBM 400-800 µm pore sizes are achievable (GE Additive 2022f).

Also, this technology can be used in the aerospace industry, as it as allows produce lightweight components with a very efficient buy-to-fly ratio. Figure 39 shows an example of sleek turbine blades.

Figure 39 - Sleek Turbine Blades (GE News 2022)

2.4.4. Direct Energy Deposition

Laser Engineered Net Shaping

LENS systems use directed energy deposition, where high-powered lasers build structures layer-by-layer directly from powdered metals, alloys, ceramics, or composites to produce fully dense parts with excellent mechanical and fatigue properties. Figure 40 represents the workflow of this process.

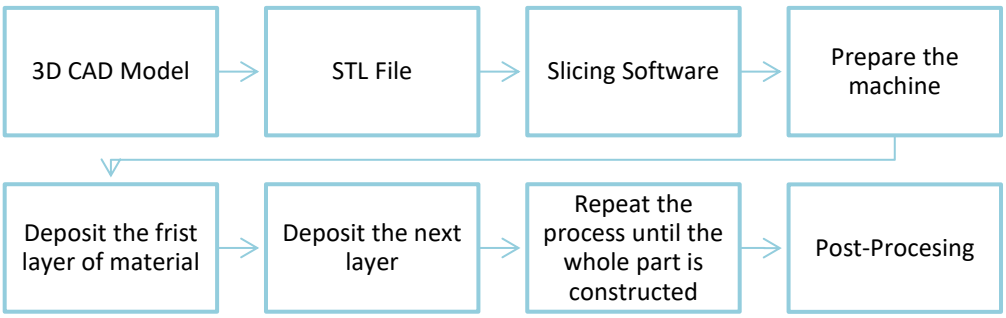

Figure 40 - Laser Engineered Net Shaping Workflow

First, a CAD model is developed, then the CAD model will be stored in an STL format, and the model is then sliced into layers and communicated to the EBM machine. The LENS process is housed in a hermetically sealed chamber purged with argon so that the oxygen and moisture levels stay below 10 parts per million. This keeps the part clean, preventing oxidation. The metal powder feedstock is delivered to the material deposition head by Optomec's proprietary powder-feed system, which can precisely regulate mass flow. Once a single layer has been deposited, the material deposition head moves to the next layer. By building up successive layers, the whole part is constructed. When complete, the component

is removed and can be heat-treated, hot-isostatic-pressed, machined, or finished in any customary manner (Ahn 2021).

Materials

LENS systems process engineering common materials such as stainless steel, tool steels, titanium alloys, and cobalt alloys. This technology can also process other materials, including zirconium, tantalum, tungsten, aluminium, bronze, refractory metals, and some ceramics (Optomec 2022d).

Advantages and Disadvantages

When using Laser Engineered Net Shaping technology to produce a part, it is possible to find some advantages and disadvantages, as shown in Table 13.

Table 13 - Advantages and Disadvantages of Laser Engineered Net Shaping (Semetay 2007) (Izadi et al. 2020)

Advantages	Disadvantages
Ability to fabricate with multiple materials and create functionally graded materials, owing to the multiple powder feed lines.	Distortion results from the uneven heating and cooling of the part during the process.
They have reduced environmental impact.	They are used for simple geometry.
Ability to process non-reactive and reactive metals.	Residual stress is significantly higher.

Equipments

The LENS CS 800 System (Figure 41) has an extensive range of processing capabilities from attractive geometric part contours at lower powers up to high power, high deposition rate cladding applications.

Figure 41 - LENS CS 800 System (Optomec 2022c)

The CS 800 comes standard with a Siemens 840D controller and can operate in up to a simultaneous 5-axis with the Master CAM/LENS plug-in. In addition, it can be equipped

with up to four powder feeders allowing for functional grading or special alloy blending during a build. Table 14 presents some specifications of this machine.

Table 14 - LENS CS 800 Specifications (Optomec 2018)

Machine Specifications	
Build envelope	800 x 600 x 600 mm
Controlled atmosphere	O2 levels < 10 ppm
Laser deposition head	LDH 3. X with 4-tip nozzle
Fibre laser	500 W
CNC Controller	Siemens 840D

Applications

The LENS technology has applications in hybrid manufacturing, materials discovery, medical implants, blisk repair, and component repair.

Hybrid manufacturing is the term used to describe combining metal additive manufacturing technology with conventional, subtractive technology, enabling each process to work together on the same machine and even on the same part (Optomec 2022a). Figure 42 shows an example of a hybrid part.

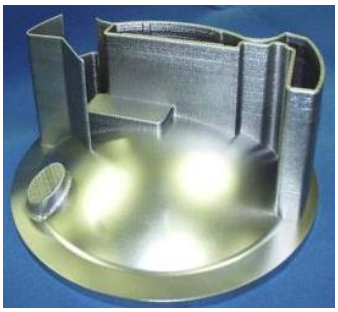

Figure 42 - Hybrid Part (Optomec 2022a)

Hybrid manufacturing machines simplify metal fabrication applications such as net shape rapid prototyping, hybrid manufacturing, in-situ repair, manufacturing rework, and more. In this example, subtractive machining was used to fabricate the housing base, and additive manufacturing was used to build and finish the thin wall structures all on the same machine (Optomec 2022a).

Another example of an application of the LENS technology is the repair of blisk. This technology can precisely add material to worn or damaged blisks and airfoils to restore their

profile. Integrally bladed rotors, also known as blisks, provide many operational and performance benefits over traditional multi-component designs. However, they can cost tens or even hundreds of thousands of dollars to manufacture, and consequently, replacing damaged blisks can significantly increase in-service operational costs (Optomec 2022b). Figures 43 and 44 present the blisk before LENS leading edge repair and after.

Figure 43 - Blisk (Before) (Optomec 2022b)

Figure 44 - Blisk (After) (Optomec 2022b)

The challenge, therefore, is to develop an effective repair technique that can guarantee that all airfoils can be repaired – for if one airfoil is unrepairable, the entire blisk must be scrapped. To respond to this challenge, a front edge has been developed for repair using Stellite® 21, a cobalt-based wear-resistant material (Optomec 2022b).

Laser Metal Deposition

Laser metal deposition (LMD) is an additive manufacturing process for metals. This is the most common designation for this process, but it is also known as direct metal deposition (DMD) and laser-direct energy deposition (L-DED) (TRUMPF 2021). In Figure 45 is represented the workflow of this process.

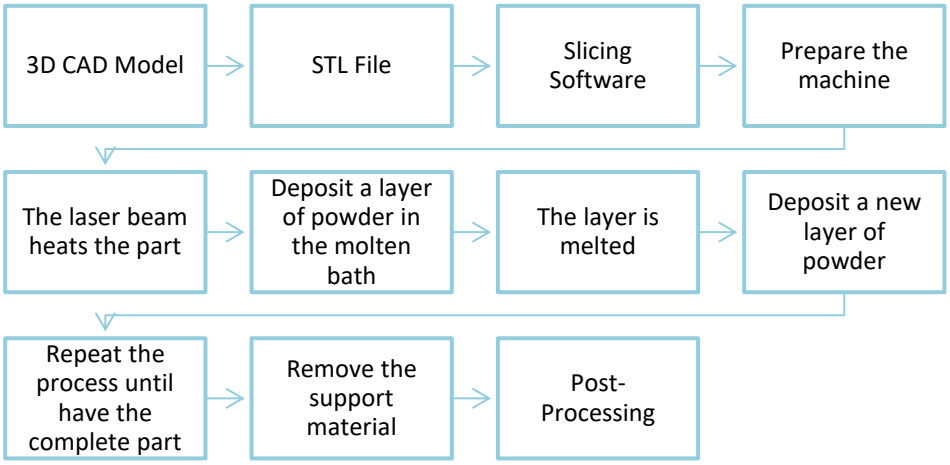

Figure 45 - Laser Metal Deposition Workflow

The starting point is a 3D CAD model subdivided into layers of a defined thickness. The actual part is fabricated by a repeating process of applying new material layers and transferring the geometrical information of each layer into the material using a laser beam (Gasser, Gerhard Backes, et al. 2010). First, the laser beam heats the part in place and creates a molten bath. Next, a fine metallic powder comes from a nozzle in the optical processing system, sprayed directly into the molten bath. There this powder is melted and binds to the base material. The metal powder is deposited layer-by-layer on the base material, where it fuses with the substrate without forming any pores or cracks. The shielding gas normally used is argon. The optical processing system moves through the piece with automatic control to apply in lines, surfaces, and shapes. The smart sensor system ensures that the layer thickness is uniform at all points. This method can apply successive metal coatings of either the same or even a different material (TRUMPF 2021).

Materials

In laser metal deposition, it is possible to use a wide variety of materials, like cast iron, nickel alloys, cobalt alloys, titanium alloys, aluminium, and copper, among others (TRUMPF 2021).

Advantages and Disadvantages

Table 15 presents some advantages and disadvantages of the laser metal deposition technology.

Table 15 - Advantages and Disadvantages of Laser Metal Deposition (Thomas 2022) (Gasser, Backes, et al. 2010)

Advantages	Disadvantages
Freedom of form	The process is very complex, requiring trained operators to tune LMD machines
Improvement of mechanical performance of high-value products	Surface finishes can be rough and porous
Customization	LMD is mainly suited for small components, as larger ones take a long time to print because of the low deposition rate.
It can be used on existing and uneven surfaces	Oxygen contamination is more common in LMD, which increases shield gas wastage and the risk of brittleness/part failure.

Equipment

The 5-axis TruLaser Cell 3000 (Figure 46) laser machine allows welding and cutting in two and three dimensions. In addition, the 3D laser machine is suitable for overlay welding. In the case of larger quantities of parts, the machine can be automated according to the customer's needs (Trumpf 2022).

Figure 46 - TruLaser Cell 3000 (TRUMPF 2022)

This machine used by the Laser Metal Deposition technology has the following specifications, shown in Table 16.

Table 16 - TruLaser Cell 3000 Specifications (TRUMPF 2022)

Machine Specifications	
Max. Speed of the shaft, parallel to the x-axis, y-axis, and y-axis	50 m/min
Mas. acceleration parallel to the x-axis, y-axis, and y-axis	10 m/s2
Max. laser power	8000 W
Available lasers	TruDisk, TruFiber, TruDiode

Applications

The laser metal deposition technology can be used for repairs, additive manufacturing, coatings, and gap filling during welding. It is a principle with broad applications in the aerospace, energy, and heavy industries, the automotive industry, research and development, tool and mould making, and medicine, among others (TRUMPF 2021). An example of these applications is the fan blade shown in Figure 47.

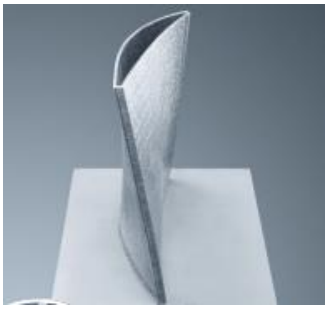

Figure 47 - Fan Blade (TRUMPF 2021)

Additive manufacturing using LMD provides considerable design freedom, even in the case of delicate and highly complex geometries. Create components from scratch or add 3D structures to base shapes (TRUMPF 2021).

2.4.5. **Material Extrusion**

Fused Deposition Modeling

The FDM technology is a layer additive manufacturing process to produce prototype and end-use parts. Figure 48 presents the workflow process of this technology. Figure 48 represents the Fused Deposition Modeling Workflow.

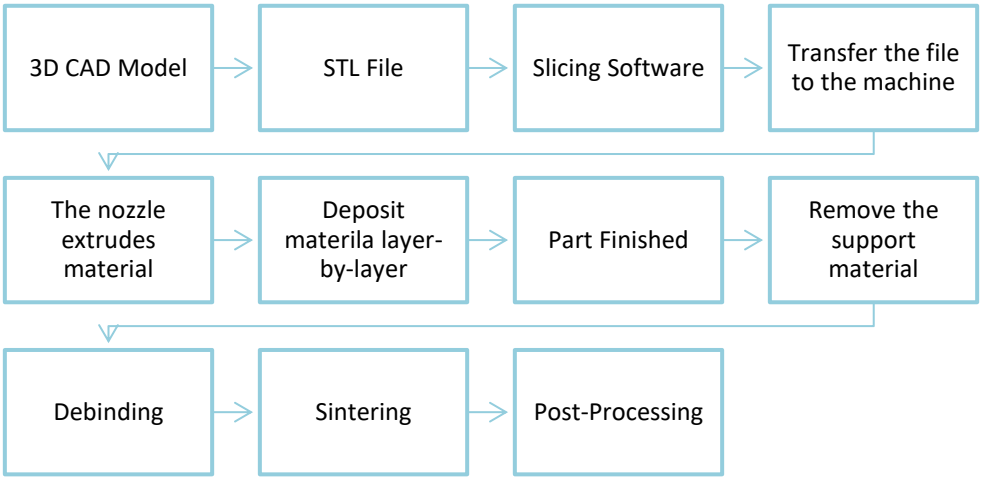

Figure 48 - Fused Deposition Modeling Workflow

This process begins by creating a CAD model of a part and then converting it into STL format, then, the file is sliced into layers, and the data is transferred to a machine that constructs the part layer-by-layer upon a build platform. First, thin thread-like spools of the filament-based feedstock material and support material are used to create each cross-section of the part. Next, the uncoiled material is slowly extruded through to dual heated nozzles. The extrusion nozzles lay down support and filament material upon the preceding layers. The extrusion nozzle moves in a horizontal XY plane while the build platform moves down, building the part layer by layer. Finally, the finished part is removed from the build platform and cleaned as support material (Solid Concepts 2010). If the part is made of metal, it needs to undergo the debinding and sintering process, and they can be necessary applied post-processing in part. In the process of printing a part, it is necessary to take into account the following parameters: layer thickness, the type of filling of the parts, the deposition orientation, the width of the deposited filaments, the diameter of the printer ribbon, the deposition temperature, the base temperature, among others. These parameters influence the surface finish of the parts as well as the mechanical properties and geometric resolution (Lopes 2015).

Materials

The material used with this technology is a solid filament made of thermoplastics or metal. This filament is characterized by extreme length relative to its cross-section. Many materials can be used, like ABS plus, ABS-M30i, Polylactic Acid, Nylon 12 Carbon Fiber, Polycarbonate (PC) (Stratasys 2022a), Ultrafuse 316L, and Ultrafuse 17-4 PH.

Advantages and Disadvantages

Table 17 presents some positive and negative points of the FDM technology.

Table 17 - Advantages and Disadvantages of Fused Deposition Modeling (Harshit K. Dave and Sandip T. Patel 2022)

Advantages	Disadvantages
FDM is more affordable, accessible, and cost-effective.	Surface quality (shape deviation and surface finish).
The process is relatively clean and safe and does not require the use of harsh chemicals.	High-detail prints are hard to achieve.
Feedstock materials are very diverse.	Unsuitable for thin-walled products.

Equipment

Artillery Sidewinder X2 is a 3D printer that uses FDM technology which comprises a large-size printing area, an automatic bed levelling, and a tempered glass platform (Artillery 2020). Figure 49 shows an example of this machine.

Figure 49 - Artillery Sidewinder X2 (Artillery 2020)

This machine used by the Fused Deposition Modeling technology has the following specifications, shown in Table 18.

Table 18 – Artillery Sidewinder X2 (Artillery 2020)

Machine Specifications	
Build Volume	300 x 300 x 400 mm
Layer Resolution	0.1mm – 0.35mm
Build speed	60mm/s – 150mm/S
Number of extruders	1

Applications

FDM technology can produce complex functional parts, prototypes, and function testing in small quantities. Figures 50 a) and 50 b) show some examples of products that can be printed using this technology.

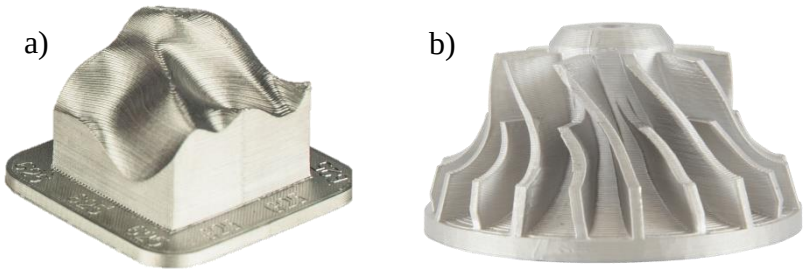

Figure 50 - Application examples of FDM technology (PTZ Prototypen GmbH 2022) (Ampower 2022)

Fused Filament Fabrication

Fused filament fabrication is an additive manufacturing technology in which a fused filament is deposited in a controlled manner over or adjoining previous deposited filaments, leading to the construction of a structural part (Yin, He, and Ye 2021). The study developed during the thesis uses this technology. Is presented, in the Figure 51, the workflow process of this technology.

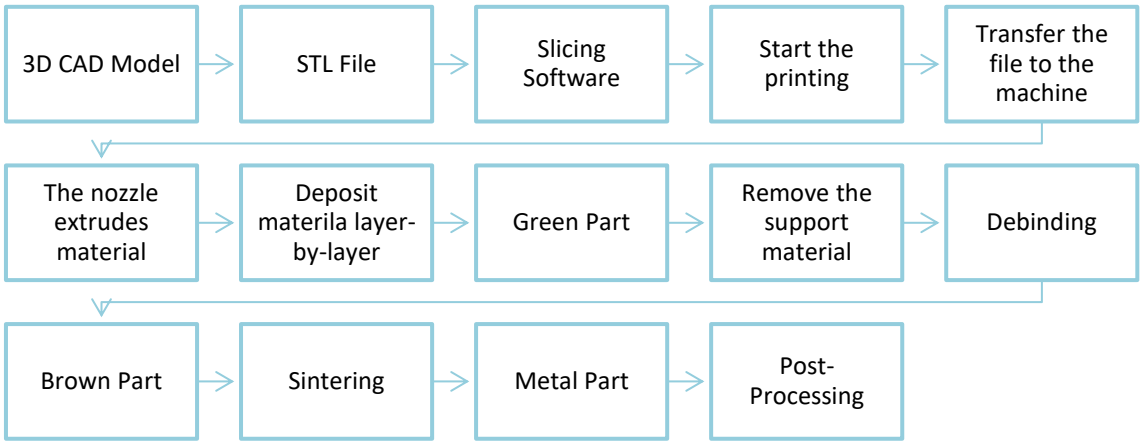

Figure 51 - Fused Filament Fabrication Workflow

The first step is the preparation and slicing, where the CAD is done and then translated into an STL, and that is the input to a slicer, which will convert the model into g-code. After this, the part is printed in the printer, where a heated nozzle ejects molten metal, depositing it in thin layers, one on top of another, onto a print bed, eventually forming the 3D printed part. The filament is led to the extruder, which uses torque and a pinch system to feed and retract the filament in precise amounts. After, a heather block melts the filament to use a usable temperature. The heated filament is pushed through the nozzle, and the extruded material is laid down on the model where it is needed. The print head or bed is moving to the correct X/Y/Z positions for placing the material. After the part is printed, there is the so-called Green Part. It is a part containing a polymeric carrier with a metal. The Green Part must then go through the debinding process, where most of the binder is removed, and the model enters its next phase, the so-called Brown part. At the end of the process, the part is sintered, in here is performed a heat treatment obtains the metal part (Hélio Rui Caldeira da Silva 2008). In Figure 52, the sintering phases are presented. In phase 1, the powder is loose. After that, in the early phase, there is an increase in the interparticle contact area and density. In the intermediate phase, there is a further increase in the contact area, a phase characterized by continuous pore channels along three-grain edges. In the final stage, the pore channel elimination occurs along three-grain boundaries.

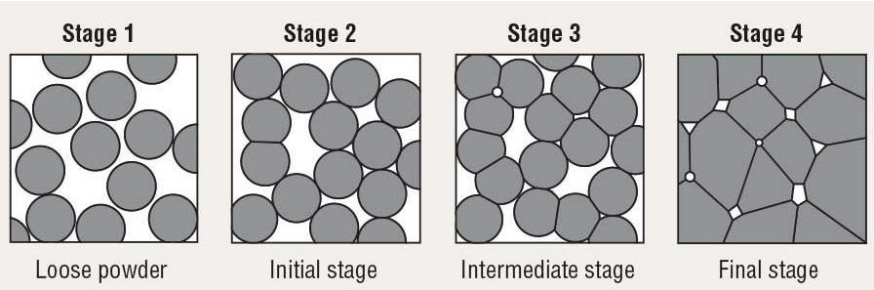

Figure 52 - Sintering Phases (Nguyen Van, Koundinya Sistla, and van Kempen 2016)

Materials

This technology also used a solid filament made of thermoplastics or metal. With the FFF technology, it is possible using the following materials: Ultrafuse 316L and Ultrafuse 17-4 PH.

Advantages and Disadvantages

In Table 19 is presented some benefits and some drawbacks of FFF (BASF 2022a):

Table 19 - Advantages and Disadvantages of Fused Filament Fabrication

Advantages	Disadvantages
Fast printing.	Low speed.
Easy to implement.	Detail resolution.
Easy operation.	Reduced mechanical properties.
Large range of engineering materials.	Surface Finish (visible layer lines).

Equipment and Applications

With FFF, we can use different type of technologies, such as Desktop Metal, filament feedstock, feedstock rods, and feedstock directly.

Desktop Metal Studio System

The Studio System (Figure 53) was developed by Desktop metal, a company founded in 2015. This system is a two-part solution that streamlines metal 3D printing, prints the part, and places it in the furnace for sintering.

Figure 53 - Metal Studio System (Desktop Metal 2022c)

The printer of this system extrudes bound metal rods, eliminating requirements associated with metal AM. The furnace first heats parts to remove all binders from parts, then ramps up the temperature to a near-melting point to deliver industrial-strength sintering. Built-in temperature profiles are tuned to every build and material, ensuring uniform heating and cooling without the residual stresses introduced in laser-based systems (Desktop Metal 2022d). In Table 20 are presented the metal studio system specifications.

Table 20 - Metal Studio System Specifications (Desktop Metal 2022c)

Machine Specifications	
External Dimensions	94.8 x 82.3 x 52.9 cm
Build envelope	300 x 200 x 200 mm
Build plate	Heated, up to 70 °C
Nozzle diameter	0.40 mm and 0.25 mm
Supported file types	STL, IGES, JT, STEP, VDA-FS, U3D, VRML and native file types

Studio System Process

The printing process of this technology consists of four steps: preparation, printing, sintering, and post-processing.

In the first step, the secure, web-based software creates build plans from STL or CAD files, automatically generating media and control parameters based on the part geometry and material. In addition, it can directly process the CAD file. After the file is sent to a printer, layer by layer, a green part is built by extrusion of bonded metal bars – metal powder bonded by polymer binders – in a process called Bound Metal Deposition™. Once printed, the parts are placed in the furnace. As the part is heated to temperatures near melting, the binder is removed, and metal particles fuse, causing the part to densify up to 98%. At the end of the

process, optional finishing methods, such as machining or shot blasting, can be applied for critical tolerances and finishes. Finally, support structures are removed manually (Desktop Metal 2022d).

Studio System Materials

Depending on the finishing and the resistance that the part being produced needs, the studio system can use five materials: stainless steel 17-4 PH, stainless steel 316L, steel H13, steel 4140, and copper (CODI 2022).

Benefits of Studio System

The Studio System extrudes bound metal, which eliminates many safety requirements often associated with metal 3D printing while enabling new features like fully closed-cell infill for lightweight strength (CODI 2022).

Studio System Applications

With a desktop metal studio, it is possible to manufacture products for the following areas: the automotive industry, consumer goods, education, machine design, heavy industry, and manufacturing tooling.

The Rook Chess Piece (Figure 54) is a unique chess piece design that can easily be 3D printed without the long lead times and costs associated with tooling. The Studio System's high-resolution print head produces small parts with fine features and a surface finish. Using the 3D printer, it is possible to have a cost reduction of 52,68% (Desktop Metal 2022d).

Figure 54 - Rook Chess Piece (Desktop Metal 2022d)

Another example is a Putter (Figure 55), and this is typically cast or machined. Manufacturers can achieve excellent material properties with the Studio System without tooling or expensive CNC machining. This system allows for the customization of parts like putters, so each player can have a design that is best suited to them. Moreover, when those

designs go into mass production, they can be manufactured via binder jetting. Using the 3D printer, it is possible to have a cost reduction of 94,00% (Desktop Metal 2022d).

Figure 55 – Putter (Desktop Metal 2022d)

2.5.Support Structures

Support structures hold up elements of a 3D printed part that have no supporting material during manufacture (Fast Radius 2022). Supports are created simultaneously as the model, usually from the same material but with different printing parameters, to be easily removable (Kechagias et al. 2022).

In additive manufacturing, support structures are required in several processes to sustain overhanging parts, and to produce metal components. However, supports are typically hollow or cellular structures removed after metallic AM. Thus, they represent a considerable waste of material, energy, and time employed for their construction and removal (Strano et al., 2012). In this context, it becomes increasingly evident that it is necessary to understand the mechanical behaviour of this structure to make the process faster, and with lower costs without compromising the strength of the parts produced by it (Martins 2016).

Support structures are used in almost all 3D printing technologies and help ensure a part's printability during the 3D printing process. Supports can help to prevent part deformation, secure a part to the printing bed, and ensure that parts are attached to the main body of the printed part. Parts with complex design features like overhangs, holes, and bridges are more challenging to print. Since these features are likely to collapse if not supported, support structures can aid in preventing collapse during the printing process. Supports can also work as heat dissipaters in processes with high temperatures, as with metal 3D printing. With metal AM technologies, support structures help to draw heat away from the part preventing residual stresses that occur due to high temperatures experienced during the printing process (AMFG 2022).

2.5.1. Support Structures Disadvantages

Using support structures brings some disadvantages to the printing process, such as (AMFG 2022):

Material costs: Support generation will require additional material during the printing process, increasing both time and material costs. It is also important to note that supports are not reusable and are usually disposed of, resulting in wasted material.

Limited geometric freedom: When manually removing supports, hand or tool access must be factored in when designing supports. However, this can restrict you from designing specific geometries that require support structures but cannot be reached by hand or tool.

Extra time: Designing a part to accommodate support structures and designing the supports themselves requires extra time.

Additional post-processing: Once a part is complete, it will have to be removed, sometimes manually, increasing the time needed for post-processing.

Risk of damage: Removing supports may leave marks on the surface of a part, which can affect its dimensional accuracy and aesthetics. Additionally, when supports are incorrectly placed on fine features, these can break off along with the support structure – ruining a part all together.

2.5.2. Characteristics of 3D Printing Technologies in Support Structures

Table 21 presents the Characteristics of 3D Printing Technologies, the technology and material used, whether the technology requires support structures and what their functions are.

Table 21 - Characteristics of 3D Printing Technologies in Support Structures (Adapted from Jiang, Xu, and Stringer 2018)

3D Printing Category	Technologies	Material Used	Need Support Structures?	Functions of Support Structure		
				For Thermal Dissipation	For Printability	For Plate Balance
Vat photopolymerization	SLA	Photopolymers	Yes		X	X
Binder jetting	3DP	Powder materials	Yes		X	X
Material jetting	MJM	Liquid materials	No			
Powder bed fusion	SLM	Powder materials, including stainless steel, tool steel, cobalt chrome, titanium and aluminium	Yes	X	X	X
	EBM	Metal powder	Yes	X	X	X
Material extrusion	FDM	Thermoplastic material	Yes	X	X	X
Directed energy deposition	LENS	Metal powder	Yes	X	X	X
Sheet lamination	LOM	Adhesive backed paper	No			

2.5.3. When using support structures

1) When an angle exceeds 45°, the overhanging element generally requires support, or the weight of the unsupported material will cause the element to collapse and the print to fail (Fast Radius 2022). Figure 56 presents an example of when it is necessary to use support structures; on the left if the overhang is 45° or less taken from the vertical, support is generally not needed, and on the right if the overhang is greater than 45° taken from the vertical, supports are generally needed (Fast Radius 2022).

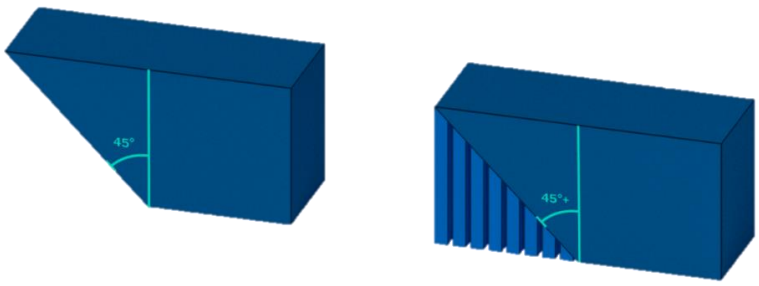

Figure 56 - Support Structures (Fast Radius 2022)

2) The 'YHT' principle - when conceived as 3D printed models, standing upright, the letters Y, H, and T help illustrate the necessity for additive manufacturing support structures. This principle is illustrated in Figure 57.

The letter Y: Two arms extend from the letter Y at 45° – the angle of their overhang does not necessitate support structures. The further the overhang angle exceeds 45°, the more likely support structures will be needed.

The letter H: If the two vertical elements of the letter H are within 5 mm of each other, it may be possible to 3D print the horizontal element of the H with a bridge. If the vertical elements are further than 5mm apart, the horizontal element may require support structures.

The letter T: The two arms of the letter T extend from the vertical element at 90° and will require support structures.

Figure 57 - YHT principle (Filament2Print 2022)

2.5.4. Types of Support Structure

Not-Soluble Supports

There are two main support structures in 3D Printing: tree supports and linear supports.

Tree supports resemble branches or trunks. Tree supports may enclose a part and fit neatly to angled surfaces for easy removal. Tree supports can be designed, applied, and tested

quickly as part of a 3D printing project, enabling rapid iteration. In addition, their branch-like structure means they can reach out over distances to support specific areas. The advantage of using this type of 3D printing support is that it is easier to remove and does not significantly damage the contact points with the part. However, this type of support is only appropriate for non-flat projections (3DLAB 2022). Figure 58 presents an example of tree supports.

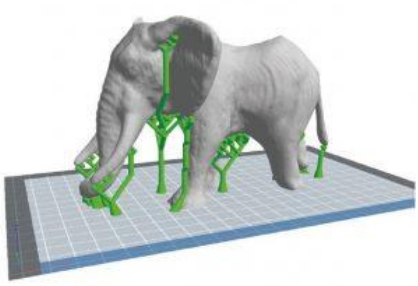

Figure 58 - Tree Supports (3DLAB 2022)

Linear supports: Resembling walls and with various mounting points, linear supports are printed perpendicular to a part's surface, often with a lattice structure (Fast Radius 2022). This type of support is the most used in 3D printing since it works for almost any projection. However, these supports are complicated to remove and much more likely to cause damage to the model's surface (3DLAB 2022). Figure 59 presents an example of linear supports.

Figure 59 - Linear Supports (3DLAB 2022)

Soluble Supports

There are still soluble support structures. If the printer is a double extruder printer, one of the extruders can be used to print the model, and the other can be used to print the support structure (material soluble in water). Once printing is complete, wash the support structure by immersing the model in water, this removal method reduces the risk of damage to the model and facilitates post-processing work (3DLAB 2022).

The range of options in FFF 3D printers with dual extruders expands, as it is not necessary to use the same material for the part and the supports. This opens the door to using materials soluble in solvents that do not dissolve the part material. This makes it possible to use dense substrates in contact with the part, ensuring an excellent finish on the contact surface (Filament2Print 2022).

When the support material is chosen, it is necessary to consider the characteristics of the material. The material must be soluble in a solvent that does not damage the properties of the material used in the part. In addition, the print temperature must be compatible with the part material; it should have good adhesion with the material used in the part; it should be easy to print and have good adhesion between layers. The main types of soluble support materials are soluble in an organic solvent, soluble in water using an activator, and soluble in water. Water soluble support structure materials are among the most sought after by the industry since it does not need organic solvents or alkaline solutions, making them the safest and most affordable alternative for most users (Filament2Print 2022). Figure 60 presents an example of a part with support structures made of Aqusys 180.

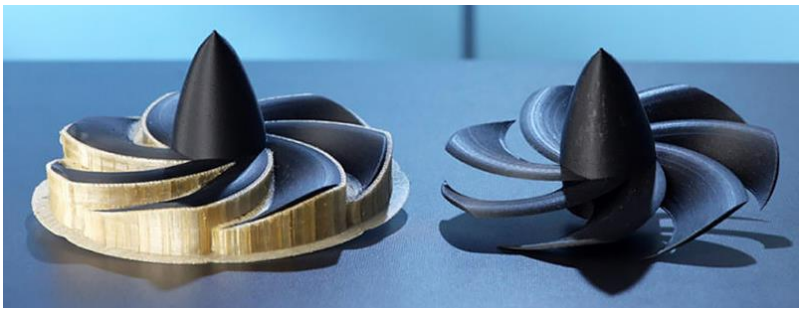

Figure 60 - Support Structures - Aqusys 180 (Filament2Print 2022)

2.5.5. Support pattern

Different patterns are available for printing support structures, resulting in sturdy or easy-to-remove support. Figure 61 shows which a user can choose from:

Figure 61 - Support Patterns (Ultimaker Support 2022b)

2.5.6. Removing Support Material

After the part is sintering, it is necessary to remove the support structures. If the support structure is soluble, the material of the support structure can be removed by simply

dissolving the material in water. For example, first, it is necessary to submerge the print in water (Figure 62), after the supports are dissolved, rinse the print with water to remove any excess of the support structure material, then let the print dry completely and apply additional post-processing to the build material if desired (Ultimaker 2022a).

Figure 62 - Support Material – Soluble (Ultimaker 2022a)

If the support structure is not soluble (Figure 63), it is necessary to break the support structures from the build material, using pliers to grab, twist, and pull the supports. First, it is required to remove the walls of the support structure with a gripping plier. After removing most of the support structure, the remaining parts can be pulled from the build material, and in the end, apply additional post-processing to the build material if desired (Ultimaker 2022a).

Figure 63 - Support Structure - Not Soluble (Ultimaker 2022a)

2.5.7. How to avoid support structures

1. Choose the optimal part orientation

Choosing the correct part orientation can have a significant impact on the printing time, costs, and a part's surface roughness. In addition, depending on a part's orientation (vertical, horizontal, or angled), fewer or more support structures may be needed (AMFG - Autonomous Manufacturing 2022).

The build orientation of an AM part refers to the direction orthogonal to the layers of the object being fabricated. AM part orientations play an essential role in AM processes as they profoundly influence the properties of the final part, influence the mechanical behaviour, the nature, and amount of support structure needed (Thrimurthulu, Pandey, and Reddy 2004). In addition, the part orientation affects the support contact area, surface roughness, build time, and cost of the fabricated part. Figure 61 illustrates a “T” example. The left needs the most support material (see Figure 64 a), followed by the example illustrated in Figure 64b, while Figure 64c does not need any support. However, different support orientations influence the final printed mechanical properties (Jiang et al. 2018).

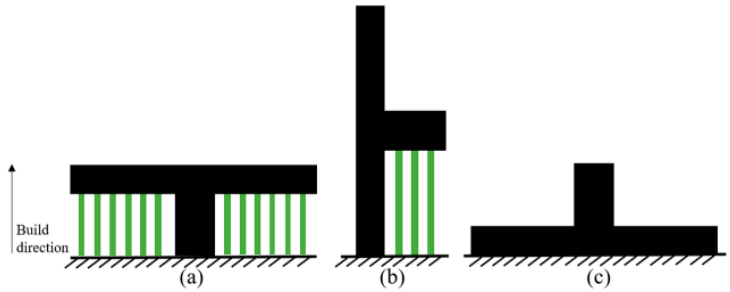

Figure 64 - T example (Jiang et al. 2018)

This example demonstrates that a part can be built up in different ways. Each side of a part can have a different surface attached to the print bed, meaning that the need for support can vary, and depend heavily on the part's orientation.

2. Optimize the support structures

When supports cannot be avoided, they should be optimized to use as little material as possible, and to speed up the printing process. For example, topology optimization can design supports with lattice structures, reducing the support volume, and saving material. With many 3D printing processes, commonly used support generation techniques are limited to producing strictly vertical structures. These are not space-efficient, mainly when there are many regions to be supported high above the print bed (AMFG - Autonomous Manufacturing 2022).

3. Use fillets and chamfers

Fillets and chamfers can be an alternative solution to creating support structures for overhanging surfaces greater than 45 degrees. Essentially, these features turn an angle

greater than 45 degrees into an angle lower than 45 degrees and can be added to a part's interior or exterior (AMFG - Autonomous Manufacturing 2022).

4. Split the part

It can often make sense for very complex 3D models to print the part separately and assemble them afterwards. This will reduce the number of supports and speed up the printing process while saving material (AMFG - Autonomous Manufacturing 2022).

3. Methodology

This chapter will present the various experimental procedures used throughout this study. To carry out this project four tasks were defined, these being the following: the first task was to print specimens with different types of infill patterns and infill densities, to perform density, tensile and roughness tests; the second task was to print small cubes with 100% infill and different patterns to perform roughness tests on the different faces of the cubes; the third task was to print specimens at 0º, 45º and 90º with support structures to perform impact tests; the fourth task was to design a part with application in the automotive industry, do the costing of the process and compare the FFF with SLM technology. Figure 65 presents a flowchart with all the steps performed.

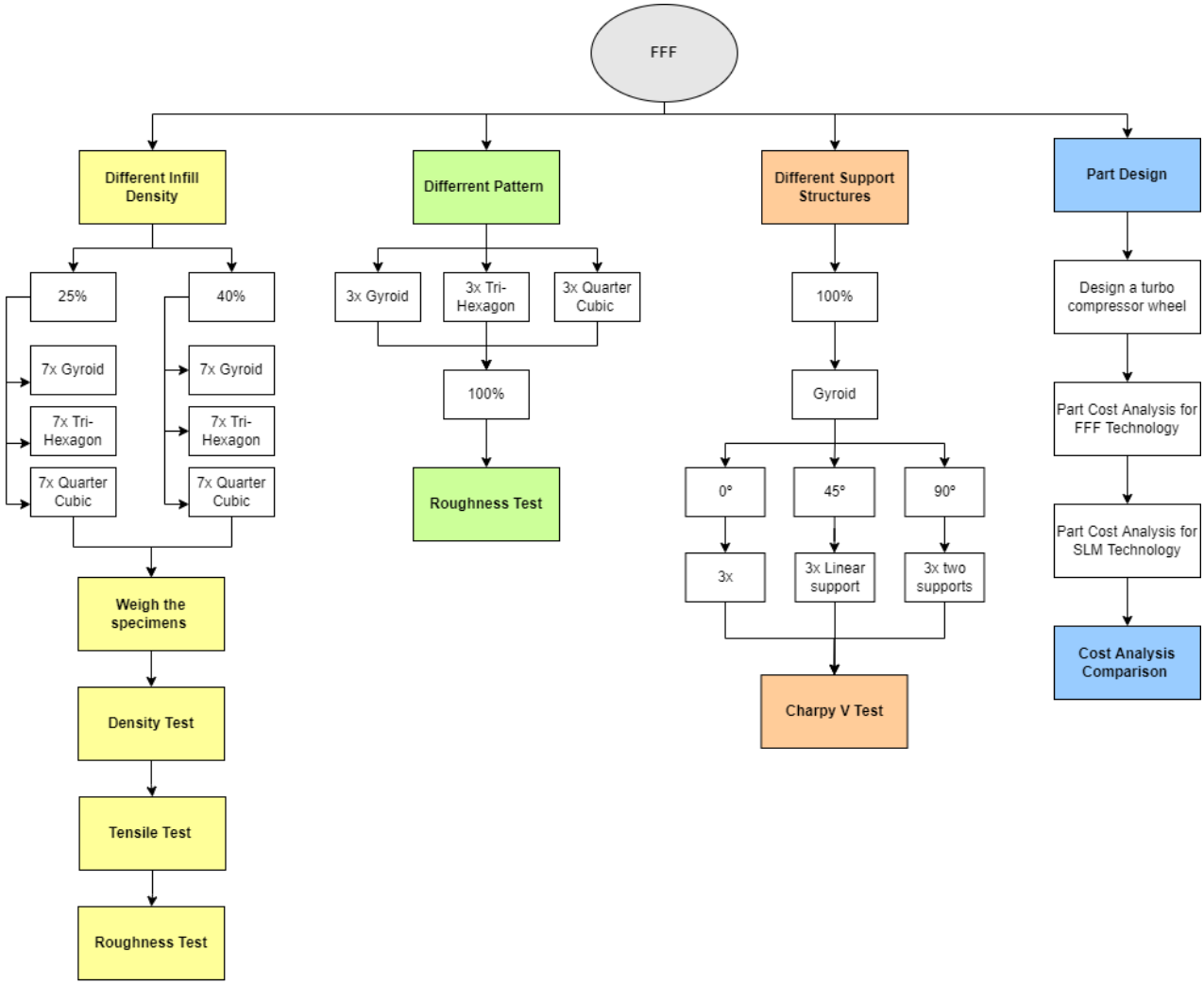

Figure 65 - Methodology Workflow

To print all the parts to perform the different studies, they were first developed in Solidworks software, Ultimaker Cura software and then printed on the Ultimaker S3-3D printer (Figure 66).

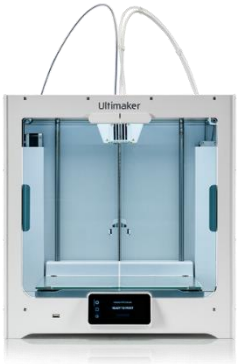

Figure 66 - Ultimaker S3 (Ultimaker 2022b)

In Table 22 are presented the Ultimaker S3 specifications.

Table 22 - Ultimaker S3 Specifications (Ultimaker 2022b)

Ultimaker S3 Specifications	
Technology	Fused Filament Fabrication
Print Head	Dual-extrusion print head with a unique auto-nozzle lifting system and swappable print cores
Build Volume (XYZ)	230 x 190 x 200 mm
Layer Resolution	0.25 mm nozzle: 150 - 60 micron 0.4 mm nozzle: 200 - 20 micron 0.6 mm nozzle: 300 - 20 micron 0.8 mm nozzle: 600 - 20 micron
Build Speed	< 24 mm3/s
Build Plate	Heated glass build plate (20 - 140 °C)
Software	Ultimaker Cura, Ultimaker Connect Ultimaker Cloud.

The Ultimaker Cura software is a default slicing, so the slicer converts the 3D model into a G-code file that will provide the 3D printer with all the necessary instructions for printing (3Dnatives 2022a).

In this specific study, the nozzle used was the CC 0.6 mm. This is used for shorter print times, and improved efficiency – resulting in easier optimization of composite applications (Reichelt elektronik 2022).

Figure 67 - Nozzle CC 0.6 (Reichelt elektronik 2022)

The Ultimaker print core CC 0.6 (Figure 67) prints with bigger line widths, meaning that the composite applications will be ready as quickly as possible – saving time in a busy, hardworking environment that requires efficiency and speed (Reichelt elektronik 2022).

The material used to print the specimens was the BASF Ultrafuse 316L Metal. This is made from 80% 316L stainless steel particles in a polymer base and is non-magnetizable with high corrosion resistance (BASF Forward AM 2022). The 316L metal is composed of nickel, iron, chromium, and molybdenum, the melting point is 164ºC, and the density is 5.4 – 5.8 g/cm^3. This material can be used for functional prototyping, medical equipment, automotive parts, chemical pipes, pumps, valves and mould inlays with near-surface cooling (BASF Forward AM 2022). Table 23 presents the filament properties.

Table 23 - Ultrafuse 316L Properties (BASF Forward AM 2022)

Ultrafuse 316L Properties	
Filament Diameter	1.75 mm / 2.85 mm
Tolerances	± 0.05 mm / ± 0.075 mm
Roundness	± 0.05 mm / ± 0.075 mm
Bending Radius	5 ± 1 mm / 10 ± 3 mm
Spool Length	250 m / 100 m
Spool Weight:	3 Kg / + 3%

3.1.Different Infill Density and Pattern

The first task developed in this study was to print specimens with different infill densities and patterns to perform density, tensile, and roughness tests. Figure 68 presents all the workflow of this task.

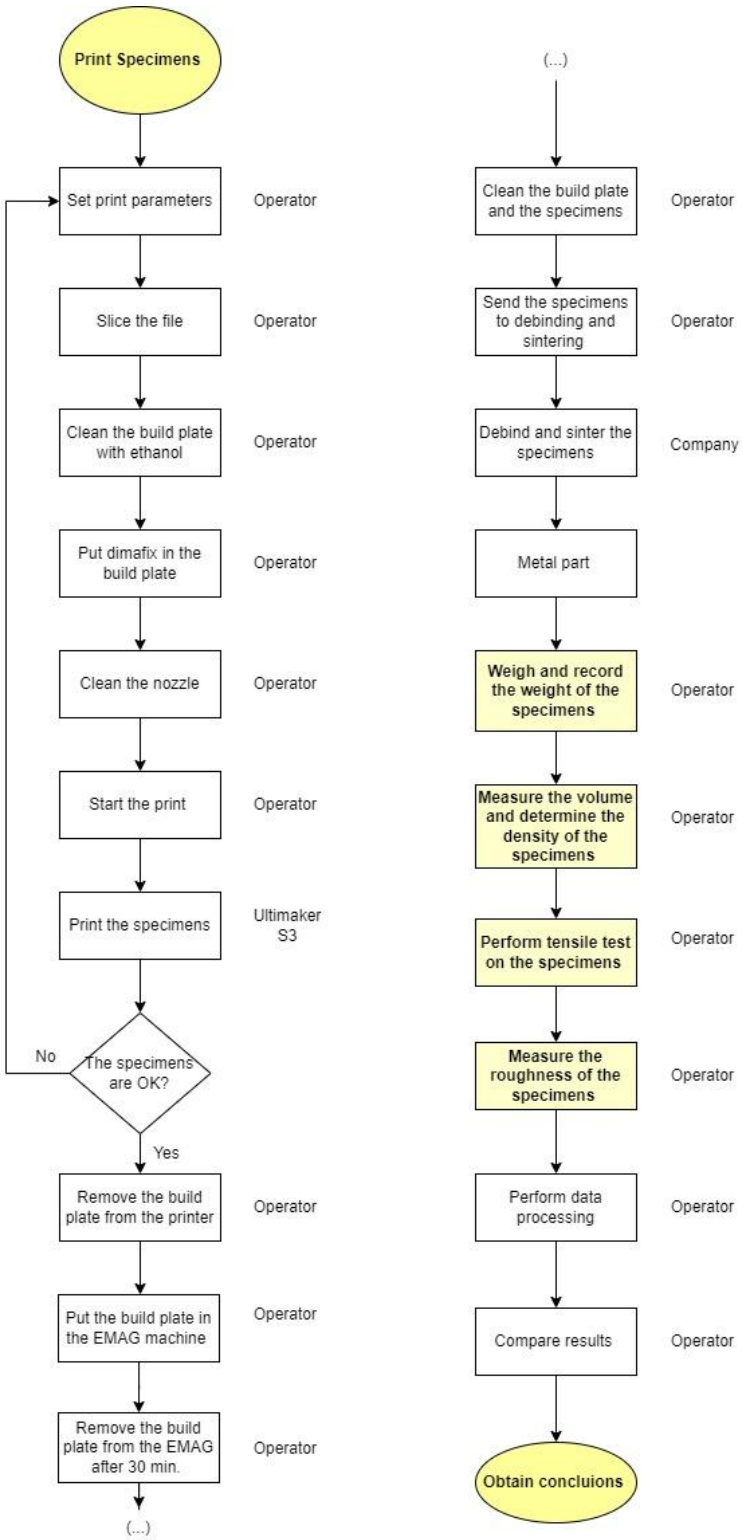

Figure 68 - Workflow Task 1

3.1.1. Print Settings and Process

The specimens used in this first practical part, shown in Figure 69 and Figure 70, have the following dimensions:

- Length: 102 mm;
- Width: 10 mm;
- Thickness: 5 mm.

Figure 69 - 3D Specimens

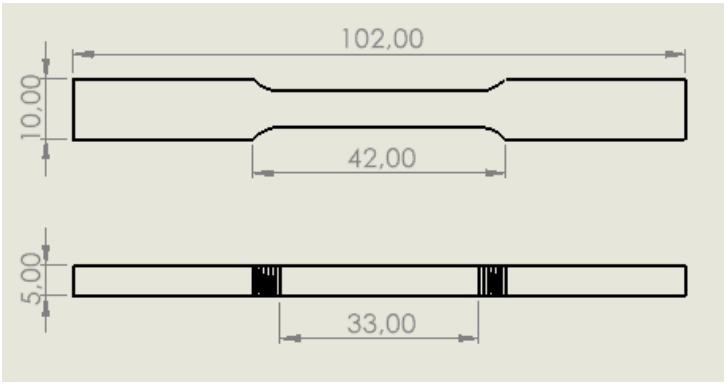

Figure 70 - 2D Specimens

In Ultimaker Cura the specimens were parametrized. In this step, the specimens were scaled, and all the print settings (Table 24), like layer height, wall line count, top and bottom layers, infill density, infill pattern, and infill line direction, among others.

Table 24 - Print Settings

Print Settings	
Layer Height [mm]	0.1
Wall Line Count	2
Layers Top/Bottom	6
Printing Temperature [ºC]	240
Plate Temperature [ºC]	100
Print Speed [mm/s]	25

In the Ultimaker Cura, it is necessary to define the print settings and scale the specimens before starting the print. When we print a part, it is necessary to consider the shrinkage, so it is required to scale the specimens. With the Ultrafuse 316L Metal, it is recommended to scale the part up by 119.82% in the X and Y, then scale the Z up by 126.10% for printing (BASF 2022b).

Through the following equations, it is possible to convert between shrinkage and oversizing factors.

$$S = 1 - \frac{L_s}{Lg};\ OFS = \frac{Lg}{Ls};\ OFS = \frac{1}{1-S}\ ;\ L_g = \frac{L_s}{1-S}$$

Where S is the shrinkage, OFS is the oversizing factor, Ls is the length of the sintering part (in mm), and Lg is the length of the green part (in mm) (BASF 2022b).

After entering all the printing settings, the slicing will start, and the file is saved to the removable disk.

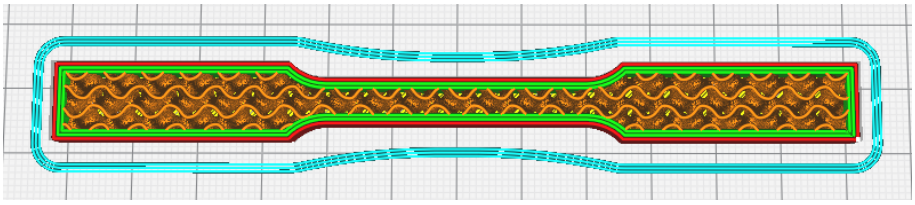

Figure 71 - Slicing Specimens

Afterwards, the preparation of the printer is done. First, it is necessary to clean the build platform with ethanol, and then, put dimafix glue, which provides a grip between the build platform and the print material in this way the test specimens are firmly attached, and the warping effect is avoided. After this, it is necessary to clean the nozzle.

To perform the tests, printing the metal tensile of each infill pattern with different infill densities was necessary. When choosing an infill pattern, it is necessary to consider: the required strength, the visual quality of the top surface, the direction and kind of flexibility necessary, the printability of the pattern, and the printing time (Ultimaker Support 2022a). The infill density defines the amount of metal used inside the print. A higher infill density means more metal inside the print, leading to a more robust object (Ultimaker Support 2022b).

This study used three infill patterns: gyroid, tri-hexagon, and quarter cubic. Figure 72 presents the infill patterns used respectively.

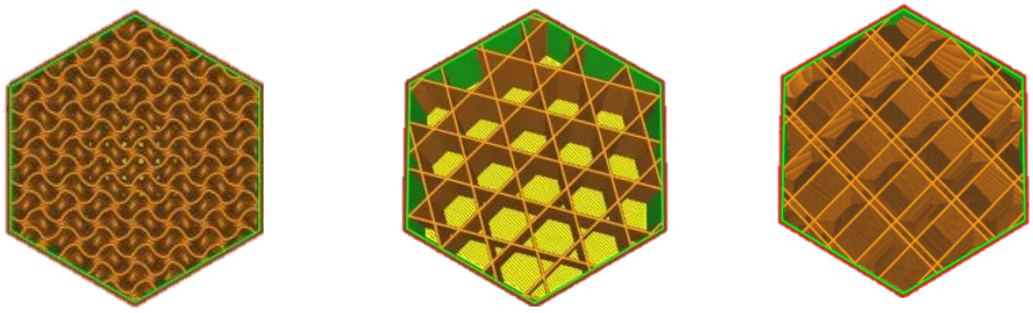

Figure 72 - Infill Patterns

The gyroid infill pattern combines waves throughout the pattern, giving excellent flexibility with good strength for the lowest weight, higher tensile and compressive strength throughout the model (isotropic), shorter printing time, less material used, and looks great without shells. Conversely, the printer vibration can be higher with denser infill percentages and increased slicing time (All3DP 2022a).

The tri-hexagon pattern has a mixture of triangles and hexagonal shapes interspersed throughout the object. It does this by creating three sets of lines in three different directions, but in a way that they do not intersect in the same position. As a result, this infill is solid in the horizontal direction and has equal strength in each horizontal direction. Hence, excellent shear resistance requires many top skin layers to get an even top surface (Fernandez-Vicente et al. 2016).

The quarter cubic pattern is a 3D pattern, that has a multiple infill lines adjacent. In this pattern, heavy loads dissipate weight to the internal structure. Reduced pillowing effect for top layers because long vertical pockets of air aren’t produced, and bridging distance for this pattern is long, so it can negatively affect top surface quality. It is not the best infill pattern when the goal is to save on filament material and time. So, it would help if it did not use this pattern where it is unnecessary to have higher strength (Fernandez-Vicente et al. 2016).

When the printing is started, the specimens begin printing (Figure 73). After the parts are printed, removing them from the build plate is necessary. For this purpose, the EMAG Emmi-100 HC is used. This machine is a small helper designed for professional cleaning. The plate is placed submerged at 60°C for 30 to 45 minutes. The last step is removing the

build plate and the machine parts and cleaning everything. After this, the specimens are ready to be sent to the company to perform the debinding and sintering.

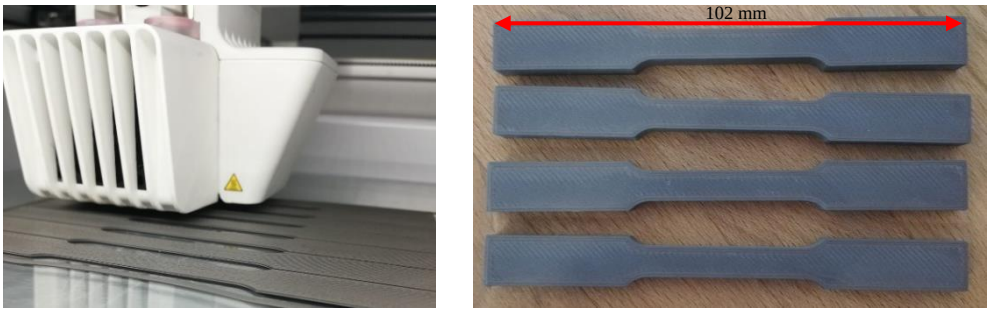

Figure 73 - Printed Specimens

During the printing process of the specimens, there were some problems. Initially, seven specimens were put to print, but during and after printing, the specimens suffered warping. This occurs due to material shrinkage, which causes the corners of the print to lift and detach from the build plate. Figure 74 shows the specimens with warping.

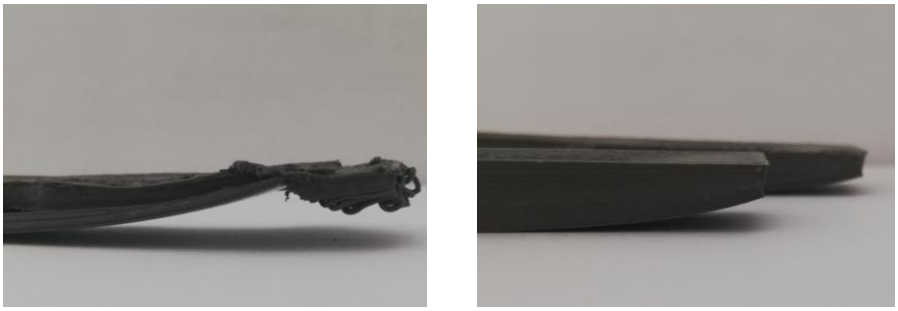

Figure 74 - Specimens With Warping

Cooling is one of the main causes of warping. Material contracts when cooling and can cause the material to pull on itself. Materials must be adequately cooled before the next layer is added, but excessive cooling should be avoided to ensure a smooth, warp-free print. For this reason, instead of printing seven specimens at once, we printed four and three specimens at a time. Table 25 presents the printing time and the material used to print all the necessary specimens.

Table 25 - Specimens Information

Infill Pattern	Infill Density	Quantity	Printing time	Grams of filament used	Meters of filament used
Gyroid	25%	3	3H24	67	2.19
Gyroid	25%	4	4H31	89	2.91
Gyroid	40%	3	3H49	77	2.50
Gyroid	40%	4	5H06	102	3.33
Tri-Hexagon	25%	3	3H24	66	2.15
Tri-Hexagon	25%	4	4H30	88	2.87
Tri-Hexagon	40%	3	3H48	77	2.50
Tri-Hexagon	40%	4	5H04	102	3.33
Quarter Cubic	25%	3	3H29	66	2.16
Quarter Cubic	25%	4	4H35	88	2.88
Quarter Cubic	40%	3	3H52	77	2.50
Quarter Cubic	40%	4	5H08	102	3.33

Debinding and Sintering

After all the specimens are printed, the next step is debinding and sintering. These processes were performed in the company Elnik Systems GmbH. The first step is debinding, and this was performed according to the BASF process at 110°C with HNO_3> 98%. As explained before, debinding removes the required binders to enable the printing process. The catalytic debinding is a thermochemical process in which green parts are exposed to gaseous nitric acid (HNO3) in a nitrogen atmosphere and heated. During this process, formaldehyde that is present in the parts during debinding can react with oxidizing agents. It should be noted that the explosion limit of formaldehyde with oxygen is 4.5% by volume. Also, it is necessary to consider that there is a slow reaction between formaldehyde and nitric acid, so high doses of nitric acid should be avoided. To achieve a safe process and based on a 50-liter debinding furnace, a nitric acid feed of typically 30 ml/h and a purge gas (nitrogen) with a capacity of 500l/h must be provided. The debinding process is complete when a minimum debinding loss of 10.5% is reached. In this process, it is necessary to consider that the thicker the part, the longer the debinding time required (BASF 2022b).

After the debinding, the part goes to the next phase, the sintering. This process combines the metal particles in the brown part into a solid mass. It is carried out under pressures and

temperatures below the melting point of the material to maintain the part's shape. To executes the sintering process, a 100% clean and dry hydrogen atmosphere with a dew point below 40ºC must be ensured. Also, as a sinter carrier, it is recommended to use an Al2O3 with a purity of 99,6%, for example, Frialit® Al2O3.

A typical sintering cycle consists of a ramp from:

1. Room temperature – 5K/min – 600ºC (hold 1H)
2. 600ºC – 5K/min – 1380ºC (hold 3H)
3. Furnace cooling

In the early stage of the sintering process, burned binder components remain, and the pyrolysis products should be extracted using a fan (BASF 2022b).

After the sintering process, the metal part is obtained. Due to its transition from a porous brown part to a dense "white" state, the part's dimensions are reduced. This size reduction is typically referred to as shrinkage.

3.1.2. Tests and Results Obtained

After all the specimens were synthesized, they were used to perform various tests. First, a weight comparison was made of the specimens before and after sintering, then the density of the specimens was determined, tensile and roughness tests were also performed.

Weight of the Tests Specimens

To verify the weight increase or decrease after sintering, the specimens were weighed after printing, in the green state, and after sintering. Figure 75 shows the results obtained for 40% density infill, and Figure 76 shows the results obtained for 25% density infill.

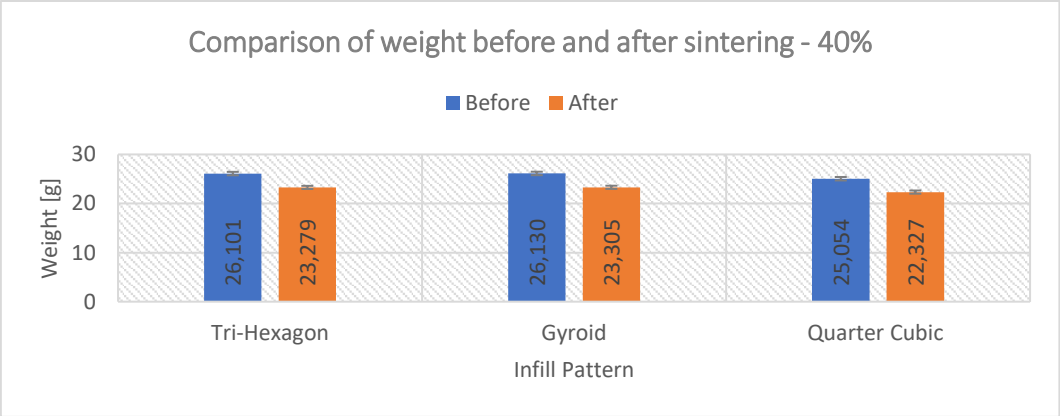

Figure 75 - Comparison Weight of the Specimens with 40% Infill

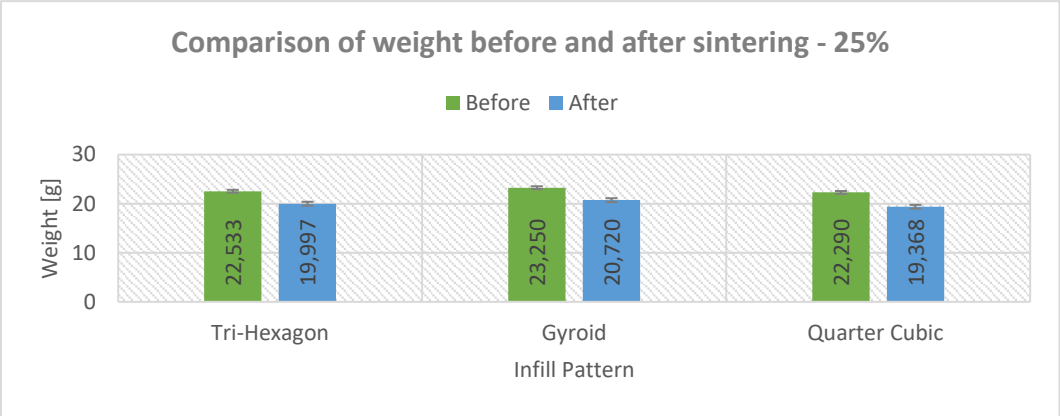

Figure 76 - Comparison Weight of the Specimens with 25% Infill

By analysing the graphs, it is possible to see that all the specimens suffered a decrease in weight after sintering, due to microstructure rearrangement and elimination of the binder present in the part. On average, both specimens with 25% infill and 40% infill reduced their weight by 2,727 grams, which is 11.256%. The specimens with the quarter cubic pattern and 25% infill exhibited the highest reduction of height (2,922 grams), followed by the specimens with the gyroid pattern and 40% infill (2,825 grams). On the other hand, the specimens with the gyroid pattern with 25% infill exhibited the lowest reduction (2,530 grams).

Density Test

After the weight of the specimens, the volume was measured to determine the density. Density is the ratio of mass to volume of a body, i.e., the concentration of mass per unit volume. Therefore, the expression for density is:

$$d = \frac{m}{V}$$

In the International System, the unit for mass is the kilogram (Kg) and for volume is the cubic meter (m^3). Thus, the International System unit for density is the kilogram per cubic meter (Kg/m^3).

To measure the volume of the specimens, a measuring cylinder with a scale and water was necessary, as shown in Figure 77.

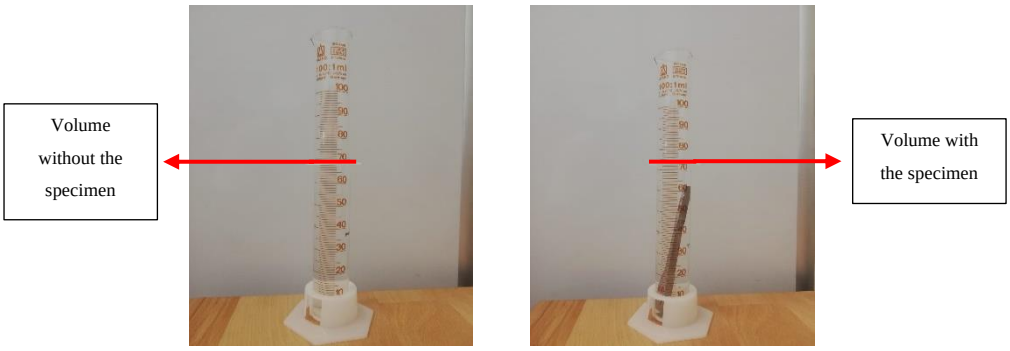

Figure 77 - Density Test

The volume is recorded without the specimen, then placed into the measuring cylinder, and the volume value is recorded. This procedure was done with three specimens of each standard and infill. The table with weight, volume, and density data for each test specimen is shown in Appendix A. In addition, in Figure 78, the results obtained from the density of the different specimens are presented.

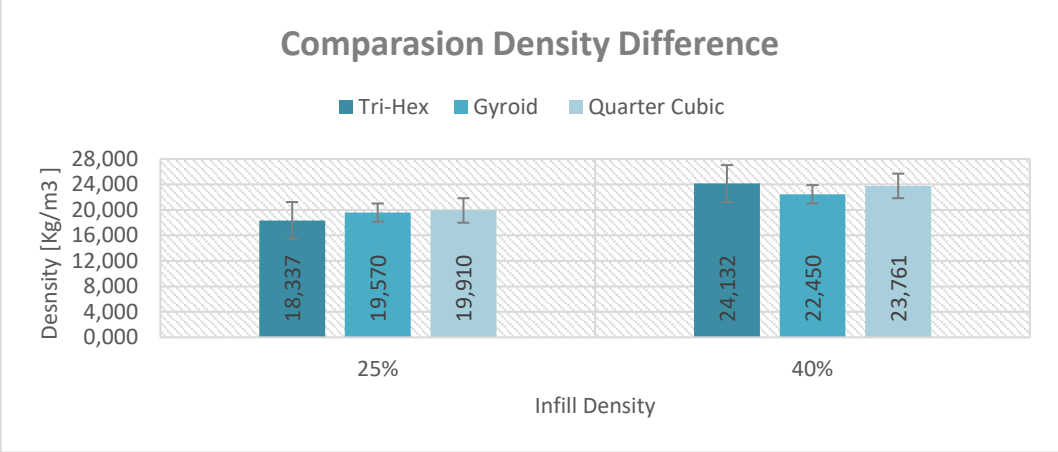

Figure 78 - Density Difference Comparasion

With the analysis of Figure 78, it is possible to conclude that the specimens with 25% infill have a lower density than specimens with 40% infill. The highest density value of 24,132 m^3 was demonstrated by the specimens with the tri-hexagon patter and 40% of infill. On the other hand, the lowest density value is 18,337 m^3 for the specimens with the tri-hexagon pattern and 25% infill.

Tensile Test

In order to study the behaviour of the specimens, tensile tests were performed on several metallic specimens with different infills and patterns. To perform the tensile tests, the machine Zwick Z100 (Figure 79) was used.

Figure 79 - Zwick Z100

Before performing the tests, the specimens' thickness and width were measured using a micrometre (Figure 80). Appendix I shows the measurements obtained from each one.

Figure 80 - Micrometer

Next, the machine was prepared for testing by defining all the set-up in Figure 81.

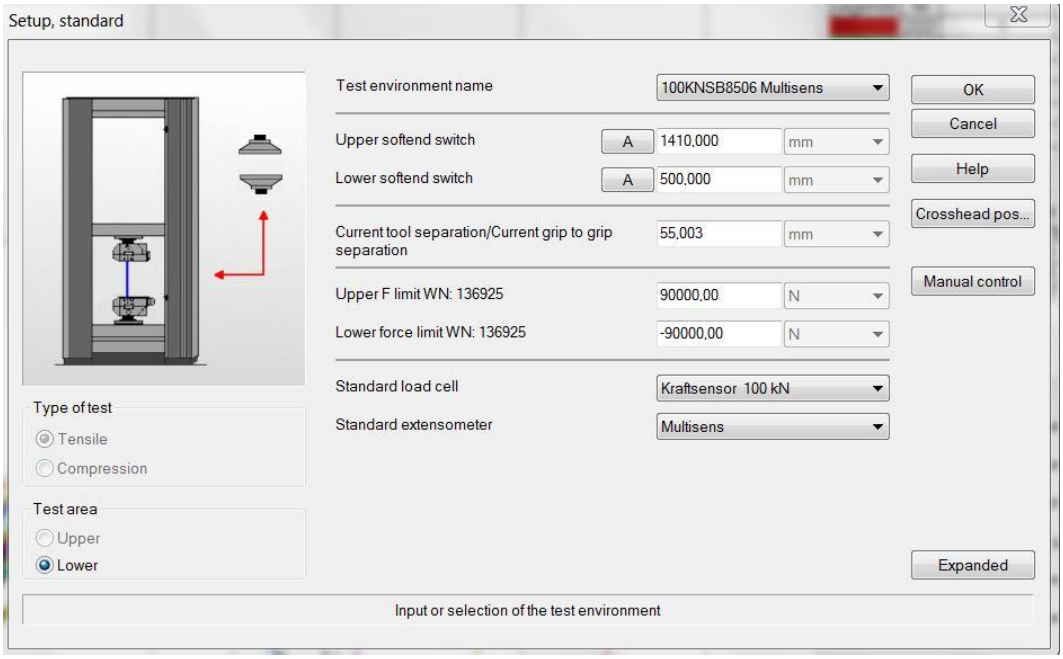

Figure 81 - Setup of the Machine

After all parameters are set, the machine is ready to start testing. First, the specimen was placed in the tensile machine. Tensile tests were performed on all specimens until failure, or if no failure occurred until the defined upper limit. Figure 82 presents some examples of specimens after the tensile test has been performed.

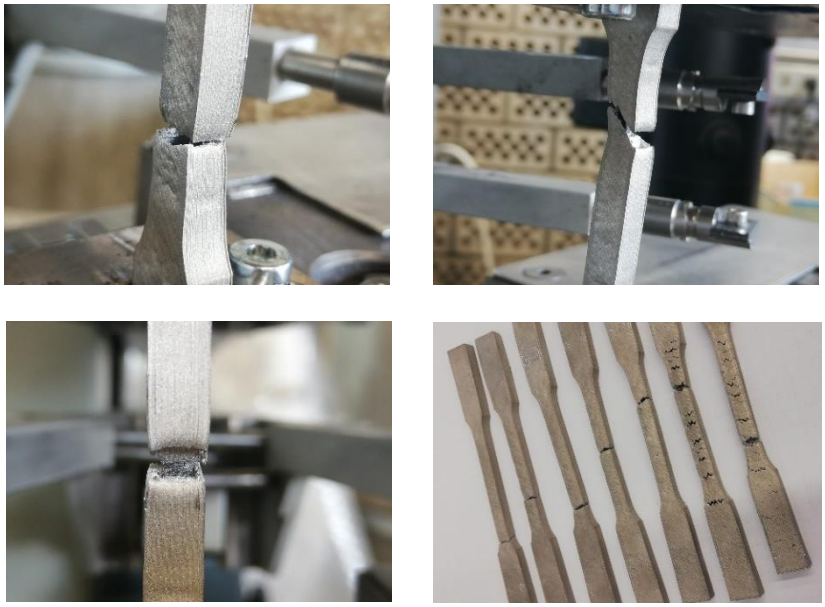

Figure 82 - Examples of Specimens After the Tensile Test

Finally, the results obtained were collected and analysed. Data treatment was performed to compare the specimens' maximum strength with different infills and patterns, as presented in Appendices J, L, M, N, O, P and Q.

After processing all the necessary data, bar graphs were created so that it was possible to make a visual analysis of the behaviour of the different specimens. Figure 83 shows the results obtained on specimens with an infill density of 25% and 40%.

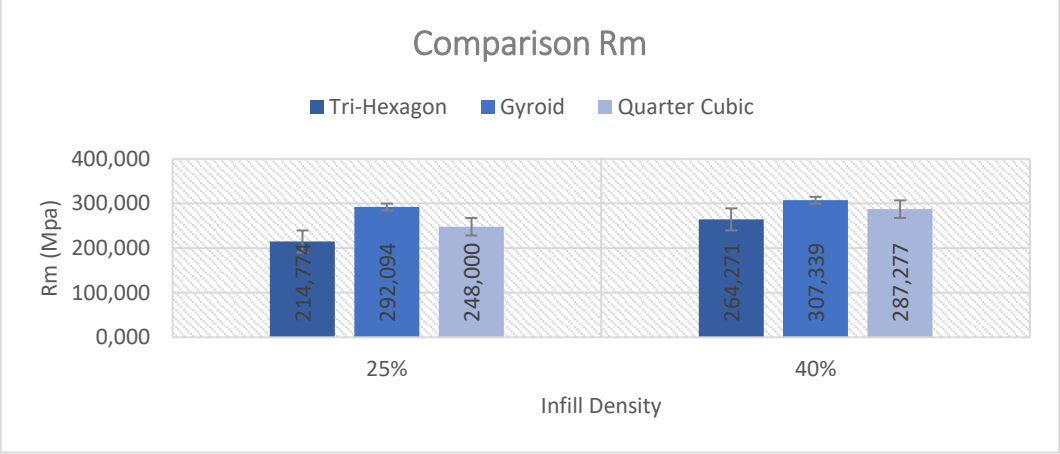

Figure 83 - Rm Results of the Specimens with 25% and 40% of Infill Density

With the analysis of Figure 83, it is possible to verify that the specimens with the highest strength are Gyroid with 40% infill, for presenting a more uniform pattern, and that the specimens with the lowest strength are Tri-Hexagon with 25% infill. In addition, the gyroid pattern generally presents a higher resistance in relation to the other patterns.

In Figure 84, the results obtained in this study are compared with studies performed by other colleagues. The results obtained with the 25% infill and 40% infill specimens are represented in green.

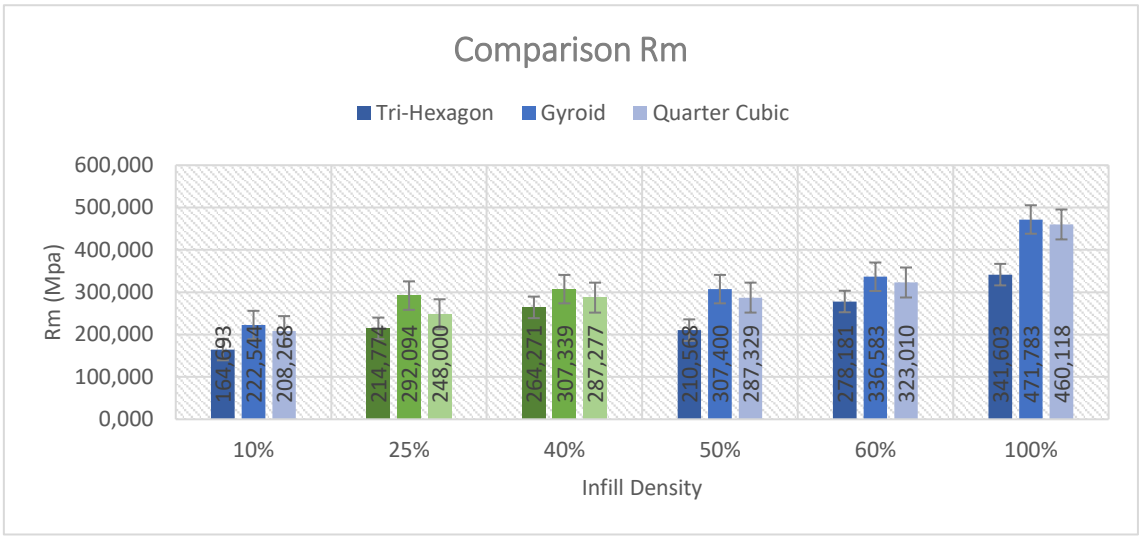

Figure 84 - Rm Results of the Specimens with Different Infill Density

With the analysis of Figure 84, it is possible to verify that the specimens with the highest strength are those with the gyroid pattern. In contrast, the specimens with the lowest strength are those with the tri-hexagon pattern. The specimens with 100% infill and gyroid pattern exhibited the highest strength with 471,783 MPa, and the specimens with the lowest strength with 164,693 MPa are tri-hexagon patterns with 10% infill. Furthermore, it is also possible to verify that the higher the percentage of infill used, the higher the strength of the specimen.

Figure 85 presents the values of Rp for FFF and SLM technologies. After the analysis, the specimens with the highest strength are those with 100% infill and the gyroid pattern. The technologies were compared with these values.

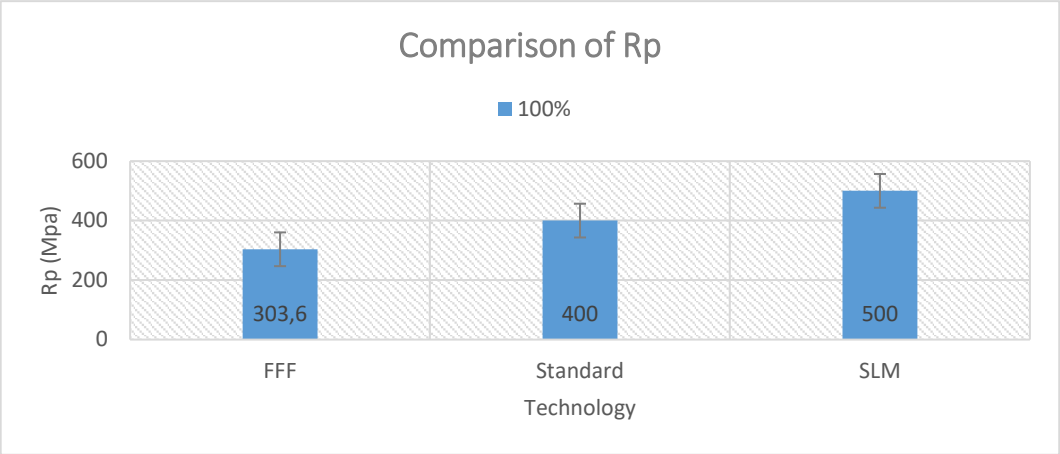

Figure 85 - Rp for FFF and SLM Technologies

By analysing Figure 85, it is possible to see that the FFF technology presents the lowest elastic limit value of 303,60 MPa. In contrast, SLM technology presents the highest elastic limit value of 500 MPa. This means that a part manufactured using SLM technology gets maximum stress or force per unit area within a solid material that can arise before the onset of permanent deformation than with FFF technology.

Figures 86, 87, 88, 89, 90, and 91 show the tensile stress-strain curves of the specimens printed with the different patterns and percentage of density infills. Comparing the pattern tri-hexagon, the specimens with 40% of infill exhibited the highest ultimate strength and strain at break. In the pattern gyroid, the specimens with 25% exhibited the highest ultimate strength and strain at break. Also, in the pattern quarter cubic, the specimens with 25% exhibited the highest ultimate strength and strain at break.

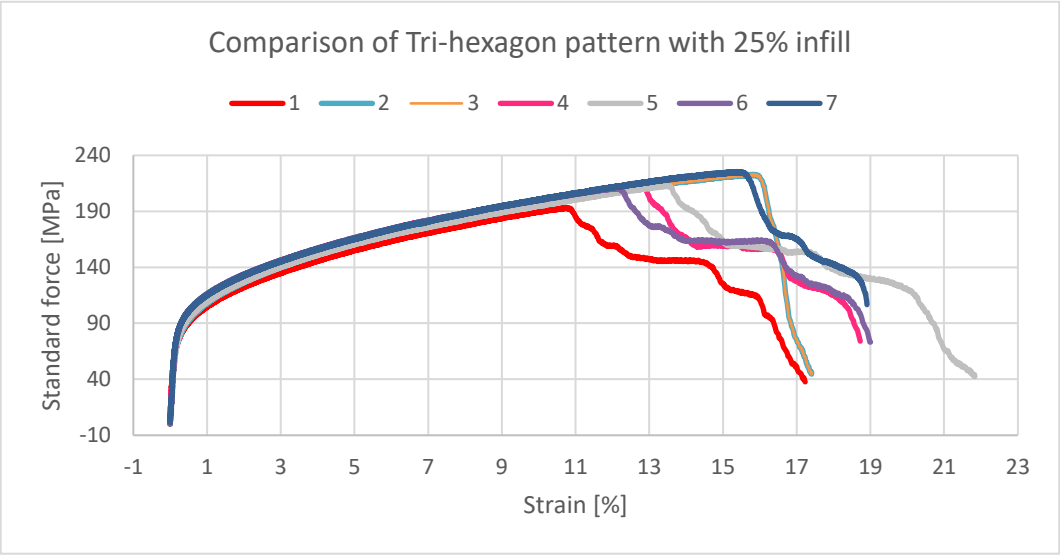

Figure 86 - Comparison of Tri-Hexagon Pattern with 25% Infill

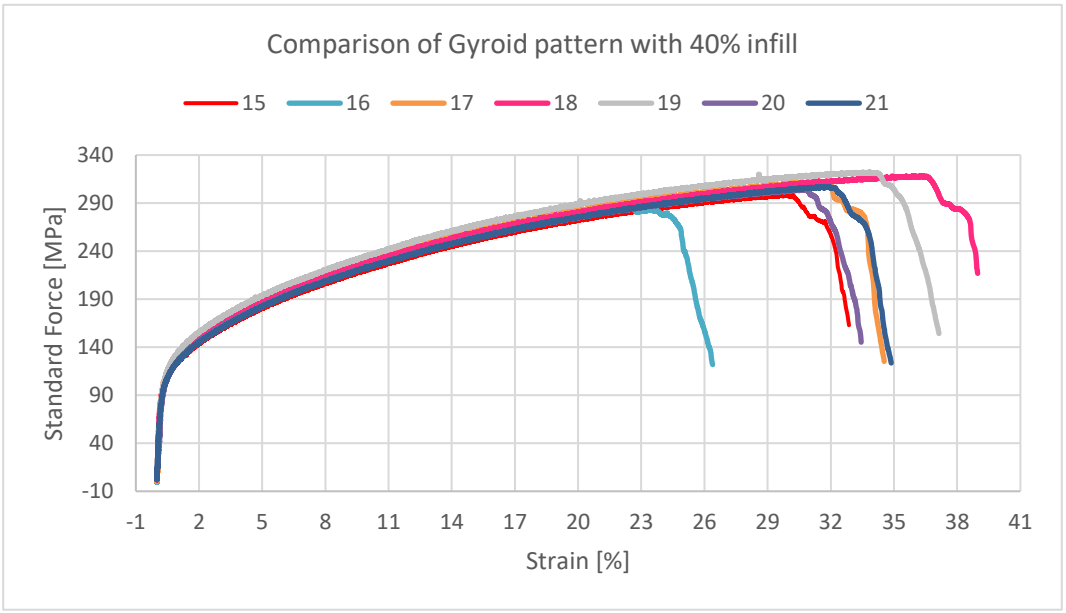

Figure 87 - Comparison of Gyroid Pattern with 40% Infill

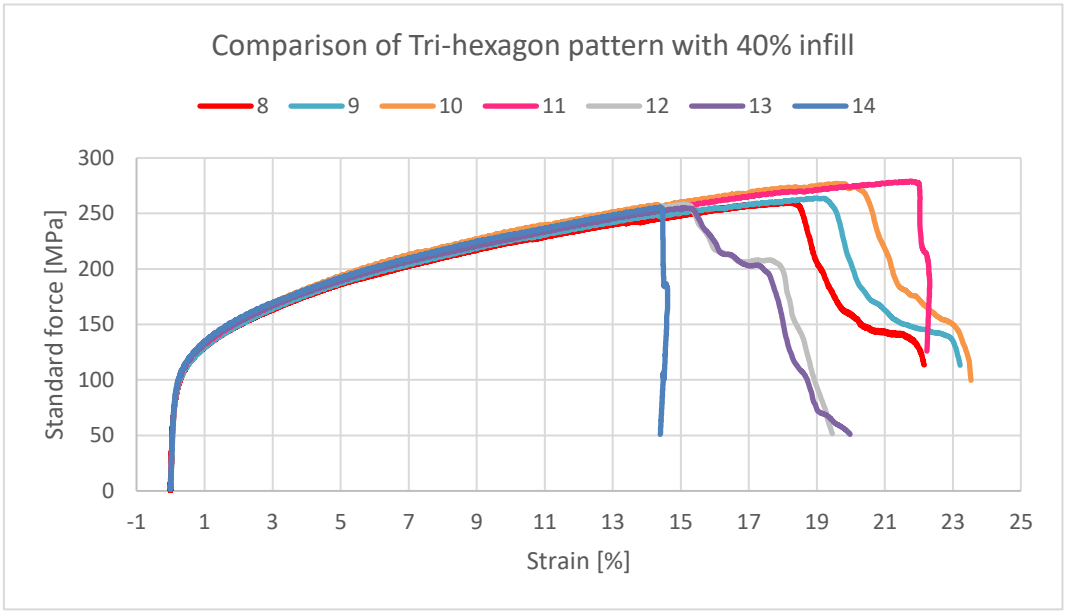

Figure 88 - Comparison of Tri-Hexagon Pattern with 40% Infill

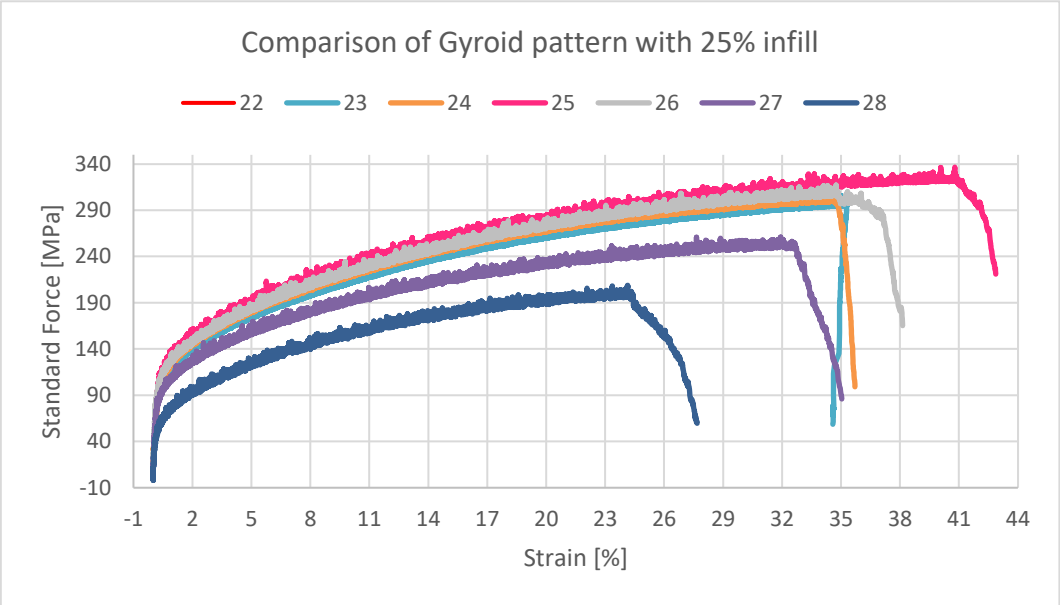

Figure 89 - Comparison of Gyroid Pattern with 25% Infill

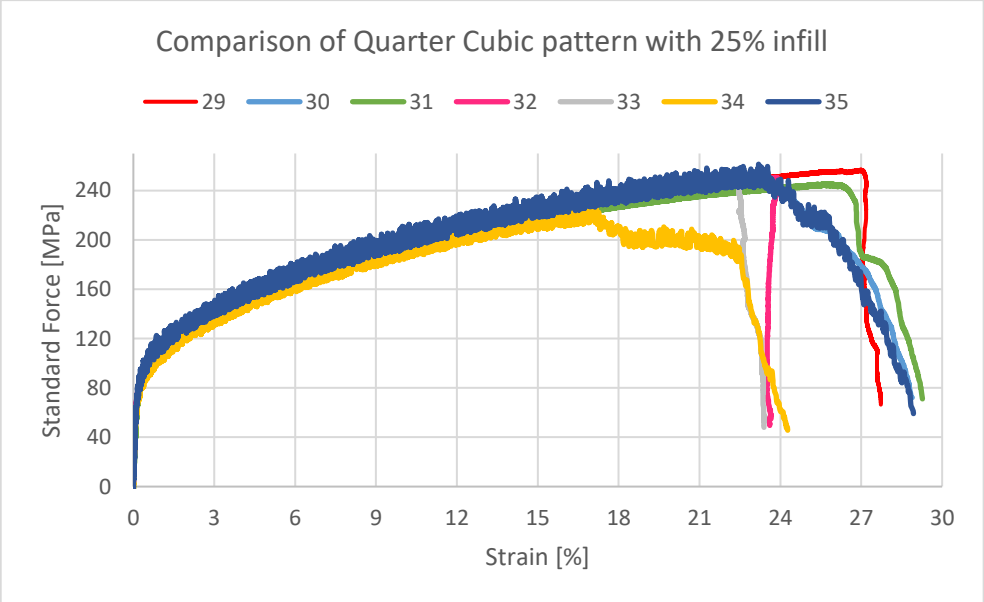

Figure 90 - Comparison of Quarter Cubic Pattern with 25% Infill

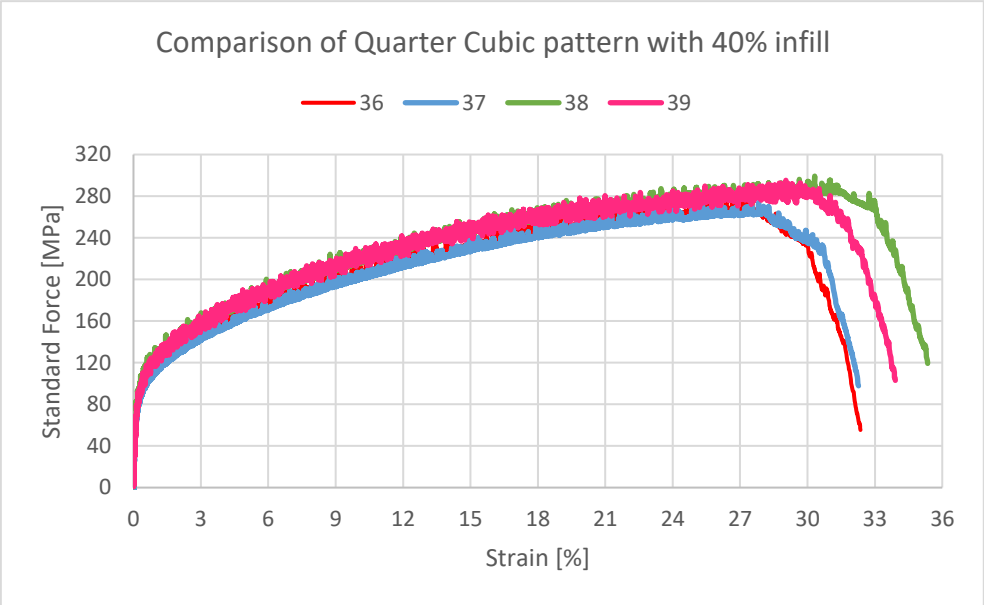

Figure 91 - Comparison of Quarter Cubic Pattern with 40% Infill

Specimen number 25 (pattern gyroid with 25% infill) exhibited the highest ultimate strength and strain at break, followed by specimen number 18 (pattern gyroid with 25% infill). The highest ultimate strength of 336 MPa and strain at break of 40% were demonstrated by specimen number 25 printed with the pattern gyroid and 25% of infill. On the other hand, specimen number 1 printed with the pattern tri-hexagon and 25% infill showed the lowest ultimate strength of 193 MPa and a strain at break of 10%.

Surface Roughness Test

Roughness is important when determining whether a surface is suitable for a specific purpose. Rough surfaces often wear out more quickly than smoother surfaces. Rougher surfaces usually are more vulnerable to corrosion and cracks but can also aid in adhesion. A roughness tester is used to quickly and accurately determine a material's surface texture or surface roughness (PCE Instruments 2022). With this test, it is possible to obtain the value of Ra and Rz.

Ra (mean roughness value) is a calculated average of the absolute individual values of a measured section that deviates upwards or downwards from the ideal profile line. Furthermore, the Rz (mean roughness depth) is the distance between an individual measurement section's highest peak and lowest valley. The average roughness depth is determined from the individual value of five individual roughness depths determined one after the other in a line (PCE Instruments 2022).

Before starting the roughness tests, preparing the equipment Surfcom Touch is necessary. Figure 92 shows the equipment used to perform the tests.

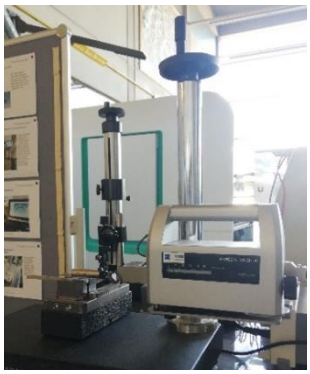

Figure 92 - Surfcom Touch

The first step is to switch on the unit then a suitable parameter is selected:

- Measuring speed: 0.3 mm/s;
- Cutoff (λc): 0.8 mm;
- Measuring length (Ln): 4 mm.

Figure 93 - Parameteres

After determining the parameters, the sample is clamped and measured from left to right. Then the measurement is started, and afterwards, the diagram is created. In the end, it is necessary to export the measurements from the unit to the computer using the *Zeiss Support Warrel* software. With the roughness test, the mean roughness value (Ra), the mean roughness depth (Rz), the primary profile curve, and the roughness profile curve can be obtained. In Table 26 is presented the Ra Values, Table 27 presents the Rz Values, and Figure 94 shows the results obtained with the roughness test in specimen 1. The other results are in Appendices B, C, D, E, F, and G.

Table 26 - Ra Values

Ra					
40%			25%		
Tri-Hexagon	**Gyroid**	**Quarter**	**Tri-Hexagon**	**Gyroid**	**Quarter**
2,979	2,471	2,016	2,889	3,857	3,150
2,676	2,626	1,224	3,353	3,969	3,372
2,871	2,778	2,125	3,077	3,825	2,511
3,651	2,448	1,336	3,140	3,624	2,664
2,878	2,605	1,359	3,362	3,914	2,648
3,381	2,583	1,238	3,333	3,442	2,491
3,132	3,065	1,271	3,395	2,943	2,612
3,535	2,524	1,188	2,926	3,915	2,598
2,778	2,889	0,904	3,050	3,531	2,436
3,098	**2,665**	**1,407**	**3,169**	**3,669**	**2,720**

Table 27 - Rz Values

Rz					
40%			25%		
Tri-Hexagon	**Gyroid**	**Quarter**	**Tri-Hexagon**	**Gyroid**	**Quarter**
20,628	16,339	10,909	20,147	33,167	20,444
20,255	20,402	6,427	24,112	33,183	19,870
21,381	19,019	8,832	22,356	28,991	17,064
21,977	17,730	7,758	27,144	26,550	20,659
20,011	17,072	7,143	28,776	27,679	16,913
20,105	16,710	7,126	27,448	22,743	19,450
20,763	19,599	6,741	26,482	20,377	18,421
21,816	17,976	6,955	27,813	29,080	19,815
21,024	21,806	5,015	23,704	27,744	17,291
20,884	**18,517**	**7,434**	**25,331**	**27,724**	**18,881**

Prüfprotokoll

ACCRETECH

Seriennummer:		Kommentar		Messdatum	21.06.2022
Teilenummer	Planetenträger	Prüfer	Kalhöfer	Messzeit	13:19:03

Messbedingung

Messtyp	Roughness measuremen	Cutoff	0,8mm	λs Filter	2,5um
Berechnungsstandard	ISO1997/2009	Filtermethode	Gaussian	Einheit	mm/um
Auswertelänge	4,00mm	Messbereich	500,0um		
Messgeschwindigkeit	0,30mm/s	Entfernen der Form	Straight		

Messergebnis

Pt	47,861	Ra_5	3,178	Rz_5	15,803
Ra	2,880	Rz	15,587	Rp	7,402
Ra_1	1,999	Rz_1	11,554	Rp_1	5,709
Ra_2	2,928	Rz_2	14,776	Rp_2	6,127
Ra_3	2,349	Rz_3	15,600	Rp_3	10,238
Ra_4	3,946	Rz_4	20,201	Rp_4	8,074

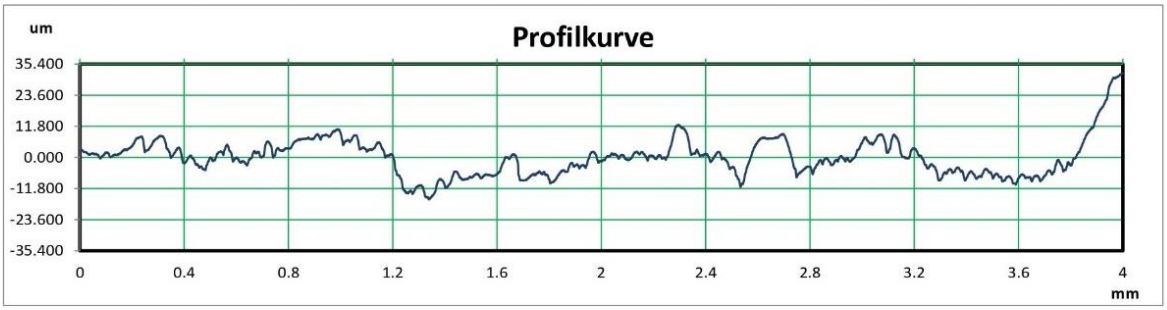

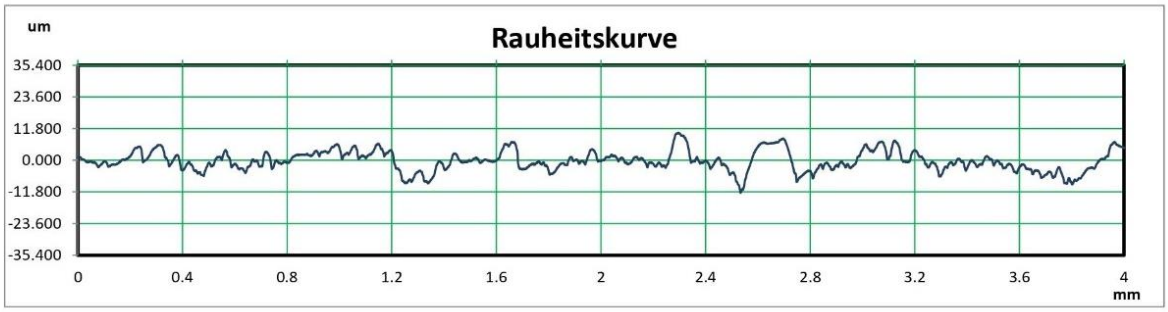

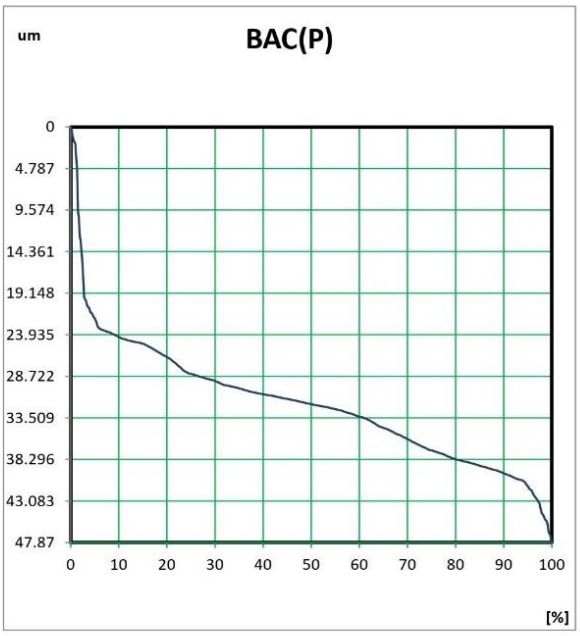

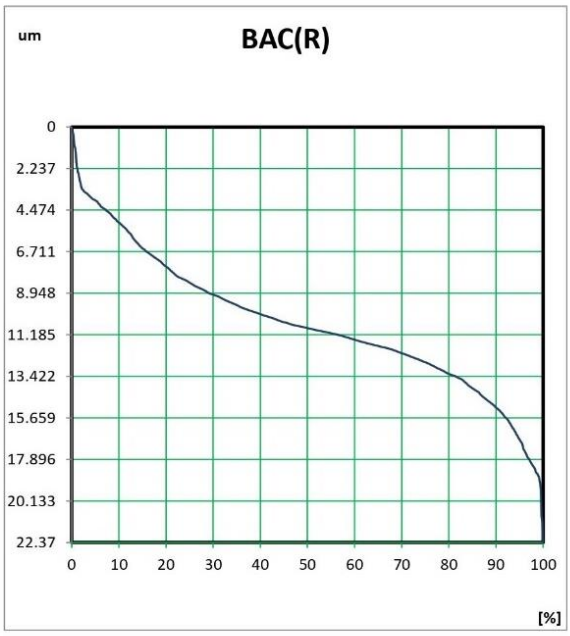

Figure 94 - Roughness Test Results

After realizing roughness tests in all the specimens, all data was processed, and values of Ra and Rz were collected. Therefore, Appendix H has the values of Ra and Rz.

To compare the values, bar graphs were created to visualise the behaviour of the roughness of the different specimens. Figure 95 shows the results obtained from the average roughness value in specimens with a 25% and 40% infill density.

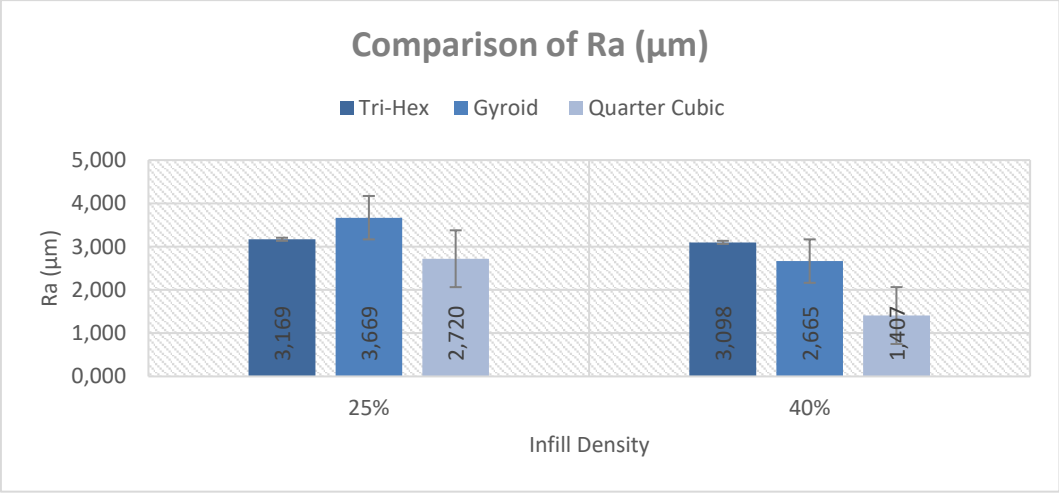

Figure 95 - Ra Results with 25% and 40% of Infill Density

With the analysis of Figure 95, it is possible to conclude that the specimens with a density infill of 40% have a lower value of Ra. In addition, the pattern quarter cubic with 40% of infill presented a lower roughness value, and the pattern gyroid with 25% of infill presented a higher roughness value.

Figure 96 presents the results obtained from the roughness depth value in the specimens with a 25% and 40%.

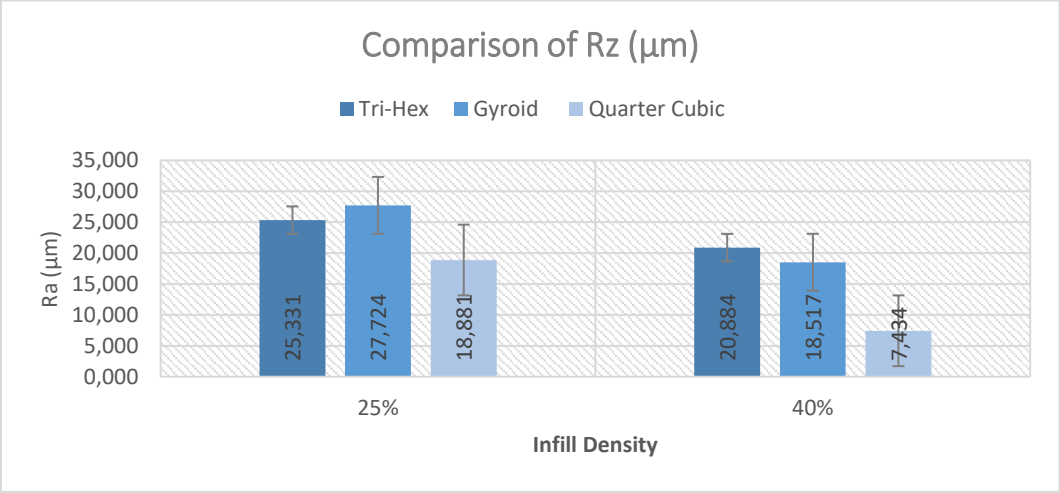

Figure 96 - Rz Results with 25% and 40% of Infill Density

With the analysis of Figure 96, it is possible to conclude that the specimens with a density infill of 40% have a lower value of Rz. In addition, the pattern quarter cubic with 40% of infill presented a lower roughness value, and the pattern quarter cubic with 25% of infill presented a higher roughness value.

3.2. Cubes Roughness Test

The second task developed in this study was to print small cubes with same infill density and different infill patterns (gyroid, tri-hexagon, and quarter cubic). This aims to compare the roughness of the cubes face. Figure 97 presents all the workflow of this task.

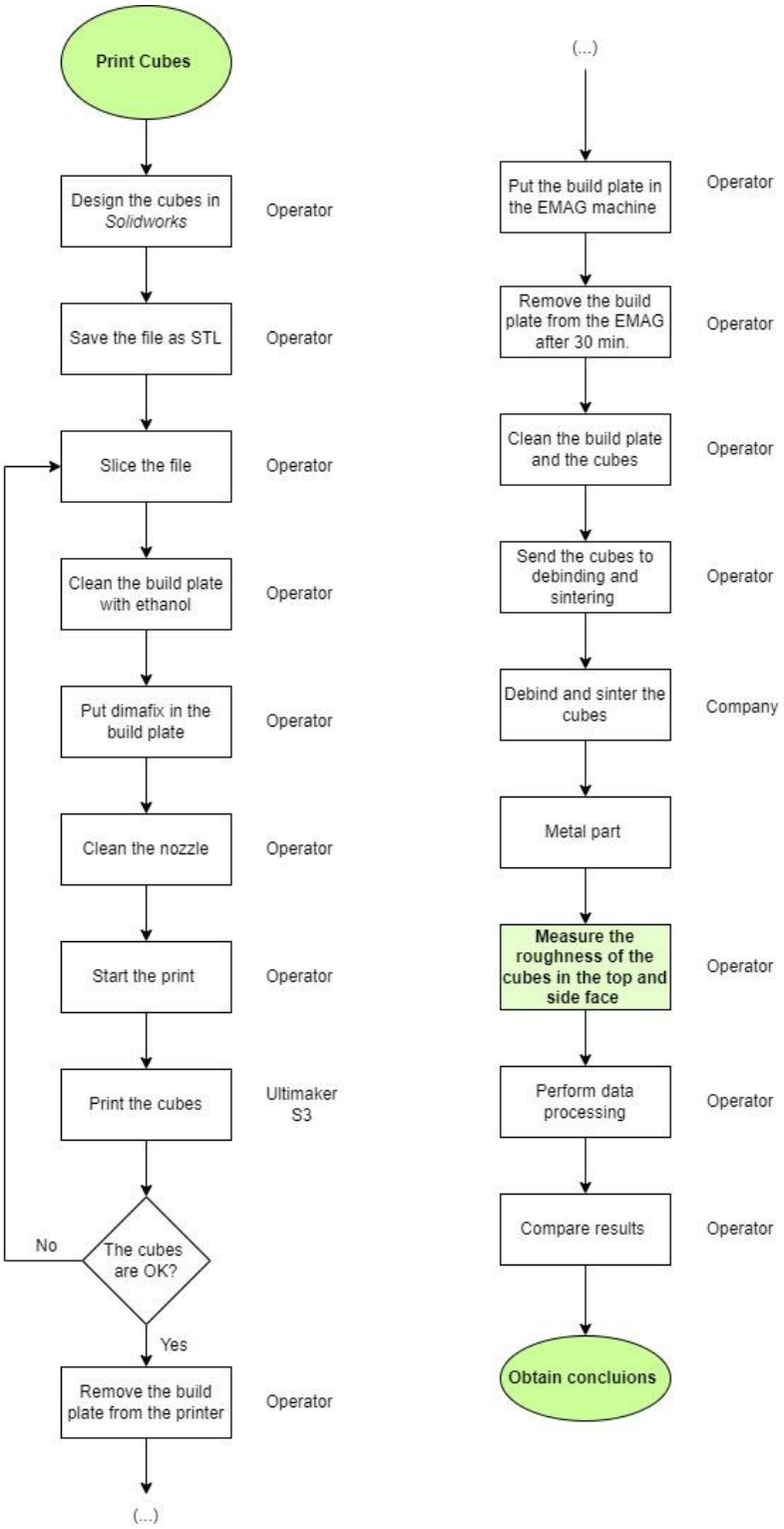

Figure 97 - Workflow Task 2

First, $1\ cm^3$ $(10\ mm\ x\ 10\ mm\ x\ 10\ mm)$ cubes were drawn in Solidworks (Figure 98), and then the document was saved in STL format and opened in Ultimaker Cura.

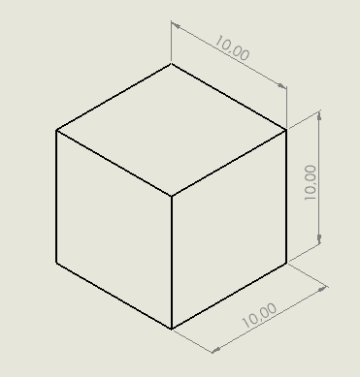

Figure 98 - 2D Cube

In Ultimaker Cura software, the print settings, like infill density, infill pattern, layer height [mm], wall line count, layers top/bottom, printing temperature [ºC], plate temperature [ºC] and print speed [mm/s] were defined. Table 28 presents the print settings used.

Table 28 - Print Settings

Print Settings	
Layer height [mm]	0.1
Wall line count	2
Layers top/bottom	6
Printing temperature [ºC]	240
Plate temperature [ºC]	100
Print speed [mm/s]	25

In total, nine cubes had to be printed: three with 100% infill density with the gyroid pattern, three with 100% infill density and with the tri-hexagon pattern, and three with 100% infill and with the quarter cubic pattern. Table 29 presents all the information about the cubes.

Table 29 - Cubes Information

Infill Density	Infill Pattern	Qty	Time [H]	Grams of filament used [g]	Meters of filament used [m]	Image
100%	Gyroid	3	52	15	0,5	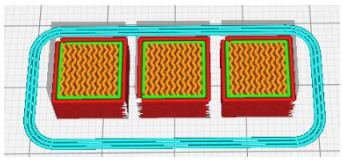
100%	Tri-Hexagon	3	50	15	0,5	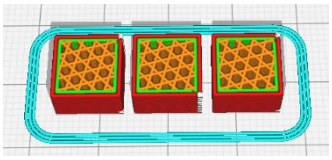
100%	Quarter Cubic	3	50	15	0,5	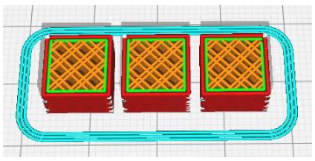

After all the print settings are set, it is necessary to clean the build platform with ethanol, put dimafix glue in the build platform so that during printing, the test pieces are firmly attached to it and do not lift, and clean the nozzle. Finalizing the last step, the printer is ready to start the job. After the cubes finished printing, the build plate was put in the EMAG machine for 30 minutes at 60º to detach the cubes from the plate. When the cubes get separated, the build plate is removed from the machine, and the cubes are cleaned. Figure 99 shows some of the cubes.

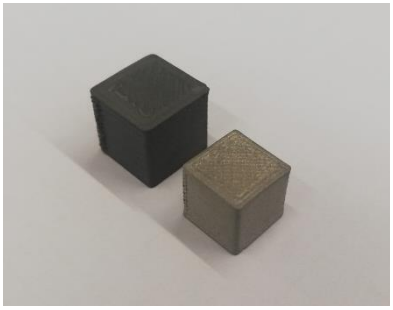

Figure 99 - Cubes Before and After Sintering

After this, the specimens are ready to be sent to the debinding and sintering company. The sintered cubes present different roughness on their faces. The cube has a flatter surface on the top face, and on the side face, it is possible to see the filament layers, as shown in Figure 100 and Figure 101.

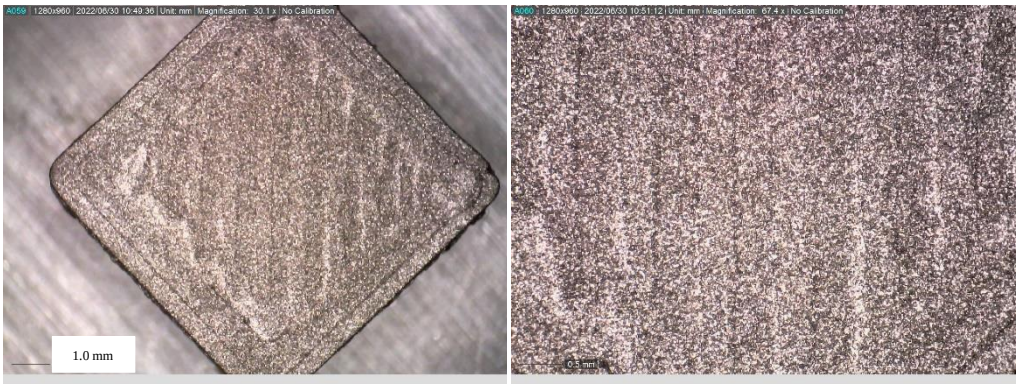

Figure 100 - Top Face of the Cube

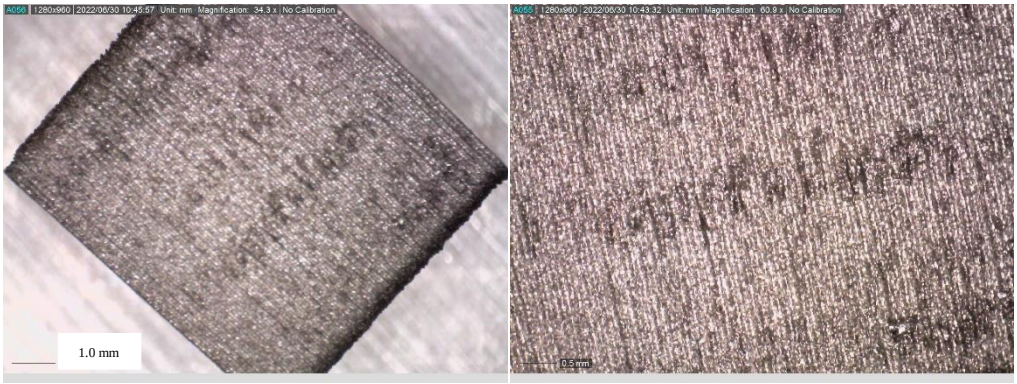

Figure 101 - Side Face of the Cube

To compare the roughness between the top face and the side face, was performed a roughness test on both faces. The other results are in Appendices R, S, T, U, V, and X. The workflow and software used to perform the roughness measurement were the same as explained above for the roughness measurement on the specimens. The results are presented in Figure 102.

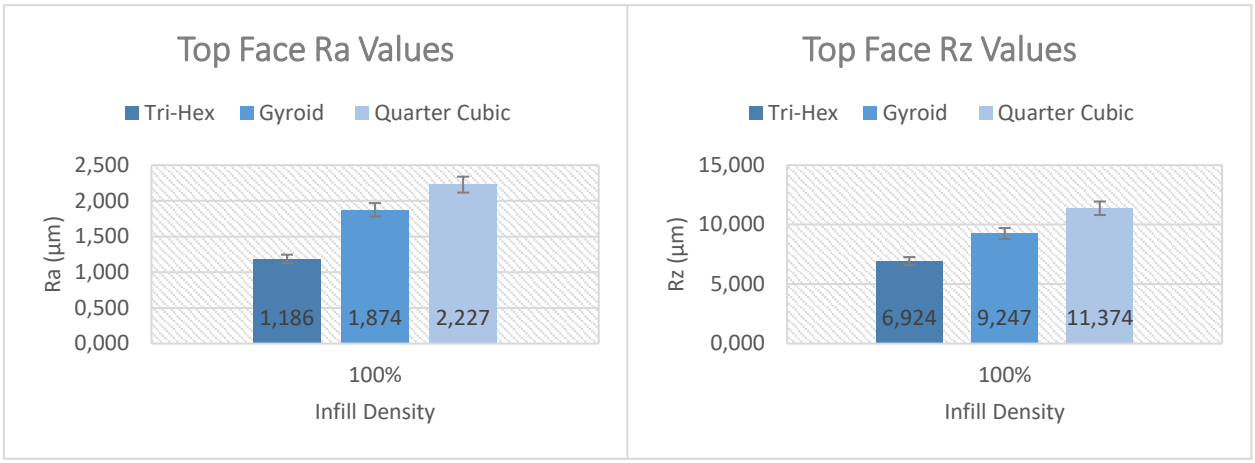

Figure 102 - Ra and Rz Results of the Top Face

With the analysis of Figure 102, it is possible to conclude that the cubes with the tri-hexagon pattern exhibited the lowest roughness value of 1,186 µm and the lowest roughness depth of 6,924 µm. On the other hand, the cubes with the quarter cubic pattern exhibited the highest roughness value of 2,227 µm and the highest roughness depth of 11,374 µm.

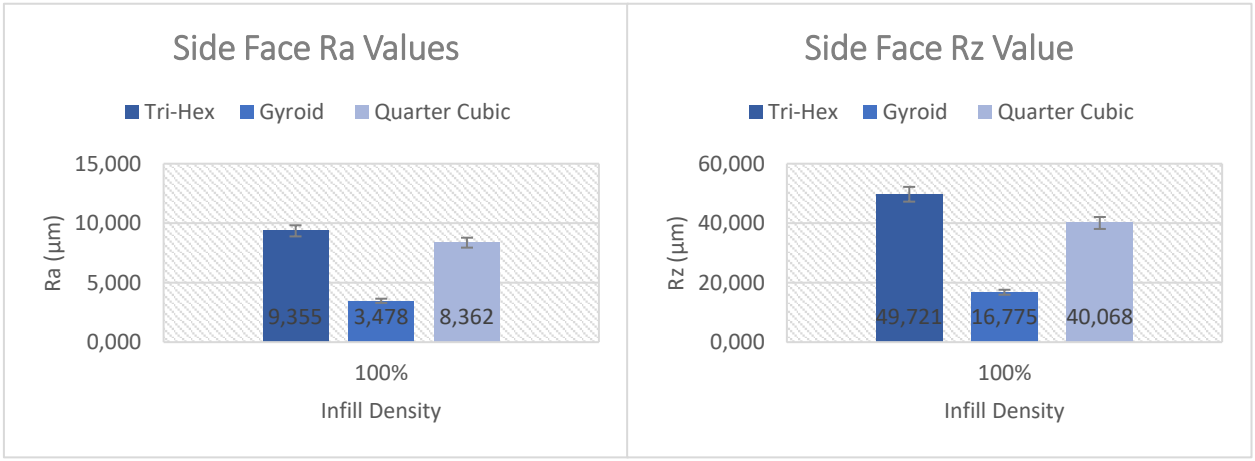

Figure 103 - Ra and Rz of the Side Face

By analysing Figure 103, it is possible to conclude that the cubes with the tri-hexagon pattern exhibited the highest roughness value of 9,355 µm and the highest roughness depth value of 49,721 µm. In contrast, the cubes with the gyroid pattern exhibited the lowest roughness value of 3,478 µm and the lowest roughness depth value of 16,775 µm. However, the roughness of the cubes should not change depending on the type of infill used, since the infill does not influence the outside of the part.

In conclusion, depending on the cube face, the roughness varies. For example, the tri-hexagon pattern exhibited a lower roughness value and roughness depth in the top face, but

the side faces exhibited a higher roughness value and roughness depth because of the printing procedure layer-by-layer, they are the edge of the printed filament.

3.3.Support Structures and Charpy V Test

The objective of the Charpy impact test to ISO 148-1 is to determine the impact energy and the impact strength of a metal. The test indicates whether the metal is tough or brittle. In addition, the tough/brittle transition can be determined based on the temperature. Impact strength is a material characteristic value. Metals with high impact strength can absorb shock and impact energies without breaking. This test is often used in the steel industry during pipe manufacturing and inspecting the pipes (ZwickRoell 2022).

Principle – This test consists of breaking a notched specimen with a single blow from a swinging pendulum under the conditions hereafter. The notch is the specimen with specified geometry and is in the middle between two supports, opposite the struck location. The energy absorbed in the impact test is determined (ISO 2006).

The impact resistance test determines the amount of energy that the material absorbs during fracture. This absorbed energy measures a given material's notch toughness and is a tool to study temperature-dependent ductile-brittle transition. In the case of Charpy or Izod, the impact is induced by a pendulum hammer on the sample. The residual energy of the hammer is measured (Centexbel - VKC 2022).

The Charpy V-notch-CVN impact test, also known as the Charpy V- notch test, is a standard test used to measure the impact energy absorbed by a material during fracture. The notch provides a point of stress concentration within the specimen and improves the reproducibility of the results. By breaking a specimen, the absorbed energy is computed by working out the potential energy lost by a pendulum. This test initiates by placing the specimen on the two ends at an anvil and struck on the opposite face by a pendulum (Figure 104). The specimen is fractured and the pendulum swings through, the height of the swing

being a measure of the amount of energy absorbed in fracturing the specimen (Total Materia Article 2019).

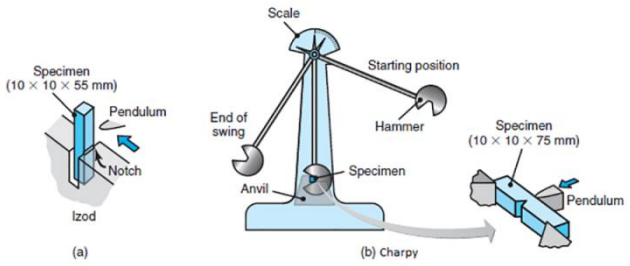

Figure 104 - Charpy V Test (Centexbel - VKC 2022)

This test is generally used for quality control and determination of the impact resistance of the materials.

Impact tests are used in studying the toughness of the material. A material's toughness is a factor in its ability to absorb energy during plastic deformation. Brittle materials have low toughness because of the small amount of plastic deformation they can endure. The impact value of a material can also changes with temperature. Generally, at lower temperatures, the impact energy of a material is decreased. The size of the specimen may also affect the value of the Izod impact test because it may allow a different number of imperfections in the material, which can act as stress risers and lower the impact energy (Mechanical Testing & Research 2022).

For the Charpy v tests, specimens with different angles (0º, 45º, and 90º) and support structures were designed in Solidworks. Figure 105 presents all the workflow of the third task of this study.

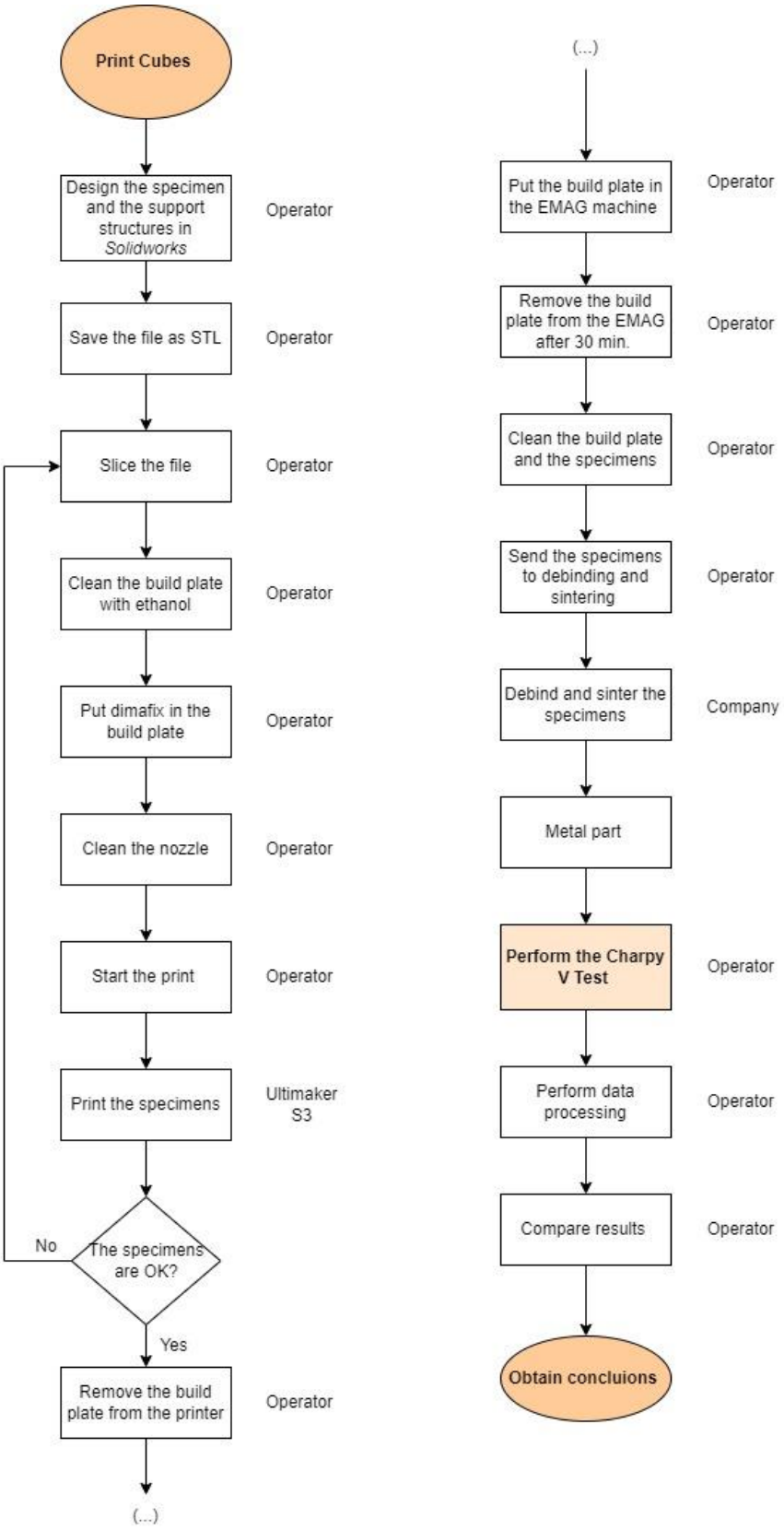

Figure 105 - Workflow Task 3

First, the test specimens (Figure 106) were designed in Solidworks, according to a standard ISO 148-1 specifies the dimensions for a so-called normal specimen (ZwickRoell 2022):

- Length:55 mm;
- Width: 10 mm;
- Thickness:10 mm;
- The notch must be placed in the centre of the length as a V or U.

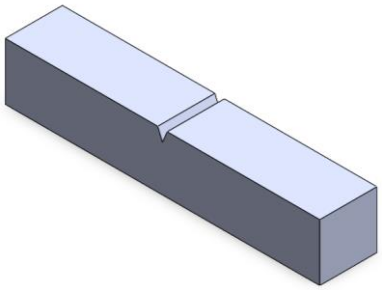

Figure 106 - Specimen Charpy V Test

After the specimen was designed in Solidworks, it was passed to the Ultimaker Cura software, where the print settings were defined, sliced, and then saved to the removable.

In Ultimaker Cura software, the print settings, like infill density, infill pattern, layer height [mm], wall line count, layers top/bottom, printing temperature [ºC], plate temperature [ºC], and print speed [mm/s] were defined. Table 30 presents the print settings used.

Table 30 - Print Settings of Task 3

Print Settings	
Layer height [mm]	0.1
Wall line count	2
Layers top/bottom	6
Printing temperature [ºC]	240
Plate temperature [ºC]	100
Print speed [mm/s]	25

Three test specimens were printed at 0º, with 100% infill density and gyroid pattern. Table 31 presents the information relative to these specimens.

Table 31 - Chapy V Test Specimens Information

Qty	Infill Density	Infill Pattern	Time	Grams of filament used	Meters of filament used
3	100%	Gyroid	7H20	1.48 g	4.83 m

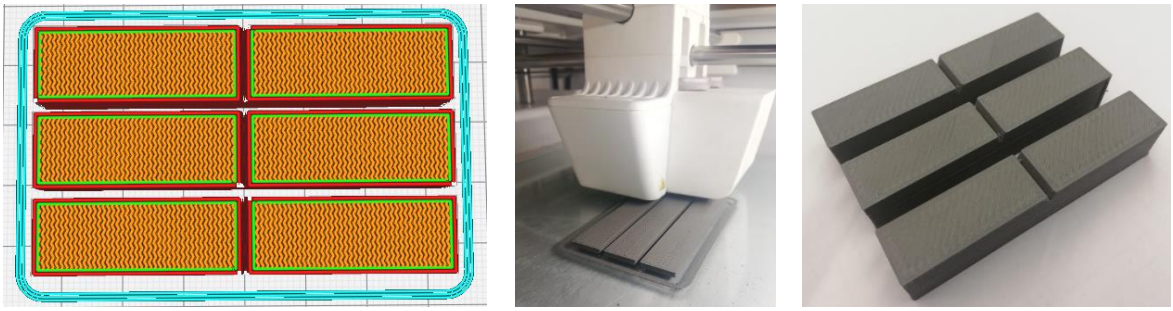

Figure 107 - Specimens with 0º

3.3.1. Support Structures 45º

After printing the specimens with 0º, the 45° specimens for the impact test were designed in Solidworks. Several support structure options were realized to select the best options later, and these are presented below.

Option 1

In Option 1, the support structures were designed with 0.4 mm of thickness and a space between them of 2 mm, as shown in Figure 108.

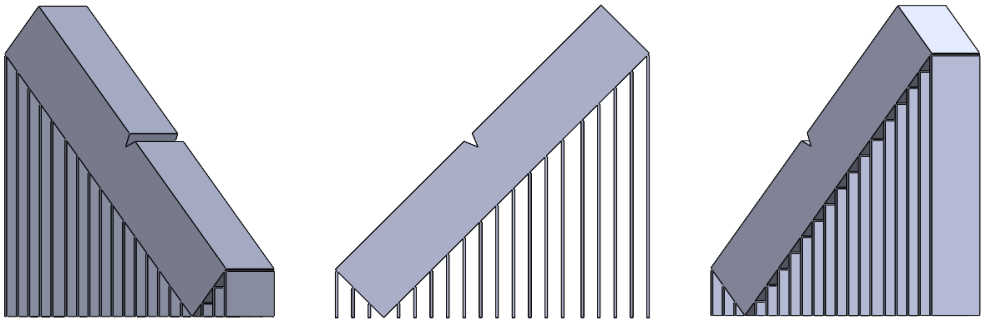

Figure 108 - Support Structures 45º - Option 1

In Figure 109, it is possible to see how the connection between the support structure and the part is made. This type of connection seeks to reduce the contact area to facilitate removal.

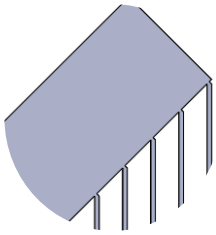

Figure 109 - Connection Option 1

In this option, the thickness of the support structure is low, so this structure will not hold the specimen part. For this reason, this option was discarded.

Option 2

In Option 2, the support structures were also designed with 0.4 mm of thickness and 2 mm of space between them. However, instead of using a support structure across its entire width, it was divided into two, as shown in Figure 110. This option was discarded because the thickness of the support structure is minimal.

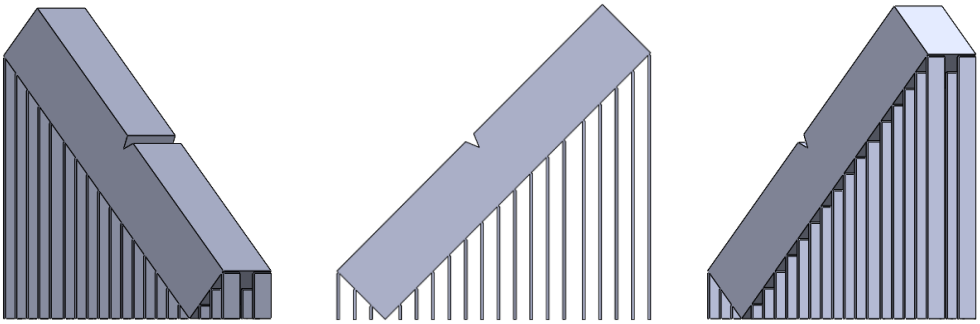

Figure 110 - Support Structures 45º - Option 2

Option 3

Option 3, support structures, were also designed with 0.4 mm of thickness and a space between them of 2 mm. Figure 111 shows Option 3.

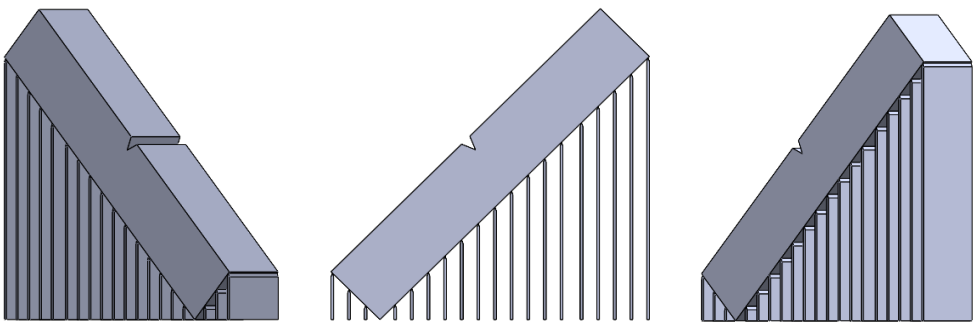

Figure 111 - Support Structures 45º - Option 3

In Figure 112, it is possible to see how the connection between the support structure and the part is made. This type of connection seeks to reduce the contact area as much as possible to facilitate removal.

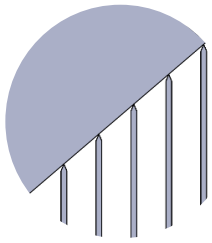

Figure 112 - Connection Option 3

However, this option was excluded because the connection between the support structure and the part during the sintering process is unreliable since it can break.

Option 4

In Option 4 the support structures were designed with 2 mm of thickness and a space between them of 4.5 mm. Figure 113 shows Option 4.

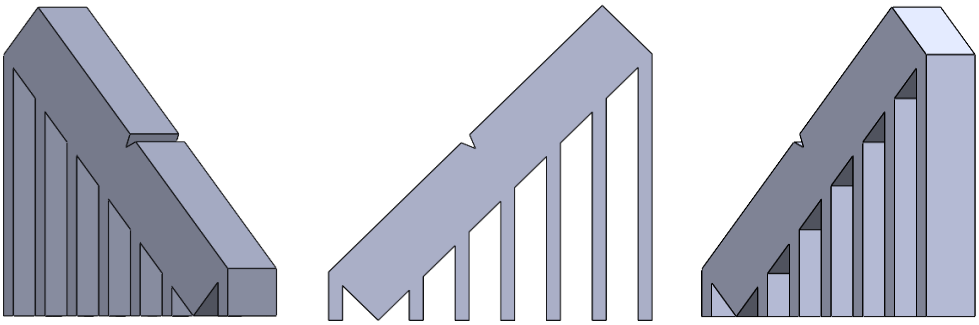

Figure 113 - Support Structures 45º - Option 4

The connection between the support structure and the part is made. This type of connection seeks to increase the contact area so that the support structure does not break during the sintering process. This support structure option was one of the chosen.

Option 5 - Mesch Structure

In Option 5, support structures were designed with a mesh pattern with 2 mm of thickness and with a space between them of 4.5 mm. Figure 114 shows Option 5.

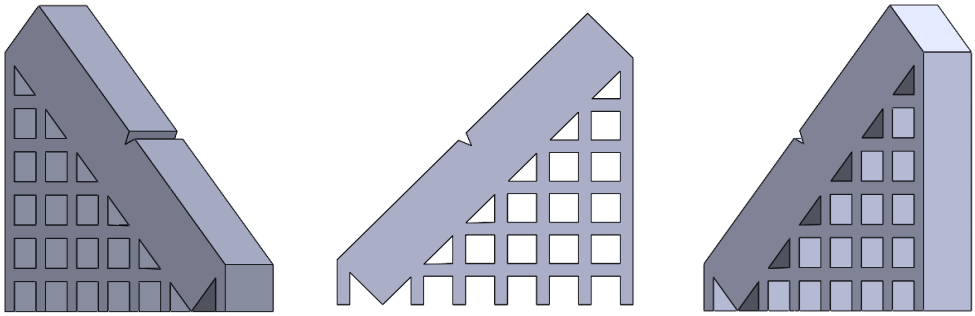

Figure 114 - Support Structures 45º - Option 5

This support structure option was one of the chosen to be possible to compare the behaviour of this design pattern with option 4. Nevertheless, during the printing, the PLA was not working with the metal, so later, this option was discarded too.

3.3.2. Support Structures 90º

After designing the 45° specimens for the impact test, the specimens were designed with 90º in Solidworks. Also, several support structure options were realized to select the best options later, and these are presented below.

Option 1

In Option 1, only one support structure was designed, and the base of the specimens was rectangular, as shown in Figure 115.

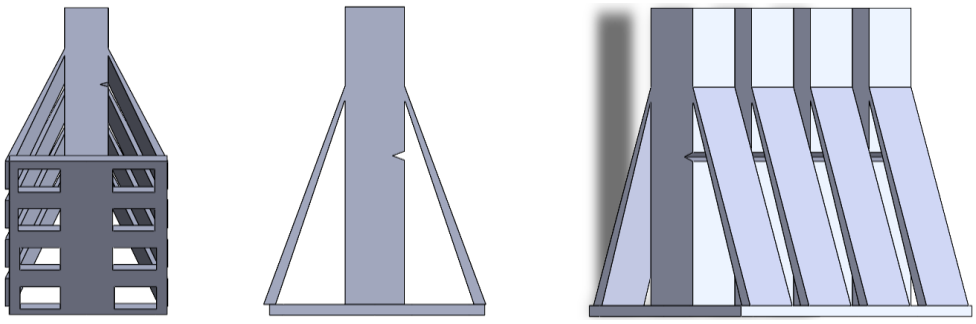

Figure 115 - Support Structures 90º - Option 1

This support structure option was discarded because during the sintering process, the specimens undergo shrinkage, and with the rectangular base, the shrinkage would not be proportional.

Option 2

Option 2 was design with two support structures, and the base of the specimens is round, as shown in Figure 116.

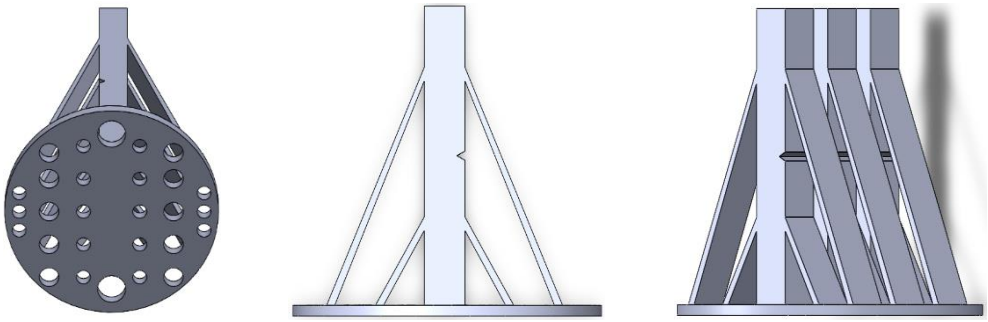

Figure 116 - Support Structures 90º - Option 2

This option of the support structure was one of the chosen ones. However, due to its round base, the sintering process will suffer proportionally shrinkage and the two support structures stabilising the specimens.

Support Structures Chosen

Finally, the support structures chosen for the 45º are the linear support structures with 2 mm of thickness and a space between them of 4.5 mm, for the 90º are the two support structures. Table 32 presents all the support structures chosen.

Table 32 - Support Structures Chosen

Degree	Nº of support structures	Type of support structure	Image
45º	-	Linear	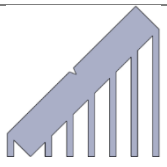
90º	2	-	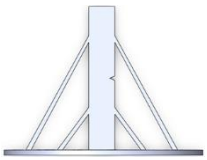

After choosing the support structures to be used, the Solidworks file was passed into STL format and opened in Ultimaker Cura to set all print settings. In Table 33, is presented the print settings.

Table 33 - Print Settings Specimens with Support Structures

Print Settings	
Layer height [mm]	0.1
Wall line count	2
Layers top/bottom	6
Printing temperature [ºC]	240
Plate temperature [ºC]	100
Print speed [mm/s]	25

Figure 117 and Figure 118 presents the specimens during the slicing, printing and after printing.

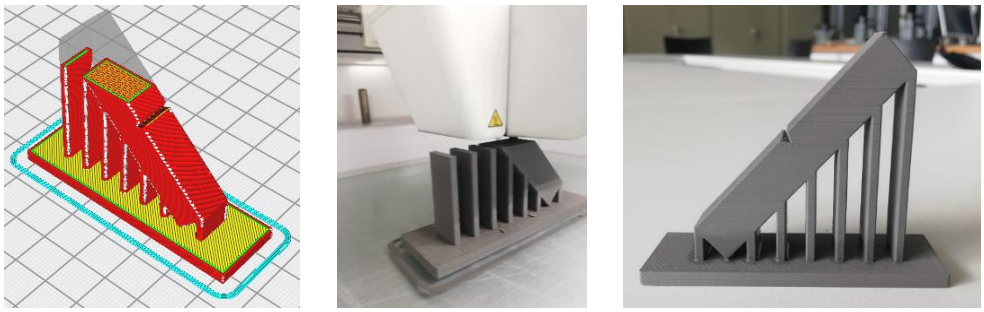

Figure 117 - Charpy V Test Specimens with 45º

Figure 118 - Charpy V Test Specimens with 90º

After printing all the specimens, when the parts were sent to the debinding and sintering company, they said they would only be able to do the job at the end of September. Consequently, it was not possible to obtain results in chapter 3.3.

3.4. Cost Analysis

In the last part of the experimental tasks, a part with application in the automotive industry, a turbo compressor wheel, was designed in *Solidworks.* After the part was designed, a cost analysis was performed, comparing the production of the same part using FFF technology and SLM technology. In Figure 119 is represented all the Workflow of Task 4.

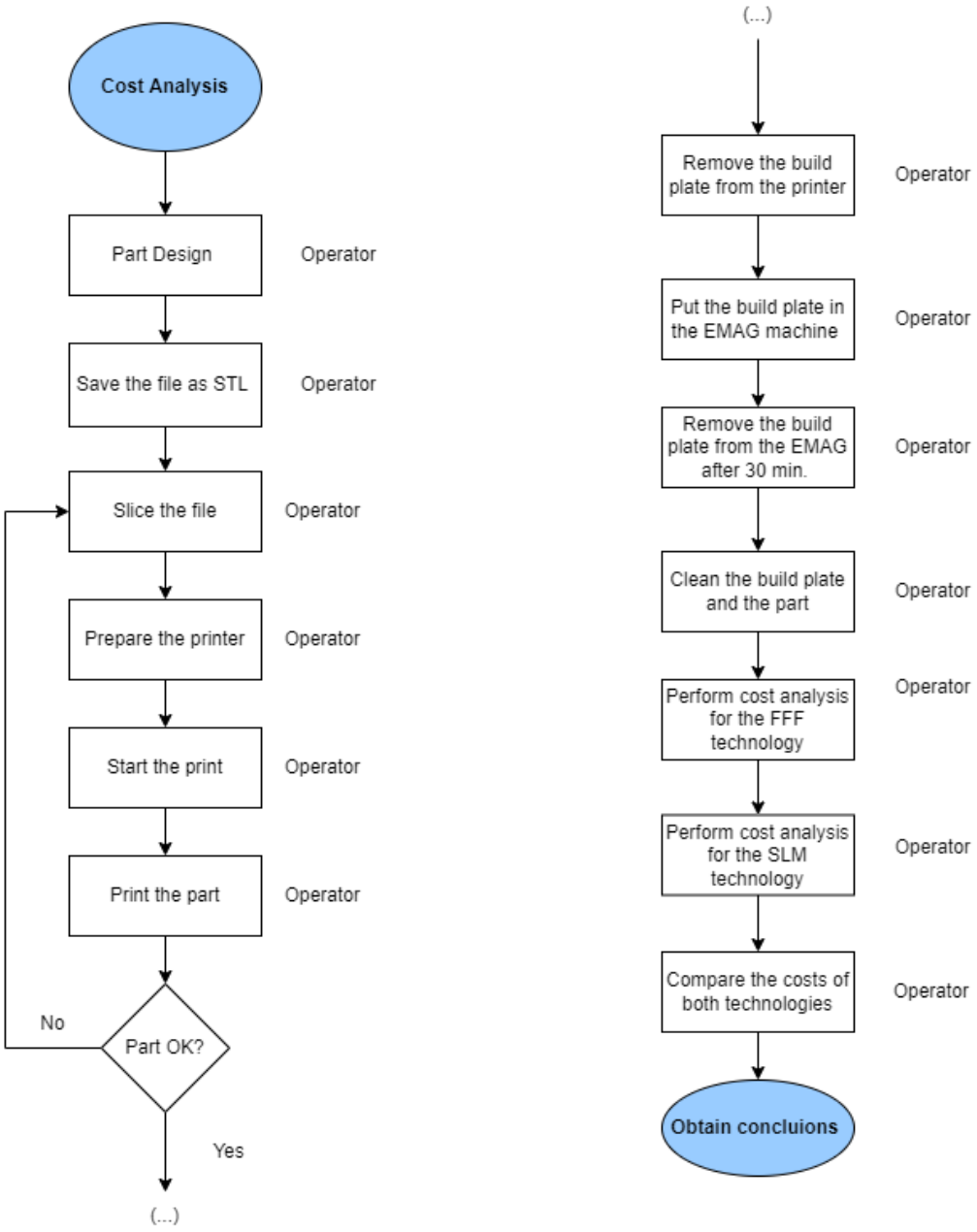

Figure 119 - Workflow Task 4

To manufacture the turbo compressor wheel using conventional manufacturing, the part must be designed (CAD), and then the part design was passed to CAM and CNC. Next, the production of the part begins with cylindrical turning, where a single tool removes material from the rotating part, and revolution surfaces are obtained. After that, the part is milled to obtain the turbine blades, and then the part is drilled, where a cylindrical hole is created, this operation is performed with a tool with two cutting edges at the end, called a drill. Finally, if necessary, post-processing is performed.

To produce the turbo compressor wheel using FFF technology the process begins by creating a CAD model of the part and then converting it into STL format. The file is sliced into layers, and the data is then transferred to the 3D printer, which constructs the part by depositing the filament layer-by-layer. After the printed part is debinded and sintered, post-processing is performed, if necessary, like heat treatments or machining processes.

By producing the part using FFF technology, it is possible to achieve a shorter production time, reduced material waste, and reduced labour costs. In Figure 120, it is presented the workflow for producing the part using conventional manufacturing and additive manufacturing.

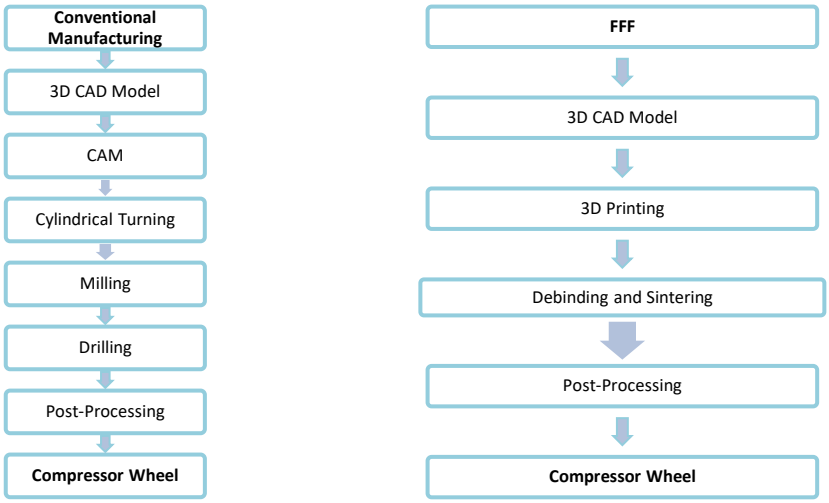

Figure 120 - Conventional Manufacturing VS FFF Technology

3.4.1. Turbocharger

One of the challenges, many engines' makers face, is how to admit more air into the combustion chamber. This problem can be solved by using a turbocharger. The turbocharger comprises two parts, the turbine (hot section) and the compressor (cold section), as shown in Figure 121.

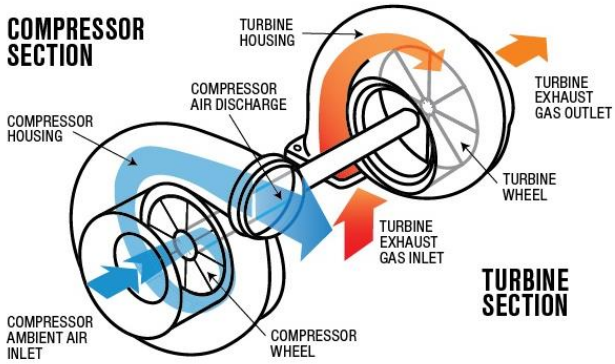

Figure 121 – Turbocharger (Eagle Ridge GM 2022)

To get more air into the engine, a turbocharging system starts with the engine exhaust gas, and this power is essentially wasted in naturally aspirated engines. This exhaust gas is channelled into the turbo, where it spins a turbine wheel. This highly engineered wheel spins quite fast, reaching a speed of up to 280000 rpm. The higher the speed of the turbine wheel, the more gases enter the turbo. On the other side of the turbine wheel, connected by a shaft, is a compressor wheel. These two wheels turn together, and the rapid spinning allows the compressor to suck in large amounts of ambient air and compress it. As a result, the air is very dense and has a higher temperature. This air then passes through a charge air cooler, which is cooled, and gains an even higher density before entering the engine. Compressed air allows the engine to burn more fuel effectively, making for highly efficient engine operation. With a turbocharger, engine makers no longer have to build more significant engines to get more power. Instead, they can use smaller, more efficient boosted engines and then match the power of the larger engine while consuming less fuel and emitting significantly less CO2.

3.4.2. Design and Print

First, the turbo compressor wheel was designed in Solidworks software, and this wheel is composed by 10 blades. as shown in Figure 122.

Figure 122 - Turbo Compressor Wheel

In Figure 123 a) and 123 b) is presented the design of the turbo compressor wheel in 2D.

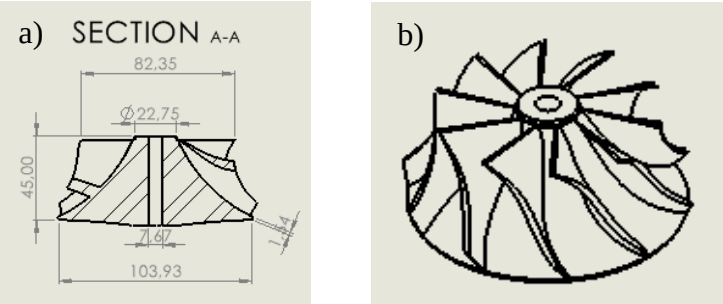

Figure 123 - 2D Turbo Compressor Wheel

After the part was designed, it was imported to Cura software, where the part was sliced (Figure 123 a) and printed on the Ultimaker S3, with the parameters shown in Table 34.

Table 34 - Printer Settings

Printer Settings	
Layer height [mm]	0.1
Wall line count	2
Layers top/bottom	6
Printing temperature [ºC]	240
Plate temperature [ºC]	100
Print speed [mm/s]	25

Table 35 shows the number of parts printed, the infill density and pattern, the printing time of the turbo compressor wheel, and the material used on the original part. The part was scaled down to print to test if it is possible to print using FFF technology.

Table 35 - Print Settings of the Turbo Compressor Wheel

Quantity	**1**
Infill Density	100%
Infill Pattern	Gyroid
Printing Time [H]	36H
Grams of Filament Used [g]	724
Meters of Filament Used [m]	23.65

As it is possible to see in Figure 124 c), there were some printing flaws on the top of the piece. This may have happened because the thickness of the veneers on the upper part is very thin, and the equipment used is not specific for printing this material.

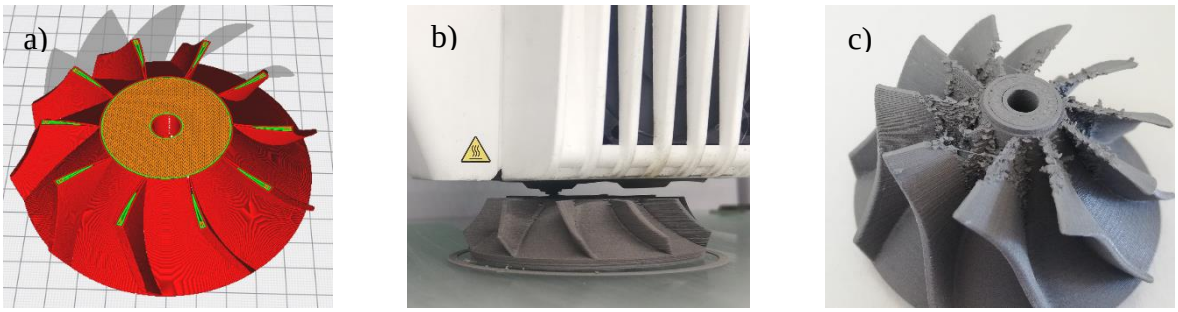

Figure 124 - Printing Turbo Compressor Wheel

3.4.3. Cost of FFF Technology *VS* Convectional Manufacturing

In order to develop a simplified cost model, the following assumptions were considered:

- The machine is operational (good machine uptime) 90% of the time.
- Electricity expenses were not considered.
- That specialized employees are needed, the average gross salary in Portugal of 1050€ was considered, which results in a value of 6€/H.
- Only the working days - 251 days.

The equation below was used to realize the cost of each of the technologies. In this equation, the main activities of the different stages necessary to produce the part included, such as part design, material, part manufacturing time, necessary labour, and post-processing.

$$Ctpart = Cd + Cm + Cs + Cds + Cpp$$

Where $Ctpart$ is the total cost of the part, Cd is the design cost, Cm is the cost of the machine, Cs is the cost of the material/stock, Cl is the cost of labour, and Cpp is the cost of the post-processing. The following explains each of the costs.

Cost of FFF Technology

Design Costs

To produce the turbo compressor wheel, it first has to be designed using software, in this case, Solidworks. In the part design phase, the function of the part can be improved through

computer simulation, generative design, and topology optimization. To calculate the design, its cost takes into account the design time (Td), the labour cost (Cl), and overheads cost (Co), such as the cost of the software. These costs also included the time and software to perform the part slicing.

$$Cd = Td \times (Cl + Co)$$

To design the turbo compressor wheel in *Solidworks* and to run simulations, it took 8 hours, then the file was converted to STL, and the software Cura was used to set all the print parameters and slice the part. This took approximately 15 minutes. Furthermore, it was assumed that the *Solidworks* license cost 4500€/year.

$$Td = 8 + (15 \div 60) = 8{,}25\ H$$

$$License\ time = 251\ days\ \times 24 = 6024\ H$$

$$Co = \frac{Td \times Solidworks\ Price}{License\ time} = \frac{8{,}25 \times 4500}{6024} = 6{,}16€/H$$

$$Cd = 8{,}25 \times (6 + 6{,}16) = 100{,}32€$$

To design and slice the turbo compressor wheel cost 100,32€.

Machine cost

To produce a turbo compressor wheel by FFF technology, the Ultimaker S3 printer was used, this printer has a cost of 4.700,50€. To calculate the design, the cost takes into account the cost of purchase (Cp), the build time (Tb), the number of parts (N), and the machine's useful life ($Ylife$).

$$Cm = \frac{Cp\ \times Tb}{N \times 0.9\ \text{Ylife}}$$

It takes 36 hours to print the turbo compressor wheel. Also, the machine use can thus be regarded as five years based on its usual depreciation time. In one year, the machine is used for approximately 5000 hours, and the total machine utilization over the five years can be considered 25 000 hours, as indicated in the equation below.

$$Ylife = 5\ years\ \times 5000\ H = 25000\ H$$

$$Cm_1 = \frac{4700{,}50 \times 36}{1 \times (0.9 \times 25000)} = 7{,}52€$$

Also, the costs of separating the part from the building plate were considered in the machine costs. This process usually takes 30 to 45 minutes. To perform this action, the EMAG machine is used and costs 629,95€. It was also considered that the machine use could thus be regarded as five years based on its usual depreciation time, and in one year, the machine is used for approximately 2500 hours.

$$Tb = 45 \div 60 = 0{,}75H$$

$$Ylife = 5\ years \times 2500\ H = 12500\ H$$

$$Cm_2 = \frac{629{,}95 \times 0{,}75}{1 \times (0.9 \times 12500)} = 0{,}04€$$

So, the total machine costs will be the sum of the Ultimaker S3 printer and the EMAG. as shown below:

$$Cm = Cm_1 + Cm_2 = 7{,}52 + 0{,}04 = 7{,}56€$$

Material Costs

To determine the material cost needed to produce the part, the material price was checked, and then how much material was needed to produce one part.

$$Cs = \frac{Amount\ of\ Material\ Used \times Total\ Material\ Cost}{Total\ Material}$$

When using FFF technology, the material used was BASF Ultrafuse 316L Filament 1,75 mm for the production of the part. Knowing that this material costs 460€ for 3Kg and to produce the part it is necessary 724g of material.

$$Cs = \frac{724 \times 460}{3000} = 111{,}01€$$

To produce the turbine, the material cost will be 111,01€.

Debinding and Sintering Costs

To perform the debinding and sintering of the part, the BASF company provides a service that is voucher-based, each voucher purchased entitles the processing maximum of

1 kg of parts and includes the cost of returning the processed parts. Each voucher has a cost of 60€/Kg. The turbo compressor wheel weighs 733g. So next, the price for debinding and sintering has been presented in part.

$$Cds = \frac{733 \times 68{,}95}{1000} = 50{,}54€$$

Debinding and sintering of the turbo compressor wheel has a cost of 50,54€.

Post-Processing Costs

If this costing model process was more complex and detailed, the cost of part quality verification, such as dimensional control and part surface quality, and post-processing cost such as heat treatments could have been considered. However, since this is a simple model, these were not considered.

$$Cpp = 0€$$

Final Costs

The final cost to produce one turbo compressor wheel using the FFF technology is 269,43€.

$$Ctpart = 100{,}32 + 7{,}56 + 111{,}01 + 50{,}54 + 0 = 269{,}43€$$

By analysing Figure 125, it can be seen that the highest cost to produce the turbo compressor wheel is the material with a percentage of the total value of 41%. The lowest cost represents the machinery needed with a percentage of 3%.

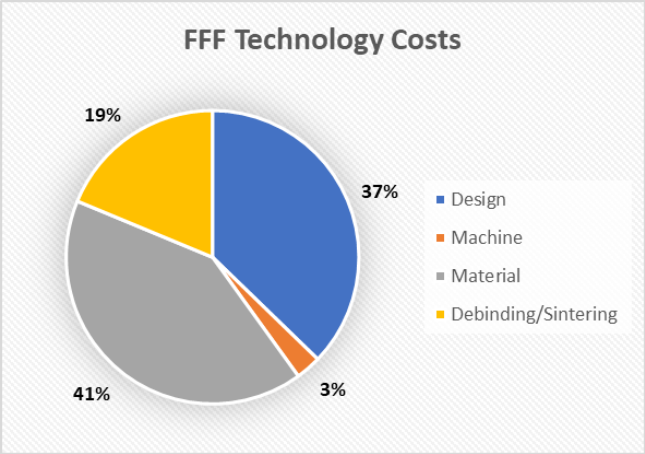

Figure 125 - FFF Technology Costs

Cost of SLM Technology

Design Costs

As in FFF technology, in SLM technology, the turbo compressor wheel is designed in Solidworks. To calculate the design costs, the equation below was used.

$$Cd = Td \times (Cl + Co)$$

To design the turbo compressor wheel in *Solidworks*, it took 2 hours, then the file was converted to STL, and the software Cura was used to set all the print parameters and slice the part. This took approximately 15 minutes. Furthermore, it was assumed that the *Solidworks* license cost 4500€/year.

$$Td = 8 + (15 \div 60) = 8{,}25\ H$$

$$License\ time = 251\ days\ \times 24 = 6024\ H$$

$$Co = \frac{Td \times Solidworks\ Price}{License\ time} = \frac{8{,}25 \times 4500}{6024} = 6{,}16€/H$$

$$Cd = 8{,}25 \times (6 + 6{,}16) = 100{,}32€$$

The design cost of the part for SLM technology is 100,32€, the same cost as for FFF technology.

Machine cost

To produce a turbo compressor wheel by SLM technology, the Kurtz Ersa Alpha 140 was used. Although this printer has a cost of 85000 €, calculating the design cost that will take into account the cost of purchase (Cp), the build time (Tb), the number of parts (N), and the machine's useful life ($Ylife$).

$$Cm = \frac{Cp\ \times Tb}{1 \times 0.9\ \text{Ylife}}$$

To calculate the build time of the part using the Kurtz Ersa Alpha 140, it was considered that:

- Part height: 48 mm
- Average area of the part: 4111,37 mm^2

- Layer height: 0,05 mm
- Focus diameter: 0,075 mm
- Printer speed: 550 mm/s

First the number of layers of the part was determined by dividing the height of the part by the height of one layer:

$$Number\ of\ layers = \frac{48}{0{,}05} = 960\ layers$$

Then, the total area of the part was calculated by multiplying the average area of the part by the number of layers:

$$\text{Total area of the part } = 4111{,}37 \times 960 = 3946915{,}20\ mm^2$$

Next, the area of the focus diameter was obtained by multiplying the printer speed by the focus diameter:

$$Area\ of\ the\ focus\ diameter = 550 \times 0{,}075 = 41{,}25\ mm^2/s$$

Finally, the printing time of the part was determined by dividing the total area of the part by the area of the focus diameter:

$$Build\ Time = \frac{3946915{,}20}{41{,}25} = 95682{,}79\ s$$

The build time was multiplied by 2, in order to consider the laser time:

$$Build\ Time = 95682{,}79\ \times 2 = 191365{,}58\ s$$

$$Build\ Time = \frac{191365{,}58\ s}{360} = 53\ hours$$

It takes 53 hours to print the turbo compressor wheel, with SLM technology. Also, the machine use can thus be regarded as five years based on its usual depreciation time. In one year, the machine is used for approximately 5000 hours, and the total machine utilization over the five years can be considered 25 000 hours, as indicated in the equation below.

$$Ylife = 5\ years\ \times 5000\ H = 25000\ H$$

$$Cm_1 = \frac{85000 \times 53}{1 \times (0.9\ \times 25000)} = 200{,}22€$$

Material Costs

To determine the material cost needed to produce the turbo compressor wheel, it is necessary know how much material is needed to produce one part and the price of the material.

$$Cs = \frac{Amount\ of\ Material\ Used\ \times Total\ Material\ Cost}{Total\ Material}$$

When using SLM technology, the material used is 316L Stainless Steel Powder for the production of the part. Knowing that this material costs 68,62€ for 1Kg. To find out the amount of material used to produce the part, from the volume of the part and the density of the material, the following equation was used:

$$d = \frac{m}{V} \leftrightarrow m = d \times V$$

Knowing the volume of the part is $0{,}000150424\ m^3$ and the density of the material is $8027\ Kg/m^3$, we get the following:

$$m = 8027 \times 0{,}000150424 = 1{,}207\ Kg$$

After the mass of material was determined, the material costs were calculated (in this calculation only the useful powder is considered):

$$Cs = \frac{1{,}207 \times 68{,}62}{1} = 82{,}82€$$

To produce the turbo compressor wheel, the material cost will be 82,82€.

Debinding and Sintering Costs

By producing the part through the SLM technology, this doesn't need to perform the debinding and sintering process, consequently, this cost will be 0€.

$$Cds = 0€$$

Post-Processing Costs

If this costing model process was more complex and detailed, the cost of part quality verification, such as dimensional control and part surface quality, and post-processing cost such as heat treatments could have been considered. However, since this is a simple model, these were not considered.

$$Cpp = 0€$$

Final Costs

As shown below, the final cost to produce one turbo compressor wheel using the SLM technology is 383,36€.

$$Ctpart = 100{,}32 + 200{,}22 + 82{,}82 + 0 + 0 = 383{,}36€$$

By analysing Figure 126, the highest cost to produce the turbo compressor wheel by SLM technology is the machinery with a percentage of the total value of 52% and the lowest cost represents the material0 with a percentage of 22%.

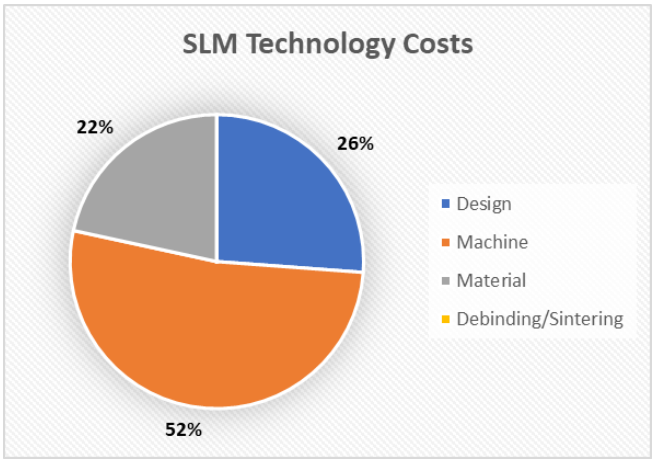

Figure 126 - SLM Technology Costs

In Figure 127 the total costs to produce the turbo compressor wheel with the FFF and SLM technologies, are presented.

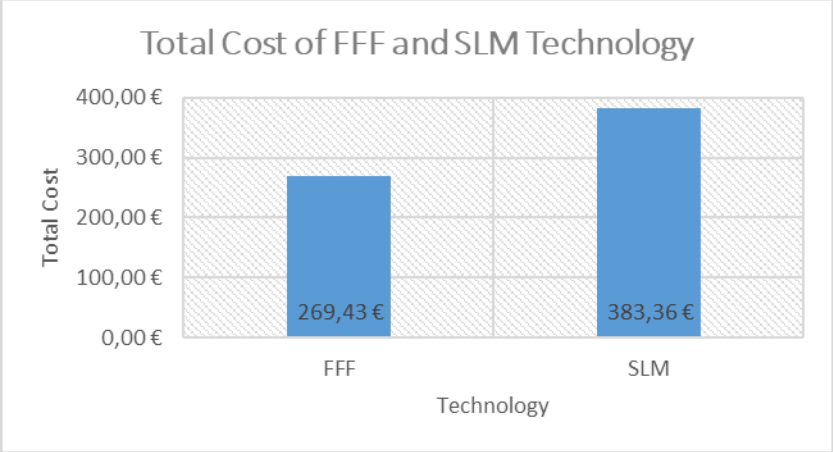

Figure 127 - Comparison of FFF and SLM Technology Costs

By analysing the Figure 127, it is possible to conclude that the FFF technology is cheaper than the SLM technology. Using FFF technology to produce one turbo compressor wheel, will result in financial costs savings of 113,93€. Furthermore, with FFF technology it is possible to achieve a shorter build time (36H) than with SLM technology (53H).

4. Conclusion

With this work and through printing specimens with 25% and 40% infill density and tri-hexagon, gyroid and quarter cubic patterns, it was possible to evaluate the mechanical properties of FFF 3D printed parts, such as weight, strength, and roughness, and it was also possible to perform a cost analysis of this technology.

After analysing all the results obtained, it is possible to conclude that:

After the debinding and sintering process, the specimens with 25% and 40% of infill density suffered an average reduction in weight of 2,727 grams, due the microstructural rearrangement and the elimination of the binder present in the part, during this processes.

The strength of the specimen depends on the infill density and pattern used, i.e., the higher the density of the infill used, higher is the strength, also the pattern that shows the best behaviour is gyroid, and the one with the lowest strength value is quarter cubic. With the performed tests it is possible to verify that the specimens with the better tensile behavior are constituted with 100% of infill density and the gyroid pattern. In other hand, the specimens with the worst tensile behavior are constituted with 10% of infill density and the tri-hexagon pattern. Compared to the SLM process, the metal FFF technology has a lower performance, this can be explained by the melting of the material that takes place in SLM technology, as opposed to FFF technology where the material is only sintered, that will influence the microstructure of the material.

Although the specimens were printed with the same layer height (0,1 mm) and with the same number of layers on the top and bottom (6), there were some differences in the roughness of the specimens. With 25% infill density they have a higher Ra and Rz value with the gyroid pattern and a lower value with the quarter cubic pattern. Specimens with 40% infill density have a higher Ra and Rz value with the tri-hexagon pattern and a lower value with the quarter cubic pattern. However, it was expected that the roughness between the different specimens would be similar, once the infill should not influence the surface, this can be because the roughness was measured after the tensile tests, in which they suffered some deformations.

With the analysis of the cubes, it was possible to verify that due to the layered filament deposition, the roughness depends on the cube face. One of the consequences of using FFF

technology is the layer bonding, how the part construction is done by deposition of a filament, a “belly” is created between consecutive layers, so the layers are not well compacted, which causes increased roughness. The side face has a higher roughness value and roughness depth, and the top face has a lower roughness value and roughness depth.

The Charpy V impact test were impossible to be performed and to obtain any results or conclusions due to the scarcity of time. However, these will be published in future reports.

Concerning the cost analysis, it was possible to determine that for producing the turbo compressor wheel, the FFF technology is cheaper and faster than the SLM. In this study by using FFF technology to produce the part, will result in financial costs savings of 113,93€. Also, with FFF technology the investment made in machinery is lower and with this technology it is possible to print in an open chamber, as opposed to the SLM technology, that requires a chamber filled with inert gas. However, it is important to note that the SLM equipment selected for comparison on this study has a kinematics quite different from several other SLM equipments. While the Kurtz SLM machine has a Cartesian kinematics, other SLM equipment use a galvanometric head to govern the LASER trajectory on the XY plane. Although, another relevant factor is that metal FFF process can be considered a low-cost process for metal parts and, thus, the comparison to a SLM machine should be performed considering a lower-cost LASER-based equipment. If in this study had been chosen an equipment with a galvanometric head to control the LASER trajectory on the XY plane, the build speed would be in the order of 7m/s to 10m/s and in this way SLM technology would be faster.

Based on the present study, future research works could focus on study the densification and porosity after sintering; study the influence of sintering on layer interface; and microstructural evaluation of sintered parts.

Bibliografia

3D Natives. n.d. “SLM 500 3D Printer.” Retrieved June 24, 2022 (https://www.3dnatives.com/3D-compare/en/3d-printers/slm-500/).

3D Systems. 2022a. “3D Printing Metal Parts and Materials .” Retrieved June 28, 2022 (https://www.3dsystems.com/3D-printing-metal-parts-and-materials).

3D Systems. 2022b. “Selective Laser Sintering (SLS) Overview | 3D Systems.” Retrieved June 20, 2022 (https://www.3dsystems.com/selective-laser-sintering).

3DLAB. 2022. “Suporte de Impressão 3D.” Retrieved June 28, 2022 (https://3dlab.com.br/suporte-de-impressao-3d/).

3Dnatives. 2022a. “Cura: All You Need to Know Before Getting Started .” Retrieved April 21, 2022 (https://www.3dnatives.com/en/cura-software-3d-printing-250320204/#!).

3Dnatives. 2022b. “The Complete Guide to Electron Beam Melting (EBM) in 3D Printing .” Retrieved August 14, 2022 (https://www.3dnatives.com/en/electron-beam-melting100420174/).

3DPrint.com. 2019. “Design Guidelines for Direct Metal Laser Sintering, Selective Laser Melting, Laser Powder Bed Fusion .” Retrieved August 15, 2022 (https://3dprint.com/237866/design-guidelines-for-direct-metal-laser-sintering-selective-laser-melting-laser-powder-bed-fusion/?fbclid=IwAR1G4f4W8tcuUwXuOkUC3z1BFp3XeNHMGCwfiwu78kJpDQtwawSdGMuYH3U).

Ahn, Dong Gyu. 2021. *Directed Energy Deposition (DED) Process: State of the Art*. Vol. 8. Korean Society for Precision Engineering.

All3DP. 2022a. “Cura Gyroid Infill: All You Need to Know .” Retrieved April 21, 2022 (https://all3dp.com/2/cura-gyroid-infill/).

All3DP. 2022b. “Electron Beam Melting (EBM) – 3D Printing Simply Explained .” Retrieved August 14, 2022 (https://all3dp.com/2/electron-beam-melting-ebm-3d-printing-simply-explained/).

All3DP. 2022c. “History of 3D Printing: When Was 3D Printing Invented?” Retrieved

November 25, 2022 (https://all3dp.com/2/history-of-3d-printing-when-was-3d-printing-invented/).

Alves, Fábio Alcino Carvalho. 2014. "Análise e Otimização Do Processo Fused Filament Fabrication."

AMFG. 2022. "3D Printing Support Structures: A Complete Guide." Retrieved June 28, 2022 (https://amfg.ai/2018/10/17/3d-printing-support-structures-guide/).

AMFG - Autonomous Manufacturing. 2022. "3D Printing Support Structures: A Complete Guide." Retrieved September 19, 2022 (https://amfg.ai/2018/10/17/3d-printing-support-structures-guide/).

Ampower. 2022. "Metal FDM Technology ." Retrieved August 16, 2022 (https://additive-manufacturing-report.com/technology/metal/metal-fdm/#007).

Aniwaa. 2022. "XJet Carmel 1400M Review - Nanoparticle Metal 3D Printer." Retrieved June 28, 2022 (https://www.aniwaa.com/product/3d-printers/xjet-carmel-1400m/).

Anon. 2022a. "3d-Printing." Retrieved August 14, 2022 (https://commons.wikimedia.org/wiki/File:3d-printing-a-2014-horizonwatching-trend-summary-report-9-638.jpg).

Anon. 2022b. "Additive vs Subtractive Manufacturing: Difference | 3DE-Shop." Retrieved April 21, 2022 (https://www.3de-shop.com/post/additive-vs-subtractive-manufacturing-difference-pros-cons/.html).

Artillery. 2020. "Artillery Sidewinder X2 Upgrade Version ABL Auto Calibration 3d Printer 550*405*640mm Larger Printed Size 11.81*11.81*15.75 Inches High Precision Dual." Retrieved August 14, 2022 (https://artillery3d.com/products/artillery-sidewinder-x2-abl-auto-calibration-3d-printer-300300400mm-larger-build-volume-titan-direct-drive-extruder-180-240℃-us-eu-free-freight).

Autodesk. 2021. "History of 3D Printing: It's Older Than You Think." Retrieved November 25, 2022 (https://redshift.autodesk.com/articles/history-of-3d-printing).

Bartolomeu, Flávio Jorge Fernandes. 2015. "Otimização Dos Parâmetros de Processamento Em Laser Melting." Universidade do Minho.

BASF. 2022a. *Exploring Fused Filament Fabrication*.

BASF. 2022b. "User Guidelines for 3D Printing Metal Parts." Retrieved September 19, 2022 (https://forward-am.com/wp-content/uploads/2021/04/UserGuidelines_2021_03_29.pdf).

BASF Forward AM. 2022. "Ultrafuse 316L 3D Printer Metal Filament ." Retrieved April 21, 2022 (https://forward-am.com/material-portfolio/ultrafuse-filaments-for-fused-filaments-fabrication-fff/metal-filaments/ultrafuse-316l/).

Beyhan, Figen, and Semra Arslan Selçuk. 2017. "3D Printing in Architecture: One Step Closer to a Sustainable Built Environment ." Retrieved August 15, 2022 (https://link.springer.com/chapter/10.1007/978-3-319-63709-9_20).

Boivie, Klas. 2022. "AM Standards: An Update on Published Work and Development in Progress." Retrieved (http://www.rm-platform.com/images/DOCUMENTS/13StandardsdevelopmentHandouts.pdf).

Bourell, David, Jean Pierre Kruth, Ming Leu, Gideon Levy, David Rosen, Allison M. Beese, and Adam Clare. 2017. *Materials for Additive Manufacturing*. Vol. 66. Elsevier USA.

Centexbel - VKC. 2022. "Charpy & Izod Impact Tests." Retrieved September 19, 2022 (https://www.centexbel.be/en/testing/charpy-izod-impact-tests).

CODI. 2022. "Desktop Metal ." Retrieved April 21, 2022 (https://www.codi.pt/solucoes-3d/).

Desktop Metal. 2022a. "Production System™." Retrieved April 21, 2022 (https://www.desktopmetal.com/products/production).

Desktop Metal. 2022b. "Production System™ ." Retrieved April 4, 2022 (https://www.desktopmetal.com/products/production).

Desktop Metal. 2022c. "Studio System™." Retrieved (https://www.desktopmetal.com/products/studio).

Desktop Metal. 2022d. "Studio System™ ." Retrieved April 21, 2022 (https://www.desktopmetal.com/products/studio).

Desktop Metal Inc. 2022. "Shop System™." Retrieved April 4, 2022

(https://www.desktopmetal.com/products/shop).

Eagle Ridge GM. 2022. “What Is a Turbocharger and How Does It Work? .” Retrieved September 20, 2022 (https://www.eagleridgegm.com/what-is-a-turbocharger-and-how-does-it-work/).

Education Department at the Museum of Arts and Design. 2022. “3D PRINTING TIMELINE Early 3D-Printing Concepts Emerge.”

Enoch Olalere, Folasayo. 2022. “Results of Integration of Rapid Prototyping Technology .” Retrieved August 15, 2022 (https://www.researchgate.net/figure/Results-of-integration-of-Rapid-Prototyping-technology-14_fig2_321489647).

fabheads. 2022. “ADDITIVE MANUFACTURING: Revolutionizing Industries around the World .” Retrieved August 14, 2022 (https://fabheads.com/blogs/additive-manufacturing-revolutionizing-industries/).

Fast Radius. 2022. “How to Design for Additive Manufacturing Support Structures .” Retrieved June 28, 2022 (https://www.fastradius.com/resources/support-structures-why-they-matter-and-how-to-design-for-them/).

Fernandez-Vicente, Miguel, Wilson Calle, Santiago Ferrandiz, and Andres Conejero. 2016. *Effect of Infill Parameters on Tensile Mechanical Behavior in Desktop 3D Printing*. Vol. 3. Mary Ann Liebert Inc.

Filament2Print. 2022. “Filamentos Solúveis Para Suporte.” Retrieved June 28, 2022 (https://filament2print.com/pt/blog/107_Filamentos-solubles-para-soporte.html).

Formlabs. 2022. “Additive vs. Subtractive Manufacturing.” Retrieved September 19, 2022 (https://formlabs.com/blog/additive-manufacturing-vs-subtractive-manufacturing/).

Gasser, Andres, Gerhard Backes, Ingomar Kelbassa, Andreas Weisheit, and Konrad Wissenbach. 2010. “Laser Additive Manufacturing Laser Metal Deposition (LmD) and Selective Laser Melting (Slm) in Turbo-Engine Applications.”

Gasser, Andres, Gerhard Backes, Ingomar Kelbassa, Andreas Weisheit, and Konrad Wissenbach. 2010. *Laser Additive Manufacturing Laser Metal Deposition (LMD) and Selective Laser Melting (SLM) in Turbo-Engine Applications*.

GE. 2022. “EBM Technology .” Retrieved May 18, 2022 (https://www.ge.com/additive/ebm).

GE Additive. 2021. *Direct Metal Laser Melting (DMLM)*.

GE Additive. 2022a. “Additive Applications .” Retrieved August 14, 2022 (https://www.ge.com/additive/additive-parts).

GE Additive. 2022b. “Arcam EBM_Q10plus_Machine .” Retrieved August 14, 2022 (https://www.ge.com/additive/additive-manufacturing/machines/ebm-machines/arcam-ebm-q10plus).

GE Additive. 2022c. “Arcam EBM A2X.” 2. Retrieved (https://www.ge.com/additive/additive-manufacturing/machines/ebm-machines/arcam-ebm-a2x).

GE Additive. 2022d. “Arcam EBM Q20plus.” 2. Retrieved May 18, 2022 (https://www.ge.com/additive/additive-manufacturing/machines/ebm-machines/arcam-ebm-a2x).

GE Additive. 2022e. “DMLM Technology.” Retrieved April 21, 2022 (https://www.ge.com/additive/direct-metal-laser-melting).

GE Additive. 2022f. “EBM for Acetabular Cups.” 300. Retrieved May 18, 2022 (https://www.ge.com/additive/sites/default/files/2021-09/GE_CS_Amplify_8.5x11_R3.pdf).

GE News. 2022. “The Blade Runners: This Factory Is 3D Printing Turbine Parts For The World’s Largest Jet Engine.” Retrieved August 14, 2022 (https://www.ge.com/news/reports/future-manufacturing-take-look-inside-factory-3d-printing-jet-engine-parts).

General Electric. 2022. “What Is Additive Manufacturing.” Retrieved February 22, 2022 (https://www.ge.com/additive/additive-manufacturing).

Gomes, Frederico. 2014. “Comparação de Processos de Fabrico Aditivo Que Utilizam Metais.” Universidade do Porto.

Harshit K. Dave, and Sandip T. Patel. 2022. *Introduction to Fused Deposition Modeling*

Based 3D Printing Process.

Hélio Rui Caldeira da Silva, Jorge. 2008. "Compounding and Processing of a Water Soluble Binder for Powder Injection Moulding." Universidade do Minho Escola de Engenharia.

Hinke, Christian. 2017. "Beam Sources for Metal Additive Manufacturing-Status Quo and Requirements." *Proceedings of the 2017 High Power Diode Lasers and Systems Conference, HPD 2017 - Co-Located with Photonex 2017* 2018-January:5–6. doi: 10.1109/HPD.2017.8261077.

ISO/ASTM. 2015. "Standard Terminology for Additive Manufacturing – General Principles – Terminology (ISO/ASTM52900)." *International Organization for Standardization: Geneva, Switzerland* i:1–9.

ISO. 2006. "ISO 148 1 Charpy."

Izadi, Mojtaba, Aidin Farzaneh, Mazher Mohammed, Ian Gibson, and Bernard Rolfe. 2020. *A Review of Laser Engineered Net Shaping (LENS) Build and Process Parameters of Metallic Parts*. Vol. 26.

Jiang, Jingchao, Xun Xu, and Jonathan Stringer. 2018. "Support Structures for Additive Manufacturing." *Journal of Manufacturing and Materials Processing* 2(4). doi: 10.3390/jmmp2040064.

Junk, S., and M. Tränkle. 2011. "DESIGN FOR ADDITIVE MANUFACTURING TECHNOLOGIES: NEW APPLICATIONS OF 3D-PRINTING FOR RAPID PROTOTYPING AND RAPID TOOLING." *Undefined*.

Kechagias, John, D. Chaidas, N. Vidakis, K. Salonitis, and N. M. Vaxevanidis. 2022. *Key Parameters Controlling Surface Quality and Dimensional Accuracy: A Critical Review of FFF Process*. Vol. 37. Taylor & Francis.

Kumar, Sanjay. 2003. *Modeling and Characterization Selective Laser Sintering: A Qualitative and Objective Approach*. Vol. 43.

Lopes, Leandro Rodrigues. 2015. "Impressão FDM de Pares de Materiais Funcionais." Universidade do Minho .

Loughborough University. 2021a. "Powder Bed Fusion." Retrieved March 22, 2022

(https://www.lboro.ac.uk/research/amrg/about/the7categoriesofadditivemanufacturing/powderbedfusion/).

Loughborough University. 2021b. “Sheet Lamination | Additive Manufacturing Research Group .” Retrieved March 22, 2022 (https://www.lboro.ac.uk/research/amrg/about/the7categoriesofadditivemanufacturing/sheetlamination/).

Loughborough University. 2021c. “VAT Photopolymerisation | Additive Manufacturing Research Group.” Retrieved March 22, 2022 (https://www.lboro.ac.uk/research/amrg/about/the7categoriesofadditivemanufacturing/vatphotopolymerisation/).

Loughborough University. 2022. “Powder Bed Fusion | Additive Manufacturing Research Group.” Retrieved April 21, 2022 (https://www.lboro.ac.uk/research/amrg/about/the7categoriesofadditivemanufacturing/powderbedfusion/).

M. Bhuvanesh Kumar, P. Sathiya, and M. Varatharajulu. 2021. *Advances in Additive Manufacturing Processes*. edited by Jeyaprakas Natarajan, Muralimohan Cheepu, and Che-Hua Yang. Bentham Science Publushers.

Make. 2022a. “3D Printing - Additive.” Retrieved August 14, 2022 (https://make.3dexperience.3ds.com/processes/3D-printing).

Make. 2022b. “Material Extrusion - FDM.” Retrieved April 21, 2022 (https://make.3dexperience.3ds.com/processes/material-extrusion).

Make. 2022c. “Material Extrusion - FDM .” Retrieved April 21, 2022 (https://make.3dexperience.3ds.com/processes/material-extrusion).

Make. 2022d. “Material Jetting - MJ, NPJ, DOD .” Retrieved September 19, 2022 (https://make.3dexperience.3ds.com/processes/material-jetting).

Manufactur3D. 2022. “Understanding XJet’s NanoParticle Jetting™ Technology.” Retrieved August 14, 2022 (https://manufactur3dmag.com/understanding-xjets-nanoparticle-jetting-technology/).

Mário Correia. 2021. “Processos Industriais Avançados.”

Marques, José. 2020. “Additive Manufacturing of a Vehicle Brake System Component.”

Martins, Joana Domingues. 2016. “ANÁLISE AO COMPORTAMENTO MECÂNICO DE ESTRUTURAS DE SUPORTE PRODUZIDAS POR FDM.” Escola Superior de Tecnologia e Gestão -IPL, Leiria.

Matmatch. 2022. “Materials Used in Selective Laser Melting (SLM) .” Retrieved April 21, 2022 (https://matmatch.com/learn/material/materials-used-in-selective-laser-melting-slm).

Mechanical Testing & Research. 2022. “Impact Testing.” Retrieved September 19, 2022 (https://www.wmtr.com/en.impact-testing.html).

Nguyen Van, Chung, Sree Koundinya Sistla, and Chung van Kempen. 2016. “A Comparative Study of Different Sintering Models for Al2O3.” Retrieved August 15, 2022 (https://www.researchgate.net/figure/Different-stages-of-sintering-1_fig3_299490787).

Nieto, Daniel Moreno, and Daniel Moreno Sánchez. 2021. “Design for Additive Manufacturing: Tool Review and a Case Study.”

Optomec. 2018. “CLASSIC SYSTEM SERIES LENS ® 800 AND LENS 600 ADDITIVE MANUFACTURING CONTROLLED ATMOSPHERE SYSTEMS Modular and Configurable.”

Optomec. 2022a. “Hybrid Metal Manufacturing .” Retrieved June 20, 2022 (https://optomec.com/hybrid-manufacturing/).

Optomec. 2022b. *LENS Blisk Repair Solution*.

Optomec. 2022c. “LENS CS 800 System.” Retrieved August 14, 2022 (https://optomec.com/lens-cs-800-system/).

Optomec. 2022d. “LENS MATERIALS FAQs.”

PCE Instruments. 2022. “Roughness Tester .” Retrieved June 24, 2022 (https://www.pce-instruments.com/english/measuring-instruments/test-meters/roughness-tester-kat_40601.htm).

Pratheesh Kumar, S., S. Elangovan, R. Mohanraj, and J. R. Ramakrishna. 2021. *Review on*

the Evolution and Technology of State-of-the-Art Metal Additive Manufacturing Processes. Vol. 46. Elsevier Ltd.

Praveena, B. A., N. Lokesh, Abdulrajak Buradi, N. Santhosh, B. L. Praveena, and R. Vignesh. 2022. *A Comprehensive Review of Emerging Additive Manufacturing (3D Printing Technology): Methods, Materials, Applications, Challenges, Trends and Future Potential*. Vol. 52. Elsevier Ltd.

Protocom. 2022. "ProX^{TM} 500 ." Retrieved August 14, 2022 (http://www.protocom3dp.com/prox-500).

PTZ Prototypen GmbH. 2022. "Metal FDM, Protótipo de Impressão Em Metal 3D ." Retrieved August 16, 2022 (https://www.ptz-prototypen.de/de/leistungen/fdm-metall.html).

Reichelt elektronik. 2022. "UM3 PC CC 0.6: 3D Printing, Ultimaker S5, Print Core CC 0.6 ." Retrieved April 21, 2022 (https://www.reichelt.com/de/en/3d-printing-ultimaker-s5-print-core-cc-0-6-um3-pc-cc-0-6-p244893.html?&trstct=pol_1&nbc=1).

Sam Davies. 2020. "Retiring Stratasys Founder Scott Crump on His 3D Printing Legacy." Retrieved August 14, 2022 (https://www.tctmagazine.com/api/amp/additive-manufacturing-3d-printing-news/exclusive-stratasys-scott-crump-3d-printing-legacy/?fbclid=IwAR1rGP47H60PKPM0j8kwn3SJDeo2CynkHzIYVG42y-0MX-8SHyS_0rtR-t0).

Santos, David Mendes. 2014. "Caracterização Mecânica Da Liga AlSi10Mg Obtida Por SLM Para Aplicação Em Componentes Automóveis."

Sculpteo. 2022. "Discover the History of 3D Printer." Retrieved March 22, 2022 (https://www.sculpteo.com/blog/2017/03/01/whos-behind-the-three-main-3d-printing-technologies/).

Semetay, Cumali. 2007. *LASER ENGINEERED NET SHAPING (LENS) MODELING USING WELDING SIMULATION CONCEPTS*.

Siemens Software. 2022. "Sheet Lamination." Retrieved March 22, 2022 (https://www.plm.automation.siemens.com/global/pt/our-story/glossary/sheet-lamination/55512).

SLM Soluctions. 2022. *Additive Design Optimization with CellCore GmbH Monolithic Thrust Chamber*.

SLM Solutions. 2022a. *3D-Printing Success Story*.

SLM Solutions. 2022b. “Explore Metals Used in 3D Printing .” Retrieved May 18, 2022 (https://www.slm-solutions.com/products-and-solutions/powders/).

SLM Solutions. 2022c. *Generative Manufacturing Processes at MonaLab GmbH Single-Piece Extrusion Tool*.

SLM Solutions. 2022d. “High-Quality Industrial Metal 3D Printers .” Retrieved August 14, 2022 (https://www.slm-solutions.com/products-and-solutions/machines/).

Solid Concepts. 2010. *Fused Deposition Modeling (FDM) Technology* .

Solutions, SLM. 2020. “Slm 500.”

Strano, G., L. Hao, R. M. Everson, and K. E. Evans. 2012. *A New Approach to the Design and Optimisation of Support Structures in Additive Manufacturing*.

Stratasys. 2022a. “FDM Materials .” Retrieved June 28, 2022 (https://www.stratasys.com/en/materials/materials-catalog/fdm-materials/?filter=MT_FDM).

Stratasys. 2022b. “Stratasys and Objet Complete Merger .” Retrieved September 19, 2022 (https://investors.stratasys.com/news-events/press-releases/detail/40/stratasys-and-objet-complete-merger).

Thomas. 2022. “All About Laser Metal Deposition 3D Printing.” Retrieved August 14, 2022 (https://www.thomasnet.com/articles/custom-manufacturing-fabricating/all-about-laser-metal-deposition-3d-printing/).

Thrimurthulu, K., Pulak M. Pandey, and N. Venkata Reddy. 2004. *Optimum Part Deposition Orientation in Fused Deposition Modeling*. Vol. 44.

Total Materia Article. 2019. “Charpy Impact Steel Testing: Part One .” Retrieved September 19, 2022 (https://www.totalmateria.com/page.aspx?ID=CheckArticle&site=kts&LN=DE&NM=534).

Trumpf. 2022. “TruLaser Cell 3000 LASERS.”

TRUMPF. 2021. “Laser Metal Deposition and High-Speed Laser Metal Deposition Tapping New Potential.”

TRUMPF. 2022. “TruLaser Cell 3000 .” Retrieved August 14, 2022 (https://www.trumpf.com/de_DE/produkte/maschinen-systeme/laserschweissanlagen-und-lichtbogenschweisszelle/trulaser-cell-3000/).

Ultimaker. 2022a. “Remove Support Material .” Retrieved June 28, 2022 (https://support.ultimaker.com/hc/en-us/articles/360011544439-Remove-support-material).

Ultimaker. 2022b. “Ultimaker S3: Easy-to-Use 3D Printing Starts Here.” Retrieved August 14, 2022 (https://ultimaker.com/3d-printers/ultimaker-s3).

Ultimaker Support. 2022a. “Infill Pattern & Density.”

Ultimaker Support. 2022b. “Infill Settings .” Retrieved April 21, 2022 (https://support.ultimaker.com/hc/en-us/articles/360012607079-Infill-settings).

Unleashed. 2022. “12 Benefits of Additive Manufacturing and 5 Disadvantages.” Retrieved March 22, 2022 (https://www.unleashedsoftware.com/blog/12-benefits-of-additive-manufacturing-and-5-disadvantages).

Xjet. 2022. “Systems.” Retrieved June 28, 2022 (https://www.xjet3d.com/systems-3-3/).

XJet. 2019. *Tech Movie* .

XJet. 2022. “Materials.” Retrieved May 18, 2022 (https://www.xjet3d.com/materials-2-2/).

XJET. 2022. “XJet & NanoParticle Jetting - Technology Brochure.” Retrieved (https://www.xjet3d.com/wp-content/uploads/2022/04/Xjet_Marketing_brochure-2022-3.pdf).

Yin, Binghong, Qinghao He, and Lin Ye. 2021. “Advanced Industrial and Engineering Polymer Research Effects of Deposition Speed and Extrusion Temperature on Fusion between Fi Laments in Single-Layer Polymer Fi Lms Printed with FFF.” Elsevier Inc.

ZwickRoell. 2022. “Charpy Impact Test on Metals.” Retrieved August 16, 2022

(https://www.zwickroell.com/industries/materials-testing/impact-test/charpy-impact-test-metals-iso-148-1/).

Appendices

Appendix A

Specimen	Weight [Kg]	Volume Before [m^3]	Density Before [Kg/m^3]	Volume After [ml]	Density After [Kg/m^3]	Density differnce [Kg/m^3]		
1	0,0199	0,000069	288,261	0,000074	268,784	19,477		
2	0,0200	0,000069	289,812	0,000074	270,230	19,582	**SD**	**1,688**
3	0,0201	0,000069	291,101	0,000073	275,151	15,951	**Average**	**18,337**
8	0,0232	0,000068	340,941	0,000073	317,589	23,352		
9	0,0233	0,000068	342,338	0,000073	318,890	23,448	**SD**	**1,036**
10	0,0233	0,000068	342,044	0,000074	316,449	25,595	**Average**	**24,132**
15	0,0232	0,000068	341,147	0,000073	319,972	21,175		
16	0,0233	0,000067	347,194	0,000072	323,083	24,111	**SD**	**1,107**
17	0,0235	0,000067	350,582	0,000072	328,517	22,065	**Average**	**22,450**
22	0,0209	0,000067	313,534	0,000072	291,608	21,925		
23	0,0207	0,000066	313,939	0,000069	300,290	13,650	**SD**	**4,215**
24	0,0204	0,000064	319,250	0,000069	296,116	23,134	**Average**	**19,570**
30	0,0194	0,0000635	305,008	0,000068	284,824	20,184		
32	0,0195	0,0000630	309,762	0,000067	291,269	18,493	**SD**	**1,063**
34	0,0196	0,0000625	313,456	0,000067	292,403	21,053	**Average**	**19,910**
40	0,0225	0,0000620	362,306	0,000067	337,789	24,517		
41	0,0223	0,0000620	360,113	0,000066	338,288	21,825	**SD**	**1,380**
42	0,0225	0,0000615	365,805	0,000066	340,864	24,941	**Average**	**23,761**

Appendix B - Tri-Hexagon | 25%

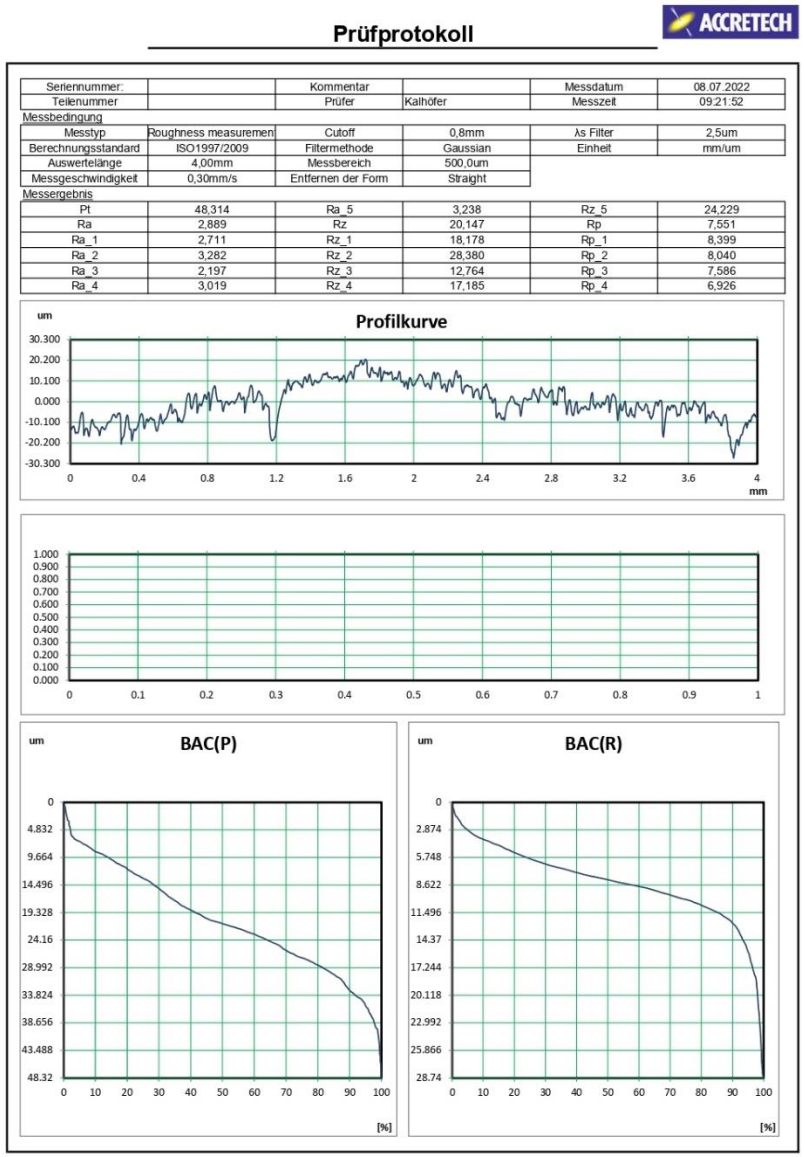

Prüfprotokoll

Seriennummer:		Kommentar		Messdatum	08.07.2022
Teilenummer		Prüfer	Kalhöfer	Messzeit	09:21:52

Messbedingung

Messtyp	Roughness measuremen	Cutoff	0,8mm	λs Filter	2,5um
Berechnungsstandard	ISO1997/2009	Filtermethode	Gaussian	Einheit	mm/um
Auswertelänge	4,00mm	Messbereich	500,0um		
Messgeschwindigkeit	0,30mm/s	Entfernen der Form	Straight		

Messergebnis

Pt	48,314	Ra_5	3,238	Rz_5	24,229
Ra	2,889	Rz	20,147	Rp	7,551
Ra_1	2,711	Rz_1	18,178	Rp_1	8,399
Ra_2	3,282	Rz_2	28,380	Rp_2	8,040
Ra_3	2,197	Rz_3	12,764	Rp_3	7,586
Ra_4	3,019	Rz_4	17,185	Rp_4	6,926

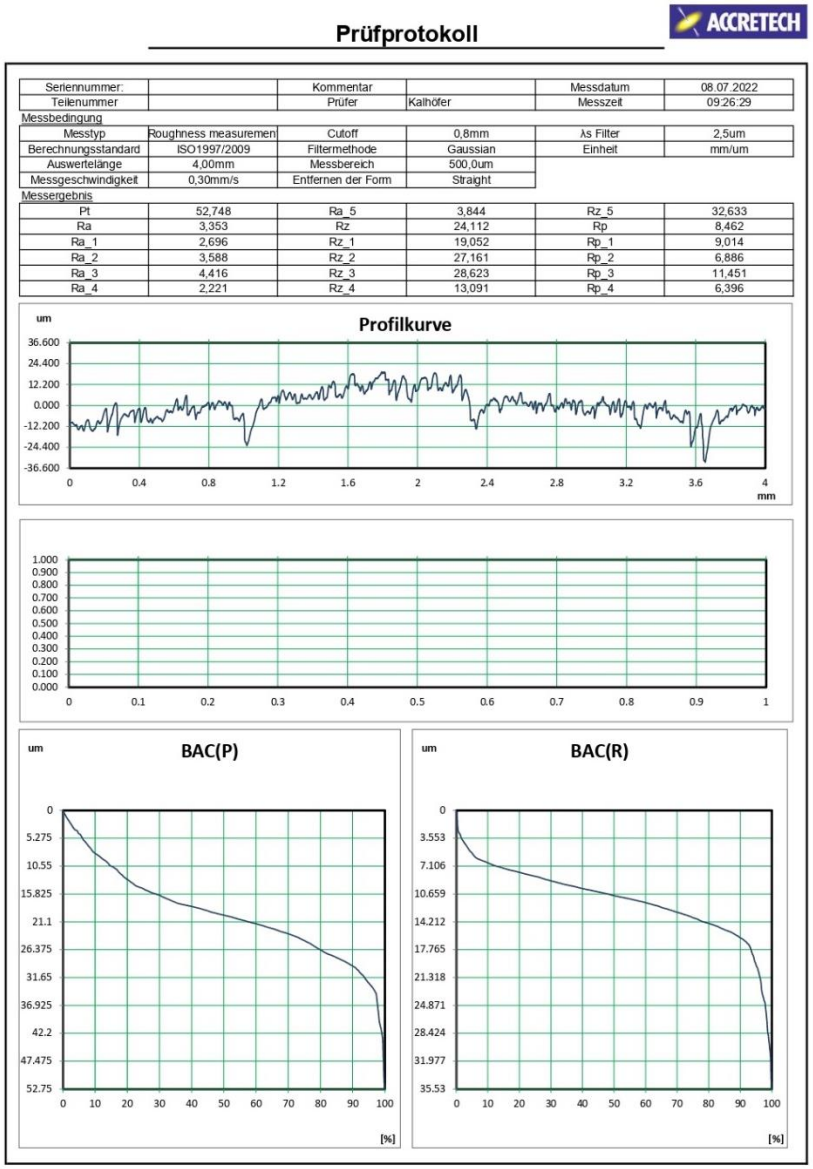

Prüfprotokoll

Seriennummer:		Kommentar		Messdatum	08.07.2022
Teilenummer		Prüfer	Kalhöfer	Messzeit	09:26:29

Messbedingung

Messtyp	Roughness measuremen	Cutoff	0,8mm	λs Filter	2,5um
Berechnungsstandard	ISO1997/2009	Filtermethode	Gaussian	Einheit	mm/um
Auswertelänge	4,00mm	Messbereich	500,0um		
Messgeschwindigkeit	0,30mm/s	Entfernen der Form	Straight		

Messergebnis

Pt	52,748	Ra_5	3,844	Rz_5	32,633
Ra	3,353	Rz	24,112	Rp	8,462
Ra_1	2,696	Rz_1	19,052	Rp_1	9,014
Ra_2	3,588	Rz_2	27,161	Rp_2	6,886
Ra_3	4,416	Rz_3	28,623	Rp_3	11,451
Ra_4	2,221	Rz_4	13,091	Rp_4	6,396

Prüfprotokoll

ACCRETECH

Seriennummer:		Kommentar		Messdatum	08.07.2022
Teilenummer		Prüfer	Kalhöfer	Messzeit	09:27:25

Messbedingung

Messtyp	Roughness measuremen	Cutoff	0,8mm	λs Filter	2,5um
Berechnungsstandard	ISO1997/2009	Filtermethode	Gaussian	Einheit	mm/um
Auswertelänge	4,00mm	Messbereich	500,0um		
Messgeschwindigkeit	0,30mm/s	Entfernen der Form	Straight		

Messergebnis

Pt	36,541	Ra_5	3,337	Rz_5	22,270
Ra	3,077	Rz	22,356	Rp	8,026
Ra_1	2,650	Rz_1	16,258	Rp_1	8,490
Ra_2	3,821	Rz_2	35,648	Rp_2	10,388
Ra_3	3,078	Rz_3	19,194	Rp_3	7,763
Ra_4	2,499	Rz_4	18,407	Rp_4	5,017

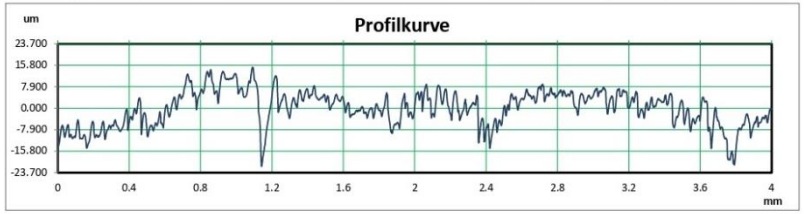

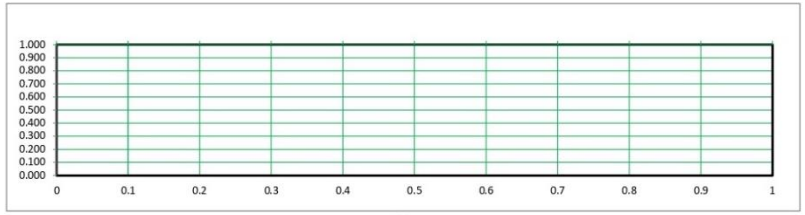

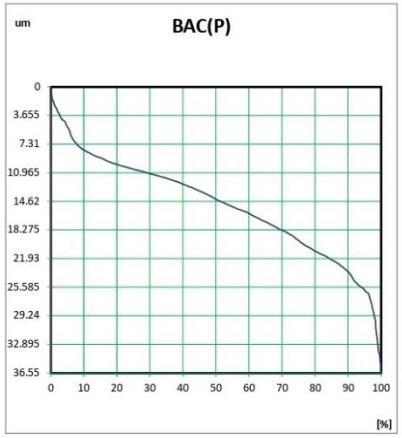

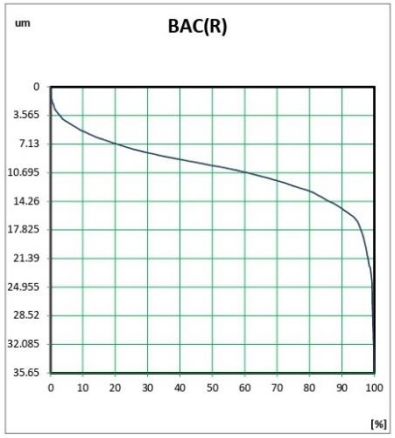

Prüfprotokoll

ACCRETECH

Seriennummer:		Kommentar		Messdatum	27.07.2022
Teilenummer		Prüfer	Kalhöfer	Messzeit	12:33:07

Messbedingung

Messtyp	Roughness measuremen	Cutoff	0,8mm	λs Filter	2,5um
Berechnungsstandard	ISO1997/2009	Filtermethode	Gaussian	Einheit	mm/um
Auswertelänge	4,00mm	Messbereich	500,0um		
Messgeschwindigkeit	0,30mm/s	Entfernen der Form	Straight		

Messergebnis

Pt	93,571	Ra_5	3,863	Rz_5	40,998
Ra	3,140	Rz	27,144	Rp	10,349
Ra_1	2,682	Rz_1	26,904	Rp_1	11,220
Ra_2	3,072	Rz_2	20,825	Rp_2	7,151
Ra_3	2,961	Rz_3	19,441	Rp_3	9,422
Ra_4	3,124	Rz_4	27,553	Rp_4	13,536

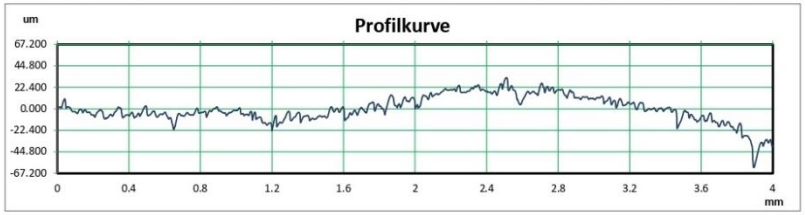

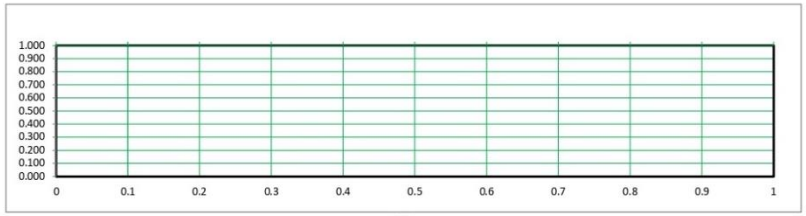

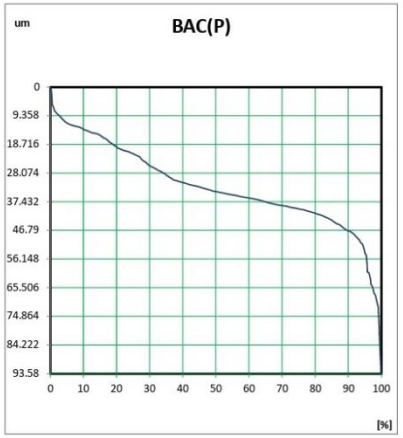

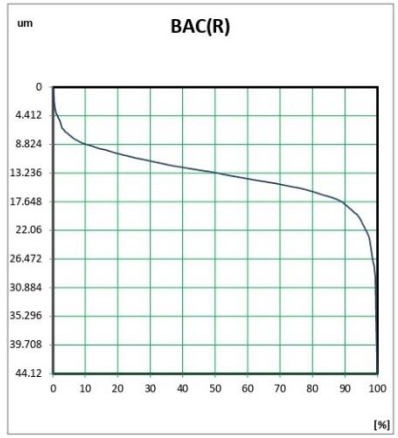

Prüfprotokoll

ACCRETECH

Seriennummer:		Kommentar		Messdatum	27.07.2022
Teilenummer		Prüfer	Kalhöfer	Messzeit	12:37:04

Messbedingung

Messtyp	Roughness measuremen	Cutoff	0,8mm	λs Filter	2,5um
Berechnungsstandard	ISO1997/2009	Filtermethode	Gaussian	Einheit	mm/um
Auswertelänge	4,00mm	Messbereich	500,0um		
Messgeschwindigkeit	0,30mm/s	Entfernen der Form	Straight		

Messergebnis

Pt	82,253	Ra_5	3,507	Rz_5	37,139
Ra	3,362	Rz	28,766	Rp	10,995
Ra_1	3,515	Rz_1	32,844	Rp_1	8,530
Ra_2	2,535	Rz_2	18,510	Rp_2	8,910
Ra_3	4,407	Rz_3	37,204	Rp_3	13,320
Ra_4	2,845	Rz_4	18,135	Rp_4	11,751

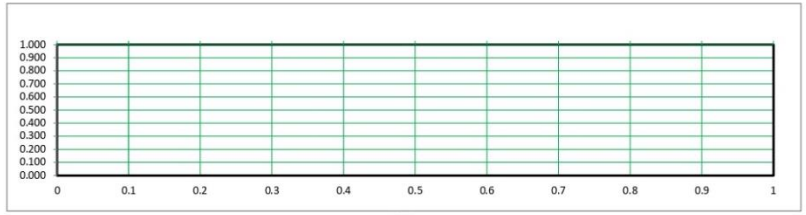

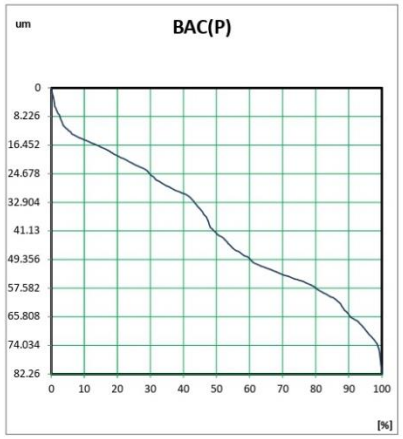

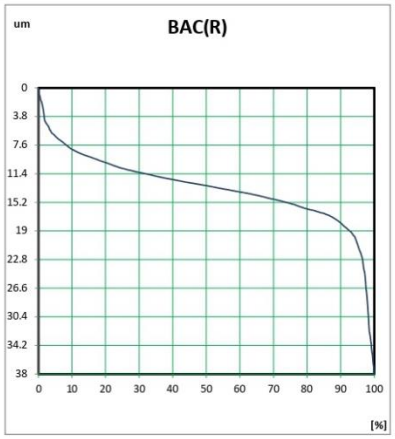

Prüfprotokoll

ACCRETECH

Seriennummer:		Kommentar		Messdatum	27.07.2022
Teilenummer		Prüfer	Kalhöfer	Messzeit	12:38:34

Messbedingung

Messtyp	Roughness measuremen	Cutoff	0,8mm	λs Filter	2,5um
Berechnungsstandard	ISO1997/2009	Filtermethode	Gaussian	Einheit	mm/um
Auswertelänge	4,00mm	Messbereich	500,0um		
Messgeschwindigkeit	0,30mm/s	Entfernen der Form	Straight		

Messergebnis

Pt	60,397	Ra_5	2,627	Rz_5	19,262
Ra	3,333	Rz	27,448	Rp	9,823
Ra_1	3,825	Rz_1	44,004	Rp_1	18,312
Ra_2	3,647	Rz_2	19,592	Rp_2	7,859
Ra_3	3,525	Rz_3	36,412	Rp_3	6,600
Ra_4	3,041	Rz_4	17,972	Rp_4	8,125

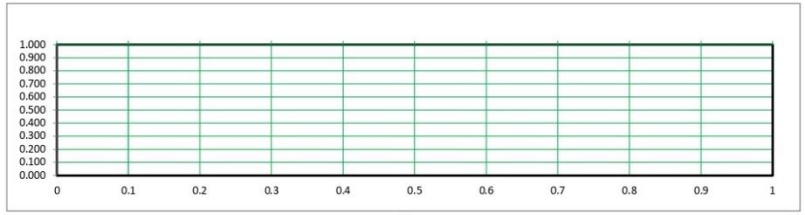

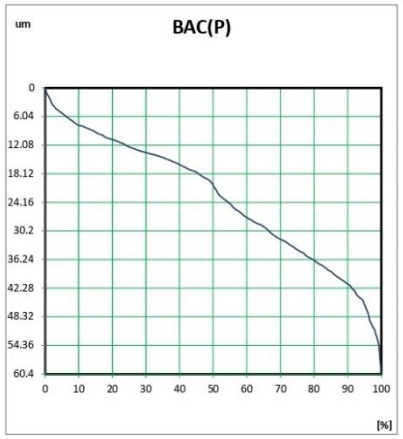

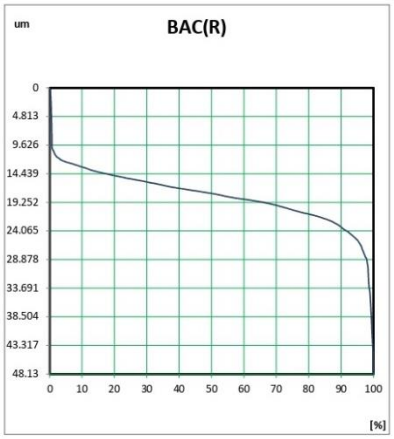

Prüfprotokoll

ACCRETECH

Seriennummer:		Kommentar		Messdatum	27.07.2022
Teilenummer		Prüfer	Kalhöfer	Messzeit	12:41:40

Messbedingung

Messtyp	Roughness measuremen	Cutoff	0,8mm	λs Filter	2,5um
Berechnungsstandard	ISO1997/2009	Filtermethode	Gaussian	Einheit	mm/um
Auswertelänge	4,00mm	Messbereich	500,0um		
Messgeschwindigkeit	0,30mm/s	Entfernen der Form	Straight		

Messergebnis

Pt	56,802	Ra_5	2,368	Rz_5	14,029
Ra	3,395	Rz	26,482	Rp	7,990
Ra_1	3,324	Rz_1	27,502	Rp_1	10,275
Ra_2	2,118	Rz_2	12,928	Rp_2	6,270
Ra_3	5,027	Rz_3	35,060	Rp_3	8,853
Ra_4	4,136	Rz_4	42,892	Rp_4	7,380

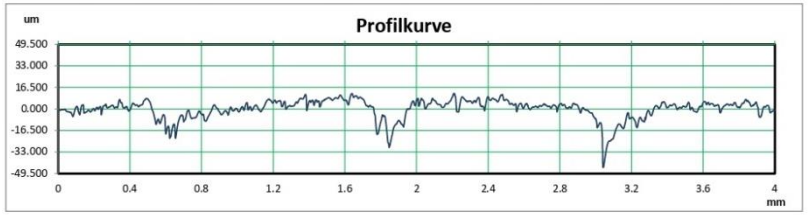

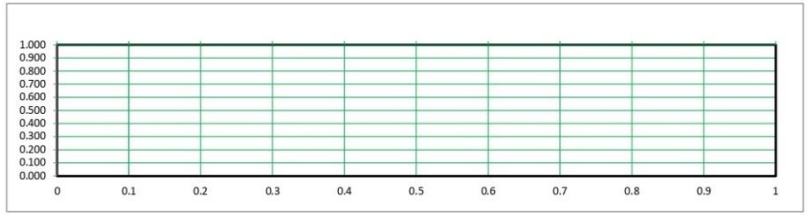

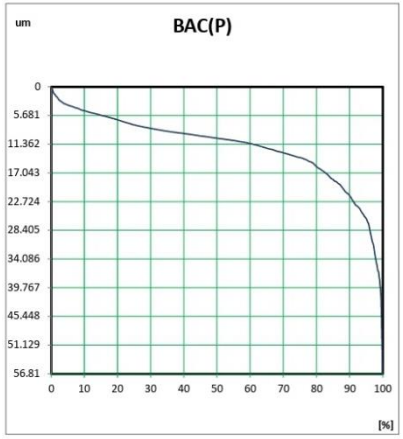

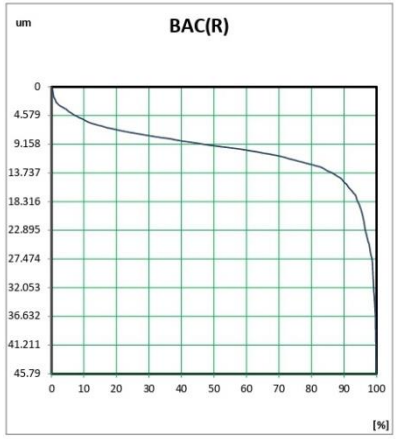

Prüfprotokoll

ACCRETECH

Seriennummer:		Kommentar		Messdatum	27.07.2022
Teilenummer		Prüfer	Kalhöfer	Messzeit	12:44:56

Messbedingung

Messtyp	Roughness measuremen	Cutoff	0,8mm	λs Filter	2,5um
Berechnungsstandard	ISO1997/2009	Filtermethode	Gaussian	Einheit	mm/um
Auswertelänge	4,00mm	Messbereich	500,0um		
Messgeschwindigkeit	0,30mm/s	Entfernen der Form	Straight		

Messergebnis

Pt	46,037	Ra_5	3,382	Rz_5	27,002
Ra	2,926	Rz	27,813	Rp	8,043
Ra_1	2,785	Rz_1	29,832	Rp_1	5,283
Ra_2	2,847	Rz_2	28,654	Rp_2	5,818
Ra_3	1,993	Rz_3	18,035	Rp_3	5,895
Ra_4	3,623	Rz_4	35,539	Rp_4	15,845

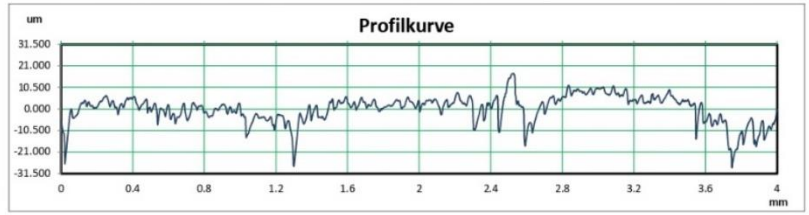

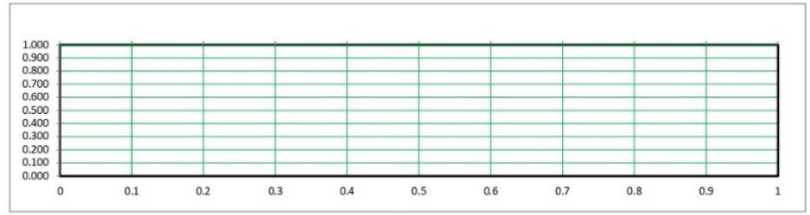

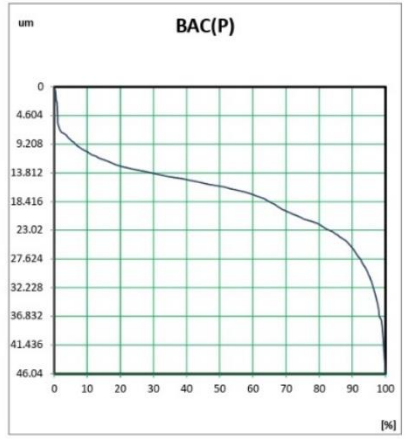

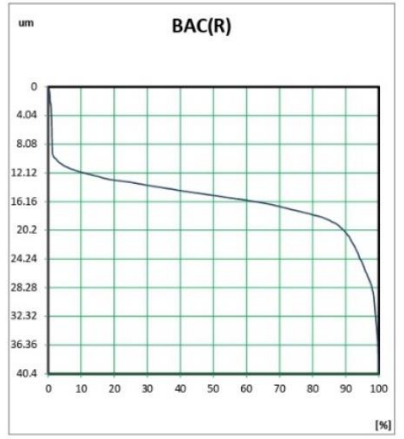

Prüfprotokoll

ACCRETECH

Seriennummer:		Kommentar		Messdatum	27.07.2022
Teilenummer		Prüfer	Kalhöfer	Messzeit	12:46:00

Messbedingung

Messtyp	Roughness measuremen	Cutoff	0,8mm	λs Filter	2,5um
Berechnungsstandard	ISO1997/2009	Filtermethode	Gaussian	Einheit	mm/um
Auswertelänge	4,00mm	Messbereich	500,0um		
Messgeschwindigkeit	0,30mm/s	Entfernen der Form	Straight		

Messergebnis

Pt	42,106	Ra_5	2,061	Rz_5	12,041
Ra	3,050	Rz	23,704	Rp	7,958
Ra_1	2,922	Rz_1	27,793	Rp_1	5,809
Ra_2	2,644	Rz_2	18,526	Rp_2	11,131
Ra_3	3,431	Rz_3	30,785	Rp_3	6,627
Ra_4	4,190	Rz_4	29,374	Rp_4	9,093

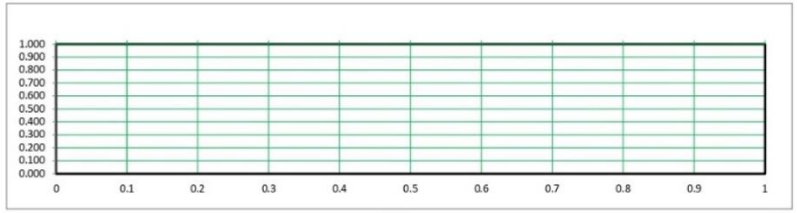

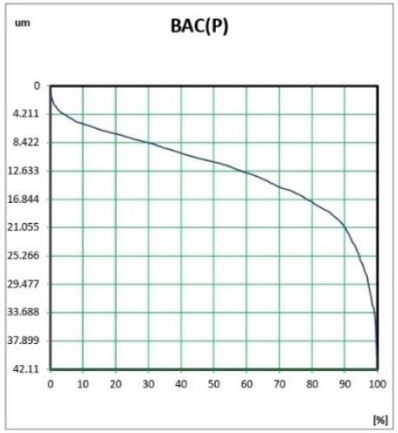

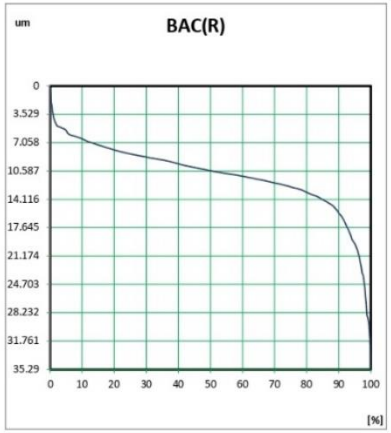

Appendix C - Tri-Hexagon | 40%

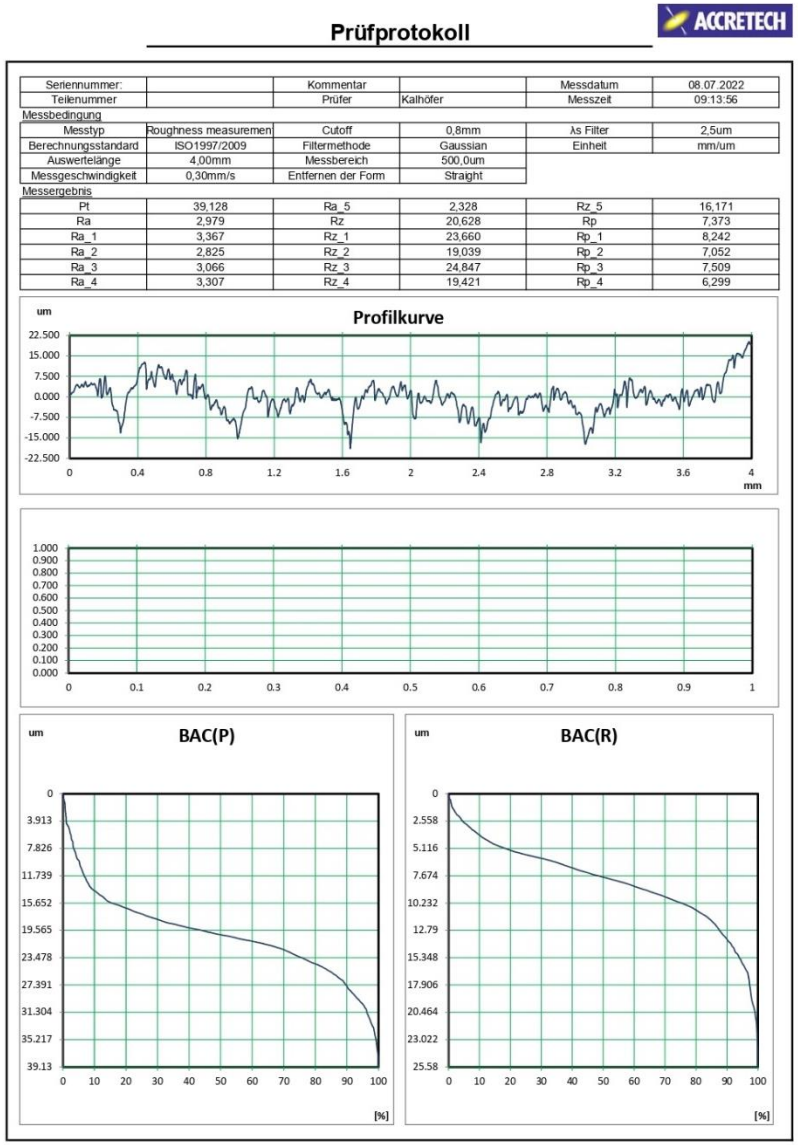

Prüfprotokoll

ACCRETECH

Seriennummer:		Kommentar		Messdatum	08.07.2022
Teilenummer		Prüfer	Kalhöfer	Messzeit	09:13:56

Messbedingung

Messtyp	Roughness measuremen	Cutoff	0,8mm	λs Filter	2,5um
Berechnungsstandard	ISO1997/2009	Filtermethode	Gaussian	Einheit	mm/um
Auswertelänge	4,00mm	Messbereich	500,0um		
Messgeschwindigkeit	0,30mm/s	Entfernen der Form	Straight		

Messergebnis

Pt	39,128	Ra_5	2,328	Rz_5	16,171
Ra	2,979	Rz	20,628	Rp	7,373
Ra_1	3,367	Rz_1	23,660	Rp_1	8,242
Ra_2	2,825	Rz_2	19,039	Rp_2	7,052
Ra_3	3,066	Rz_3	24,847	Rp_3	7,509
Ra_4	3,307	Rz_4	19,421	Rp_4	6,299

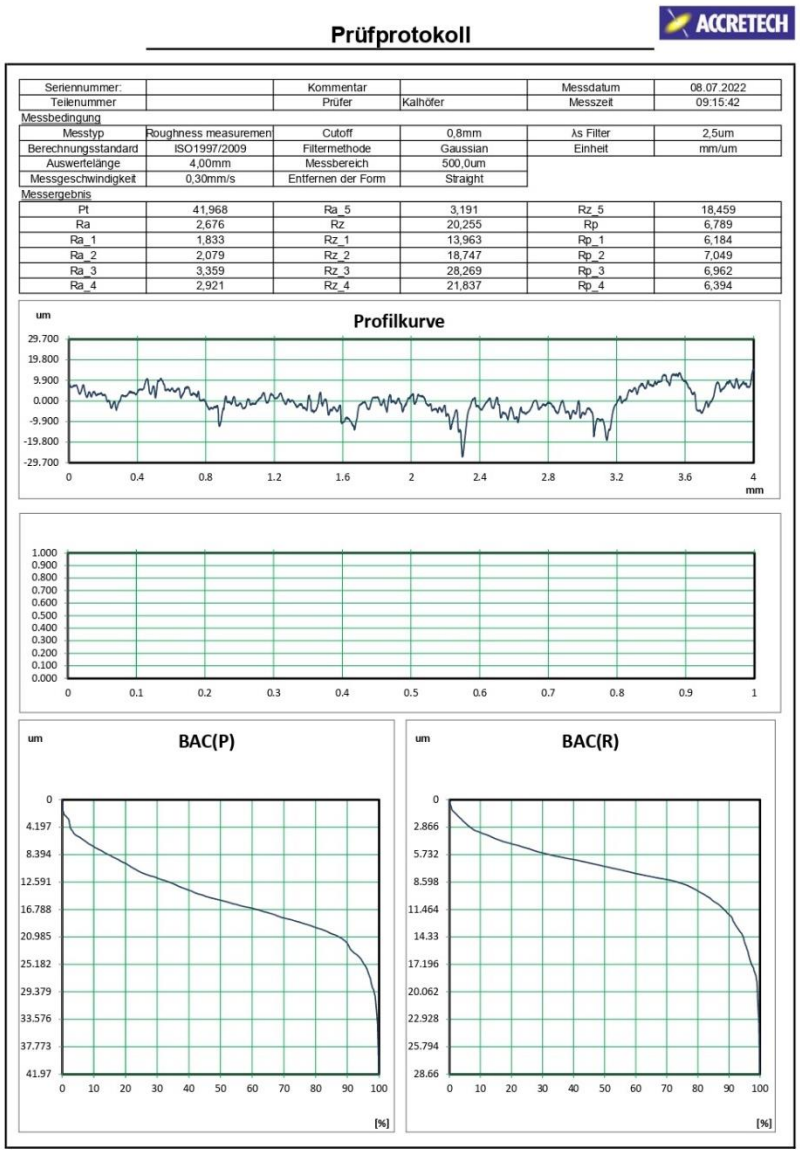

Prüfprotokoll

ACCRETECH

Seriennummer:		Kommentar		Messdatum	08.07.2022
Teilenummer		Prüfer	Kalhöfer	Messzeit	09:15:42

Messbedingung

Messtyp	Roughness measuremen	Cutoff	0,8mm	λs Filter	2,5um
Berechnungsstandard	ISO1997/2009	Filtermethode	Gaussian	Einheit	mm/um
Auswertelänge	4,00mm	Messbereich	500,0um		
Messgeschwindigkeit	0,30mm/s	Entfernen der Form	Straight		

Messergebnis

Pt	41,968	Ra_5	3,191	Rz_5	18,459
Ra	2,676	Rz	20,255	Rp	6,789
Ra_1	1,833	Rz_1	13,963	Rp_1	6,184
Ra_2	2,079	Rz_2	18,747	Rp_2	7,049
Ra_3	3,359	Rz_3	28,269	Rp_3	6,962
Ra_4	2,921	Rz_4	21,837	Rp_4	6,394

Prüfprotokoll

ACCRETECH

Seriennummer:		Kommentar		Messdatum	08.07.2022
Teilenummer		Prüfer	Kalhöfer	Messzeit	09:18:55

Messbedingung

Messtyp	Roughness measuremen	Cutoff	0,8mm	λs Filter	2,5um
Berechnungsstandard	ISO1997/2009	Filtermethode	Gaussian	Einheit	mm/um
Auswertelänge	4,00mm	Messbereich	500,0um		
Messgeschwindigkeit	0,30mm/s	Entfernen der Form	Straight		

Messergebnis

Pt	34,236	Ra_5	3,310	Rz_5	20,953
Ra	2,871	Rz	21,381	Rp	7,728
Ra_1	2,225	Rz_1	18,346	Rp_1	6,817
Ra_2	2,386	Rz_2	26,295	Rp_2	9,471
Ra_3	3,543	Rz_3	22,731	Rp_3	7,067
Ra_4	2,891	Rz_4	18,580	Rp_4	9,123

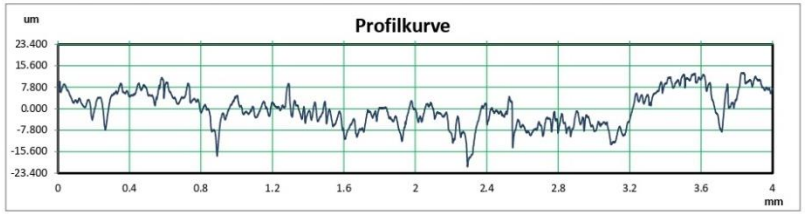

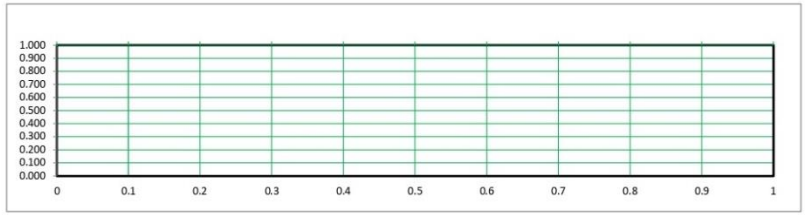

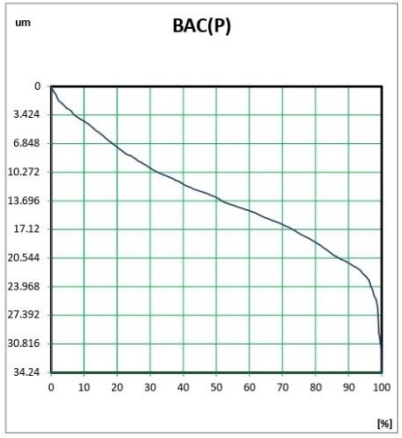

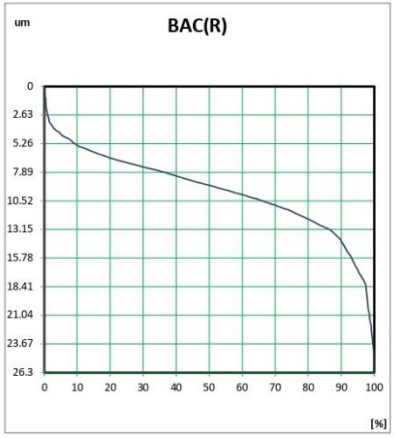

Prüfprotokoll

ACCRETECH

Seriennummer:		Kommentar		Messdatum	27.07.2022
Teilenummer		Prüfer	Kalhöfer	Messzeit	12:49:05

Messbedingung

Messtyp	Roughness measuremen	Cutoff	0,8mm	λs Filter	2,5um
Berechnungsstandard	ISO1997/2009	Filtermethode	Gaussian	Einheit	mm/um
Auswertelänge	4,00mm	Messbereich	500,0um		
Messgeschwindigkeit	0,30mm/s	Entfernen der Form	Straight		

Messergebnis

Pt	56,077	Ra_5	2,708	Rz_5	14,874
Ra	3,651	Rz	21,977	Rp	9,262
Ra_1	3,195	Rz_1	20,792	Rp_1	9,318
Ra_2	5,004	Rz_2	29,217	Rp_2	13,516
Ra_3	3,854	Rz_3	20,141	Rp_3	7,606
Ra_4	3,496	Rz_4	24,863	Rp_4	9,349

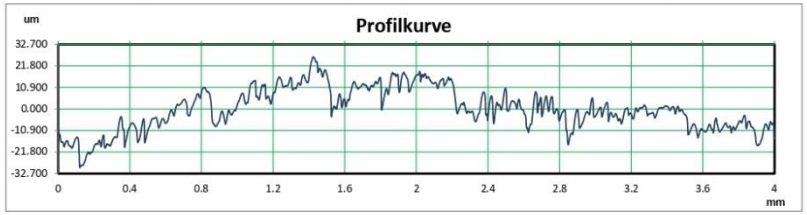

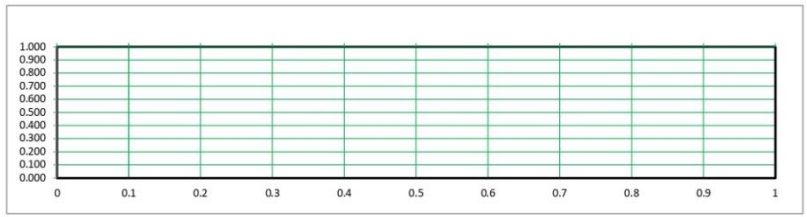

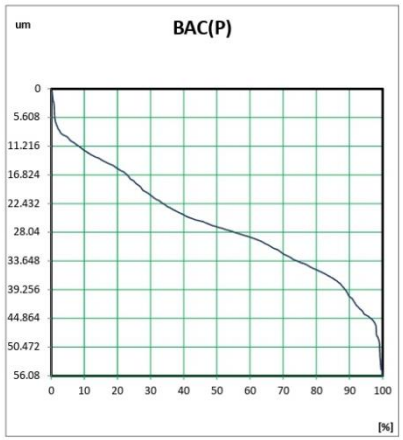

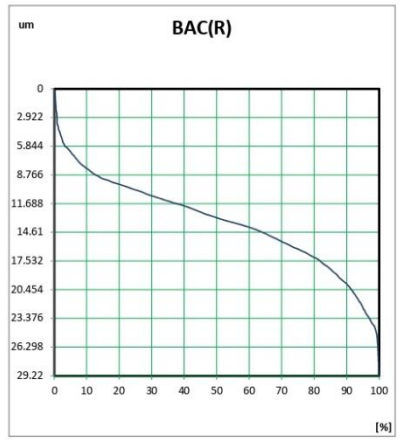

Prüfprotokoll

ACCRETECH

Seriennummer:		Kommentar		Messdatum	27.07.2022
Teilenummer		Prüfer	Kalhöfer	Messzeit	12:51:33

Messbedingung

Messtyp	Roughness measuremen	Cutoff	0,8mm	λs Filter	2,5um
Berechnungsstandard	ISO1997/2009	Filtermethode	Gaussian	Einheit	mm/um
Auswertelänge	4,00mm	Messbereich	500,0um		
Messgeschwindigkeit	0,30mm/s	Entfernen der Form	Straight		

Messergebnis

Pt	29,923	Ra_5	2,667	Rz_5	19,131
Ra	2,878	Rz	20,011	Rp	7,950
Ra_1	3,934	Rz_1	24,444	Rp_1	11,315
Ra_2	2,748	Rz_2	18,649	Rp_2	6,927
Ra_3	2,354	Rz_3	15,948	Rp_3	6,394
Ra_4	2,687	Rz_4	21,885	Rp_4	7,950

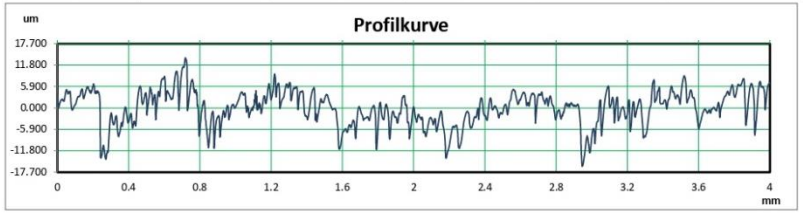

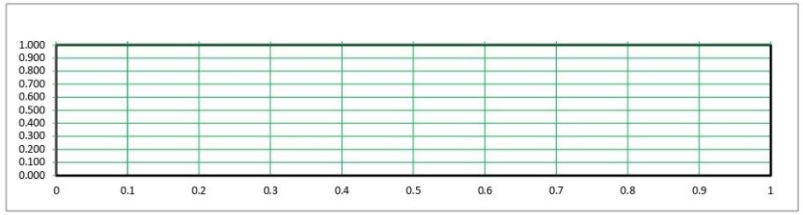

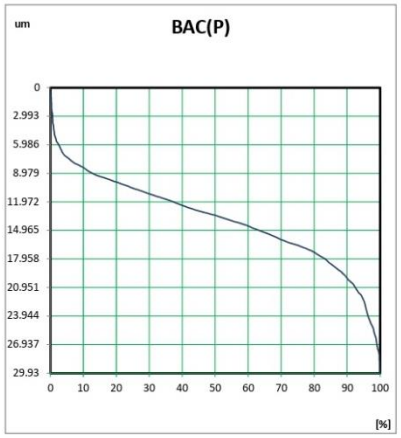

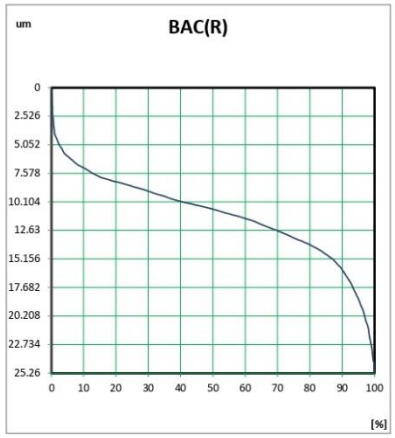

Prüfprotokoll

ACCRETECH

Seriennummer:		Kommentar		Messdatum	27.07.2022
Teilenummer		Prüfer	Kalhöfer	Messzeit	12:52:39

Messbedingung

Messtyp	Roughness measuremen	Cutoff	0,8mm	λs Filter	2,5um
Berechnungsstandard	ISO1997/2009	Filtermethode	Gaussian	Einheit	mm/um
Auswertelänge	4,00mm	Messbereich	500,0um		
Messgeschwindigkeit	0,30mm/s	Entfernen der Form	Straight		

Messergebnis

Pt	46,409	Ra_5	2,155	Rz_5	15,097
Ra	3,381	Rz	20,105	Rp	7,987
Ra_1	3,992	Rz_1	26,056	Rp_1	8,467
Ra_2	4,109	Rz_2	23,099	Rp_2	8,546
Ra_3	3,774	Rz_3	21,154	Rp_3	9,988
Ra_4	2,874	Rz_4	15,118	Rp_4	6,442

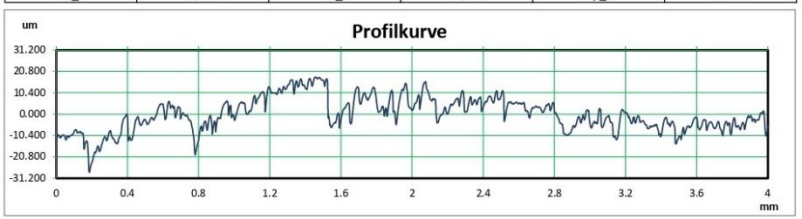

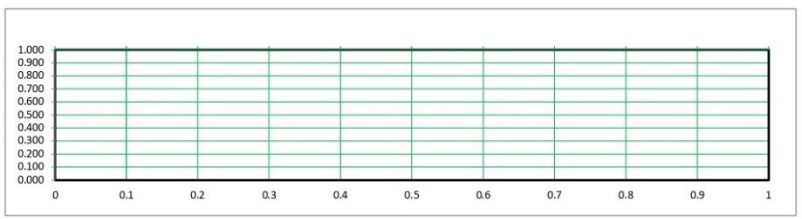

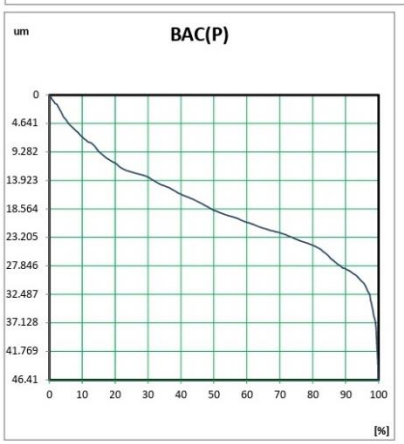

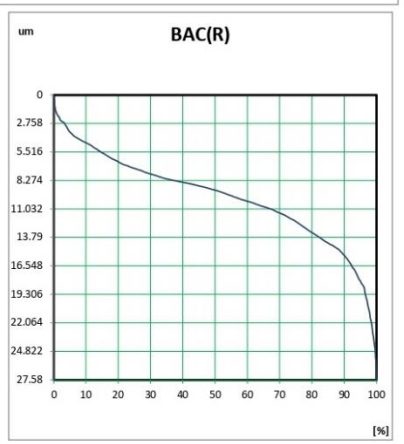

Prüfprotokoll

ACCRETECH

Seriennummer:		Kommentar		Messdatum	27.07.2022
Teilenummer		Prüfer	Kalhöfer	Messzeit	12:54:47

Messbedingung

Messtyp	Roughness measuremen	Cutoff	0,8mm	λs Filter	2,5um
Berechnungsstandard	ISO1997/2009	Filtermethode	Gaussian	Einheit	mm/um
Auswertelänge	4,00mm	Messbereich	500,0um		
Messgeschwindigkeit	0,30mm/s	Entfernen der Form	Straight		

Messergebnis

Pt	41,246	Ra_5	2,484	Rz_5	19,161
Ra	3,132	Rz	20,763	Rp	8,488
Ra_1	3,879	Rz_1	23,561	Rp_1	11,861
Ra_2	2,867	Rz_2	24,261	Rp_2	7,949
Ra_3	2,580	Rz_3	15,443	Rp_3	4,821
Ra_4	3,849	Rz_4	21,388	Rp_4	7,523

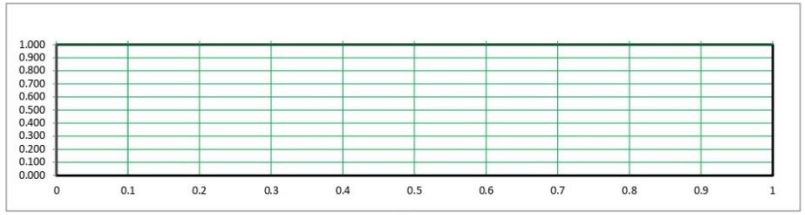

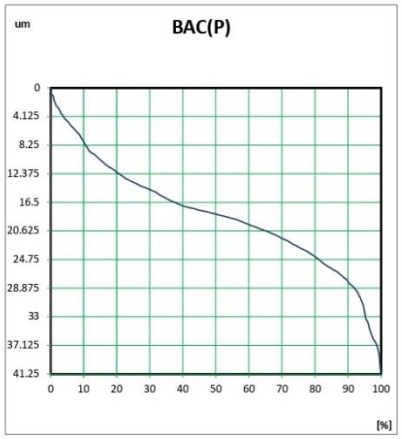

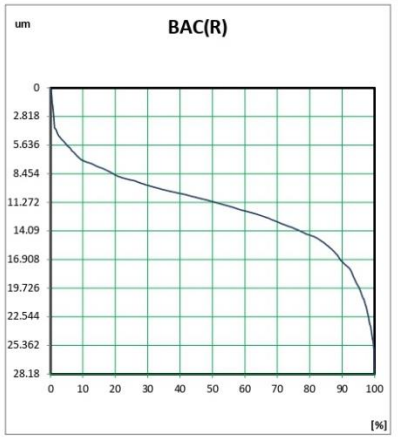

Prüfprotokoll

ACCRETECH

Seriennummer:		Kommentar		Messdatum	27.07.2022
Teilenummer		Prüfer	Kalhöfer	Messzeit	12:56:16

Messbedingung

Messtyp	Roughness measuremen	Cutoff	0,8mm	λs Filter	2,5um
Berechnungsstandard	ISO1997/2009	Filtermethode	Gaussian	Einheit	mm/um
Auswertelänge	4,00mm	Messbereich	500,0um		
Messgeschwindigkeit	0,30mm/s	Entfernen der Form	Straight		

Messergebnis

Pt	52,623	Ra_5	2,702	Rz_5	13,069
Ra	3,535	Rz	21,816	Rp	8,428
Ra_1	2,519	Rz_1	20,033	Rp_1	5,414
Ra_2	6,184	Rz_2	39,627	Rp_2	17,219
Ra_3	3,768	Rz_3	21,706	Rp_3	7,593
Ra_4	2,500	Rz_4	14,645	Rp_4	6,490

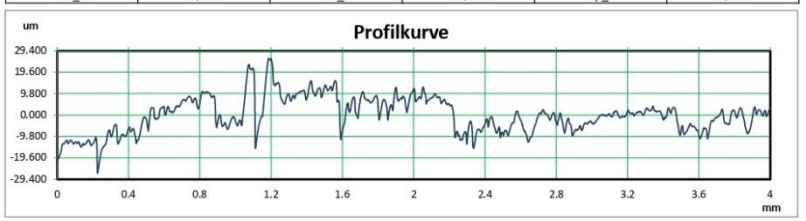

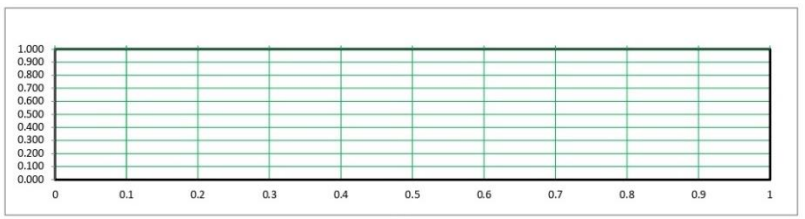

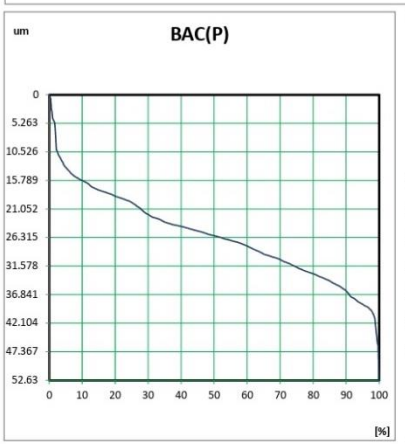

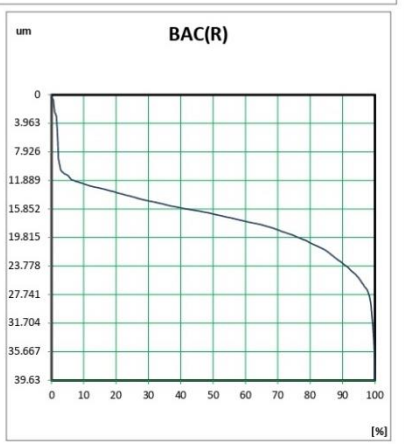

Prüfprotokoll

ACCRETECH

Seriennummer:		Kommentar		Messdatum	27.07.2022
Teilenummer		Prüfer	Kalhöfer	Messzeit	12:57:44

Messbedingung

Messtyp	Roughness measuremen	Cutoff	0,8mm	λs Filter	2,5um
Berechnungsstandard	ISO1997/2009	Filtermethode	Gaussian	Einheit	mm/um
Auswertelänge	4,00mm	Messbereich	500,0um		
Messgeschwindigkeit	0,30mm/s	Entfernen der Form	Straight		

Messergebnis

Pt	41,262	Ra_5	2,753	Rz_5	19,926
Ra	2,778	Rz	21,024	Rp	8,025
Ra_1	3,336	Rz_1	33,799	Rp_1	10,293
Ra_2	3,039	Rz_2	18,127	Rp_2	7,181
Ra_3	2,655	Rz_3	15,565	Rp_3	8,446
Ra_4	2,110	Rz_4	17,705	Rp_4	7,115

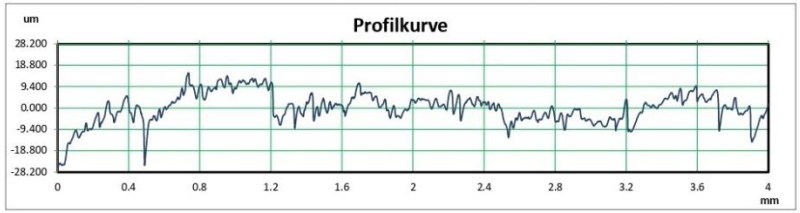

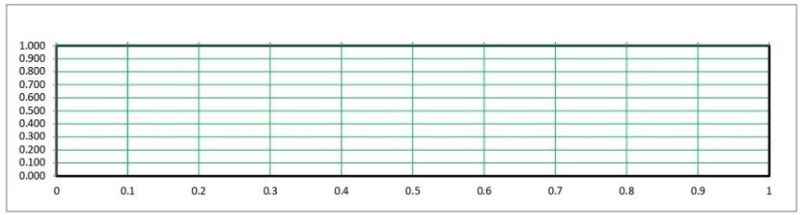

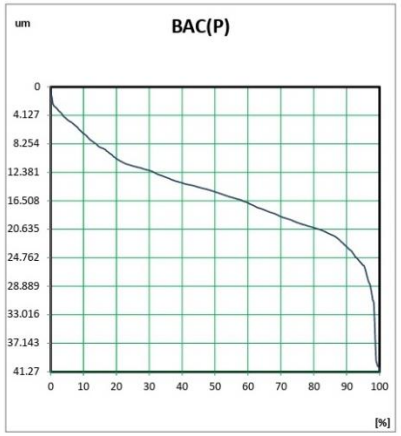

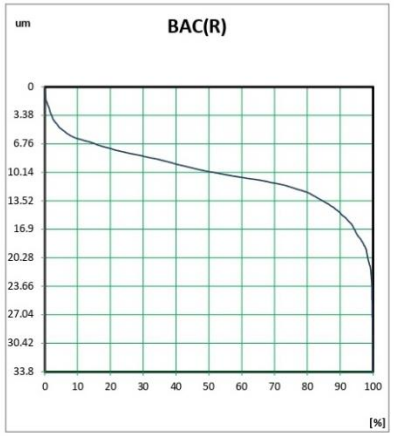

Appendix D -Gyroid | 40%

Prüfprotokoll

Seriennummer:		Kommentar		Messdatum	08.07.2022
Teilenummer		Prüfer	Kalhöfer	Messzeit	09:31:07

Messbedingung

Messtyp	Roughness measuremen	Cutoff	0,8mm	λs Filter	2,5um
Berechnungsstandard	ISO1997/2009	Filtermethode	Gaussian	Einheit	mm/um
Auswertelänge	4,00mm	Messbereich	500,0um		
Messgeschwindigkeit	0,30mm/s	Entfernen der Form	Straight		

Messergebnis

Pt	34,711	Ra_5	2,828	Rz_5	19,812
Ra	2,471	Rz	16,339	Rp	6,643
Ra_1	2,166	Rz_1	13,570	Rp_1	6,955
Ra_2	2,431	Rz_2	16,407	Rp_2	7,102
Ra_3	2,364	Rz_3	14,720	Rp_3	5,916
Ra_4	2,568	Rz_4	17,186	Rp_4	5,678

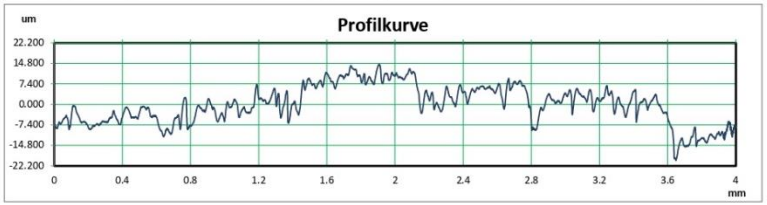

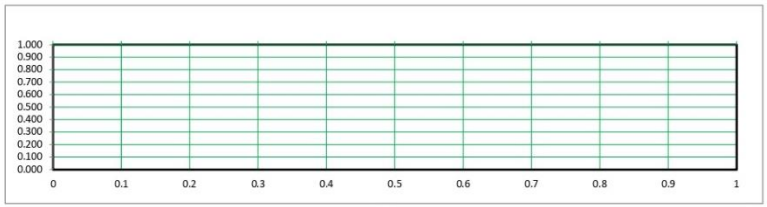

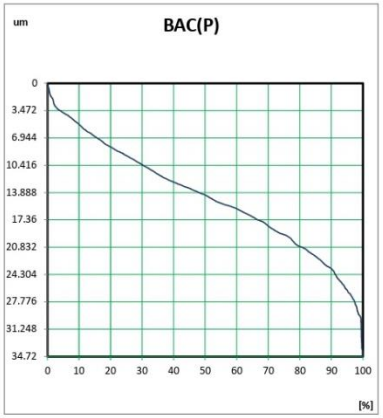

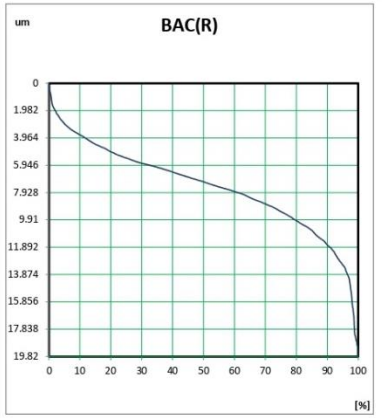

Prüfprotokoll

Seriennummer:		Kommentar		Messdatum	08.07.2022
Teilenummer		Prüfer	Kalhöfer	Messzeit	09:33:19

Messbedingung

Messtyp	Roughness measuremen	Cutoff	0,8mm	λs Filter	2,5um
Berechnungsstandard	ISO1997/2009	Filtermethode	Gaussian	Einheit	mm/um
Auswertelänge	4,00mm	Messbereich	500,0um		
Messgeschwindigkeit	0,30mm/s	Entfernen der Form	Straight		

Messergebnis

Pt	48,149	Ra_5	2,527	Rz_5	27,184
Ra	2,626	Rz	20,402	Rp	6,604
Ra_1	2,062	Rz_1	13,125	Rp_1	5,102
Ra_2	2,988	Rz_2	21,596	Rp_2	6,329
Ra_3	2,577	Rz_3	19,710	Rp_3	7,464
Ra_4	2,975	Rz_4	20,398	Rp_4	7,998

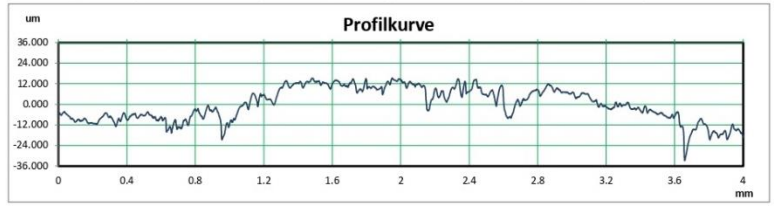

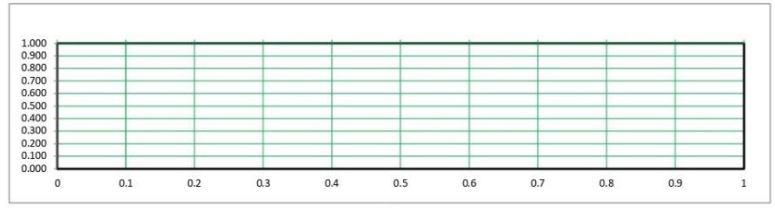

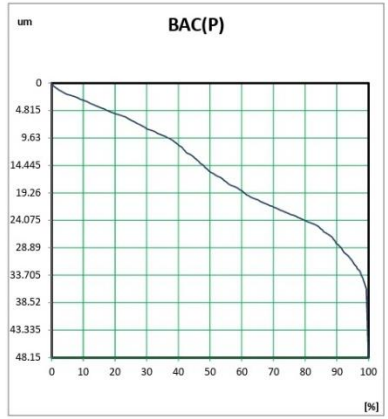

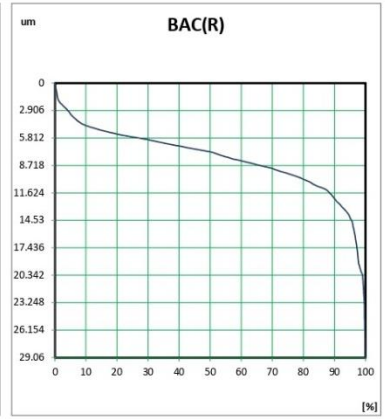

Prüfprotokoll

ACCRETECH

Seriennummer:		Kommentar		Messdatum	08.07.2022
Teilenummer		Prüfer	Kalhöfer	Messzeit	09:34:21

Messbedingung

Messtyp	Roughness measuremen	Cutoff	0,8mm	λs Filter	2,5um
Berechnungsstandard	ISO1997/2009	Filtermethode	Gaussian	Einheit	mm/um
Auswertelänge	4,00mm	Messbereich	500,0um		
Messgeschwindigkeit	0,30mm/s	Entfernen der Form	Straight		

Messergebnis

Pt	34,660	Ra_5	2,762	Rz_5	17,062
Ra	2,778	Rz	19,019	Rp	6,880
Ra_1	3,018	Rz_1	23,114	Rp_1	6,608
Ra_2	2,712	Rz_2	19,291	Rp_2	5,804
Ra_3	3,474	Rz_3	23,426	Rp_3	8,078
Ra_4	1,925	Rz_4	12,200	Rp_4	6,014

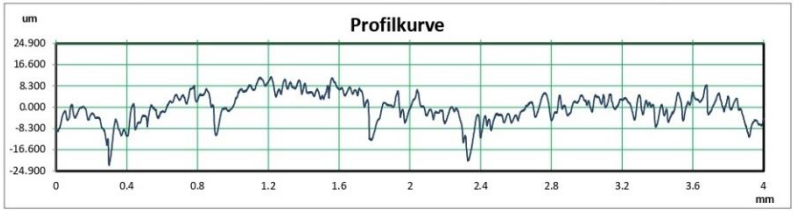

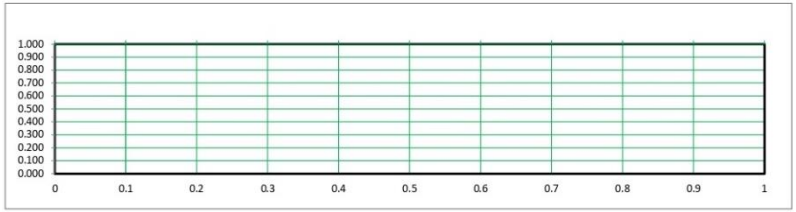

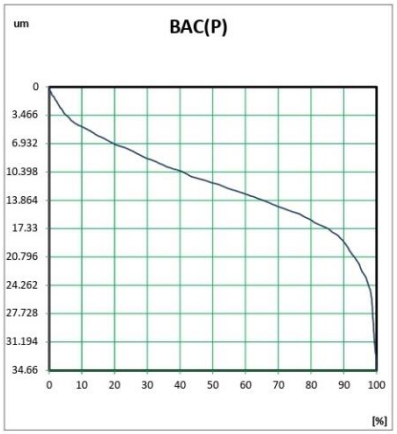

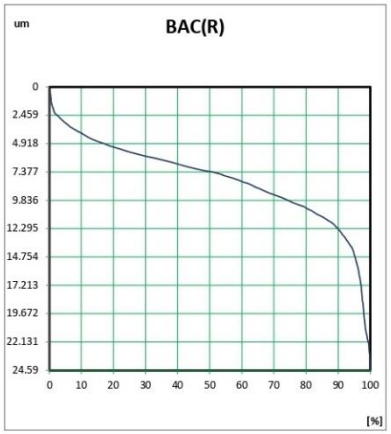

Prüfprotokoll

ACCRETECH

Seriennummer:		Kommentar		Messdatum	27.07.2022
Teilenummer		Prüfer	Kalhöfer	Messzeit	13:20:51

Messbedingung

Messtyp	Roughness measuremen	Cutoff	0,8mm	λs Filter	2,5um
Berechnungsstandard	ISO1997/2009	Filtermethode	Gaussian	Einheit	mm/um
Auswertelänge	4,00mm	Messbereich	500,0um		
Messgeschwindigkeit	0,30mm/s	Entfernen der Form	Straight		

Messergebnis

Pt	24,752	Ra_5	2,716	Rz_5	17,482
Ra	2,448	Rz	17,730	Rp	6,721
Ra_1	1,807	Rz_1	17,521	Rp_1	6,229
Ra_2	2,833	Rz_2	16,930	Rp_2	5,617
Ra_3	2,147	Rz_3	18,267	Rp_3	7,786
Ra_4	2,740	Rz_4	18,451	Rp_4	6,088

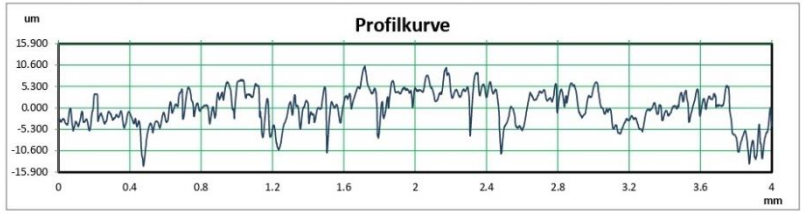

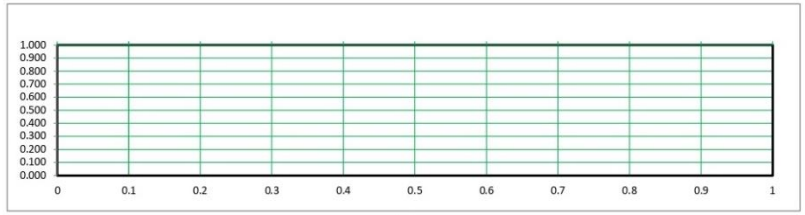

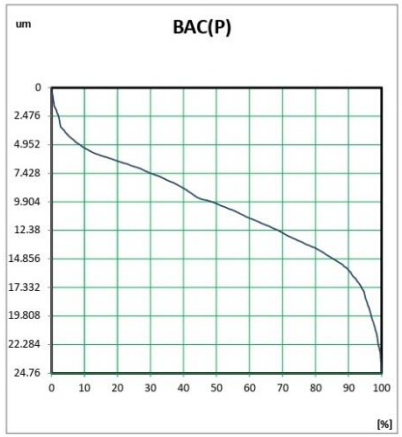

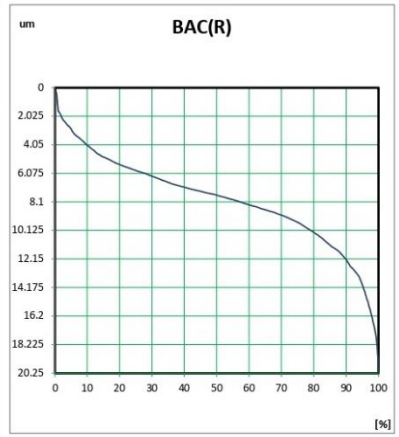

Prüfprotokoll

ACCRETECH

Seriennummer:		Kommentar		Messdatum	27.07.2022
Teilenummer		Prüfer	Kalhöfer	Messzeit	13:22:20

Messbedingung

Messtyp	Roughness measuremen	Cutoff	0,8mm	λs Filter	2,5um
Berechnungsstandard	ISO1997/2009	Filtermethode	Gaussian	Einheit	mm/um
Auswertelänge	4,00mm	Messbereich	500,0um		
Messgeschwindigkeit	0,30mm/s	Entfernen der Form	Straight		

Messergebnis

Pt	23,872	Ra_5	2,987	Rz_5	20,289
Ra	2,605	Rz	17,072	Rp	6,015
Ra_1	2,666	Rz_1	16,593	Rp_1	3,848
Ra_2	2,636	Rz_2	17,302	Rp_2	7,093
Ra_3	1,895	Rz_3	11,967	Rp_3	4,467
Ra_4	2,839	Rz_4	19,210	Rp_4	7,688

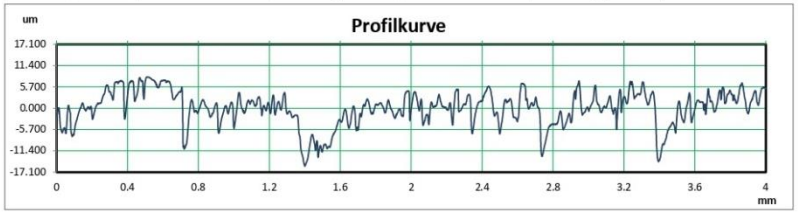

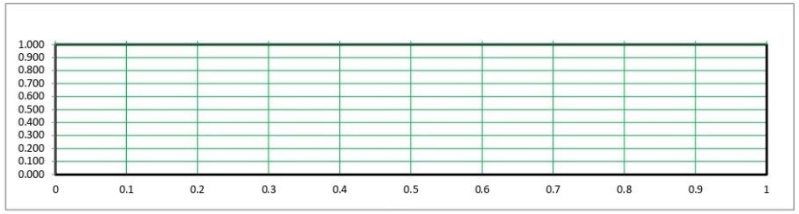

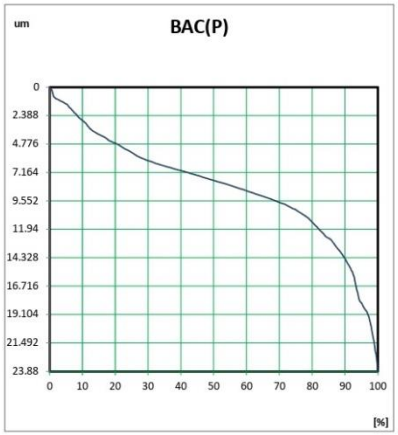

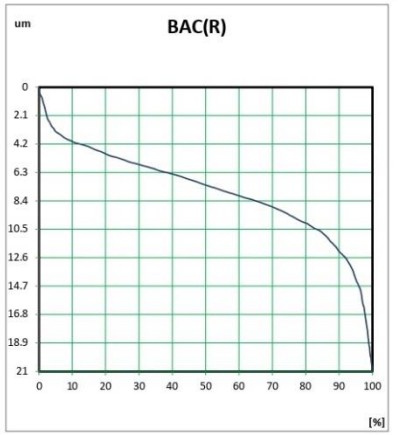

Prüfprotokoll

ACCRETECH

Seriennummer:		Kommentar		Messdatum	27.07.2022
Teilenummer		Prüfer	Kalhöfer	Messzeit	13:23:39

Messbedingung

Messtyp	Roughness measuremen	Cutoff	0,8mm	λs Filter	2,5um
Berechnungsstandard	ISO1997/2009	Filtermethode	Gaussian	Einheit	mm/um
Auswertelänge	4,00mm	Messbereich	500,0um		
Messgeschwindigkeit	0,30mm/s	Entfernen der Form	Straight		

Messergebnis

Pt	25,118	Ra_5	2,974	Rz_5	19,021
Ra	2,583	Rz	16,710	Rp	6,994
Ra_1	2,250	Rz_1	14,151	Rp_1	6,147
Ra_2	2,679	Rz_2	16,868	Rp_2	6,480
Ra_3	2,237	Rz_3	12,987	Rp_3	6,179
Ra_4	2,777	Rz_4	20,523	Rp_4	8,871

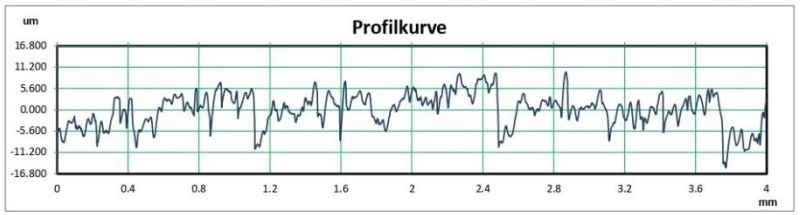

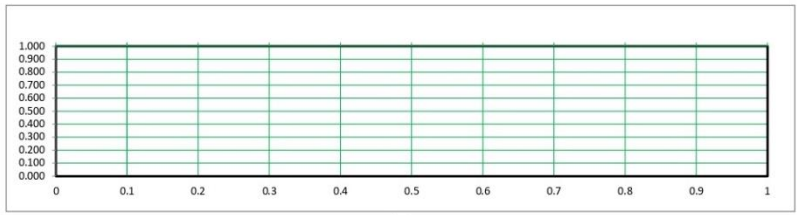

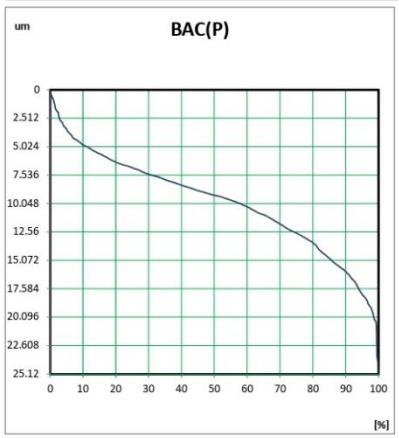

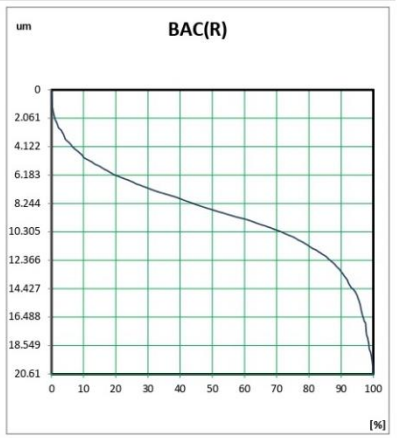

Prüfprotokoll

ACCRETECH

Seriennummer:		Kommentar		Messdatum	27.07.2022
Teilenummer		Prüfer	Kalhöfer	Messzeit	13:25:50

Messbedingung

Messtyp	Roughness measuremen	Cutoff	0,8mm	λs Filter	2,5um
Berechnungsstandard	ISO1997/2009	Filtermethode	Gaussian	Einheit	mm/um
Auswertelänge	4,00mm	Messbereich	500,0um		
Messgeschwindigkeit	0,30mm/s	Entfernen der Form	Straight		

Messergebnis

Pt	27,552	Ra_5	2,602	Rz_5	20,345
Ra	3,065	Rz	19,599	Rp	7,760
Ra_1	2,681	Rz_1	19,807	Rp_1	7,454
Ra_2	3,829	Rz_2	21,096	Rp_2	7,778
Ra_3	2,597	Rz_3	14,561	Rp_3	4,917
Ra_4	3,614	Rz_4	22,184	Rp_4	10,988

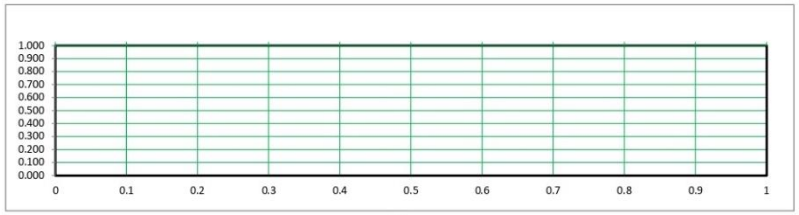

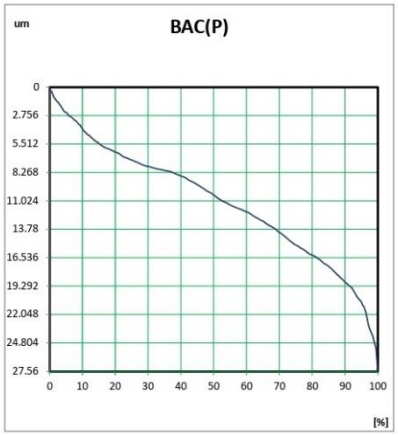

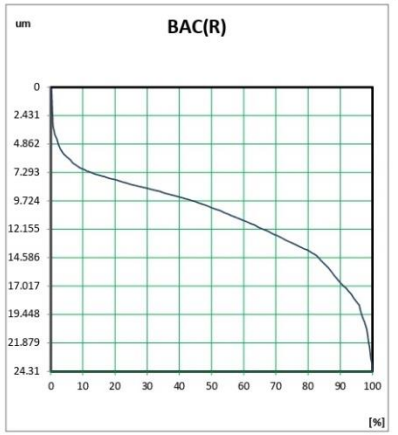

Prüfprotokoll

ACCRETECH

Seriennummer:		Kommentar		Messdatum	27.07.2022
Teilenummer		Prüfer	Kalhöfer	Messzeit	13:26:51

Messbedingung

Messtyp	Roughness measuremen	Cutoff	0,8mm	λs Filter	2,5um
Berechnungsstandard	ISO1997/2009	Filtermethode	Gaussian	Einheit	mm/um
Auswertelänge	4,00mm	Messbereich	500,0um		
Messgeschwindigkeit	0,30mm/s	Entfernen der Form	Straight		

Messergebnis

Pt	26,719	Ra_5	2,644	Rz_5	17,236
Ra	2,524	Rz	17,976	Rp	6,918
Ra_1	2,530	Rz_1	15,563	Rp_1	5,605
Ra_2	2,143	Rz_2	13,818	Rp_2	5,322
Ra_3	2,626	Rz_3	28,278	Rp_3	10,319
Ra_4	2,675	Rz_4	14,984	Rp_4	6,453

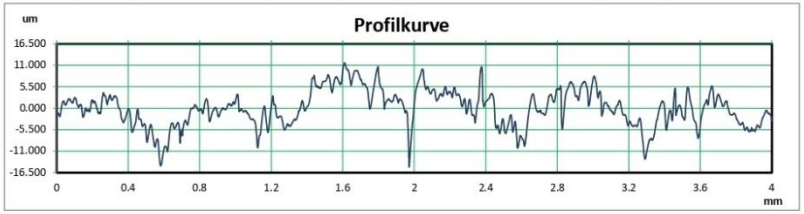

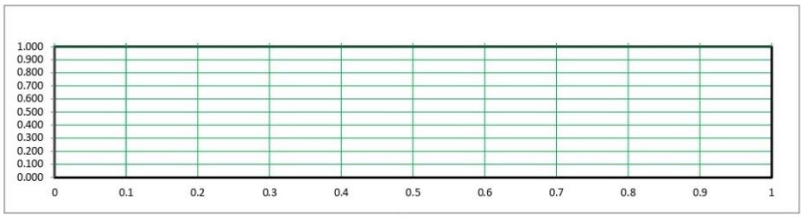

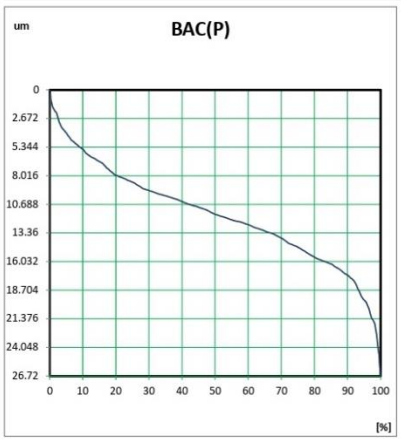

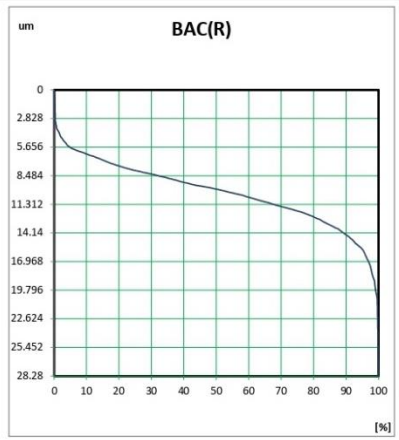

Prüfprotokoll

ACCRETECH

Seriennummer:		Kommentar		Messdatum	27.07.2022
Teilenummer		Prüfer	Kalhöfer	Messzeit	13:28:39

Messbedingung

Messtyp	Roughness measuremen	Cutoff	0,8mm	λs Filter	2,5um
Berechnungsstandard	ISO1997/2009	Filtermethode	Gaussian	Einheit	mm/um
Auswertelänge	4,00mm	Messbereich	500,0um		
Messgeschwindigkeit	0,30mm/s	Entfernen der Form	Straight		

Messergebnis

Pt	38,944	Ra_5	2,950	Rz_5	18,051
Ra	2,889	Rz	21,806	Rp	6,702
Ra_1	2,965	Rz_1	28,516	Rp_1	7,560
Ra_2	2,188	Rz_2	12,527	Rp_2	6,083
Ra_3	3,425	Rz_3	19,290	Rp_3	5,658
Ra_4	2,919	Rz_4	30,646	Rp_4	6,253

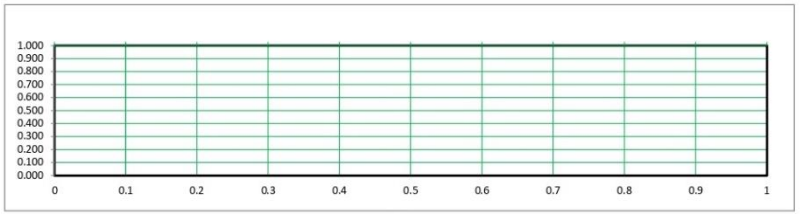

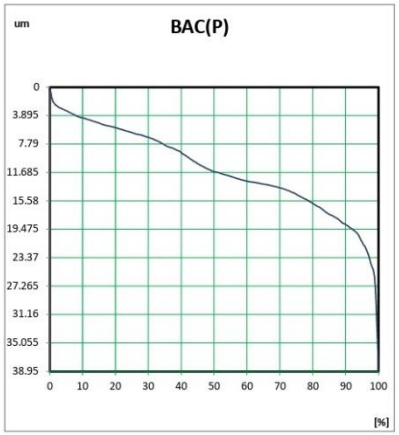

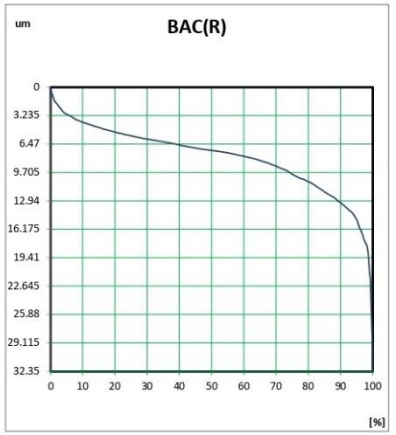

Appendix E – Gyroid | 25%

Prüfprotokoll

Seriennummer:		Kommentar		Messdatum	08.07.2022
Teilenummer		Prüfer	Kalhöfer	Messzeit	09:38:51

Messbedingung

Messtyp	Roughness measuremen	Cutoff	0,8mm	λs Filter	2,5um
Berechnungsstandard	ISO1997/2009	Filtermethode	Gaussian	Einheit	mm/um
Auswertelänge	4,00mm	Messbereich	500,0um		
Messgeschwindigkeit	0,30mm/s	Entfernen der Form	Straight		

Messergebnis

Pt	69,216	Ra_5	3,415	Rz_5	33,322
Ra	3,857	Rz	33,167	Rp	8,501
Ra_1	4,779	Rz_1	45,390	Rp_1	8,546
Ra_2	3,162	Rz_2	28,896	Rp_2	8,380
Ra_3	5,688	Rz_3	43,383	Rp_3	9,791
Ra_4	2,244	Rz_4	14,844	Rp_4	8,313

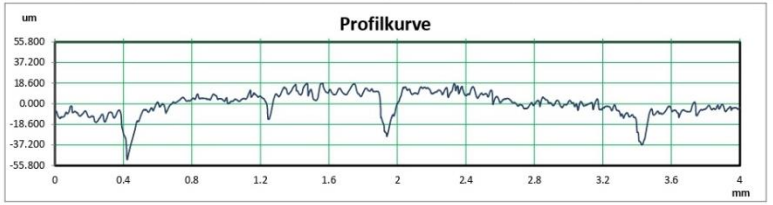

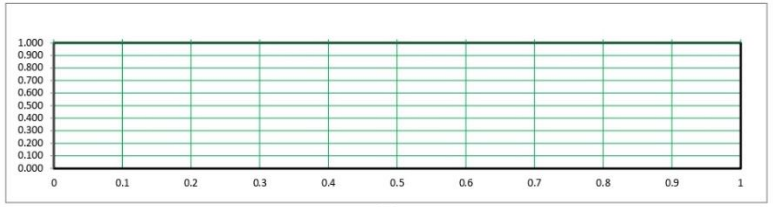

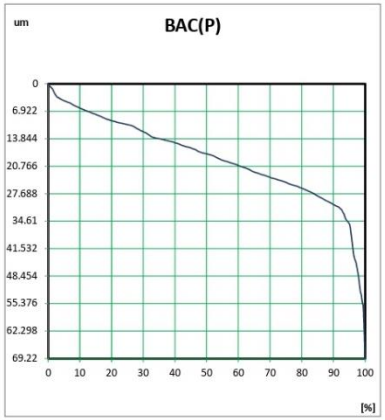

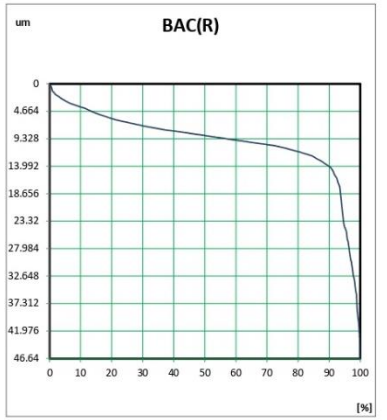

Prüfprotokoll

Seriennummer:		Kommentar		Messdatum	08.07.2022
Teilenummer		Prüfer	Kalhöfer	Messzeit	09:40:22

Messbedingung

Messtyp	Roughness measuremen	Cutoff	0,8mm	λs Filter	2,5um
Berechnungsstandard	ISO1997/2009	Filtermethode	Gaussian	Einheit	mm/um
Auswertelänge	4,00mm	Messbereich	500,0um		
Messgeschwindigkeit	0,30mm/s	Entfernen der Form	Straight		

Messergebnis

Pt	57,289	Ra_5	5,023	Rz_5	40,967
Ra	3,969	Rz	33,183	Rp	10,899
Ra_1	5,424	Rz_1	49,028	Rp_1	11,914
Ra_2	2,842	Rz_2	18,761	Rp_2	9,126
Ra_3	4,003	Rz_3	37,121	Rp_3	9,896
Ra_4	2,552	Rz_4	20,038	Rp_4	11,395

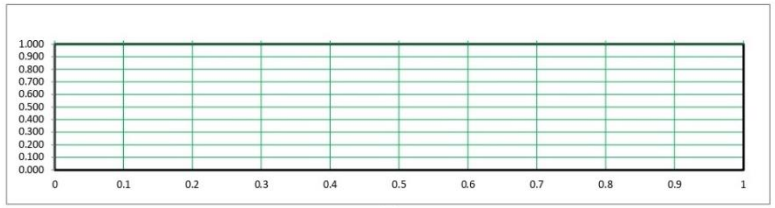

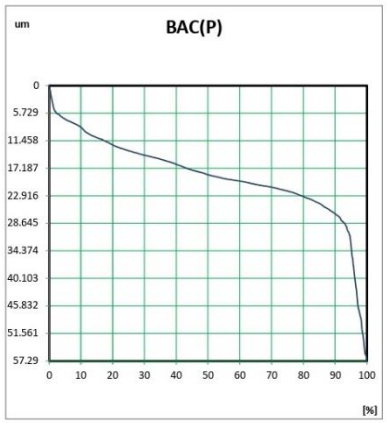

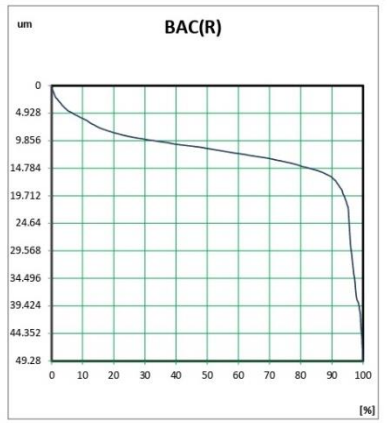

Prüfprotokoll

ACCRETECH

Seriennummer:		Kommentar		Messdatum	08.07.2022
Teilenummer		Prüfer	Kalhöfer	Messzeit	09:41:20

Messbedingung

Messtyp	Roughness measuremen	Cutoff	0,8mm	λs Filter	2,5um
Berechnungsstandard	ISO1997/2009	Filtermethode	Gaussian	Einheit	mm/um
Auswertelänge	4,00mm	Messbereich	500,0um		
Messgeschwindigkeit	0,30mm/s	Entfernen der Form	Straight		

Messergebnis

Pt	62,645	Ra_5	3,855	Rz_5	36,625
Ra	3,825	Rz	28,991	Rp	8,831
Ra_1	4,976	Rz_1	36,574	Rp_1	11,176
Ra_2	2,767	Rz_2	18,433	Rp_2	8,562
Ra_3	5,112	Rz_3	38,200	Rp_3	10,851
Ra_4	2,413	Rz_4	15,123	Rp_4	6,333

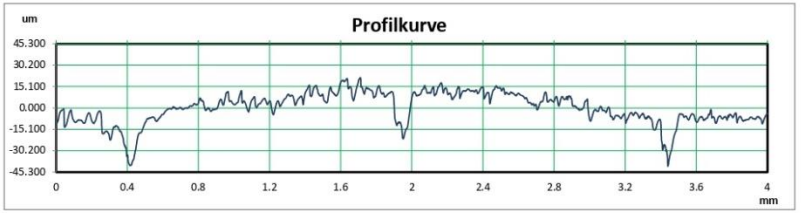

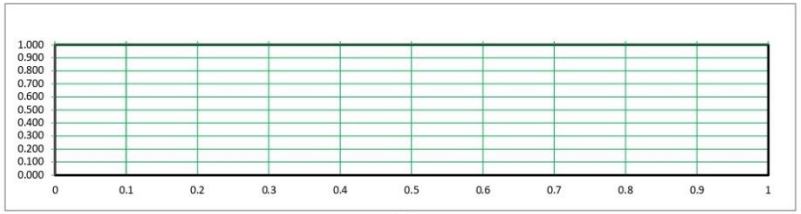

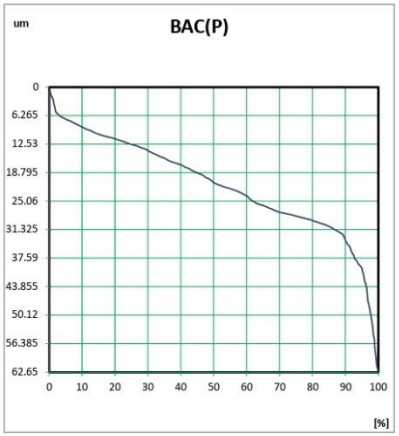

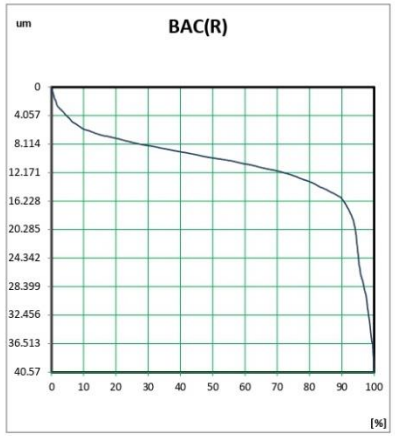

Prüfprotokoll

ACCRETECH

Seriennummer:		Kommentar		Messdatum	27.07.2022
Teilenummer		Prüfer	Kalhöfer	Messzeit	13:02:04

Messbedingung

Messtyp	Roughness measuremen	Cutoff	0,8mm	λs Filter	2,5um
Berechnungsstandard	ISO1997/2009	Filtermethode	Gaussian	Einheit	mm/um
Auswertelänge	4,00mm	Messbereich	500,0um		
Messgeschwindigkeit	0,30mm/s	Entfernen der Form	Straight		

Messergebnis

Pt	39,993	Ra_5	3,937	Rz_5	28,034
Ra	3,624	Rz	26,550	Rp	8,938
Ra_1	4,113	Rz_1	33,620	Rp_1	10,232
Ra_2	2,424	Rz_2	16,439	Rp_2	8,256
Ra_3	4,273	Rz_3	30,199	Rp_3	7,923
Ra_4	3,370	Rz_4	24,456	Rp_4	9,039

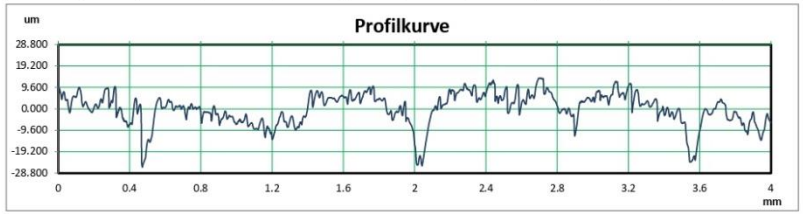

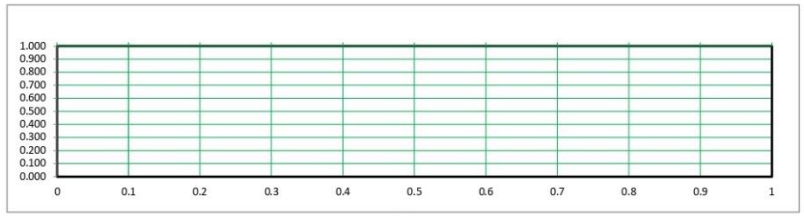

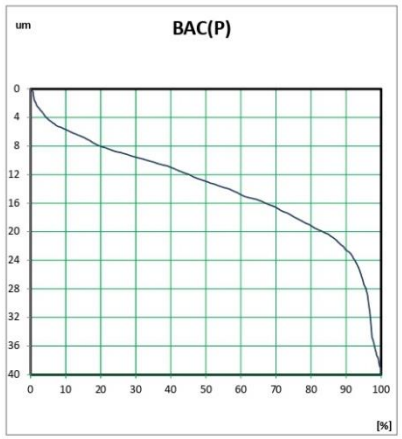

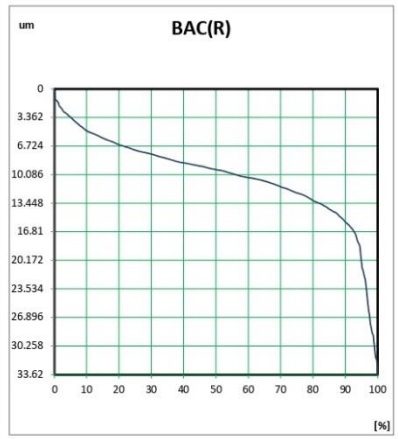

Prüfprotokoll

ACCRETECH

Seriennummer:		Kommentar		Messdatum	27.07.2022
Teilenummer		Prüfer	Kalhöfer	Messzeit	13:03:35

Messbedingung

Messtyp	Roughness measuremen	Cutoff	0,8mm	λs Filter	2,5um
Berechnungsstandard	ISO1997/2009	Filtermethode	Gaussian	Einheit	mm/um
Auswertelänge	4,00mm	Messbereich	500,0um		
Messgeschwindigkeit	0,30mm/s	Entfernen der Form	Straight		

Messergebnis

Pt	45,136	Ra_5	2,761	Rz_5	19,040
Ra	3,914	Rz	27,679	Rp	9,369
Ra_1	3,639	Rz_1	37,961	Rp_1	10,934
Ra_2	5,005	Rz_2	31,414	Rp_2	11,552
Ra_3	3,942	Rz_3	20,172	Rp_3	10,228
Ra_4	4,221	Rz_4	29,809	Rp_4	7,440

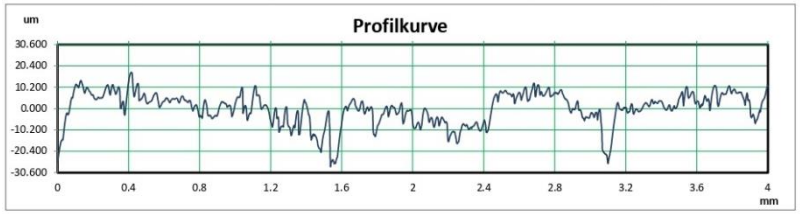

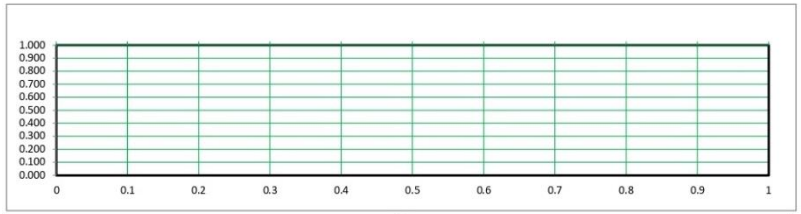

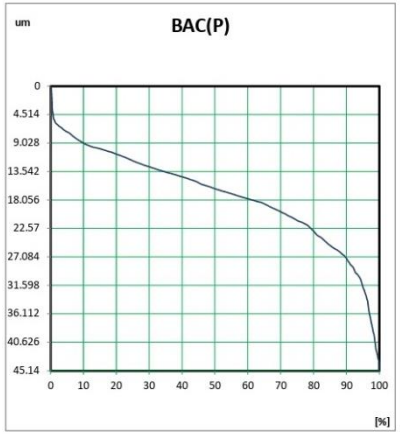

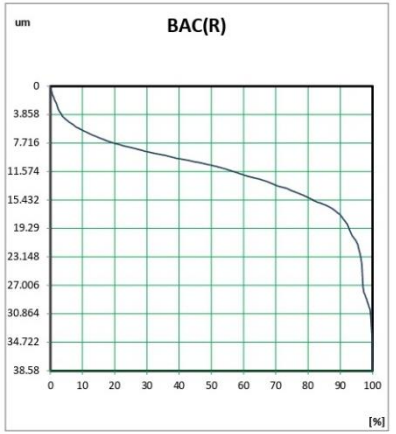

Prüfprotokoll

ACCRETECH

Seriennummer:		Kommentar		Messdatum	27.07.2022
Teilenummer		Prüfer	Kalhöfer	Messzeit	13:04:52

Messbedingung

Messtyp	Roughness measuremen	Cutoff	0,8mm	λs Filter	2,5um
Berechnungsstandard	ISO1997/2009	Filtermethode	Gaussian	Einheit	mm/um
Auswertelänge	4,00mm	Messbereich	500,0um		
Messgeschwindigkeit	0,30mm/s	Entfernen der Form	Straight		

Messergebnis

Pt	51,976	Ra_5	4,151	Rz_5	33,279
Ra	3,442	Rz	22,743	Rp	8,775
Ra_1	4,667	Rz_1	26,329	Rp_1	9,560
Ra_2	2,350	Rz_2	14,613	Rp_2	7,939
Ra_3	3,610	Rz_3	26,727	Rp_3	10,475
Ra_4	2,430	Rz_4	12,765	Rp_4	5,667

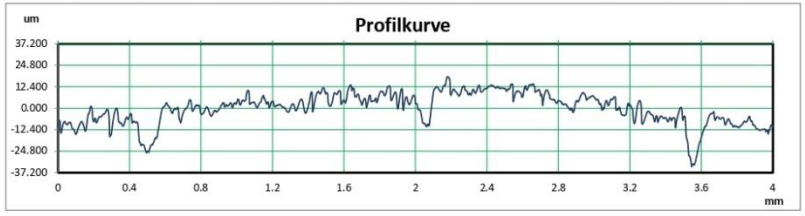

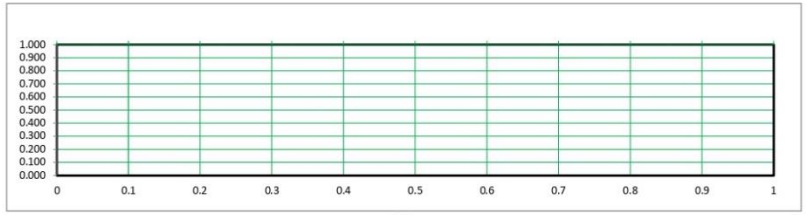

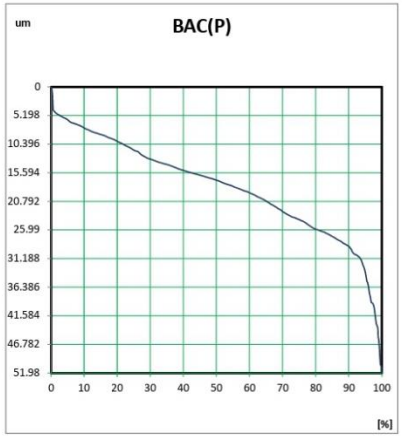

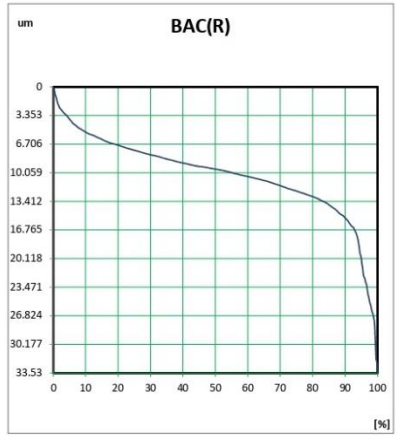

Prüfprotokoll

ACCRETECH

Seriennummer:		Kommentar		Messdatum	27.07.2022
Teilenummer		Prüfer	Kalhöfer	Messzeit	13:15:44

Messbedingung

Messtyp	Roughness measuremen	Cutoff	0,8mm	λs Filter	2,5um
Berechnungsstandard	ISO1997/2009	Filtermethode	Gaussian	Einheit	mm/um
Auswertelänge	4,00mm	Messbereich	500,0um		
Messgeschwindigkeit	0,30mm/s	Entfernen der Form	Straight		

Messergebnis

Pt	35,778	Ra_5	3,087	Rz_5	20,644
Ra	2,943	Rz	20,377	Rp	7,691
Ra_1	2,775	Rz_1	17,579	Rp_1	8,447
Ra_2	2,914	Rz_2	16,649	Rp_2	7,801
Ra_3	2,920	Rz_3	19,700	Rp_3	7,421
Ra_4	3,020	Rz_4	27,312	Rp_4	8,014

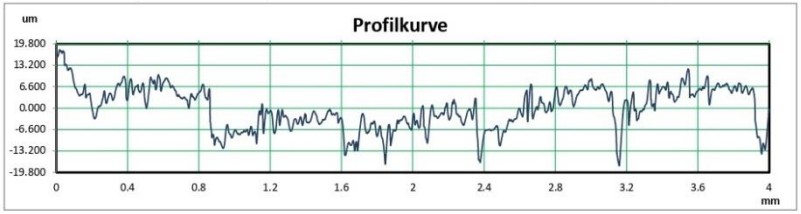

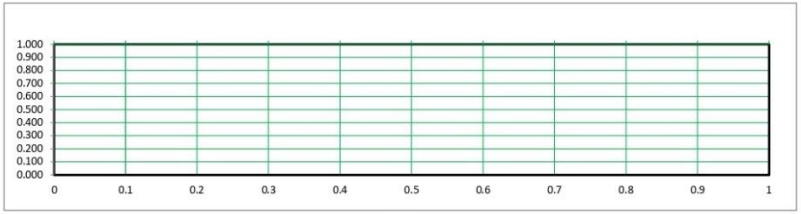

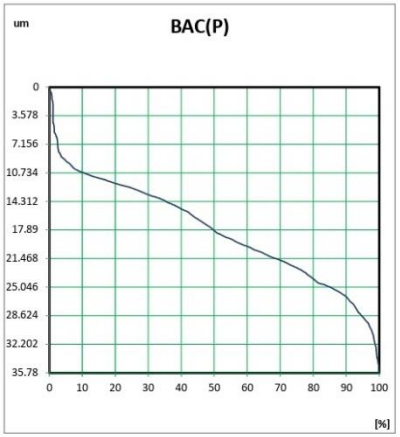

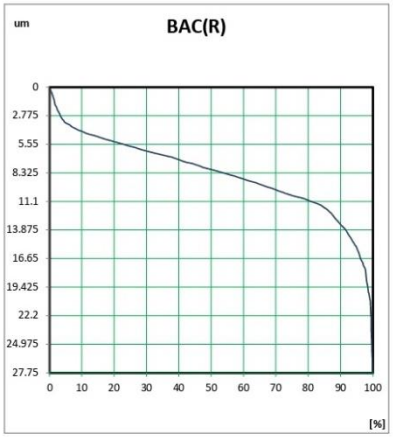

Prüfprotokoll

ACCRETECH

Seriennummer:		Kommentar		Messdatum	27.07.2022
Teilenummer		Prüfer	Kalhöfer	Messzeit	13:16:53

Messbedingung

Messtyp	Roughness measuremen	Cutoff	0,8mm	λs Filter	2,5um
Berechnungsstandard	ISO1997/2009	Filtermethode	Gaussian	Einheit	mm/um
Auswertelänge	4,00mm	Messbereich	500,0um		
Messgeschwindigkeit	0,30mm/s	Entfernen der Form	Straight		

Messergebnis

Pt	51,378	Ra_5	3,698	Rz_5	29,207
Ra	3,915	Rz	29,080	Rp	8,143
Ra_1	3,180	Rz_1	22,566	Rp_1	9,070
Ra_2	4,843	Rz_2	33,917	Rp_2	8,420
Ra_3	4,085	Rz_3	28,053	Rp_3	7,824
Ra_4	3,769	Rz_4	31,656	Rp_4	8,154

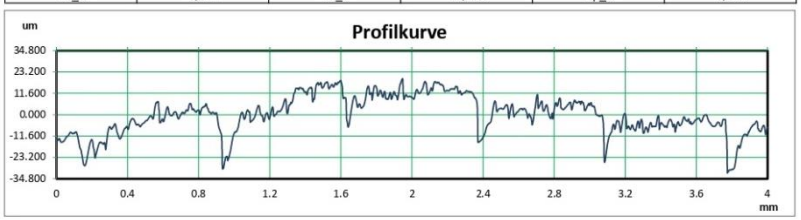

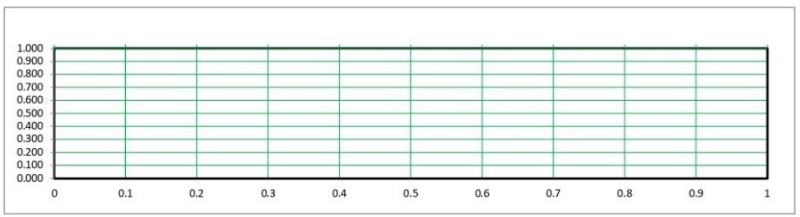

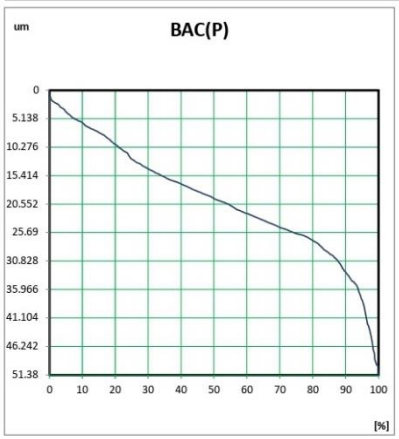

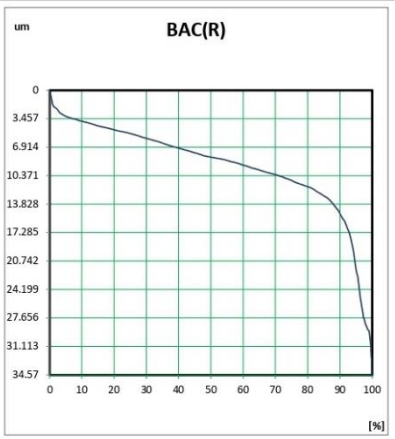

Prüfprotokoll

ACCRETECH

Seriennummer:		Kommentar		Messdatum	27.07.2022
Teilenummer		Prüfer	Kalhöfer	Messzeit	13:17:55

Messbedingung

Messtyp	Roughness measuremen	Cutoff	0,8mm	λs Filter	2,5um
Berechnungsstandard	ISO1997/2009	Filtermethode	Gaussian	Einheit	mm/um
Auswertelänge	4,00mm	Messbereich	500,0um		
Messgeschwindigkeit	0,30mm/s	Entfernen der Form	Straight		

Messergebnis

Pt	52,189	Ra_5	2,961	Rz_5	20,310
Ra	3,531	Rz	27,744	Rp	8,325
Ra_1	3,103	Rz_1	18,120	Rp_1	7,209
Ra_2	4,140	Rz_2	41,337	Rp_2	7,956
Ra_3	3,754	Rz_3	23,072	Rp_3	9,123
Ra_4	3,698	Rz_4	35,883	Rp_4	9,709

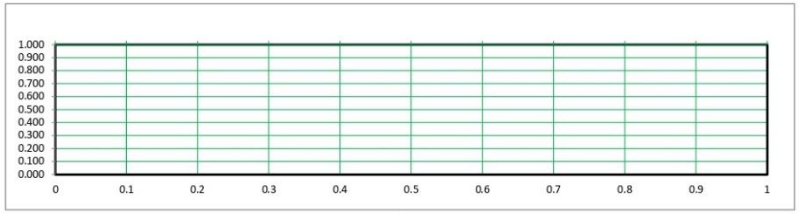

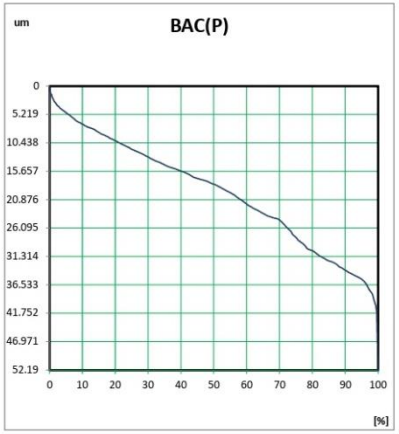

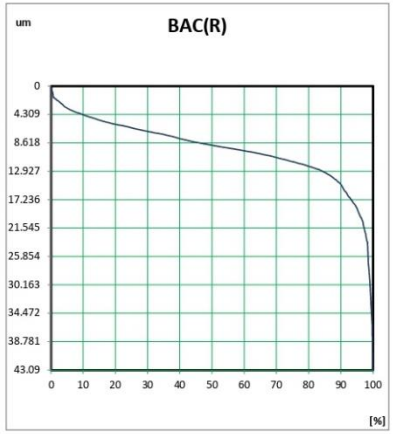

Appendix F - Quarter Cubic | 25%

Prüfprotokoll

Seriennummer:		Kommentar		Messdatum	08.07.2022
Teilenummer		Prüfer	Kalhöfer	Messzeit	09:21:52

Messbedingung

Messtyp	Roughness measuremen	Cutoff	0,8mm	λs Filter	2,5um
Berechnungsstandard	ISO1997/2009	Filtermethode	Gaussian	Einheit	mm/um
Auswertelänge	4,00mm	Messbereich	500,0um		
Messgeschwindigkeit	0,30mm/s	Entfernen der Form	Straight		

Messergebnis

Pt	48,314	Ra_5	3,238	Rz_5	24,229
Ra	2,889	Rz	20,147	Rp	7,551
Ra_1	2,711	Rz_1	18,178	Rp_1	8,399
Ra_2	3,282	Rz_2	28,380	Rp_2	8,040
Ra_3	2,197	Rz_3	12,764	Rp_3	7,586
Ra_4	3,019	Rz_4	17,185	Rp_4	6,926

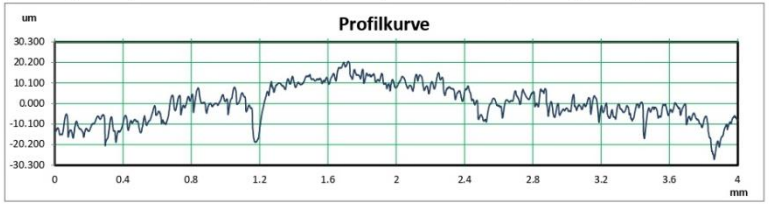

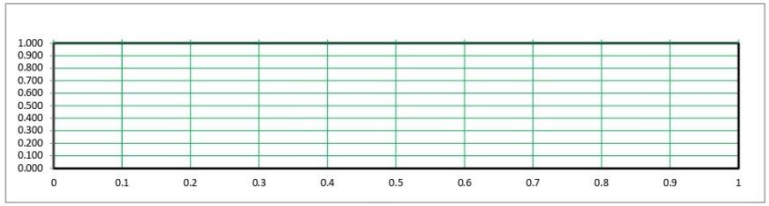

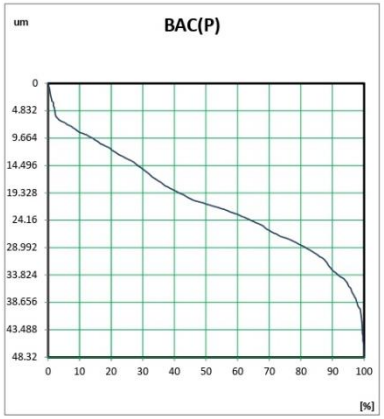

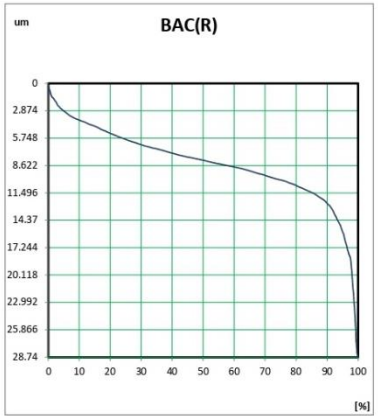

Prüfprotokoll

Seriennummer:		Kommentar		Messdatum	08.07.2022
Teilenummer		Prüfer	Kalhöfer	Messzeit	09:26:29

Messbedingung

Messtyp	Roughness measuremen	Cutoff	0,8mm	λs Filter	2,5um
Berechnungsstandard	ISO1997/2009	Filtermethode	Gaussian	Einheit	mm/um
Auswertelänge	4,00mm	Messbereich	500,0um		
Messgeschwindigkeit	0,30mm/s	Entfernen der Form	Straight		

Messergebnis

Pt	52,748	Ra_5	3,844	Rz_5	32,633
Ra	3,353	Rz	24,112	Rp	8,462
Ra_1	2,696	Rz_1	19,052	Rp_1	9,014
Ra_2	3,588	Rz_2	27,161	Rp_2	6,886
Ra_3	4,416	Rz_3	28,623	Rp_3	11,451
Ra_4	2,221	Rz_4	13,091	Rp_4	6,396

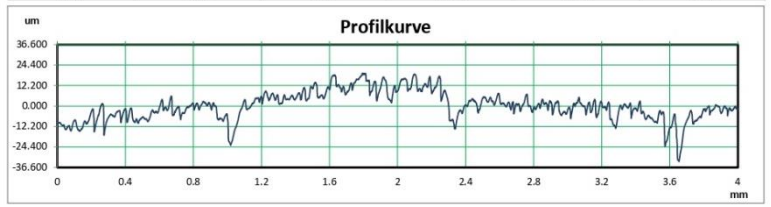

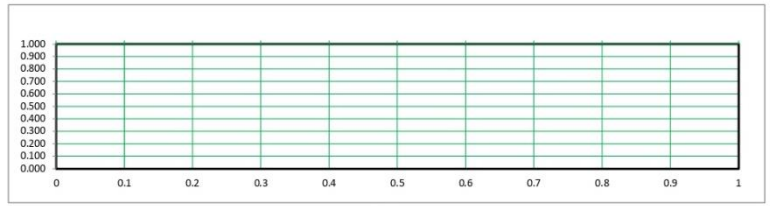

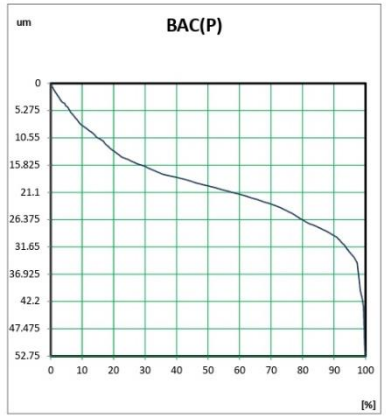

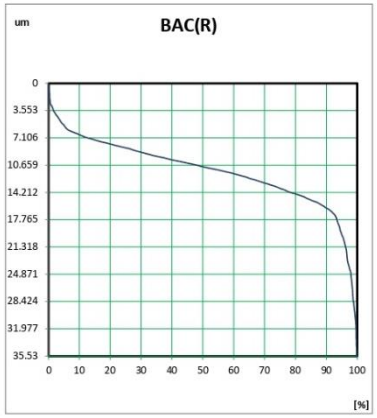

Prüfprotokoll

ACCRETECH

Seriennummer:		Kommentar		Messdatum	08.07.2022
Teilenummer		Prüfer	Kalhöfer	Messzeit	09:27:25

Messbedingung

Messtyp	Roughness measuremen	Cutoff	0,8mm	λs Filter	2,5um
Berechnungsstandard	ISO1997/2009	Filtermethode	Gaussian	Einheit	mm/um
Auswertelänge	4,00mm	Messbereich	500,0um		
Messgeschwindigkeit	0,30mm/s	Entfernen der Form	Straight		

Messergebnis

Pt	36,541	Ra_5	3,337	Rz_5	22,270
Ra	3,077	Rz	22,356	Rp	8,026
Ra_1	2,650	Rz_1	16,258	Rp_1	8,490
Ra_2	3,821	Rz_2	35,648	Rp_2	10,388
Ra_3	3,078	Rz_3	19,194	Rp_3	7,763
Ra_4	2,499	Rz_4	18,407	Rp_4	5,017

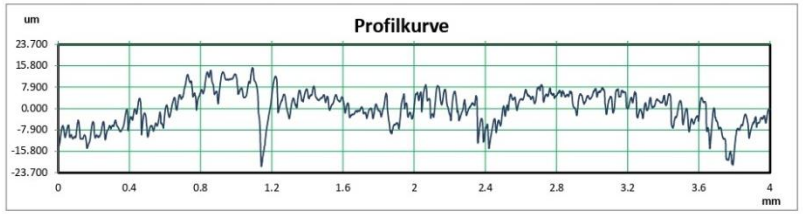

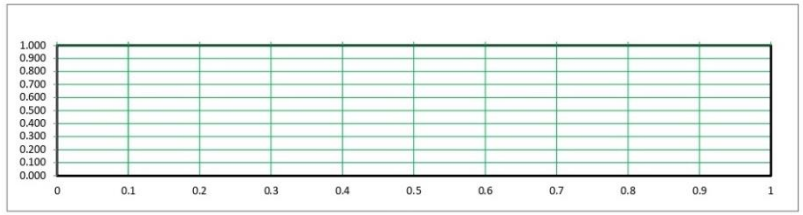

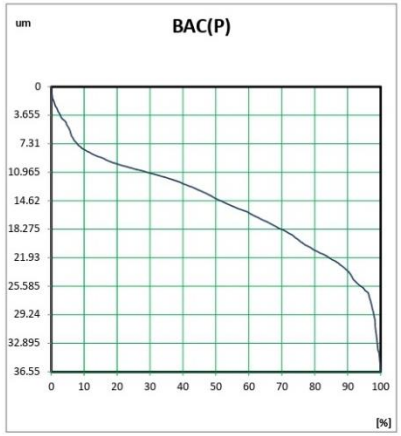

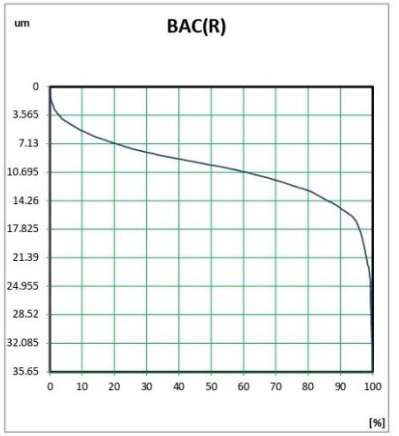

Prüfprotokoll

ACCRETECH

Seriennummer:		Kommentar		Messdatum	27.07.2022
Teilenummer		Prüfer	Kalhöfer	Messzeit	12:33:07

Messbedingung

Messtyp	Roughness measuremen	Cutoff	0,8mm	λs Filter	2,5um
Berechnungsstandard	ISO1997/2009	Filtermethode	Gaussian	Einheit	mm/um
Auswertelänge	4,00mm	Messbereich	500,0um		
Messgeschwindigkeit	0,30mm/s	Entfernen der Form	Straight		

Messergebnis

Pt	93,571	Ra_5	3,863	Rz_5	40,998
Ra	3,140	Rz	27,144	Rp	10,349
Ra_1	2,682	Rz_1	26,904	Rp_1	11,220
Ra_2	3,072	Rz_2	20,825	Rp_2	7,151
Ra_3	2,961	Rz_3	19,441	Rp_3	9,422
Ra_4	3,124	Rz_4	27,553	Rp_4	13,536

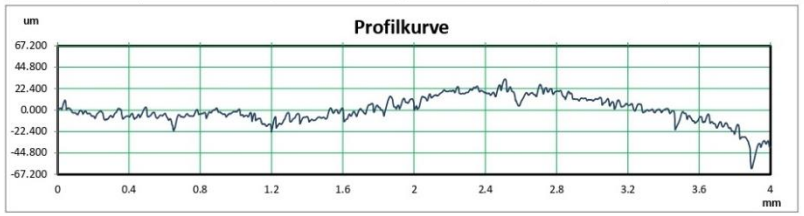

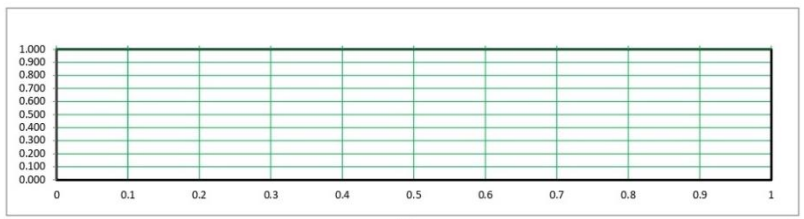

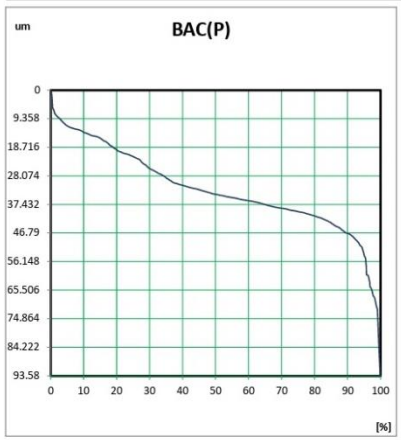

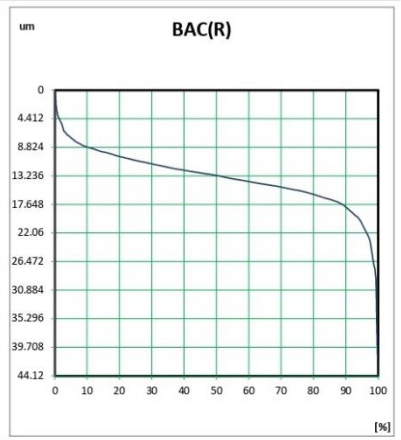

Prüfprotokoll

ACCRETECH

Seriennummer:		Kommentar		Messdatum	27.07.2022
Teilenummer		Prüfer	Kalhöfer	Messzeit	12:37:04

Messbedingung

Messtyp	Roughness measuremen	Cutoff	0,8mm	λs Filter	2,5um
Berechnungsstandard	ISO1997/2009	Filtermethode	Gaussian	Einheit	mm/um
Auswertelänge	4,00mm	Messbereich	500,0um		
Messgeschwindigkeit	0,30mm/s	Entfernen der Form	Straight		

Messergebnis

Pt	82,253	Ra_5	3,507	Rz_5	37,139
Ra	3,362	Rz	28,766	Rp	10,995
Ra_1	3,515	Rz_1	32,844	Rp_1	8,530
Ra_2	2,535	Rz_2	18,510	Rp_2	8,910
Ra_3	4,407	Rz_3	37,204	Rp_3	13,320
Ra_4	2,845	Rz_4	18,135	Rp_4	11,751

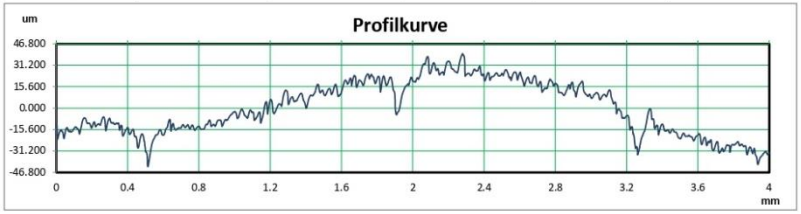

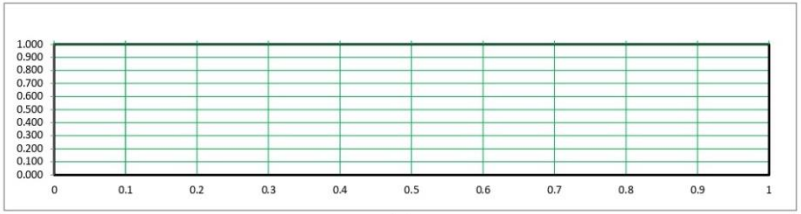

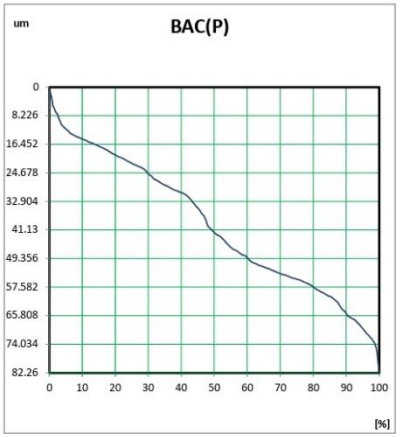

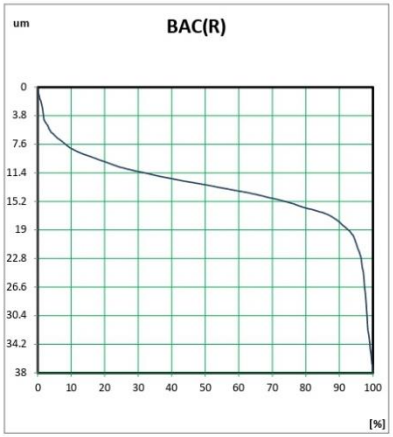

Prüfprotokoll

ACCRETECH

Seriennummer:		Kommentar		Messdatum	27.07.2022
Teilenummer		Prüfer	Kalhöfer	Messzeit	12:38:34

Messbedingung

Messtyp	Roughness measuremen	Cutoff	0,8mm	λs Filter	2,5um
Berechnungsstandard	ISO1997/2009	Filtermethode	Gaussian	Einheit	mm/um
Auswertelänge	4,00mm	Messbereich	500,0um		
Messgeschwindigkeit	0,30mm/s	Entfernen der Form	Straight		

Messergebnis

Pt	60,397	Ra_5	2,627	Rz_5	19,262
Ra	3,333	Rz	27,448	Rp	9,823
Ra_1	3,825	Rz_1	44,004	Rp_1	18,312
Ra_2	3,647	Rz_2	19,592	Rp_2	7,859
Ra_3	3,525	Rz_3	36,412	Rp_3	6,600
Ra_4	3,041	Rz_4	17,972	Rp_4	8,125

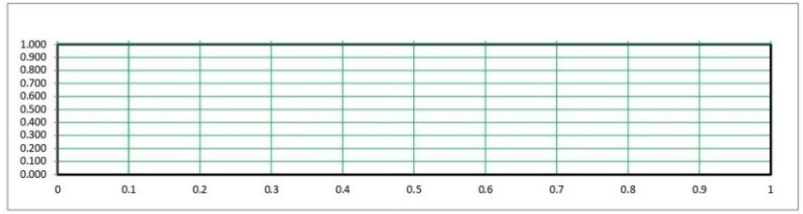

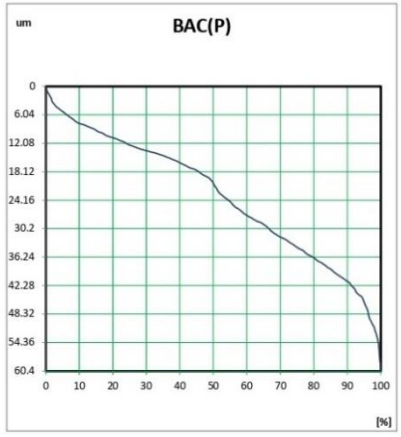

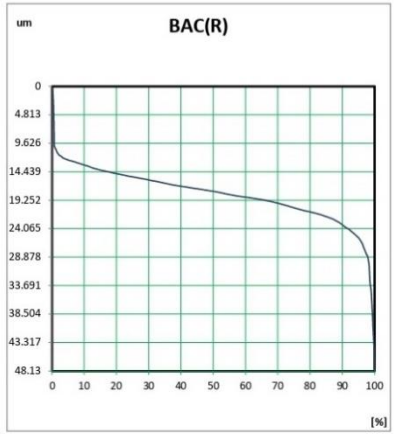

Prüfprotokoll

ACCRETECH

Seriennummer:		Kommentar		Messdatum	27.07.2022
Teilenummer		Prüfer	Kalhöfer	Messzeit	12:41:40

Messbedingung

Messtyp	Roughness measuremen	Cutoff	0,8mm	λs Filter	2,5um
Berechnungsstandard	ISO1997/2009	Filtermethode	Gaussian	Einheit	mm/um
Auswertelänge	4,00mm	Messbereich	500,0um		
Messgeschwindigkeit	0,30mm/s	Entfernen der Form	Straight		

Messergebnis

Pt	56,802	Ra_5	2,368	Rz_5	14,029
Ra	3,395	Rz	26,482	Rp	7,990
Ra_1	3,324	Rz_1	27,502	Rp_1	10,275
Ra_2	2,118	Rz_2	12,928	Rp_2	6,270
Ra_3	5,027	Rz_3	35,060	Rp_3	8,853
Ra_4	4,136	Rz_4	42,892	Rp_4	7,380

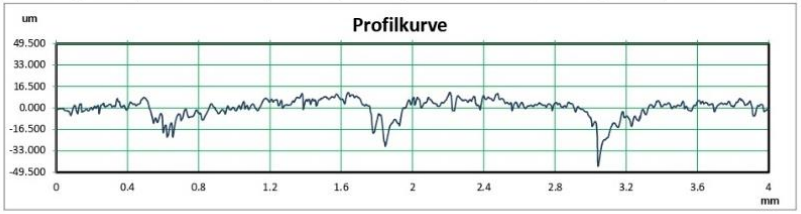

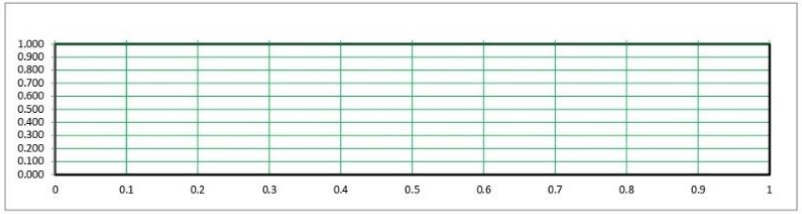

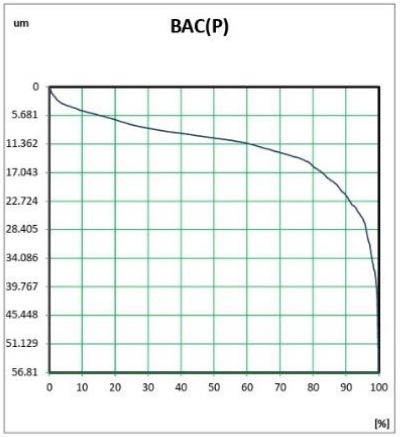

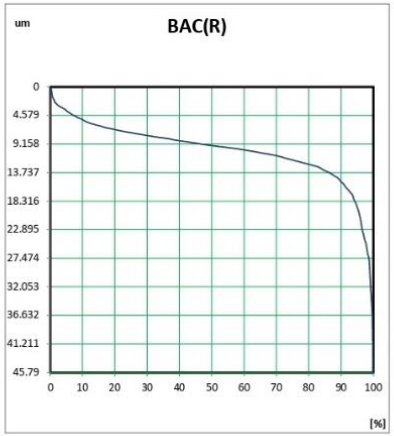

Prüfprotokoll

ACCRETECH

Seriennummer:		Kommentar		Messdatum	27.07.2022
Teilenummer		Prüfer	Kalhöfer	Messzeit	12:44:56

Messbedingung

Messtyp	Roughness measuremen	Cutoff	0,8mm	λs Filter	2,5um
Berechnungsstandard	ISO1997/2009	Filtermethode	Gaussian	Einheit	mm/um
Auswertelänge	4,00mm	Messbereich	500,0um		
Messgeschwindigkeit	0,30mm/s	Entfernen der Form	Straight		

Messergebnis

Pt	46,037	Ra_5	3,382	Rz_5	27,002
Ra	2,926	Rz	27,813	Rp	8,043
Ra_1	2,785	Rz_1	29,832	Rp_1	5,283
Ra_2	2,847	Rz_2	28,654	Rp_2	5,818
Ra_3	1,993	Rz_3	18,035	Rp_3	5,895
Ra_4	3,623	Rz_4	35,539	Rp_4	15,845

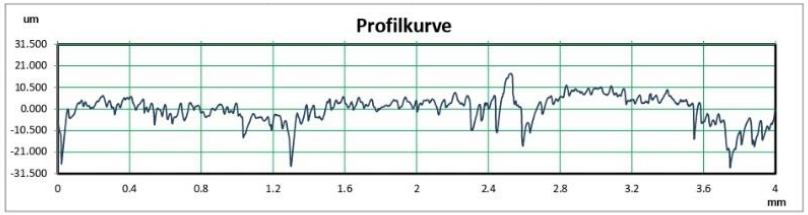

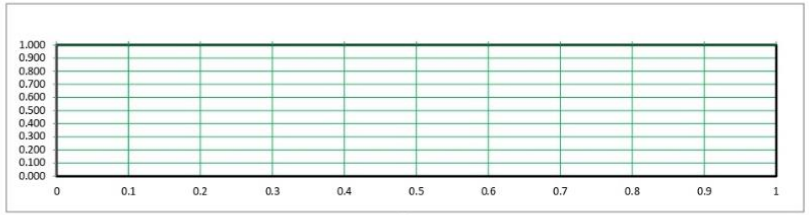

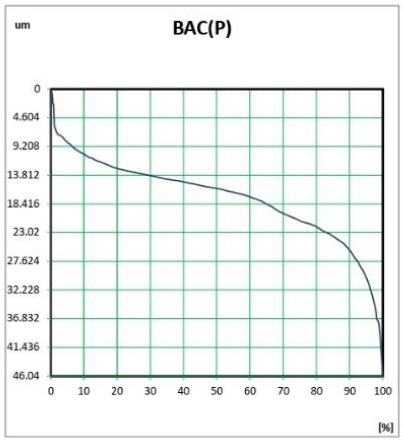

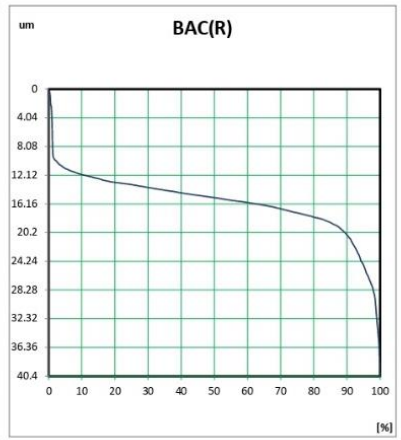

Prüfprotokoll

ACCRETECH

Seriennummer:		Kommentar		Messdatum	27.07.2022
Teilenummer		Prüfer	Kalhöfer	Messzeit	12:46:00

Messbedingung

Messtyp	Roughness measuremen	Cutoff	0,8mm	λs Filter	2,5um
Berechnungsstandard	ISO1997/2009	Filtermethode	Gaussian	Einheit	mm/um
Auswertelänge	4,00mm	Messbereich	500,0um		
Messgeschwindigkeit	0,30mm/s	Entfernen der Form	Straight		

Messergebnis

Pt	42,106	Ra_5	2,061	Rz_5	12,041
Ra	3,050	Rz	23,704	Rp	7,958
Ra_1	2,922	Rz_1	27,793	Rp_1	5,809
Ra_2	2,644	Rz_2	18,526	Rp_2	11,131
Ra_3	3,431	Rz_3	30,785	Rp_3	6,627
Ra_4	4,190	Rz_4	29,374	Rp_4	9,093

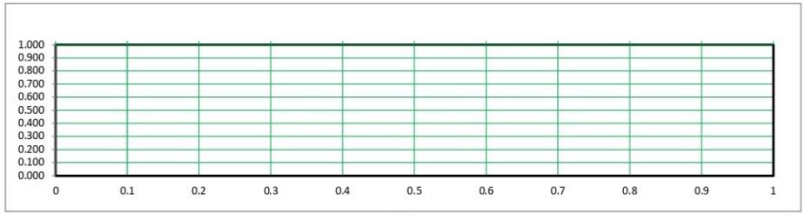

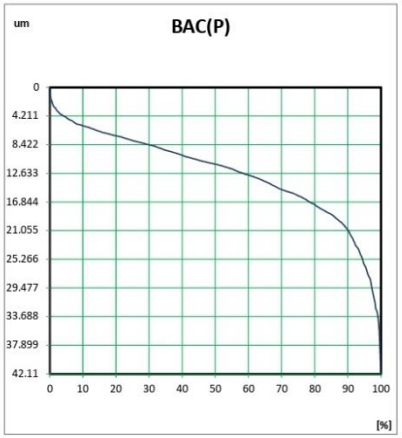

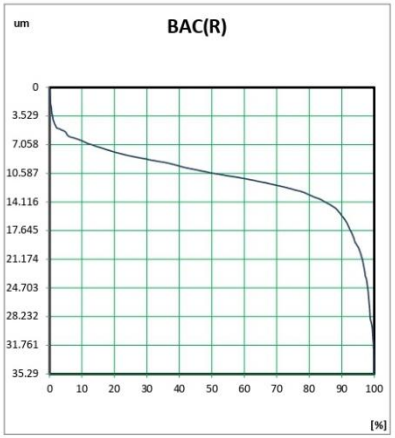

Appendix G - Quarter Cubic | 40%

Prüfprotokoll

Seriennummer:		Kommentar		Messdatum	21.06.2022
Teilenummer	Planetenträger	Prüfer	Kalhöfer	Messzeit	16:17:47

Messbedingung

Messtyp	Roughness measuremen	Cutoff	0,8mm	λs Filter	2,5um
Berechnungsstandard	ISO1997/2009	Filtermethode	Gaussian	Einheit	mm/um
Auswertelänge	4,00mm	Messbereich	500,0um		
Messgeschwindigkeit	0,30mm/s	Entfernen der Form	Straight		

Messergebnis

Pt	26,282	Ra_5	1,555	Rz_5	9,198
Ra	1,336	Rz	7,758	Rp	3,866
Ra_1	1,141	Rz_1	6,235	Rp_1	2,720
Ra_2	1,138	Rz_2	7,200	Rp_2	3,744
Ra_3	1,407	Rz_3	7,412	Rp_3	3,614
Ra_4	1,440	Rz_4	8,745	Rp_4	3,817

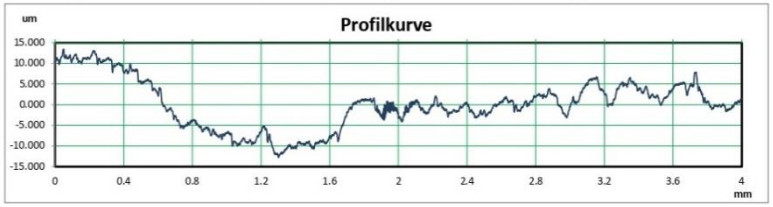

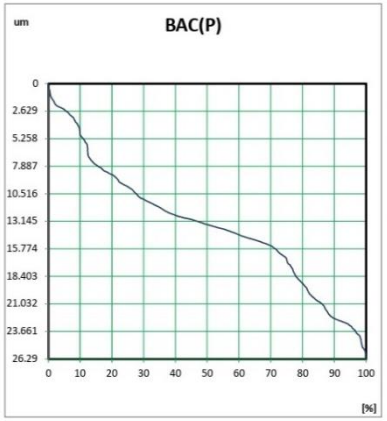

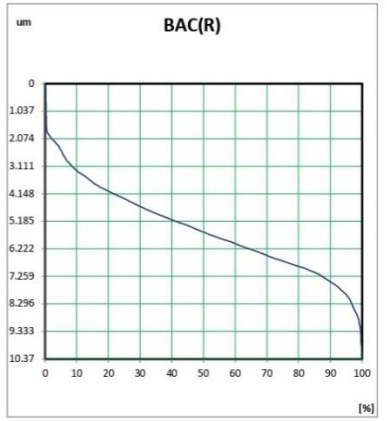

Prüfprotokoll

Seriennummer:		Kommentar		Messdatum	21.06.2022
Teilenummer	Planetenträger	Prüfer	Kalhöfer	Messzeit	16:19:15

Messbedingung

Messtyp	Roughness measuremen	Cutoff	0,8mm	λs Filter	2,5um
Berechnungsstandard	ISO1997/2009	Filtermethode	Gaussian	Einheit	mm/um
Auswertelänge	4,00mm	Messbereich	500,0um		
Messgeschwindigkeit	0,30mm/s	Entfernen der Form	Straight		

Messergebnis

Pt	16,848	Ra_5	1,564	Rz_5	8,029
Ra	1,359	Rz	7,143	Rp	3,249
Ra_1	1,221	Rz_1	7,247	Rp_1	3,887
Ra_2	1,730	Rz_2	8,353	Rp_2	3,976
Ra_3	1,109	Rz_3	6,182	Rp_3	2,929
Ra_4	1,173	Rz_4	5,905	Rp_4	2,483

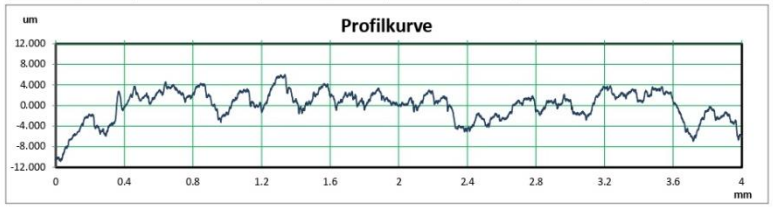

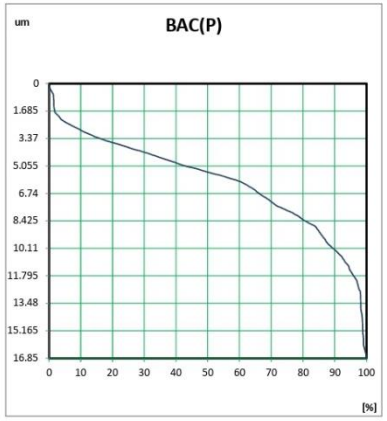

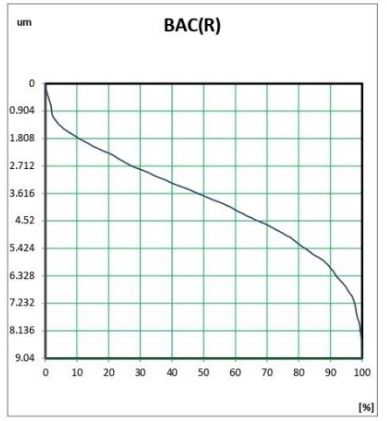

Prüfprotokoll

ACCRETECH

Seriennummer:		Kommentar		Messdatum	21.06.2022
Teilenummer	Planetenträger	Prüfer	Kalhöfer	Messzeit	16:20:04

Messbedingung

Messtyp	Roughness measuremen	Cutoff	0,8mm	λs Filter	2,5um
Berechnungsstandard	ISO1997/2009	Filtermethode	Gaussian	Einheit	mm/um
Auswertelänge	4,00mm	Messbereich	500,0um		
Messgeschwindigkeit	0,30mm/s	Entfernen der Form	Straight		

Messergebnis

Pt	18,513	Ra_5	0,949	Rz_5	5,504
Ra	1,238	Rz	7,126	Rp	3,477
Ra_1	0,990	Rz_1	5,470	Rp_1	2,890
Ra_2	1,652	Rz_2	8,239	Rp_2	3,743
Ra_3	1,608	Rz_3	9,771	Rp_3	5,478
Ra_4	0,990	Rz_4	6,643	Rp_4	2,391

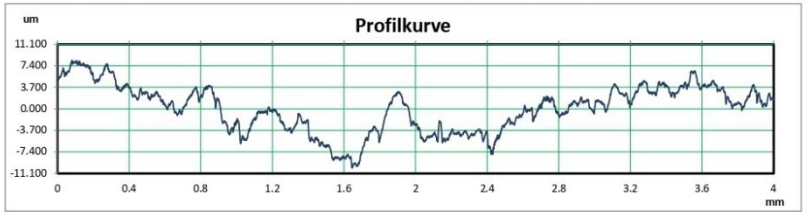

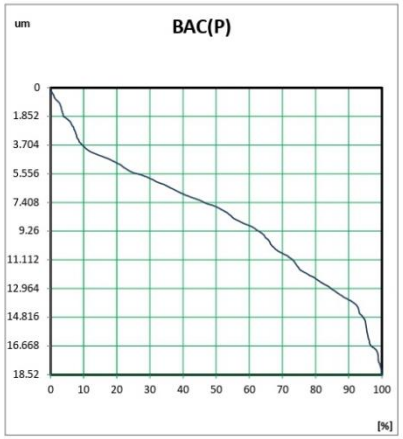

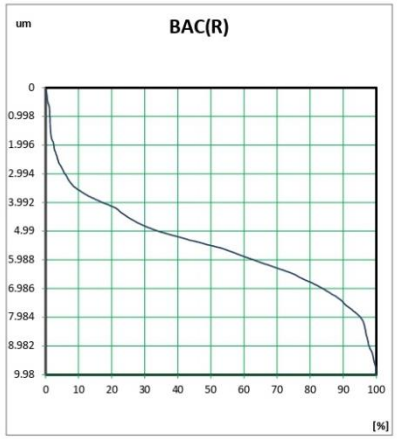

Prüfprotokoll

ACCRETECH

Seriennummer:		Kommentar		Messdatum	21.06.2022
Teilenummer	Planetenträger	Prüfer	Kalhöfer	Messzeit	16:21:16

Messbedingung

Messtyp	Roughness measuremen	Cutoff	0,8mm	λs Filter	2,5um
Berechnungsstandard	ISO1997/2009	Filtermethode	Gaussian	Einheit	mm/um
Auswertelänge	4,00mm	Messbereich	500,0um		
Messgeschwindigkeit	0,30mm/s	Entfernen der Form	Straight		

Messergebnis

Pt	19,964	Ra_5	0,660	Rz_5	5,607
Ra	1,271	Rz	6,741	Rp	3,614
Ra_1	1,569	Rz_1	7,541	Rp_1	4,159
Ra_2	1,307	Rz_2	6,516	Rp_2	4,257
Ra_3	1,337	Rz_3	6,274	Rp_3	2,889
Ra_4	1,482	Rz_4	7,765	Rp_4	3,700

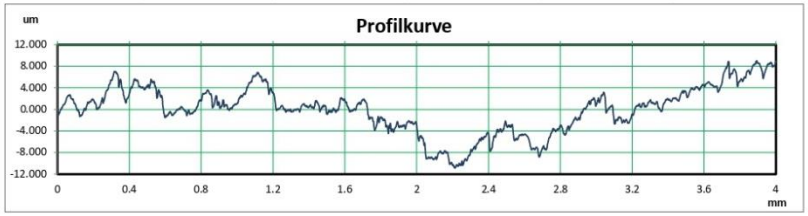

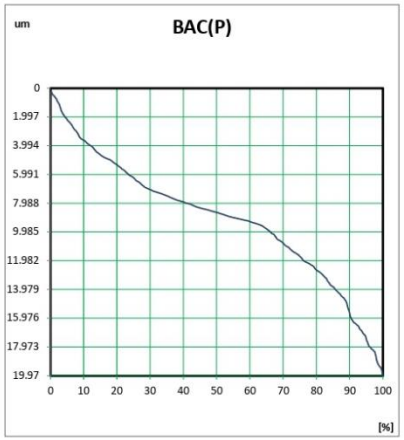

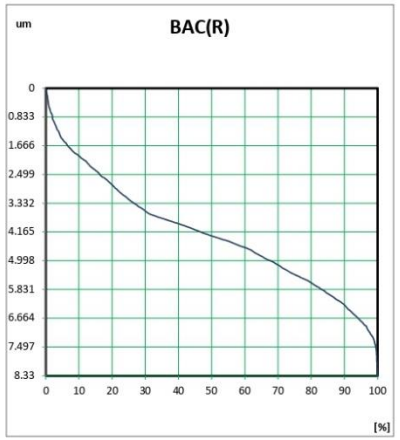

Prüfprotokoll

ACCRETECH

Seriennummer:		Kommentar		Messdatum	21.06.2022
Teilenummer	Planetenträger	Prüfer	Kalhöfer	Messzeit	16:22:08

Messbedingung

Messtyp	Roughness measuremen	Cutoff	0,8mm	λs Filter	2,5um
Berechnungsstandard	ISO1997/2009	Filtermethode	Gaussian	Einheit	mm/um
Auswertelänge	4,00mm	Messbereich	500,0um		
Messgeschwindigkeit	0,30mm/s	Entfernen der Form	Straight		

Messergebnis

Pt	12,877	Ra_5	0,968	Rz_5	5,483
Ra	1,188	Rz	6,955	Rp	3,311
Ra_1	1,091	Rz_1	5,180	Rp_1	2,553
Ra_2	1,020	Rz_2	5,498	Rp_2	3,054
Ra_3	1,487	Rz_3	8,867	Rp_3	4,435
Ra_4	1,376	Rz_4	9,746	Rp_4	3,901

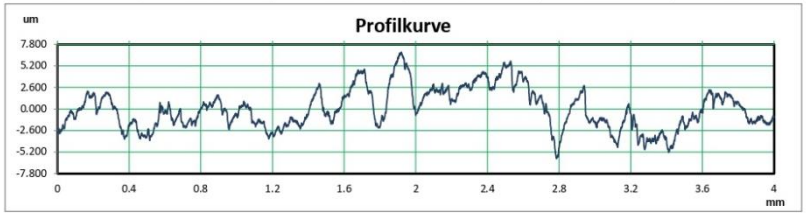

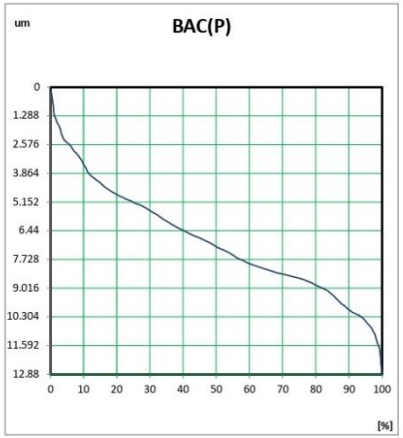

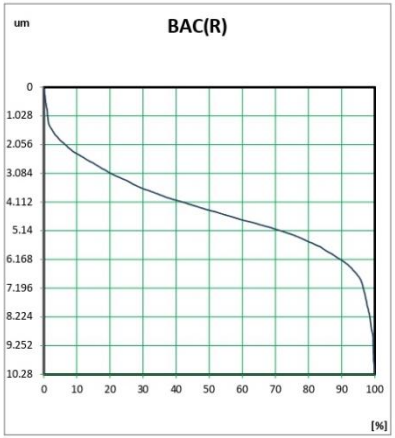

Prüfprotokoll

ACCRETECH

Seriennummer:		Kommentar		Messdatum	21.06.2022
Teilenummer	Planetenträger	Prüfer	Kalhöfer	Messzeit	16:22:58

Messbedingung

Messtyp	Roughness measuremen	Cutoff	0,8mm	λs Filter	2,5um
Berechnungsstandard	ISO1997/2009	Filtermethode	Gaussian	Einheit	mm/um
Auswertelänge	4,00mm	Messbereich	500,0um		
Messgeschwindigkeit	0,30mm/s	Entfernen der Form	Straight		

Messergebnis

Pt	8,120	Ra_5	0,750	Rz_5	4,971
Ra	0,904	Rz	5,015	Rp	2,320
Ra_1	1,080	Rz_1	6,103	Rp_1	3,319
Ra_2	0,775	Rz_2	4,397	Rp_2	1,940
Ra_3	0,881	Rz_3	4,518	Rp_3	1,981
Ra_4	1,033	Rz_4	5,086	Rp_4	2,260

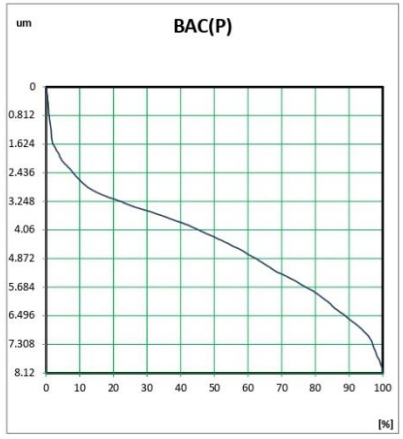

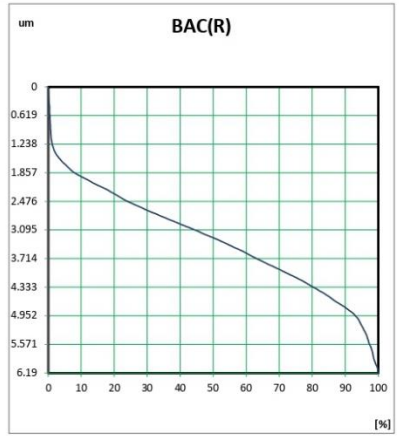

Prüfprotokoll

ACCRETECH

Seriennummer:		Kommentar		Messdatum	21.06.2022
Teilenummer	Planetenträger	Prüfer	Kalhöfer	Messzeit	16:24:09

Messbedingung

Messtyp	Roughness measuremen	Cutoff	0,8mm	λs Filter	2,5um
Berechnungsstandard	ISO1997/2009	Filtermethode	Gaussian	Einheit	mm/um
Auswertelänge	4,00mm	Messbereich	500,0um		
Messgeschwindigkeit	0,30mm/s	Entfernen der Form	Straight		

Messergebnis

Pt	24,402	Ra_5	2,200	Rz_5	11,820
Ra	1,658	Rz	9,025	Rp	4,582
Ra_1	1,490	Rz_1	8,743	Rp_1	4,883
Ra_2	1,363	Rz_2	8,132	Rp_2	3,218
Ra_3	1,681	Rz_3	9,002	Rp_3	4,948
Ra_4	1,553	Rz_4	7,430	Rp_4	3,287

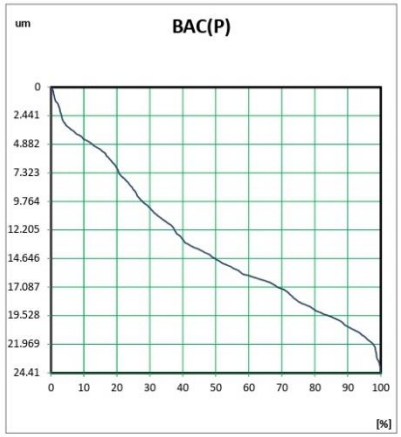

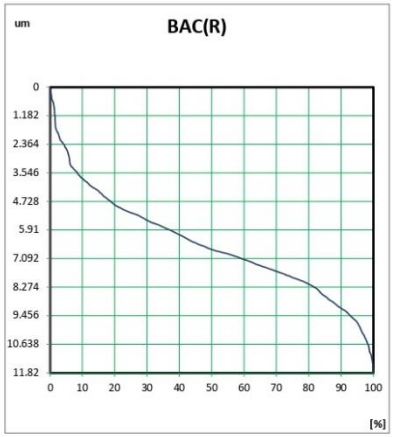

Prüfprotokoll

ACCRETECH

Seriennummer:		Kommentar		Messdatum	21.06.2022
Teilenummer	Planetenträger	Prüfer	Kalhöfer	Messzeit	16:25:24

Messbedingung

Messtyp	Roughness measuremen	Cutoff	0,8mm	λs Filter	2,5um
Berechnungsstandard	ISO1997/2009	Filtermethode	Gaussian	Einheit	mm/um
Auswertelänge	4,00mm	Messbereich	500,0um		
Messgeschwindigkeit	0,30mm/s	Entfernen der Form	Straight		

Messergebnis

Pt	31,958	Ra_5	0,823	Rz_5	4,138
Ra	0,964	Rz	5,565	Rp	2,645
Ra_1	1,206	Rz_1	6,502	Rp_1	3,098
Ra_2	1,123	Rz_2	7,101	Rp_2	3,204
Ra_3	0,918	Rz_3	5,572	Rp_3	3,176
Ra_4	0,748	Rz_4	4,512	Rp_4	1,859

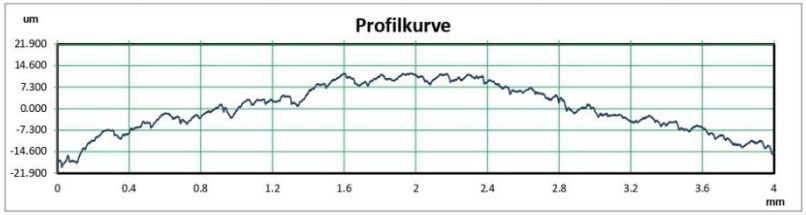

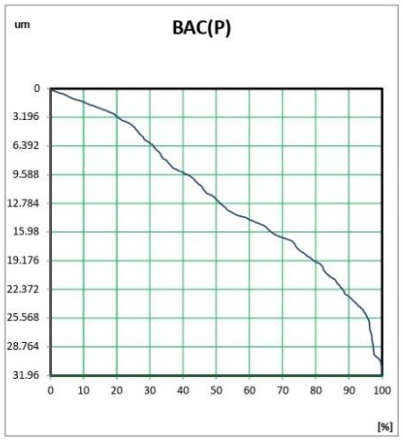

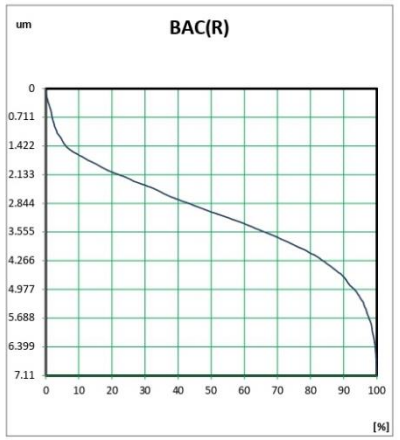

Prüfprotokoll

ACCRETECH

Seriennummer:		Kommentar		Messdatum	21.06.2022
Teilenummer	Planetenträger	Prüfer	Kalhöfer	Messzeit	16:26:17

Messbedingung

Messtyp	Roughness measuremen	Cutoff	0,8mm	λs Filter	2,5um
Berechnungsstandard	ISO1997/2009	Filtermethode	Gaussian	Einheit	mm/um
Auswertelänge	4,00mm	Messbereich	500,0um		
Messgeschwindigkeit	0,30mm/s	Entfernen der Form	Straight		

Messergebnis

Pt	20,193	Ra_5	1,608	Rz_5	8,269
Ra	1,626	Rz	8,211	Rp	3,409
Ra_1	1,760	Rz_1	9,211	Rp_1	2,978
Ra_2	1,258	Rz_2	6,361	Rp_2	2,997
Ra_3	2,450	Rz_3	10,810	Rp_3	4,744
Ra_4	1,055	Rz_4	6,404	Rp_4	3,027

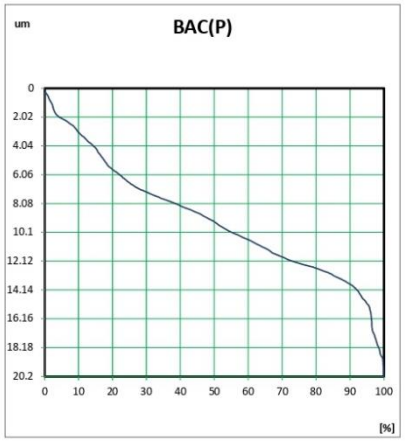

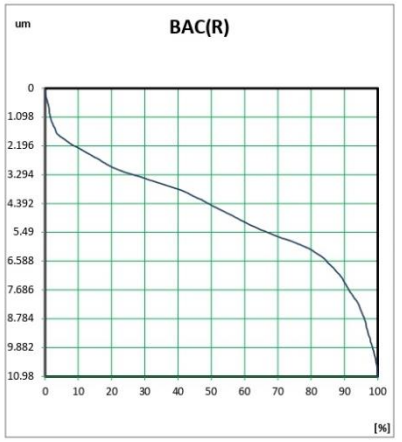

Appendix H

Ra					
40%			25%		
Tri-Hexagon	Gyroid	Quarter	Tri-Hexagon	Gyroid	Quarter
2,979	2,471	2,016	2,889	3,857	3,150
2,676	2,626	1,224	3,353	3,969	3,372
2,871	2,778	2,125	3,077	3,825	2,511
3,651	2,448	1,336	3,140	3,624	2,664
2,878	2,605	1,359	3,362	3,914	2,648
3,381	2,583	1,238	3,333	3,442	2,491
3,132	3,065	1,271	3,395	2,943	2,612
3,535	2,524	1,188	2,926	3,915	2,598
2,778	2,889	0,904	3,050	3,531	2,436
3,098	**2,665**	**1,407**	**3,169**	**3,669**	**2,720**
Rz					
40%			**25%**		
Tri-Hexagon	**Gyroid**	**Quarter**	**Tri-Hexagon**	**Gyroid**	**Quarter**
20,628	16,339	10,909	20,147	33,167	20,444
20,255	20,402	6,427	24,112	33,183	19,870
21,381	19,019	8,832	22,356	28,991	17,064
21,977	17,730	7,758	27,144	26,550	20,659
20,011	17,072	7,143	28,776	27,679	16,913
20,105	16,710	7,126	27,448	22,743	19,450
20,763	19,599	6,741	26,482	20,377	18,421
21,816	17,976	6,955	27,813	29,080	19,815
21,024	21,806	5,015	23,704	27,744	17,291
20,884	**18,517**	**7,434**	**25,331**	**27,724**	**18,881**

Appendix I

Nº	Density	Infill	Thickness [mm]	Widht [mm]
1	25%	Tri-Hex	4,89	6,01
2			4,83	5,92
3			4,85	5,94
4			5,02	5,9
5			4,94	5,93
6			5,02	5,98
7			4,93	6,01
8	40%	Tri-Hex	4,97	6,04
9			4,96	6,07
10			4,92	5,96
11			4,94	5,98
12			4,96	5,89
13			4,89	5,96
14			4,93	5,92
15	40%	Gyroid	4,97	5,96
16			4,91	5,97
17			4,89	5,89
18			4,9	5,93
19			4,86	5,94
20			4,95	6,01
21			4,92	5,93
22	25%	Gyroid	5,01	5,96
23			4,98	5,98
24			4,96	6,02
25			4,83	5,98
26			4,96	5,86
27			4,82	5,87
28			4,86	5,88
29	25%	Quarter Cubic	4,97	5,95
30			4,98	5,97

31			4,90	6,05
32			4,94	6,04
33			4,93	5,94
34			4,86	6,02
35			4,93	5,87
36	40%	Quarter Cubic	4,90	6,07
37			4,87	6,07
38			4,84	6,00
39			4,86	6,06
40			4,94	6,04
41			4,85	6,07
42			4,91	6,08

Appendix J

Tri-Hexagon					
25%			40%		
Nº	Rp0.2 [MPa]	Rm [MPa]	Nº	Rp0.2 [MPa]	Rm [MPa]
1	88,226	193,414	8	104,622	260,817
2	90,879	223,001	9	104,283	263,918
3	90,879	223,001	10	108,622	276,979
4	95,482	214,262	11	108,558	279,059
5	90,859	213,315	12	108,123	258,284
6	97,381	211,016	13	108,277	255,217
7	94,238	225,408	14	108,944	255,619
Average	**90,879**	**214,262**	**Average**	**108,277**	**260,817**
SD	**2,974**	**10,150**	**SD**	**1,849**	**9,141**

Gyroid					
40%			25%		
Nº	Rp0.2 [MPa]	Rm [MPa]	Nº	Rp0.2 [MPa]	Rm [MPa]
15		299,640	22		305,626
16	103,605	286,951	23		305,626
17	105,542	312,862	24		309,656
18	106,391	318,270	25		336,548
19	112,440	322,126	26	104,462	317,298
20	106,520	304,395	27		261,004
21	104,847	307,127	28	67,605	208,899
Average	**105,967**	**307,127**	**Average**	**86,034**	**305,626**
SD	**2,808**	**11,034**	**SD**	**18,429**	**39,953**

Quarter Cubic					
25%			40%		
Nº	Rp0.2 [MPa]	Rm [MPa]	Nº	Rp0.2 [MPa]	Rm [MPa]
29	92,406	256,954	36		280,569
30	89,966	241,843	37		274,055
31	92,275	245,397	38		299,237
32	92,334	250,625	39	96,393	295,248
33	93,430	249,199	40		
34		230,728	41		
35		261,254	42		
Average	**92,334**	**249,199**	**Average**	**96,393**	**287,908**
SD	**1,140**	**9,313**	**SD**	**0,000**	**10,325**

Appendix L – Tri-Hexagon | 25%

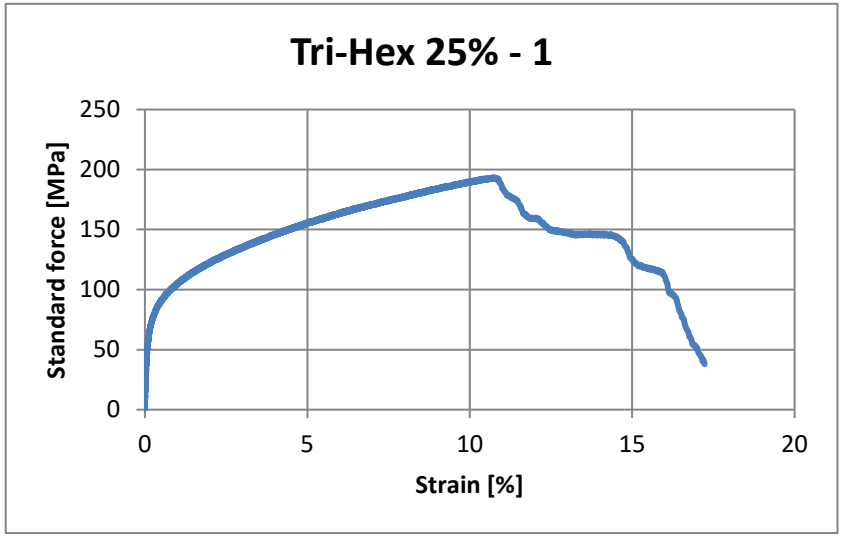

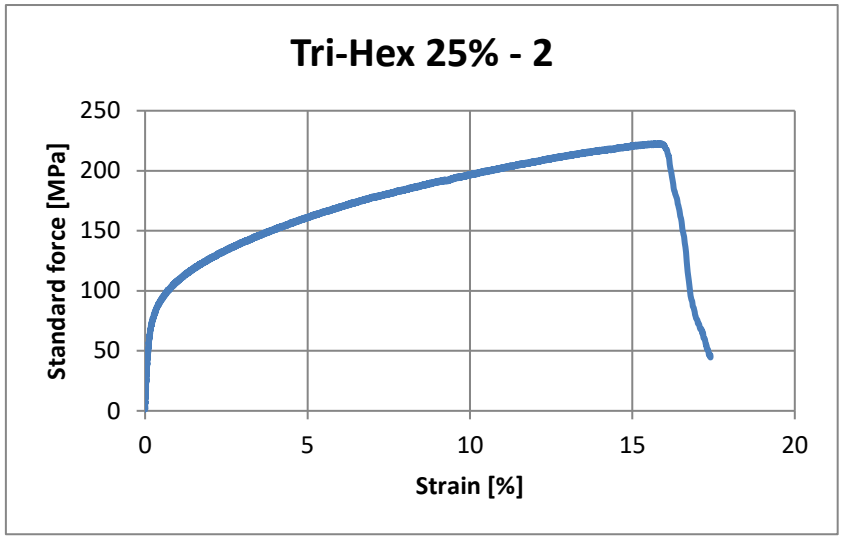

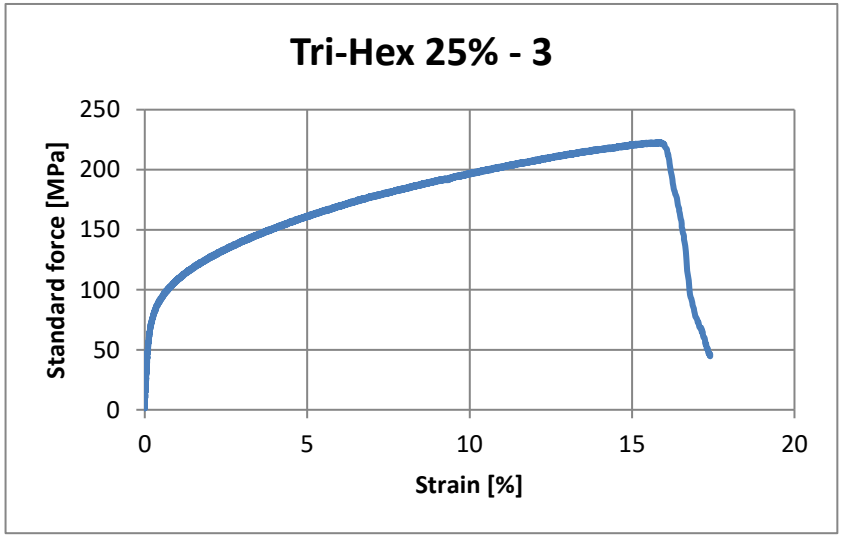

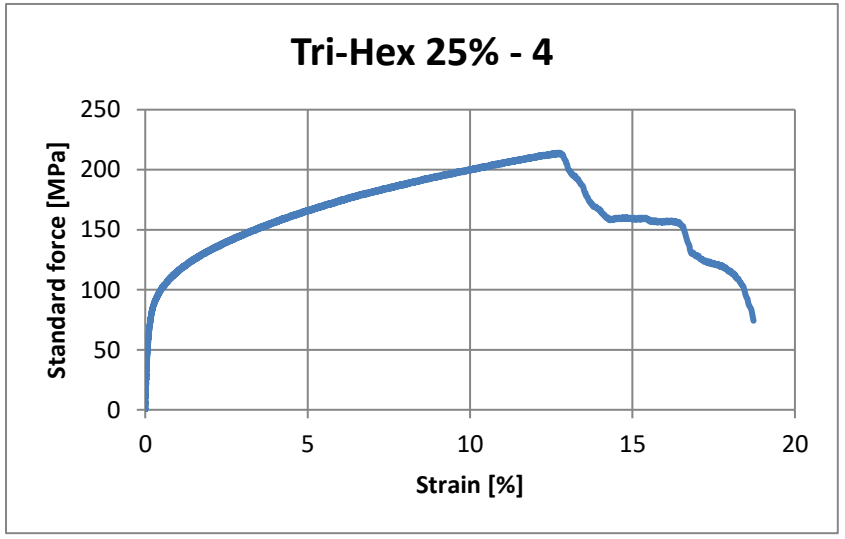

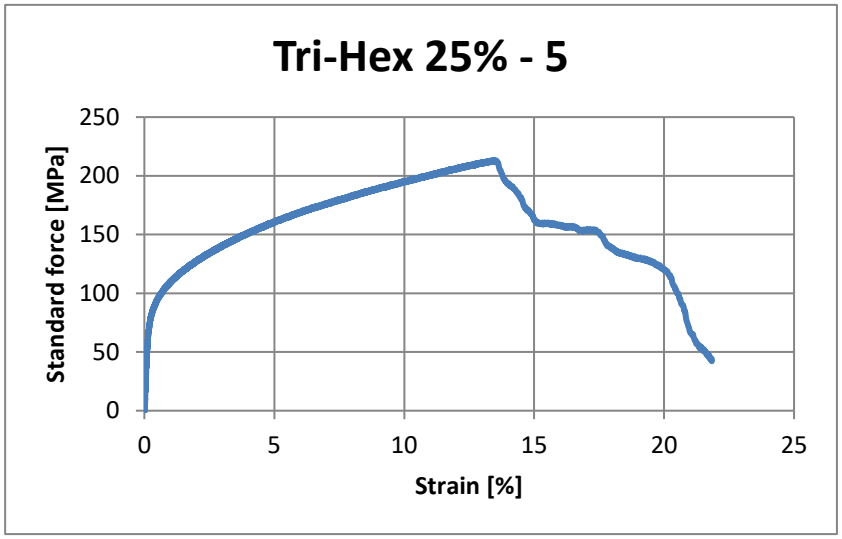
Tri-Hex 25% - 5
Standard force [MPa]
250
200
150
100
50
0
0
5
10
15
20
25
Strain [%]

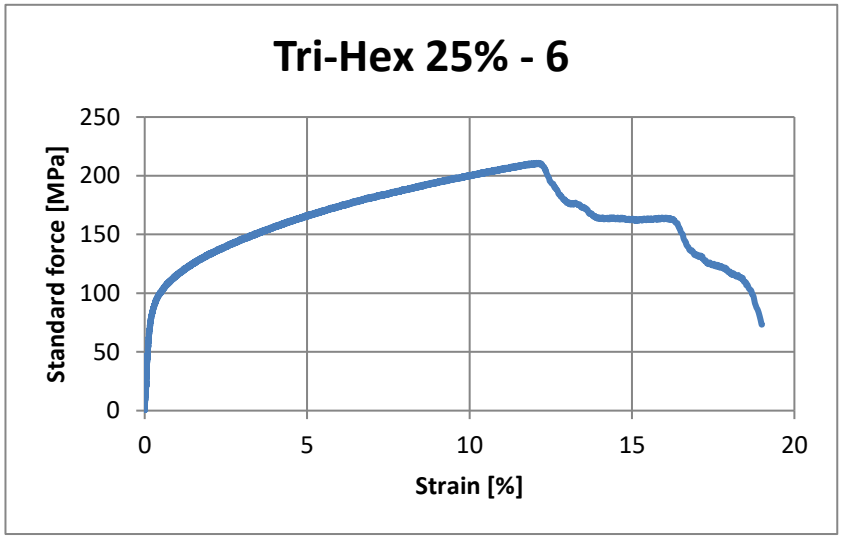
Tri-Hex 25% - 6
Standard force [MPa]
250
200
150
100
50
0
0
5
10
15
20
Strain [%]

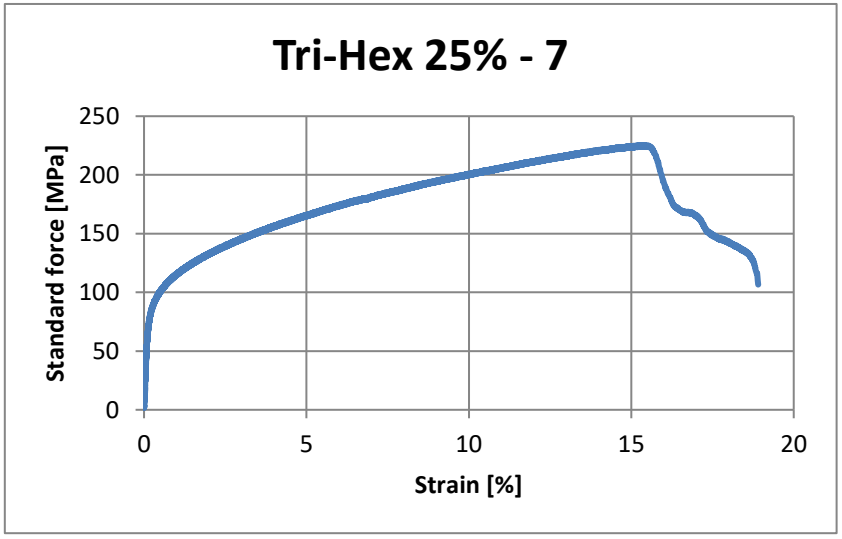
Tri-Hex 25% - 7
Standard force [MPa]
250
200
150
100
50
0
0
5
10
15
20
Strain [%]

Appendix M –Tri-Hexagon | 40%

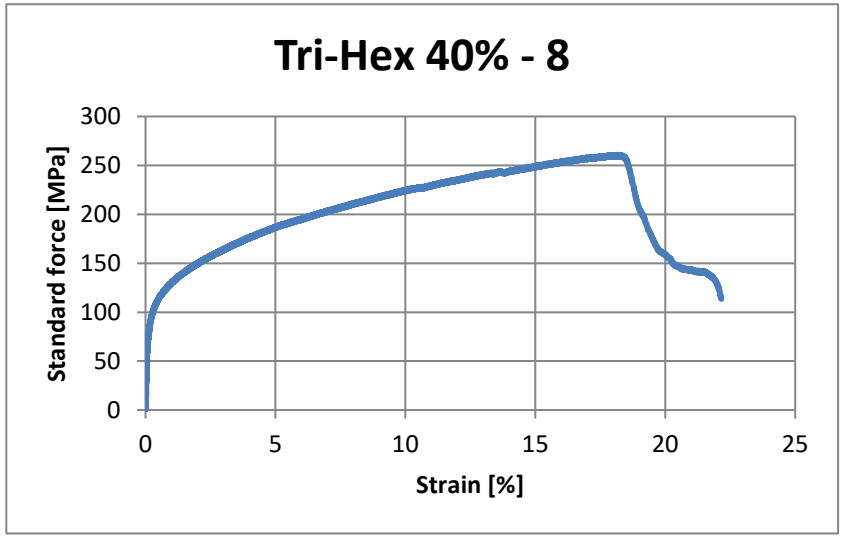

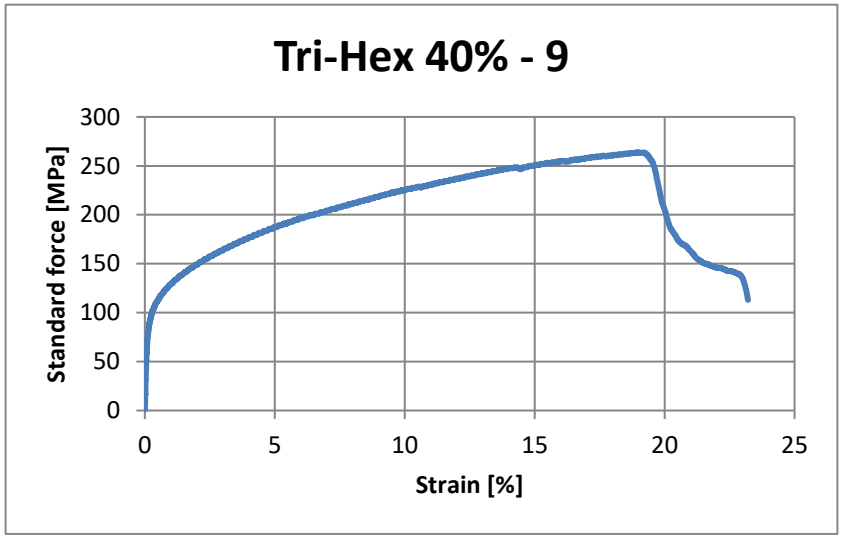

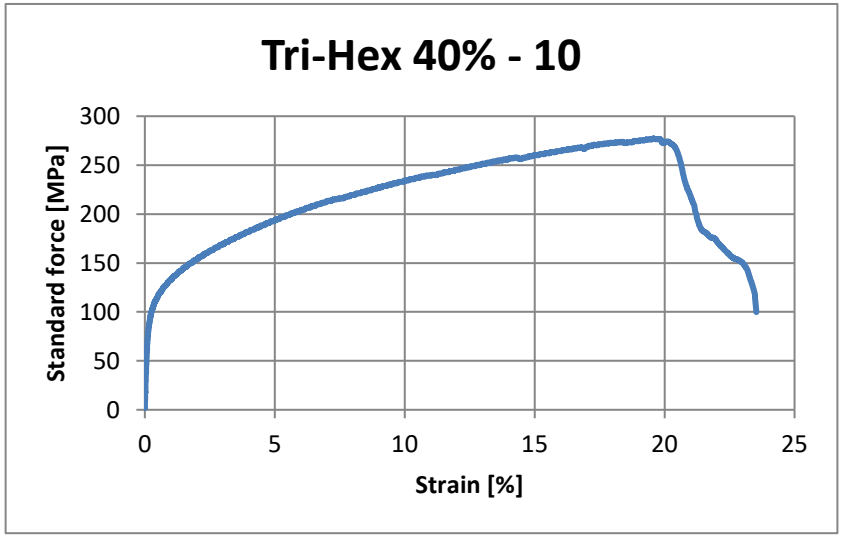

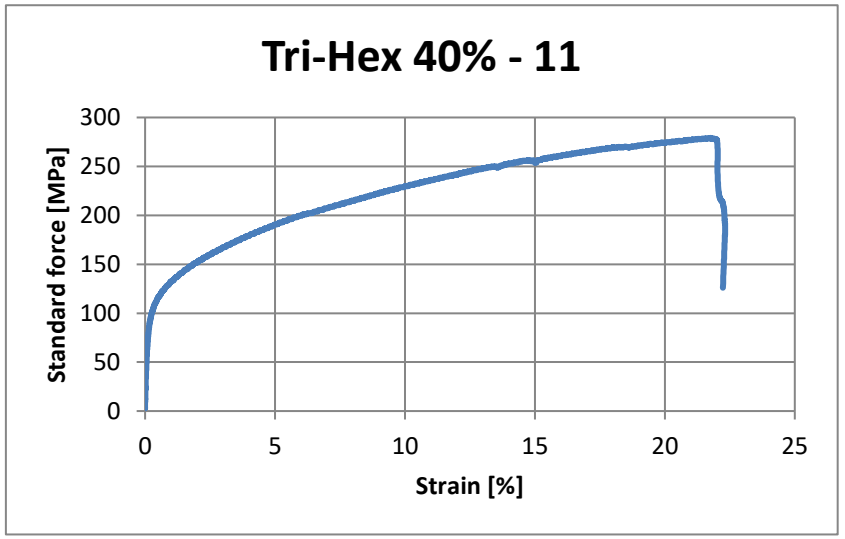

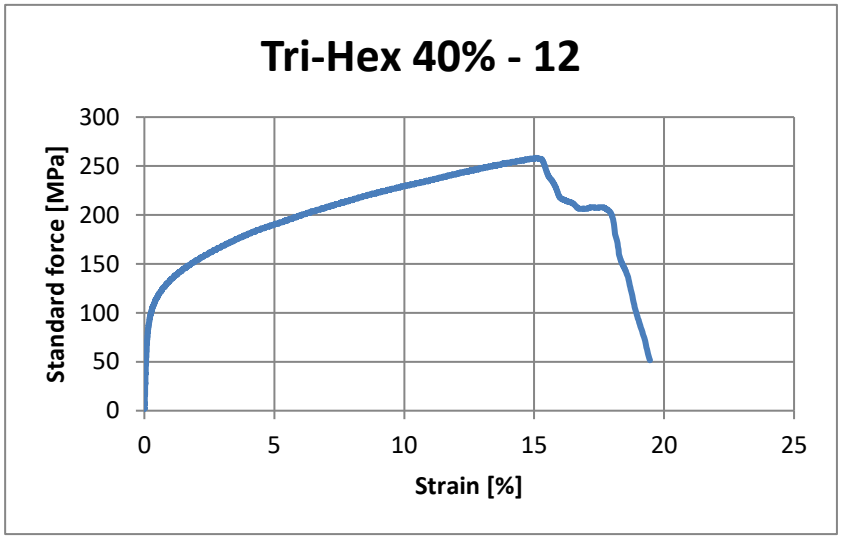
Tri-Hex 40% - 12
Standard force [MPa]
300
250
200
150
100
50
0
0
5
10
15
20
25
Strain [%]

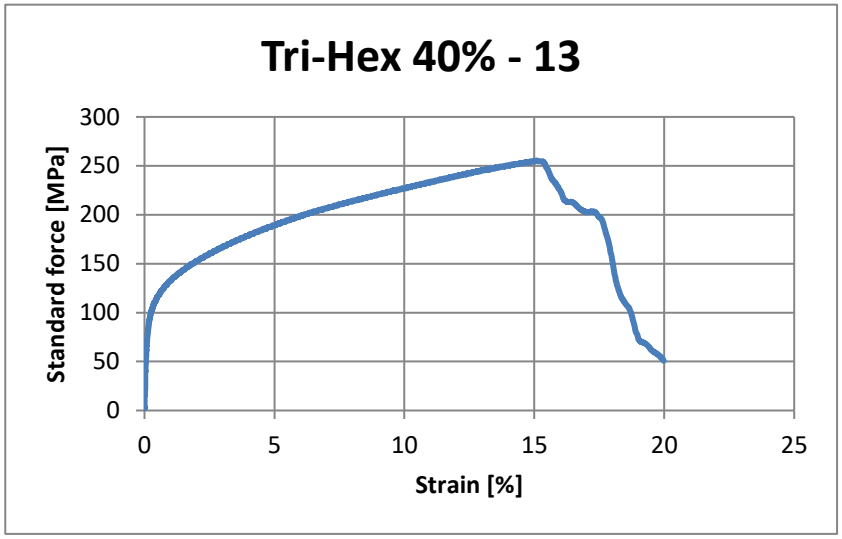
Tri-Hex 40% - 13
Standard force [MPa]
300
250
200
150
100
50
0
0
5
10
15
20
25
Strain [%]

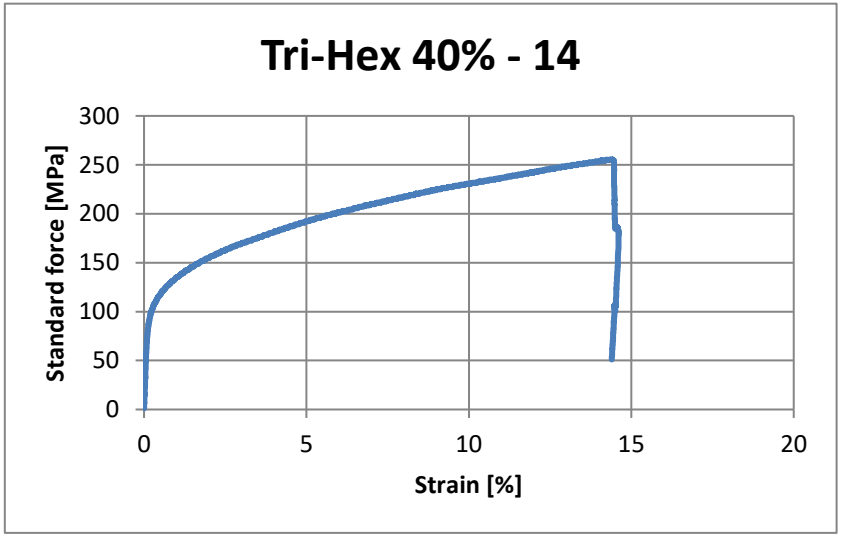
Tri-Hex 40% - 14
Standard force [MPa]
300
250
200
150
100
50
0
0
5
10
15
20
Strain [%]

Appendix N - Gyroid | 40%

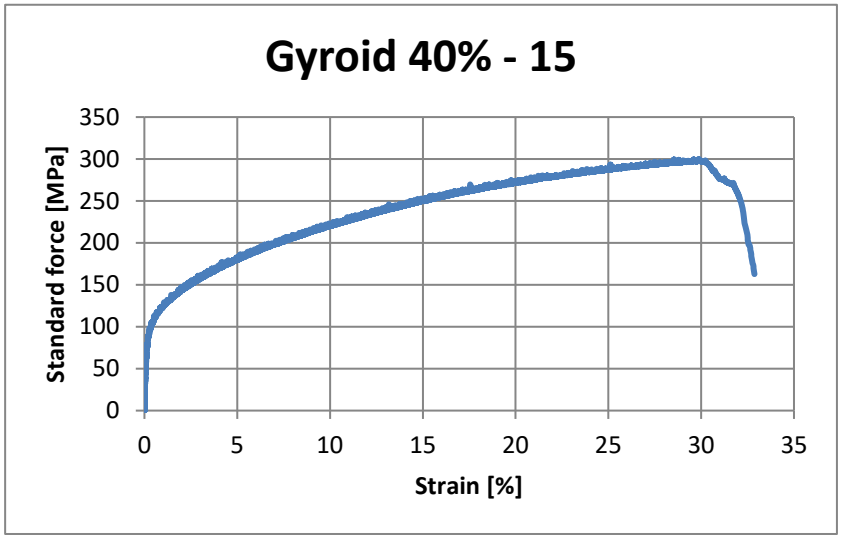

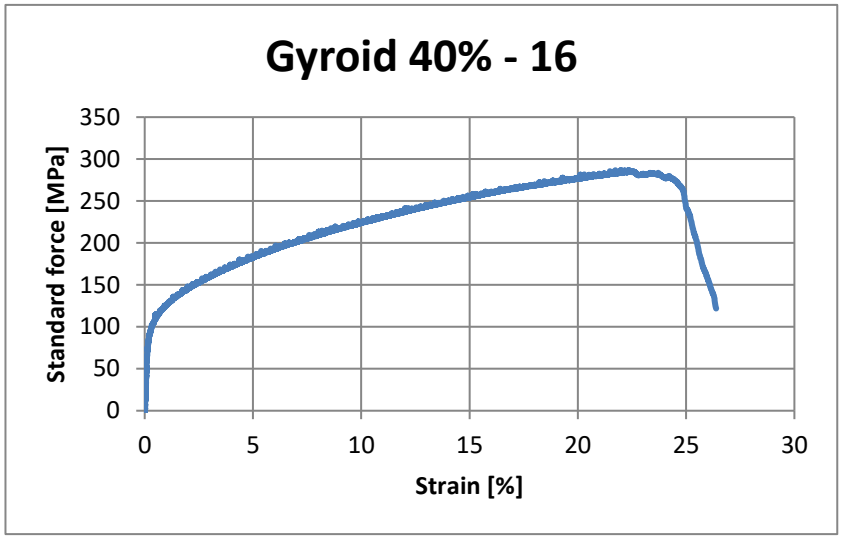

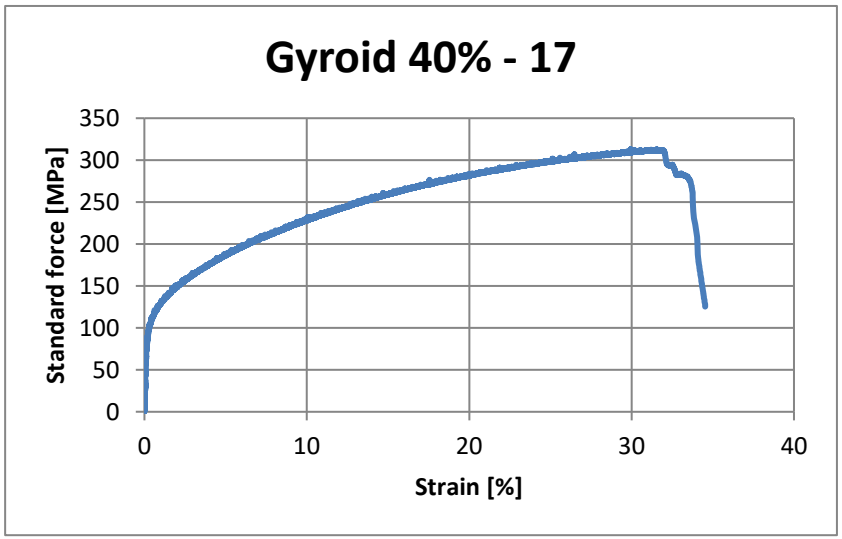

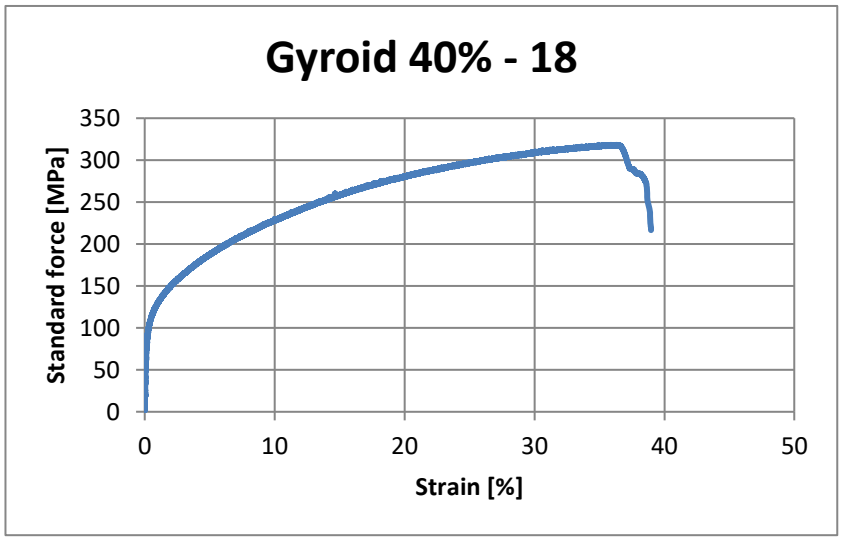

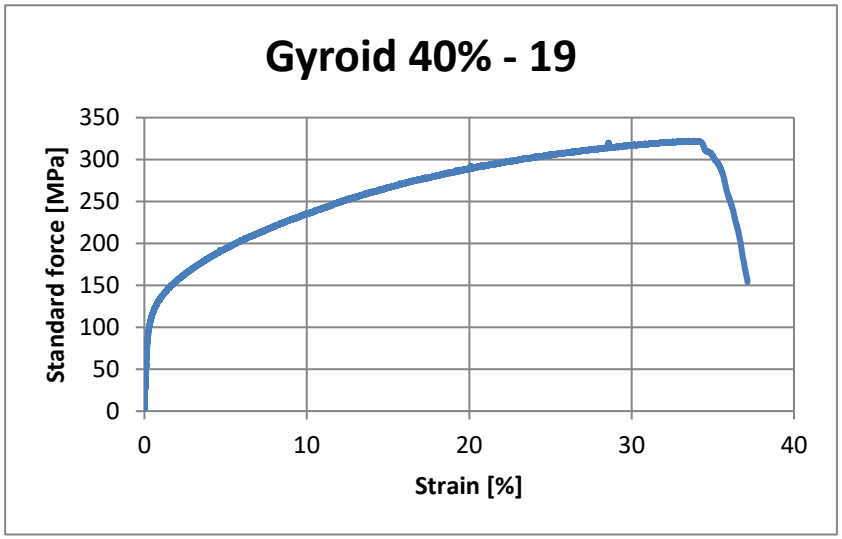
Gyroid 40% - 19
Standard force [MPa]
350
300
250
200
150
100
50
0
0
10
20
30
40
Strain [%]

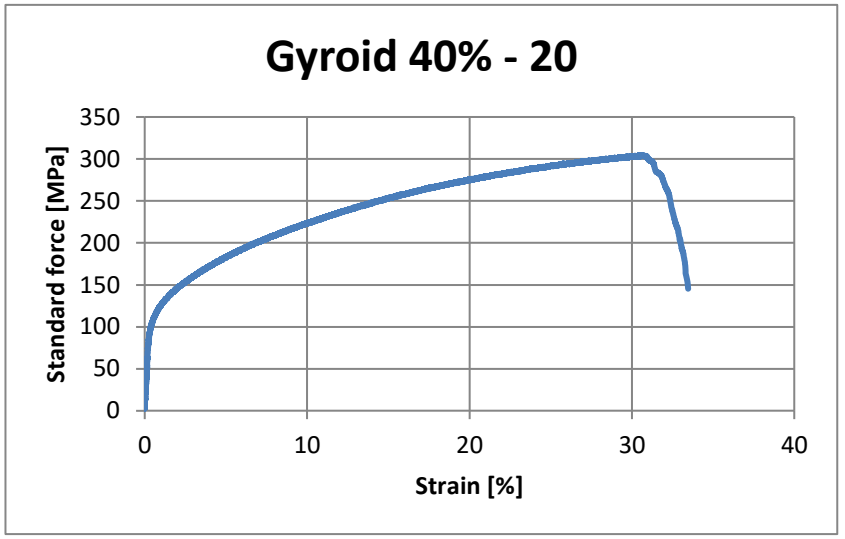
Gyroid 40% - 20
Standard force [MPa]
350
300
250
200
150
100
50
0
0
10
20
30
40
Strain [%]

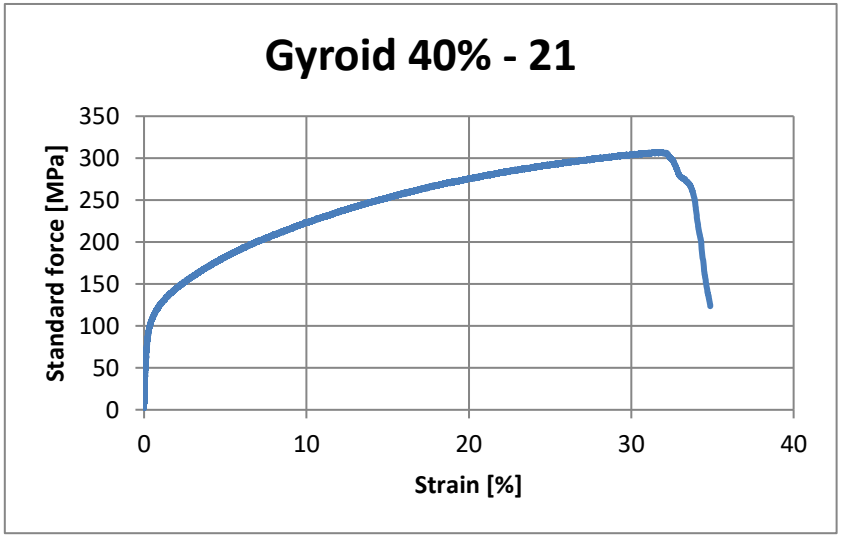
Gyroid 40% - 21
Standard force [MPa]
350
300
250
200
150
100
50
0
0
10
20
30
40
Strain [%]

Appendix O - Gyroid | 25%

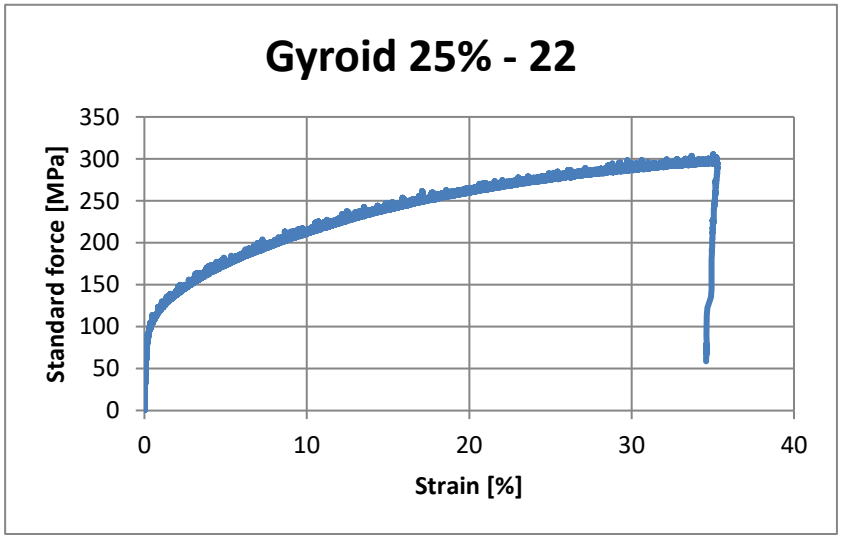

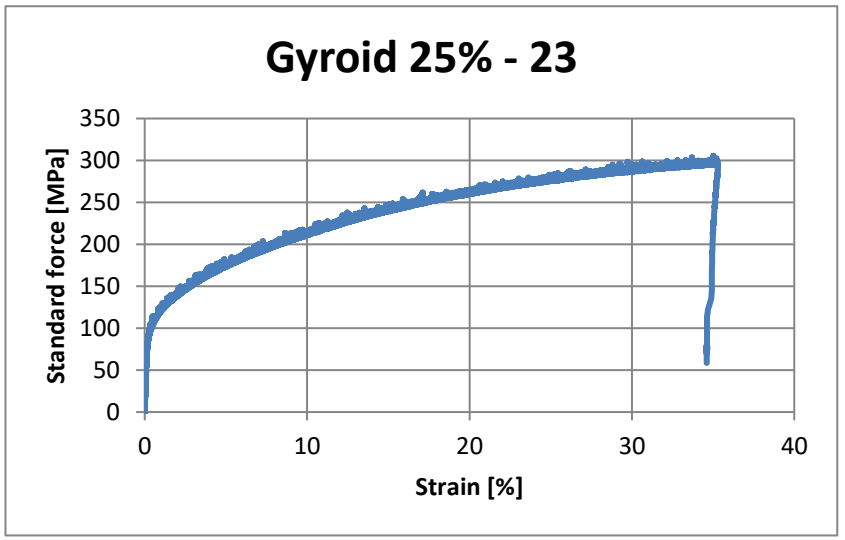

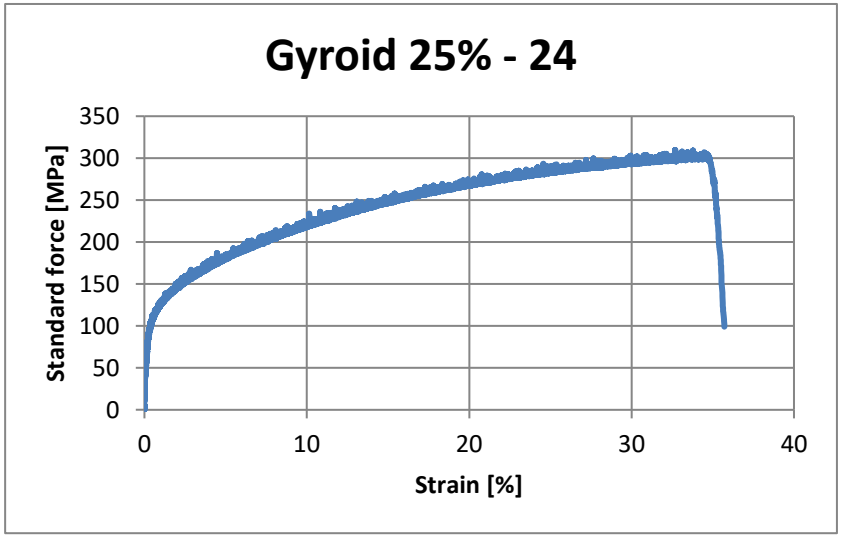

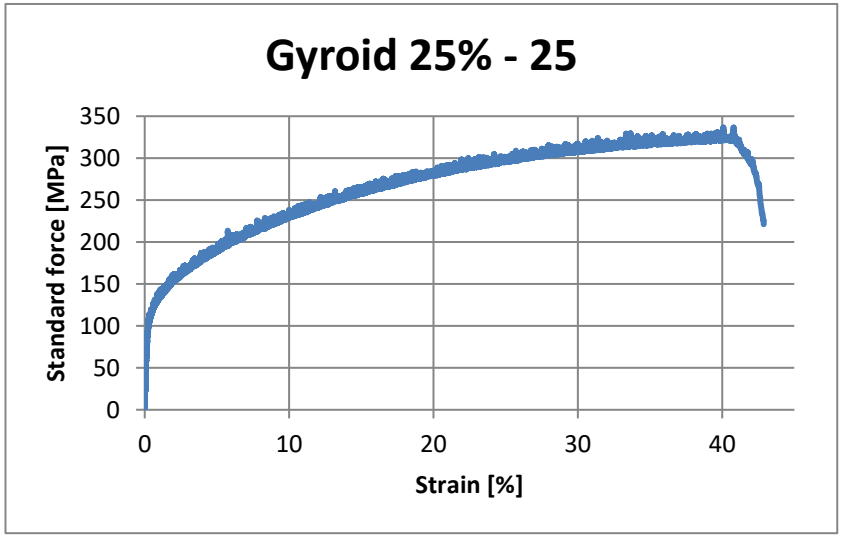

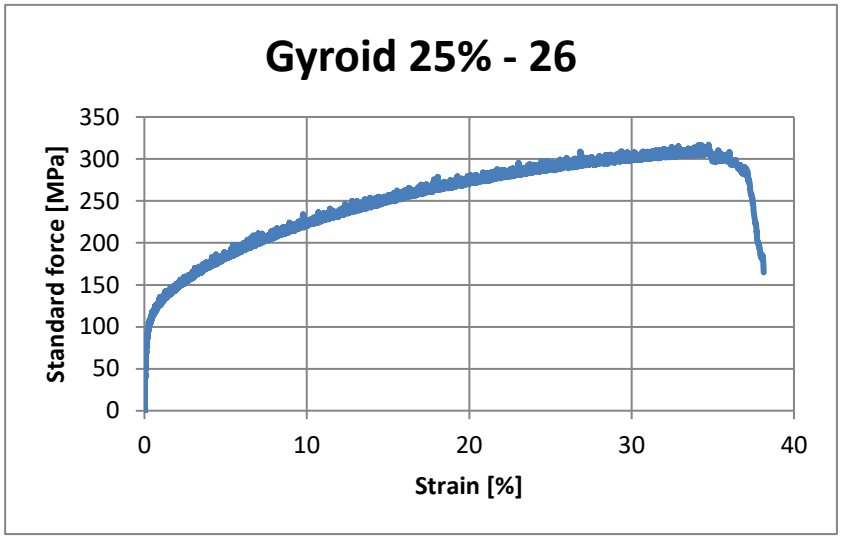
Gyroid 25% - 26
Standard force [MPa]
350
300
250
200
150
100
50
0
0
10
20
30
40
Strain [%]

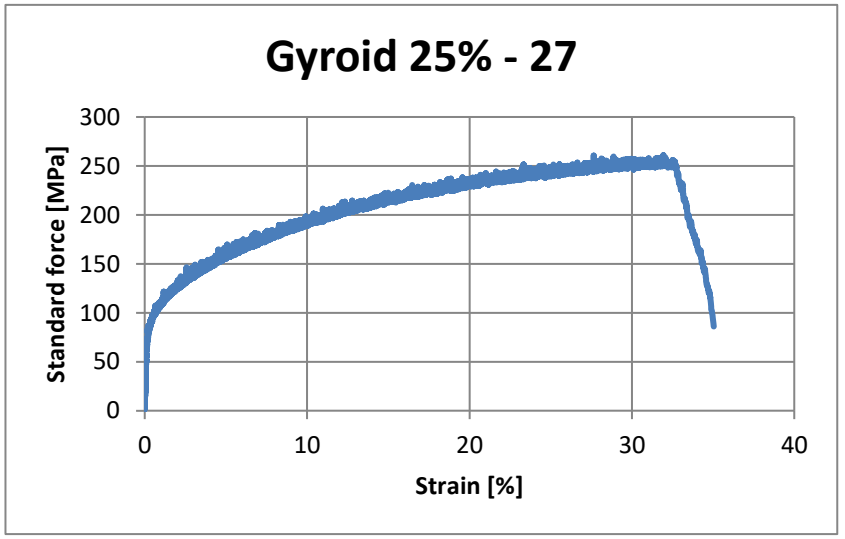
Gyroid 25% - 27
Standard force [MPa]
300
250
200
150
100
50
0
0
10
20
30
40
Strain [%]

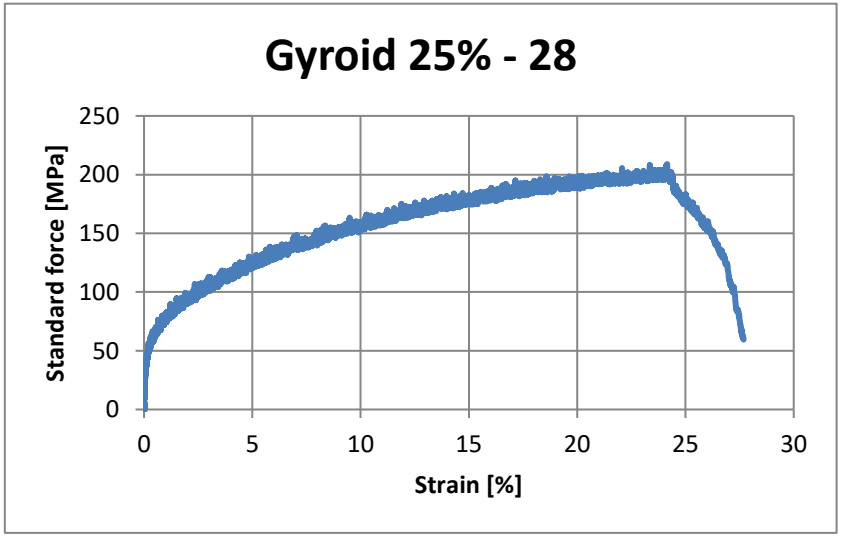
Gyroid 25% - 28
Standard force [MPa]
250
200
150
100
50
0
0
5
10
15
20
25
30
Strain [%]

Appendix P - Quarter Cubic | 25%

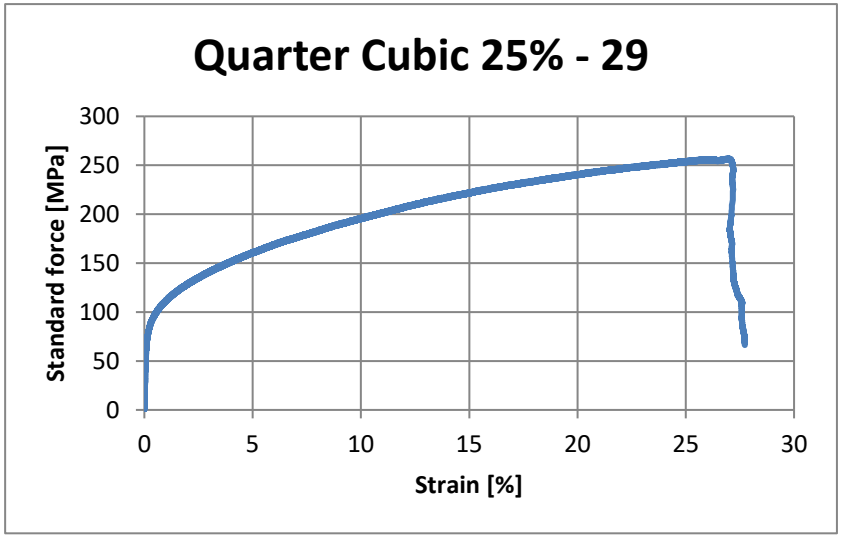

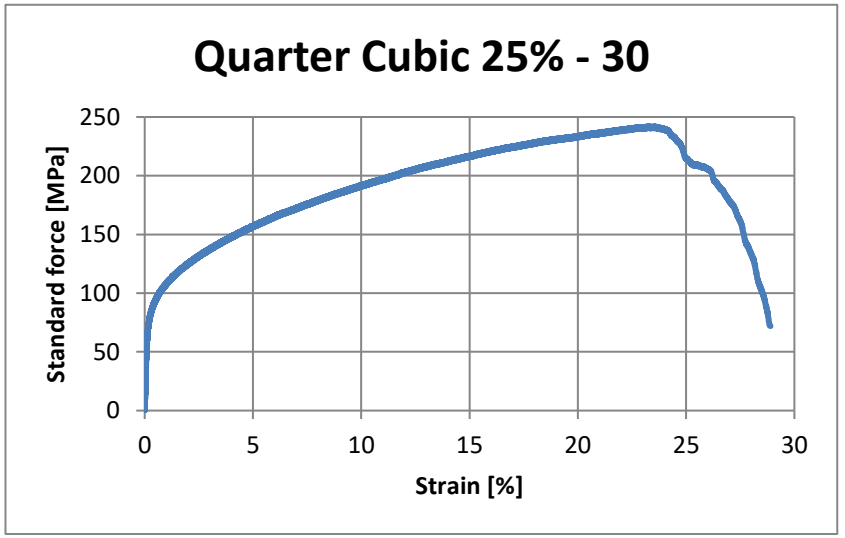

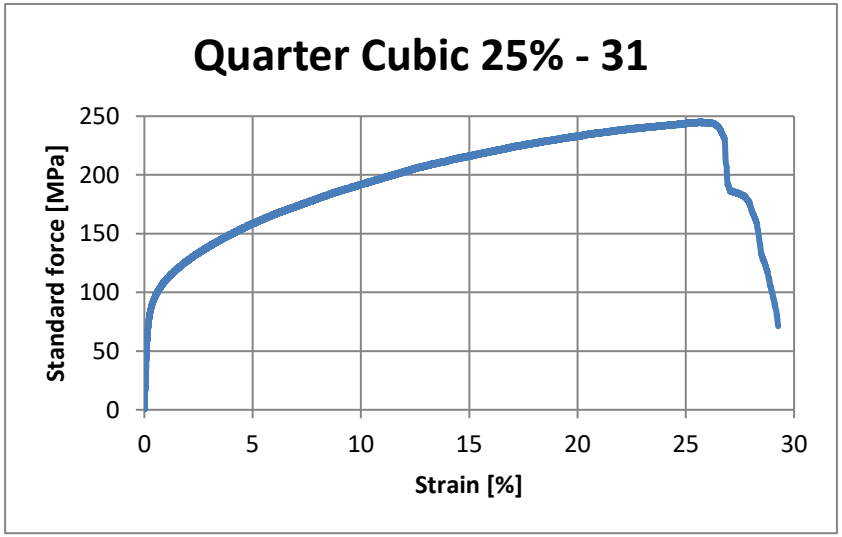

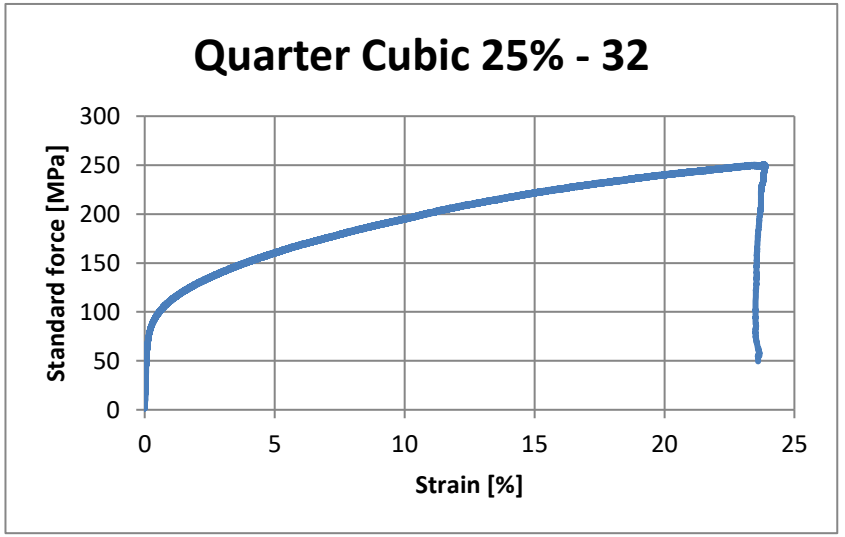

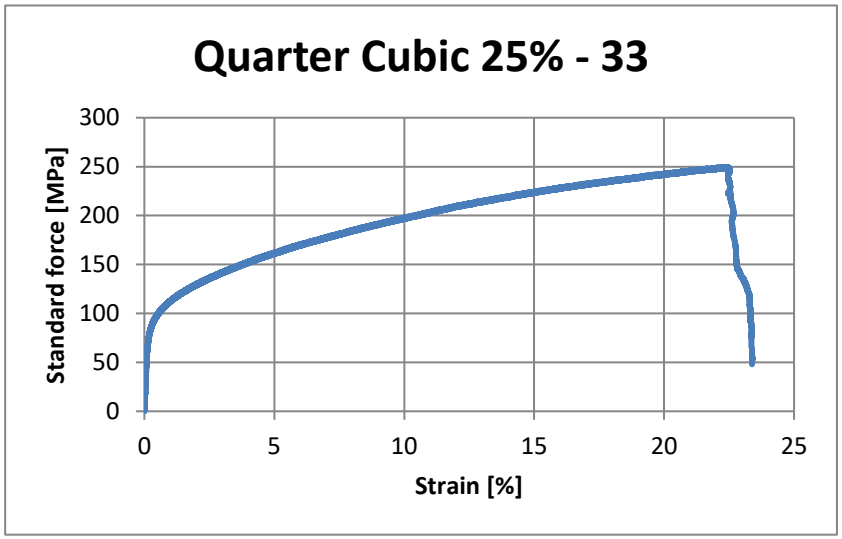
Quarter Cubic 25% - 33
Standard force [MPa]
300
250
200
150
100
50
0
0
5
10
15
20
25
Strain [%]

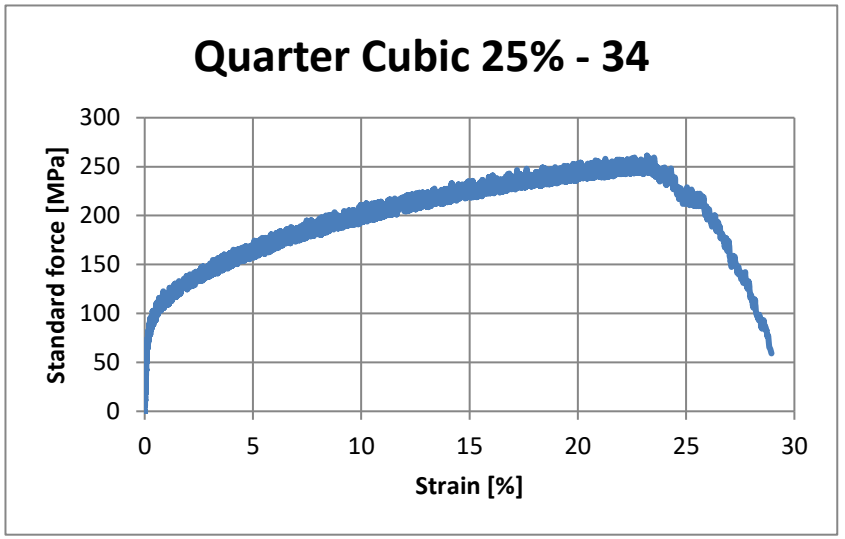
Quarter Cubic 25% - 34
Standard force [MPa]
300
250
200
150
100
50
0
0
5
10
15
20
25
30
Strain [%]

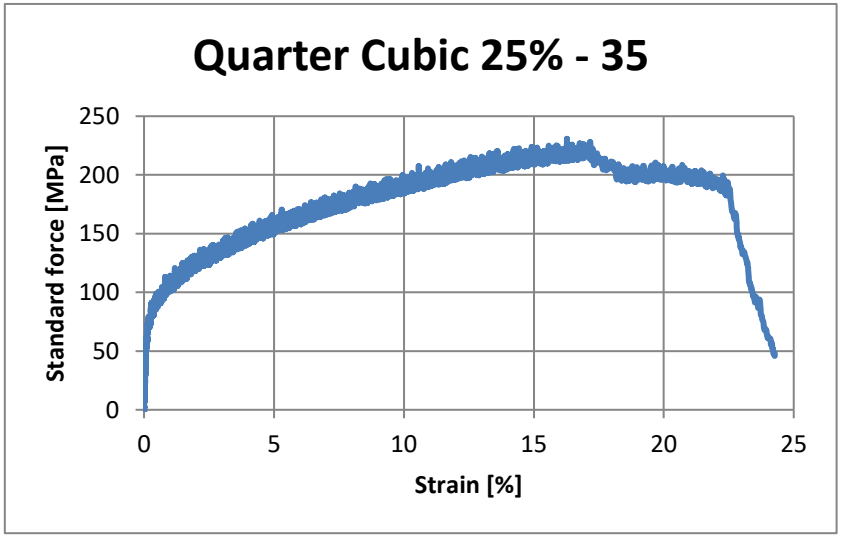
Quarter Cubic 25% - 35
Standard force [MPa]
250
200
150
100
50
0
0
5
10
15
20
25
Strain [%]

Appendix Q - Quarter Cubic | 40

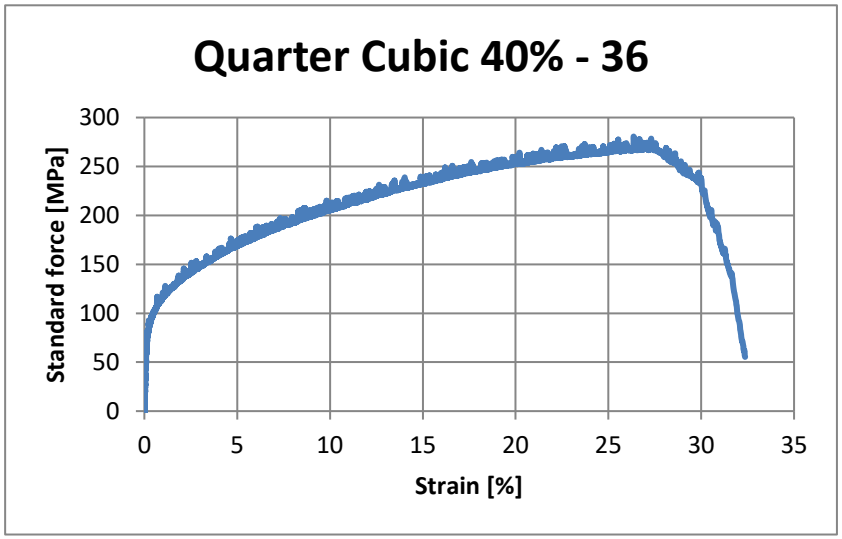

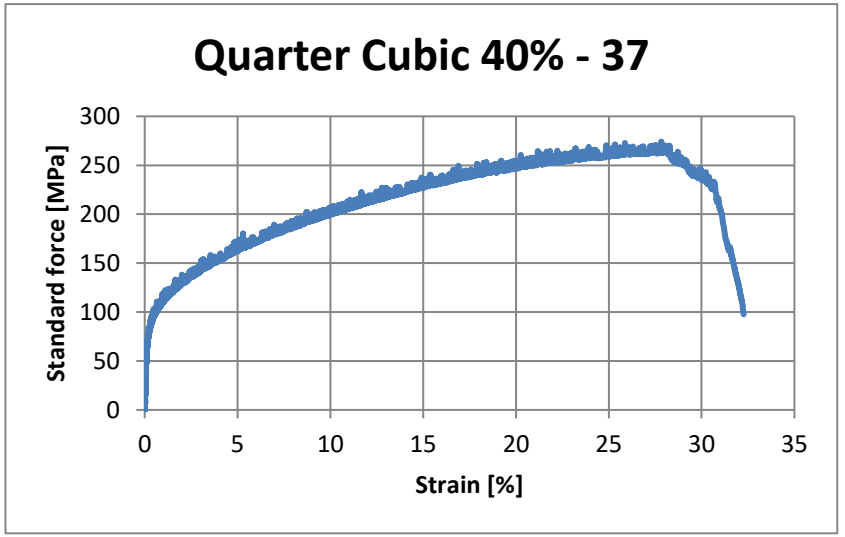

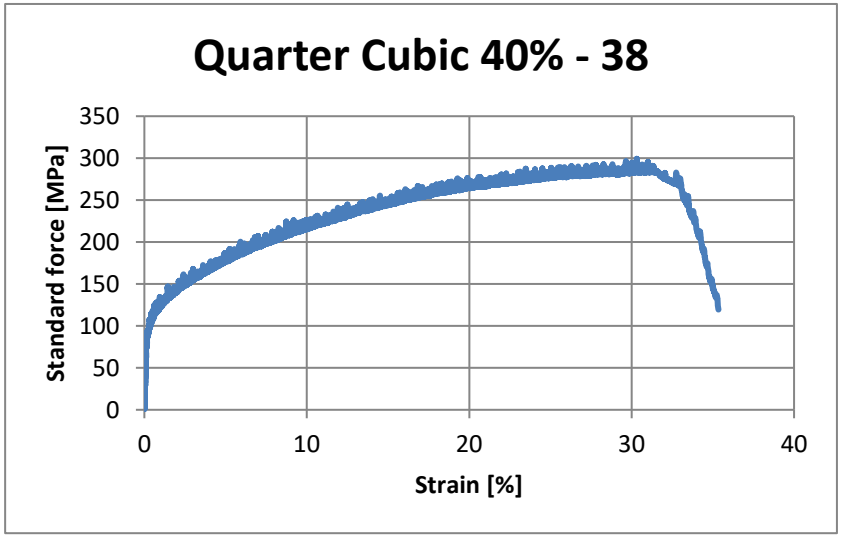

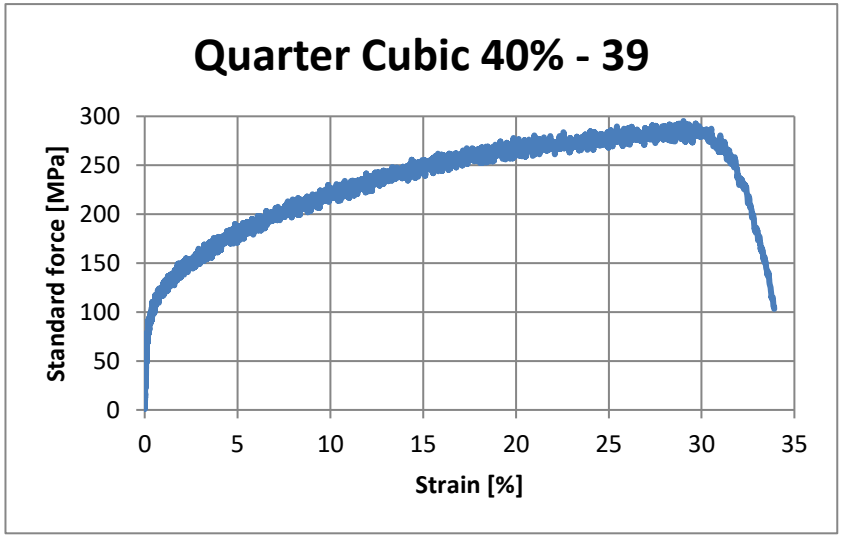

Appendix R – Tri-Hexagon | Side

Prüfprotokoll

Seriennummer:		Kommentar		Messdatum	30.06.2022
Teilenummer	Planetenträger	Prüfer	Kalhöfer	Messzeit	10:06:38

Messbedingung

Messtyp	Roughness measuremen	Cutoff	0,8mm	λs Filter	2,5um
Berechnungsstandard	ISO1997/2009	Filtermethode	Gaussian	Einheit	mm/um
Auswertelänge	4,00mm	Messbereich	500,0um		
Messgeschwindigkeit	0,30mm/s	Entfernen der Form	Straight		

Messergebnis

Pt	119,684	Ra_5	5,333	Rz_5	34,874
Ra	6,945	Rz	38,984	Rp	13,774
Ra_1	9,830	Rz_1	47,115	Rp_1	20,406
Ra_2	10,177	Rz_2	54,931	Rp_2	18,356
Ra_3	4,339	Rz_3	22,399	Rp_3	9,926
Ra_4	5,047	Rz_4	35,602	Rp_4	10,131

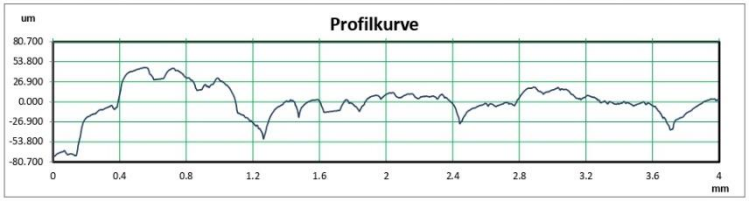

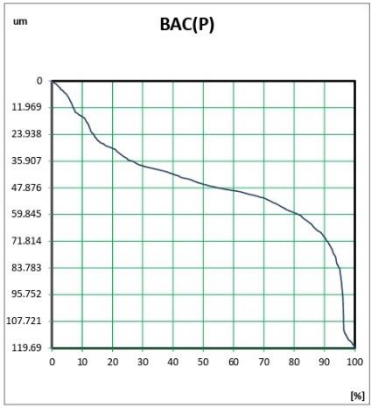

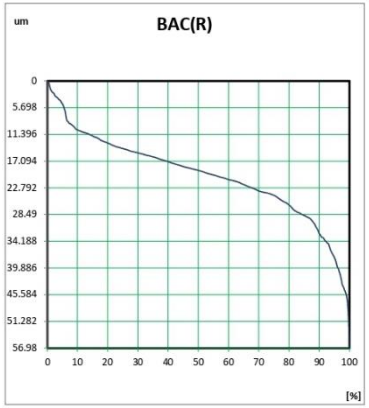

Prüfprotokoll

Seriennummer:		Kommentar		Messdatum	30.06.2022
Teilenummer	Planetenträger	Prüfer	Kalhöfer	Messzeit	10:07:42

Messbedingung

Messtyp	Roughness measuremen	Cutoff	0,8mm	λs Filter	2,5um
Berechnungsstandard	ISO1997/2009	Filtermethode	Gaussian	Einheit	mm/um
Auswertelänge	4,00mm	Messbereich	500,0um		
Messgeschwindigkeit	0,30mm/s	Entfernen der Form	Straight		

Messergebnis

Pt	119,270	Ra_5	4,753	Rz_5	29,367
Ra	6,811	Rz	39,818	Rp	17,094
Ra_1	8,128	Rz_1	43,852	Rp_1	17,900
Ra_2	12,809	Rz_2	75,137	Rp_2	40,677
Ra_3	4,660	Rz_3	32,007	Rp_3	9,040
Ra_4	3,702	Rz_4	18,726	Rp_4	9,215

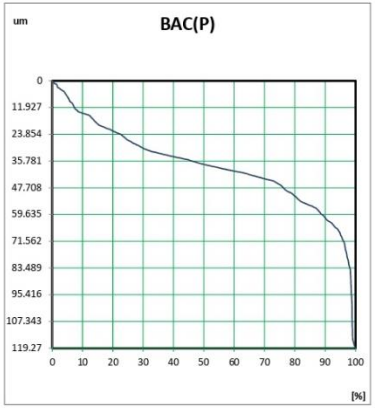

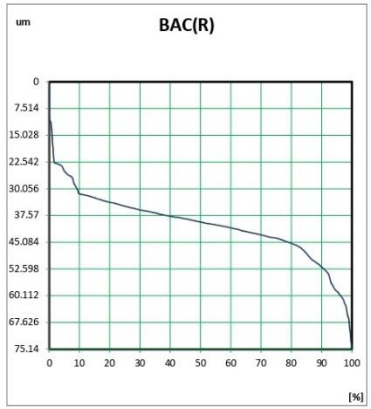

Prüfprotokoll

ACCRETECH

Seriennummer:		Kommentar		Messdatum	30.06.2022
Teilenummer	Planetenträger	Prüfer	Kalhöfer	Messzeit	10:08:41

Messbedingung

Messtyp	Roughness measuremen	Cutoff	0,8mm	λs Filter	2,5um
Berechnungsstandard	ISO1997/2009	Filtermethode	Gaussian	Einheit	mm/um
Auswertelänge	4,00mm	Messbereich	500,0um		
Messgeschwindigkeit	0,30mm/s	Entfernen der Form	Straight		

Messergebnis

Pt	125,282	Ra_5	4,522	Rz_5	27,876
Ra	6,717	Rz	40,921	Rp	18,791
Ra_1	8,013	Rz_1	44,368	Rp_1	18,965
Ra_2	12,880	Rz_2	82,609	Rp_2	48,781
Ra_3	4,499	Rz_3	31,644	Rp_3	9,130
Ra_4	3,669	Rz_4	18,106	Rp_4	8,944

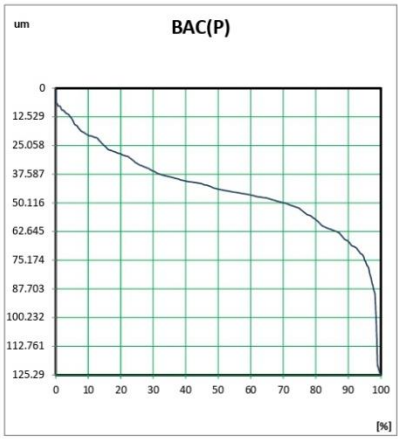

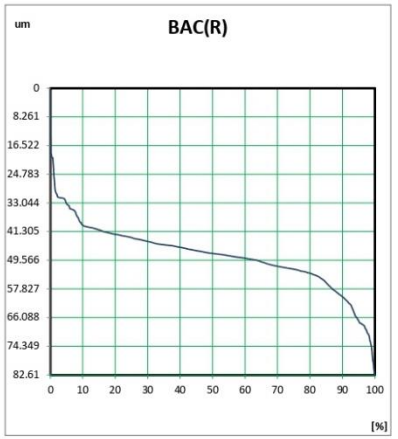

Prüfprotokoll

ACCRETECH

Seriennummer:		Kommentar		Messdatum	30.06.2022
Teilenummer	Planetenträger	Prüfer	Kalhöfer	Messzeit	10:14:31

Messbedingung

Messtyp	Roughness measuremen	Cutoff	0,8mm	λs Filter	2,5um
Berechnungsstandard	ISO1997/2009	Filtermethode	Gaussian	Einheit	mm/um
Auswertelänge	4,00mm	Messbereich	500,0um		
Messgeschwindigkeit	0,30mm/s	Entfernen der Form	Straight		

Messergebnis

Pt	148,610	Ra_5	12,880	Rz_5	49,415
Ra	11,283	Rz	66,980	Rp	17,334
Ra_1	4,911	Rz_1	33,345	Rp_1	5,031
Ra_2	7,726	Rz_2	77,614	Rp_2	17,247
Ra_3	18,366	Rz_3	99,115	Rp_3	24,489
Ra_4	12,530	Rz_4	75,412	Rp_4	22,582

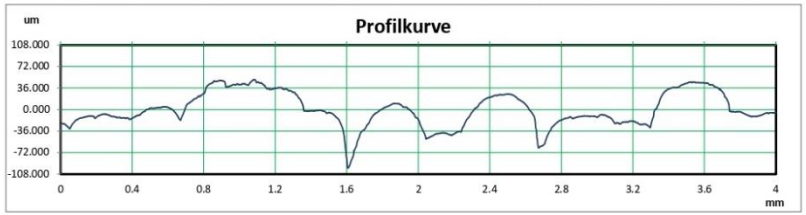

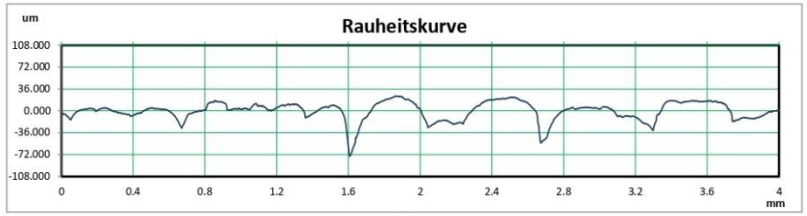

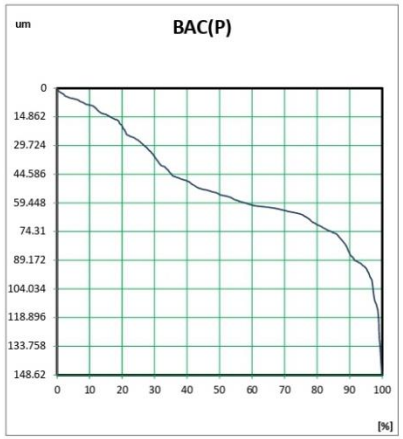

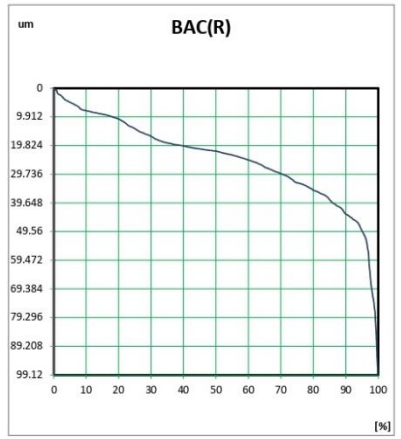

Prüfprotokoll

ACCRETECH

Seriennummer:		Kommentar		Messdatum	30.06.2022
Teilenummer	Planetenträger	Prüfer	Kalhöfer	Messzeit	10:15:23

Messbedingung

Messtyp	Roughness measuremen	Cutoff	0,8mm	λs Filter	2,5um
Berechnungsstandard	ISO1997/2009	Filtermethode	Gaussian	Einheit	mm/um
Auswertelänge	4,00mm	Messbereich	500,0um		
Messgeschwindigkeit	0,30mm/s	Entfernen der Form	Straight		

Messergebnis

Pt	133,545	Ra_5	5,097	Rz_5	25,456
Ra	11,069	Rz	56,049	Rp	18,779
Ra_1	14,526	Rz_1	94,432	Rp_1	24,415
Ra_2	18,216	Rz_2	77,244	Rp_2	23,086
Ra_3	10,564	Rz_3	49,353	Rp_3	17,689
Ra_4	6,941	Rz_4	33,760	Rp_4	15,755

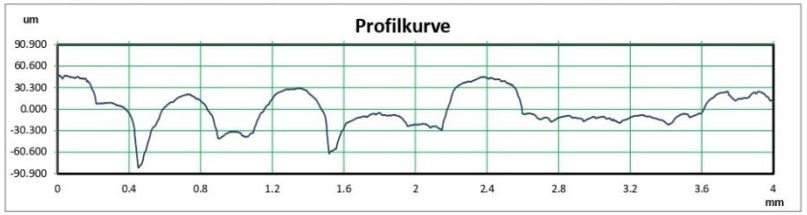

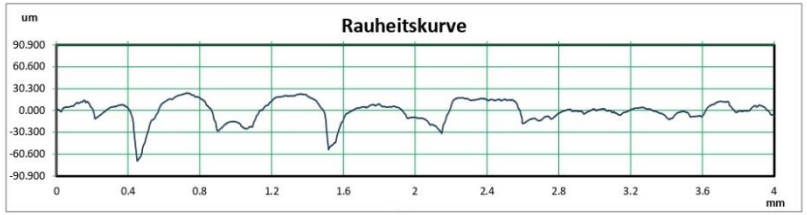

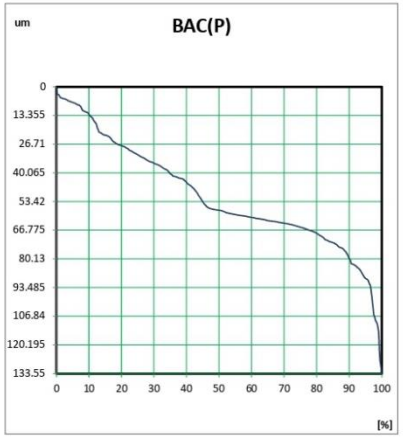

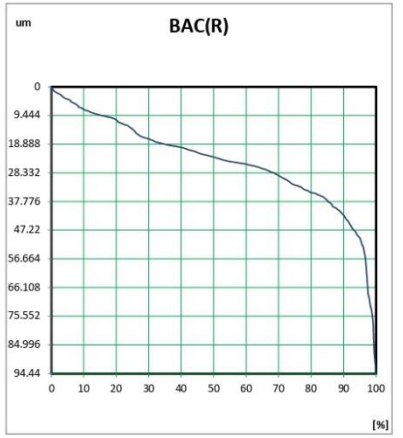

Prüfprotokoll

ACCRETECH

Seriennummer:		Kommentar		Messdatum	30.06.2022
Teilenummer	Planetenträger	Prüfer	Kalhöfer	Messzeit	10:16:23

Messbedingung

Messtyp	Roughness measuremen	Cutoff	0,8mm	λs Filter	2,5um
Berechnungsstandard	ISO1997/2009	Filtermethode	Gaussian	Einheit	mm/um
Auswertelänge	4,00mm	Messbereich	500,0um		
Messgeschwindigkeit	0,30mm/s	Entfernen der Form	Straight		

Messergebnis

Pt	123,673	Ra_5	5,620	Rz_5	25,774
Ra	11,219	Rz	56,012	Rp	19,119
Ra_1	15,178	Rz_1	91,213	Rp_1	24,396
Ra_2	17,569	Rz_2	79,027	Rp_2	23,770
Ra_3	12,203	Rz_3	48,770	Rp_3	18,111
Ra_4	5,526	Rz_4	35,273	Rp_4	16,440

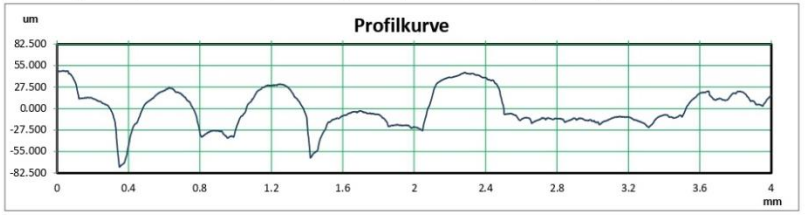

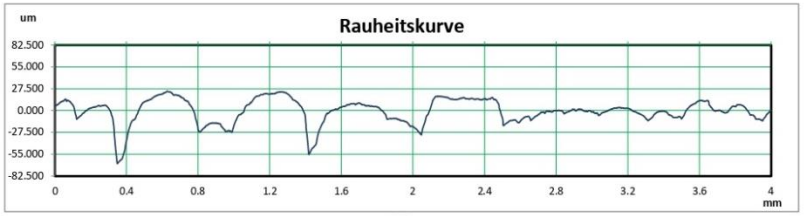

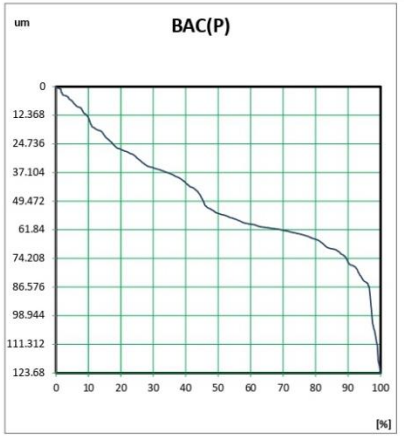

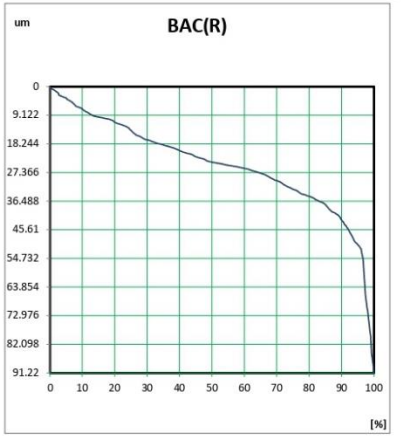

Prüfprotokoll

ACCRETECH

Seriennummer:		Kommentar		Messdatum	30.06.2022
Teilenummer	Planetenträger	Prüfer	Kalhöfer	Messzeit	10:23:10

Messbedingung

Messtyp	Roughness measuremen	Cutoff	0,8mm	λs Filter	2,5um
Berechnungsstandard	ISO1997/2009	Filtermethode	Gaussian	Einheit	mm/um
Auswertelänge	4,00mm	Messbereich	500,0um		
Messgeschwindigkeit	0,30mm/s	Entfernen der Form	Straight		

Messergebnis

Pt	101,618	Ra_5	8,821	Rz_5	47,380
Ra	10,842	Rz	51,174	Rp	22,434
Ra_1	12,864	Rz_1	53,481	Rp_1	32,635
Ra_2	10,988	Rz_2	59,734	Rp_2	27,482
Ra_3	13,182	Rz_3	62,307	Rp_3	20,229
Ra_4	8,357	Rz_4	32,970	Rp_4	13,061

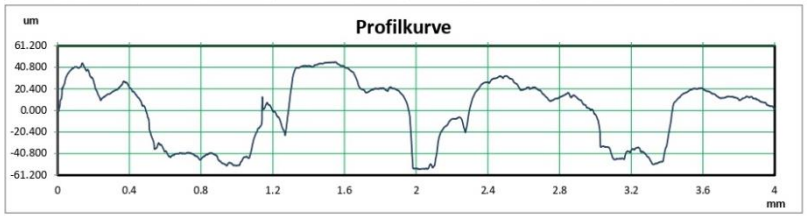

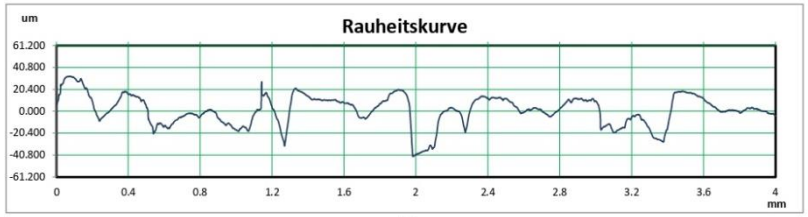

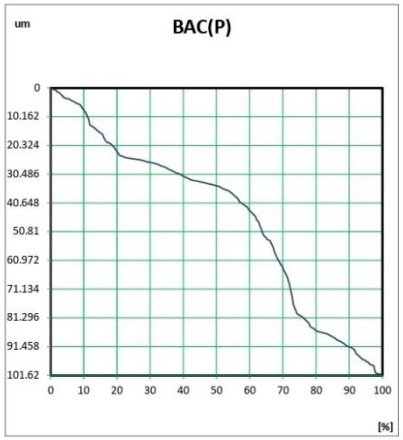

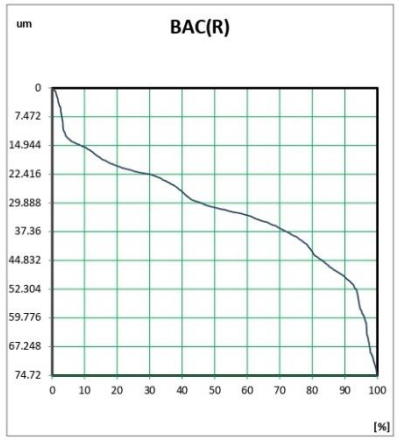

Prüfprotokoll

ACCRETECH

Seriennummer:		Kommentar		Messdatum	30.06.2022
Teilenummer	Planetenträger	Prüfer	Kalhöfer	Messzeit	10:24:10

Messbedingung

Messtyp	Roughness measuremen	Cutoff	0,8mm	λs Filter	2,5um
Berechnungsstandard	ISO1997/2009	Filtermethode	Gaussian	Einheit	mm/um
Auswertelänge	4,00mm	Messbereich	500,0um		
Messgeschwindigkeit	0,30mm/s	Entfernen der Form	Straight		

Messergebnis

Pt	103,420	Ra_5	9,476	Rz_5	47,652
Ra	11,128	Rz	54,680	Rp	23,359
Ra_1	13,971	Rz_1	66,244	Rp_1	32,473
Ra_2	10,674	Rz_2	62,749	Rp_2	30,512
Ra_3	12,979	Rz_3	62,656	Rp_3	20,427
Ra_4	8,542	Rz_4	34,097	Rp_4	14,233

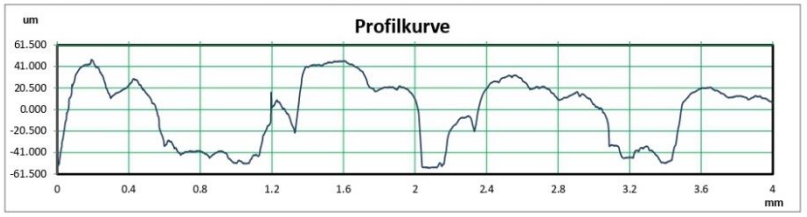

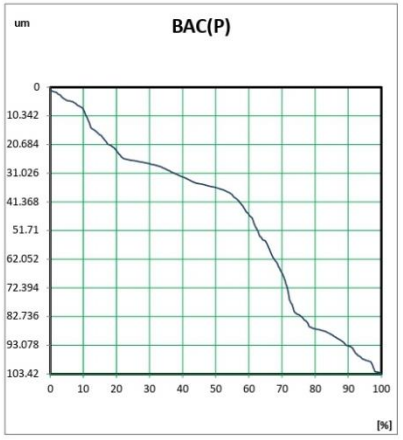

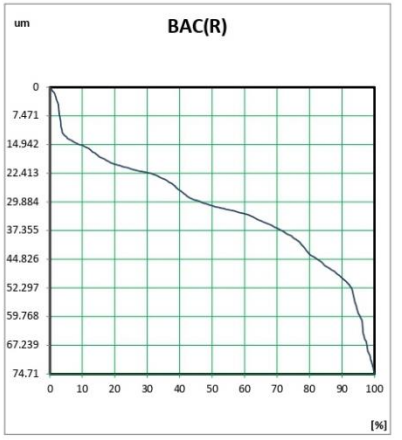

Prüfprotokoll

ACCRETECH

Seriennummer:		Kommentar		Messdatum	30.06.2022
Teilenummer	Planetenträger	Prüfer	Kalhöfer	Messzeit	10:25:22

Messbedingung

Messtyp	Roughness measuremen	Cutoff	0,8mm	λs Filter	2,5um
Berechnungsstandard	ISO1997/2009	Filtermethode	Gaussian	Einheit	mm/um
Auswertelänge	4,00mm	Messbereich	500,0um		
Messgeschwindigkeit	0,30mm/s	Entfernen der Form	Straight		

Messergebnis

Pt	98,743	Ra_5	2,220	Rz_5	12,090
Ra	8,184	Rz	42,870	Rp	19,871
Ra_1	10,421	Rz_1	66,408	Rp_1	34,542
Ra_2	12,855	Rz_2	62,556	Rp_2	20,415
Ra_3	11,533	Rz_3	47,934	Rp_3	19,705
Ra_4	3,892	Rz_4	25,360	Rp_4	19,359

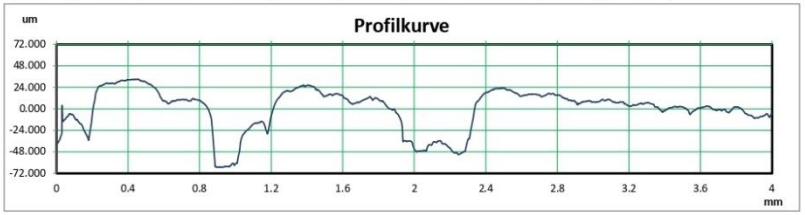

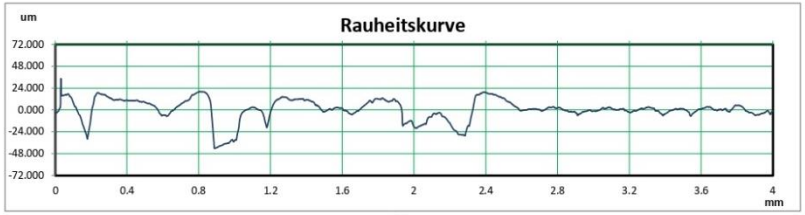

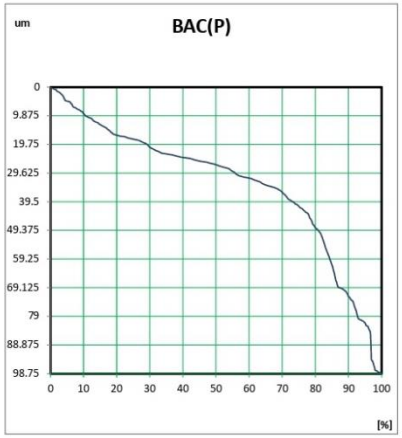

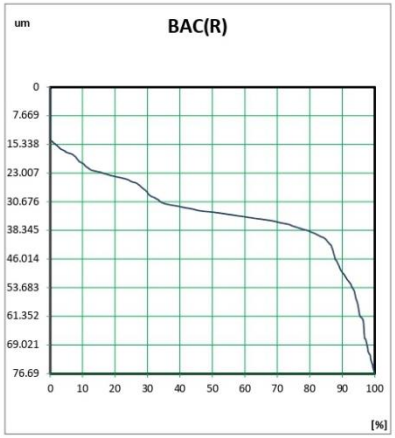

Appendix S – Gyroid | Top

Prüfprotokoll

Seriennummer:		Kommentar		Messdatum	30.06.2022
Teilenummer	Planetenträger	Prüfer	Kalhöfer	Messzeit	10:30:34

Messbedingung

Messtyp	Roughness measuremen	Cutoff	0,8mm	λs Filter	2,5um
Berechnungsstandard	ISO1997/2009	Filtermethode	Gaussian	Einheit	mm/um
Auswertelänge	4,00mm	Messbereich	500,0um		
Messgeschwindigkeit	0,30mm/s	Entfernen der Form	Straight		

Messergebnis

Pt	19,490	Ra_5	0,951	Rz_5	5,804
Ra	1,169	Rz	6,333	Rp	3,085
Ra_1	1,087	Rz_1	7,386	Rp_1	3,449
Ra_2	1,521	Rz_2	7,772	Rp_2	3,415
Ra_3	1,478	Rz_3	6,307	Rp_3	3,037
Ra_4	0,809	Rz_4	4,394	Rp_4	2,072

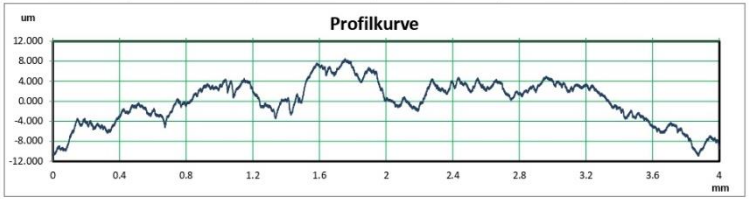

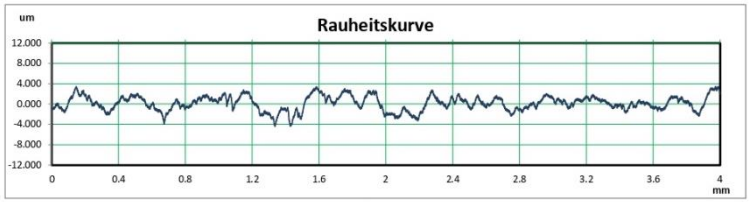

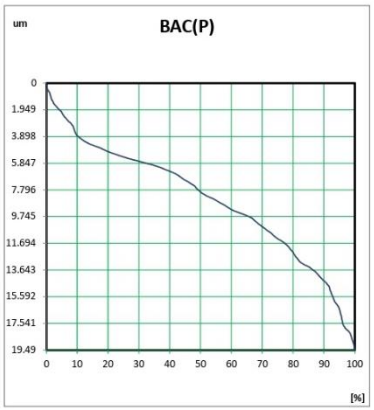

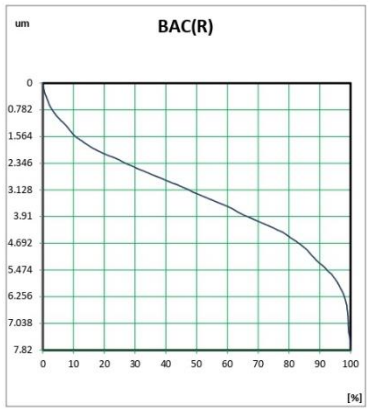

Prüfprotokoll

Seriennummer:		Kommentar		Messdatum	30.06.2022
Teilenummer	Planetenträger	Prüfer	Kalhöfer	Messzeit	10:31:49

Messbedingung

Messtyp	Roughness measuremen	Cutoff	0,8mm	λs Filter	2,5um
Berechnungsstandard	ISO1997/2009	Filtermethode	Gaussian	Einheit	mm/um
Auswertelänge	4,00mm	Messbereich	500,0um		
Messgeschwindigkeit	0,30mm/s	Entfernen der Form	Straight		

Messergebnis

Pt	24,056	Ra_5	1,095	Rz_5	6,389
Ra	1,179	Rz	6,291	Rp	2,911
Ra_1	1,166	Rz_1	6,887	Rp_1	2,568
Ra_2	1,746	Rz_2	8,786	Rp_2	3,706
Ra_3	1,099	Rz_3	5,351	Rp_3	2,556
Ra_4	0,790	Rz_4	4,042	Rp_4	2,283

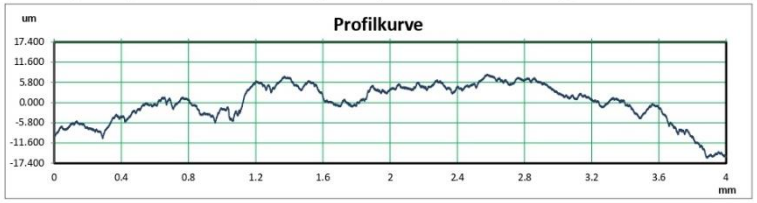

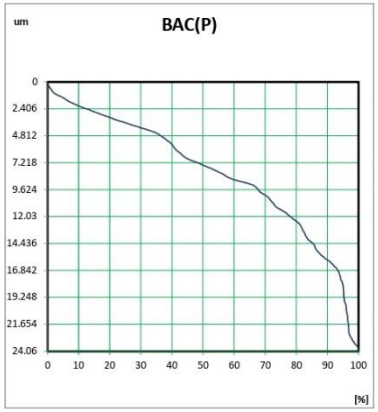

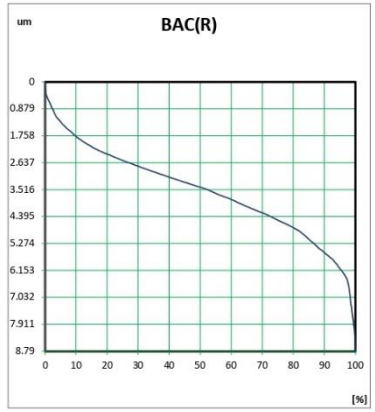

Prüfprotokoll

ACCRETECH

Seriennummer:		Kommentar		Messdatum	30.06.2022
Teilenummer	Planetenträger	Prüfer	Kalhöfer	Messzeit	10:32:45

Messbedingung

Messtyp	Roughness measuremen	Cutoff	0,8mm	λs Filter	2,5um
Berechnungsstandard	ISO1997/2009	Filtermethode	Gaussian	Einheit	mm/um
Auswertelänge	4,00mm	Messbereich	500,0um		
Messgeschwindigkeit	0,30mm/s	Entfernen der Form	Straight		

Messergebnis

Pt	21,932	Ra_5	0,977	Rz_5	5,734
Ra	1,186	Rz	6,412	Rp	3,085
Ra_1	1,103	Rz_1	7,185	Rp_1	2,965
Ra_2	1,692	Rz_2	8,654	Rp_2	3,711
Ra_3	1,309	Rz_3	5,913	Rp_3	3,085
Ra_4	0,848	Rz_4	4,572	Rp_4	2,234

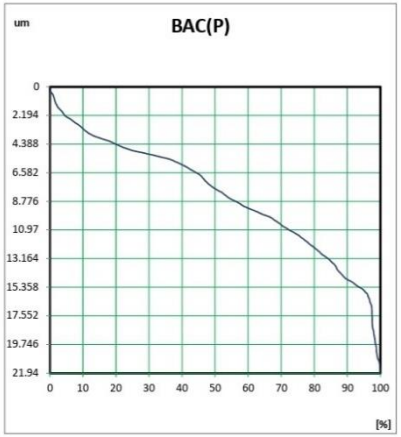

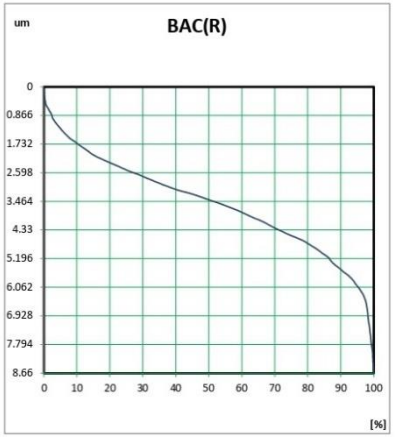

Prüfprotokoll

ACCRETECH

Seriennummer:		Kommentar		Messdatum	30.06.2022
Teilenummer	Planetenträger	Prüfer	Kalhöfer	Messzeit	10:41:55

Messbedingung

Messtyp	Roughness measuremen	Cutoff	0,8mm	λs Filter	2,5um
Berechnungsstandard	ISO1997/2009	Filtermethode	Gaussian	Einheit	mm/um
Auswertelänge	4,00mm	Messbereich	500,0um		
Messgeschwindigkeit	0,30mm/s	Entfernen der Form	Straight		

Messergebnis

Pt	25,675	Ra_5	1,494	Rz_5	6,262
Ra	2,745	Rz	12,401	Rp	5,632
Ra_1	3,521	Rz_1	16,685	Rp_1	5,951
Ra_2	2,847	Rz_2	13,362	Rp_2	5,659
Ra_3	3,523	Rz_3	14,363	Rp_3	6,772
Ra_4	2,338	Rz_4	11,333	Rp_4	6,471

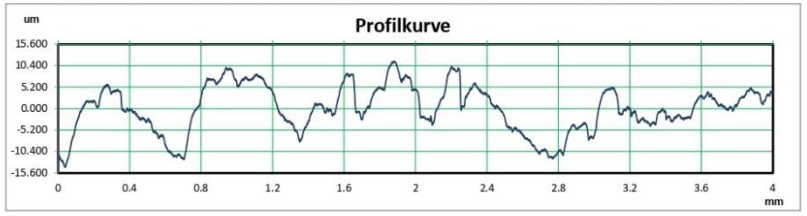

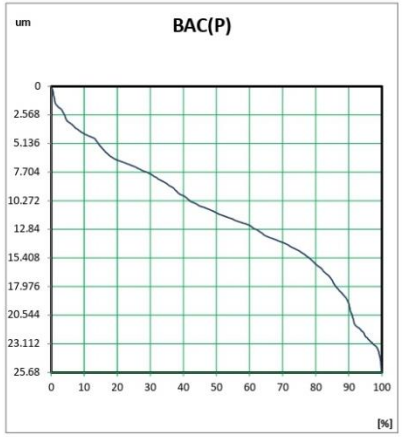

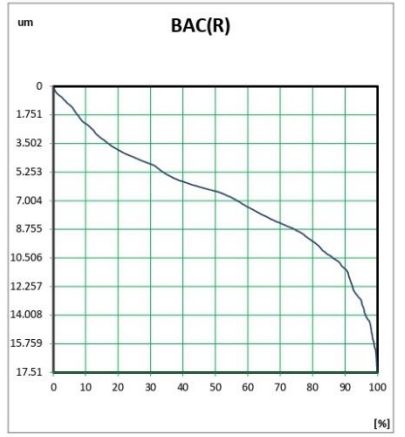

Prüfprotokoll

ACCRETECH

Seriennummer:		Kommentar		Messdatum	30.06.2022
Teilenummer	Planetenträger	Prüfer	Kalhöfer	Messzeit	10:42:53

Messbedingung

Messtyp	Roughness measuremen	Cutoff	0,8mm	λs Filter	2,5um
Berechnungsstandard	ISO1997/2009	Filtermethode	Gaussian	Einheit	mm/um
Auswertelänge	4,00mm	Messbereich	500,0um		
Messgeschwindigkeit	0,30mm/s	Entfernen der Form	Straight		

Messergebnis

Pt	24,465	Ra_5	2,126	Rz_5	10,406
Ra	2,431	Rz	11,376	Rp	5,763
Ra_1	2,867	Rz_1	14,057	Rp_1	6,367
Ra_2	3,097	Rz_2	13,430	Rp_2	6,432
Ra_3	2,321	Rz_3	11,678	Rp_3	6,833
Ra_4	1,745	Rz_4	7,311	Rp_4	3,808

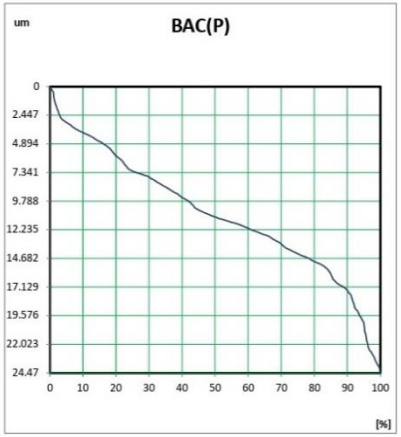

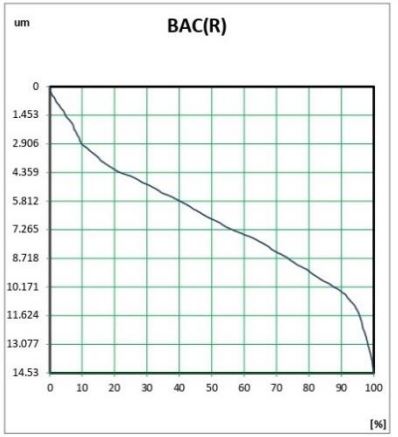

Prüfprotokoll

ACCRETECH

Seriennummer:		Kommentar		Messdatum	30.06.2022
Teilenummer	Planetenträger	Prüfer	Kalhöfer	Messzeit	10:44:03

Messbedingung

Messtyp	Roughness measuremen	Cutoff	0,8mm	λs Filter	2,5um
Berechnungsstandard	ISO1997/2009	Filtermethode	Gaussian	Einheit	mm/um
Auswertelänge	4,00mm	Messbereich	500,0um		
Messgeschwindigkeit	0,30mm/s	Entfernen der Form	Straight		

Messergebnis

Pt	24,136	Ra_5	1,606	Rz_5	8,901
Ra	2,535	Rz	12,670	Rp	5,802
Ra_1	3,067	Rz_1	15,395	Rp_1	5,660
Ra_2	2,912	Rz_2	14,421	Rp_2	6,496
Ra_3	2,748	Rz_3	12,830	Rp_3	5,914
Ra_4	2,343	Rz_4	11,804	Rp_4	7,052

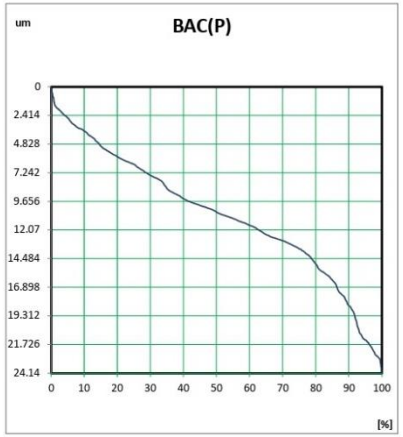

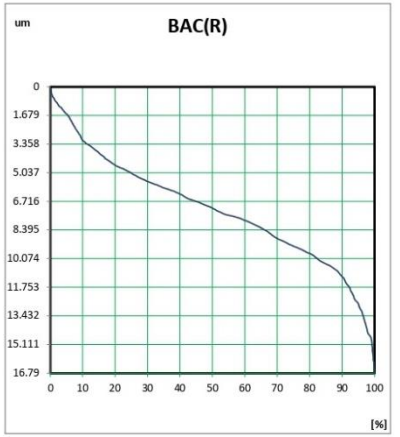

Appendix T – Quarter-Cubic | Top

Prüfprotokoll

Seriennummer:		Kommentar		Messdatum	30.06.2022
Teilenummer	Planetenträger	Prüfer	Kalhöfer	Messzeit	10:53:21

Messbedingung

Messtyp	Roughness measuremen	Cutoff	0,8mm	λs Filter	2,5um
Berechnungsstandard	ISO1997/2009	Filtermethode	Gaussian	Einheit	mm/um
Auswertelänge	4,00mm	Messbereich	500,0um		
Messgeschwindigkeit	0,30mm/s	Entfernen der Form	Straight		

Messergebnis

Pt	15,808	Ra_5	1,082	Rz_5	5,483
Ra	1,300	Rz	6,974	Rp	3,002
Ra_1	1,173	Rz_1	5,501	Rp_1	2,124
Ra_2	1,315	Rz_2	7,758	Rp_2	3,134
Ra_3	1,242	Rz_3	8,069	Rp_3	3,606
Ra_4	1,689	Rz_4	8,061	Rp_4	3,453

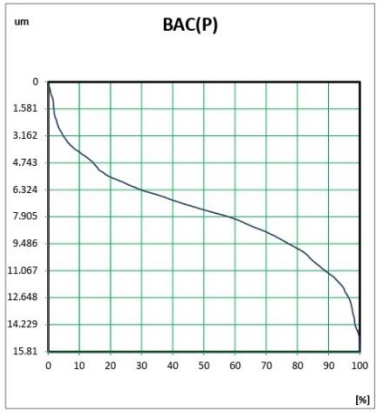

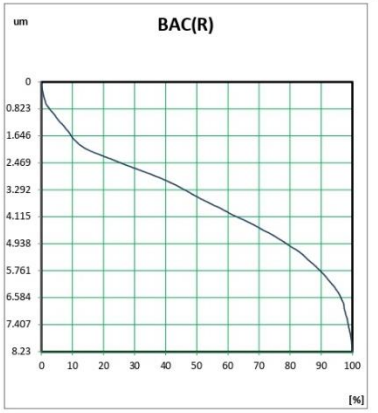

Prüfprotokoll

Seriennummer:		Kommentar		Messdatum	30.06.2022
Teilenummer	Planetenträger	Prüfer	Kalhöfer	Messzeit	10:55:16

Messbedingung

Messtyp	Roughness measuremen	Cutoff	0,8mm	λs Filter	2,5um
Berechnungsstandard	ISO1997/2009	Filtermethode	Gaussian	Einheit	mm/um
Auswertelänge	4,00mm	Messbereich	500,0um		
Messgeschwindigkeit	0,30mm/s	Entfernen der Form	Straight		

Messergebnis

Pt	16,786	Ra_5	1,324	Rz_5	9,085
Ra	1,418	Rz	8,676	Rp	3,714
Ra_1	1,319	Rz_1	7,864	Rp_1	2,377
Ra_2	1,458	Rz_2	9,944	Rp_2	3,818
Ra_3	1,413	Rz_3	9,179	Rp_3	5,486
Ra_4	1,575	Rz_4	7,311	Rp_4	2,830

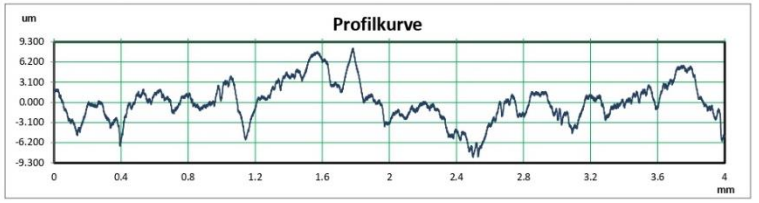

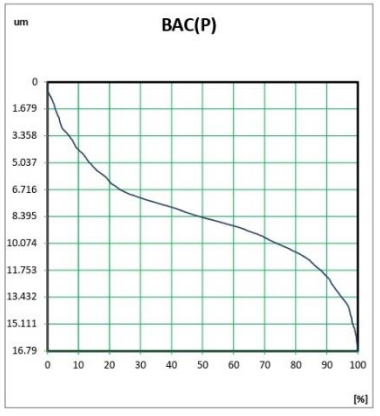

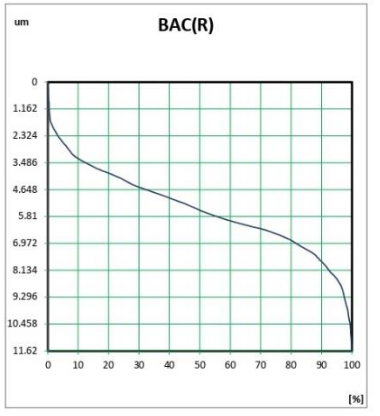

Prüfprotokoll

ACCRETECH

Seriennummer:		Kommentar		Messdatum	30.06.2022
Teilenummer	Planetenträger	Prüfer	Kalhöfer	Messzeit	10:55:16

Messbedingung

Messtyp	Roughness measuremen	Cutoff	0,8mm	λs Filter	2,5um
Berechnungsstandard	ISO1997/2009	Filtermethode	Gaussian	Einheit	mm/um
Auswertelänge	4,00mm	Messbereich	500,0um		
Messgeschwindigkeit	0,30mm/s	Entfernen der Form	Straight		

Messergebnis

Pt	16,786	Ra_5	1,324	Rz_5	9,085
Ra	1,418	Rz	8,676	Rp	3,714
Ra_1	1,319	Rz_1	7,864	Rp_1	2,377
Ra_2	1,458	Rz_2	9,944	Rp_2	3,818
Ra_3	1,413	Rz_3	9,179	Rp_3	5,486
Ra_4	1,575	Rz_4	7,311	Rp_4	2,830

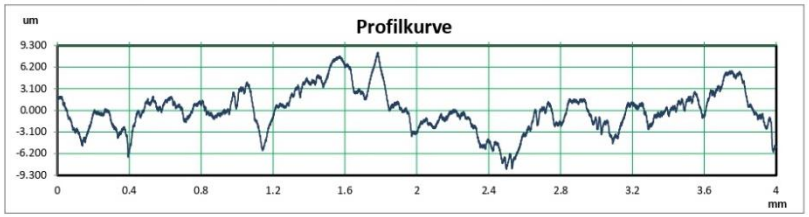

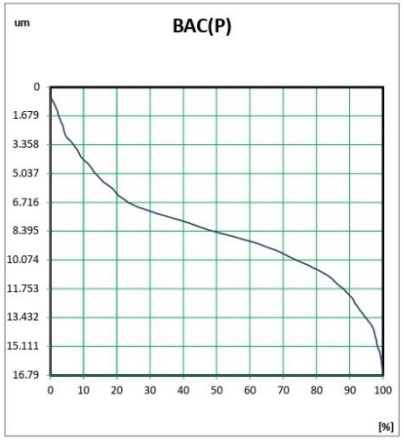

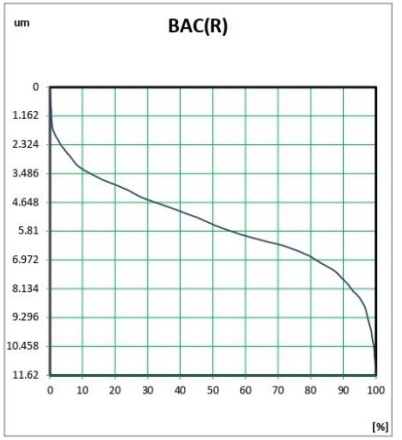

Prüfprotokoll

ACCRETECH

Seriennummer:		Kommentar		Messdatum	30.06.2022
Teilenummer	Planetenträger	Prüfer	Kalhöfer	Messzeit	10:59:49

Messbedingung

Messtyp	Roughness measuremen	Cutoff	0,8mm	λs Filter	2,5um
Berechnungsstandard	ISO1997/2009	Filtermethode	Gaussian	Einheit	mm/um
Auswertelänge	4,00mm	Messbereich	500,0um		
Messgeschwindigkeit	0,30mm/s	Entfernen der Form	Straight		

Messergebnis

Pt	25,936	Ra_5	2,699	Rz_5	12,689
Ra	2,337	Rz	12,570	Rp	4,805
Ra_1	2,499	Rz_1	14,434	Rp_1	6,385
Ra_2	2,245	Rz_2	13,389	Rp_2	4,427
Ra_3	1,903	Rz_3	13,759	Rp_3	4,430
Ra_4	2,339	Rz_4	8,580	Rp_4	4,355

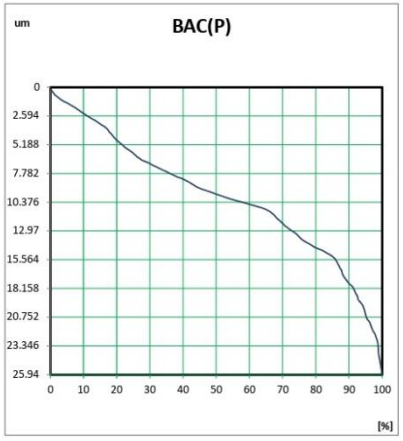

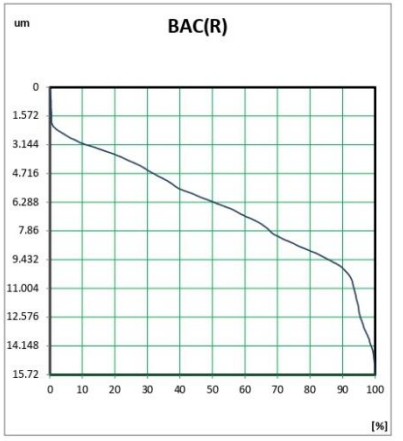

Prüfprotokoll

ACCRETECH

Seriennummer:		Kommentar		Messdatum	30.06.2022
Teilenummer	Planetenträger	Prüfer	Kalhöfer	Messzeit	11:00:51

Messbedingung

Messtyp	Roughness measuremen	Cutoff	0,8mm	λs Filter	2,5um
Berechnungsstandard	ISO1997/2009	Filtermethode	Gaussian	Einheit	mm/um
Auswertelänge	4,00mm	Messbereich	500,0um		
Messgeschwindigkeit	0,30mm/s	Entfernen der Form	Straight		

Messergebnis

Pt	25,293	Ra_5	2,836	Rz_5	13,484
Ra	2,503	Rz	12,046	Rp	5,513
Ra_1	2,695	Rz_1	12,659	Rp_1	6,457
Ra_2	2,258	Rz_2	9,409	Rp_2	4,658
Ra_3	2,639	Rz_3	15,150	Rp_3	5,435
Ra_4	2,086	Rz_4	9,527	Rp_4	4,360

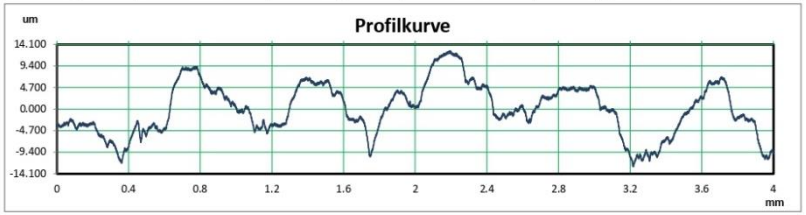

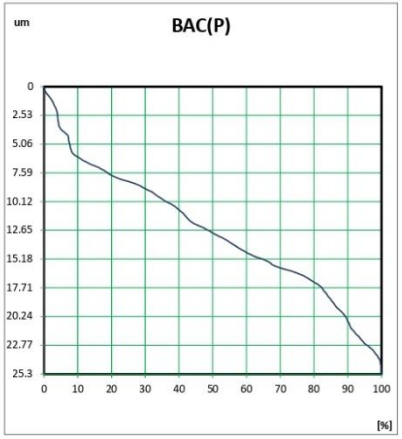

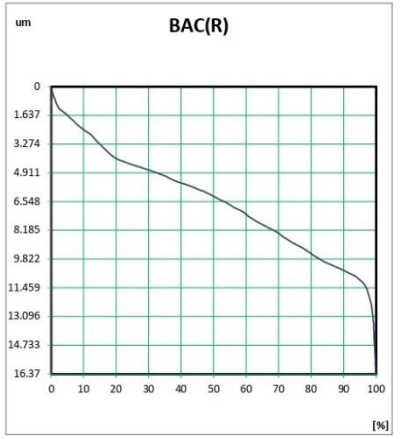

Prüfprotokoll

ACCRETECH

Seriennummer:		Kommentar		Messdatum	30.06.2022
Teilenummer	Planetenträger	Prüfer	Kalhöfer	Messzeit	11:01:50

Messbedingung

Messtyp	Roughness measuremen	Cutoff	0,8mm	λs Filter	2,5um
Berechnungsstandard	ISO1997/2009	Filtermethode	Gaussian	Einheit	mm/um
Auswertelänge	4,00mm	Messbereich	500,0um		
Messgeschwindigkeit	0,30mm/s	Entfernen der Form	Straight		

Messergebnis

Pt	25,506	Ra_5	2,830	Rz_5	12,219
Ra	2,526	Rz	12,324	Rp	5,494
Ra_1	2,626	Rz_1	12,710	Rp_1	6,170
Ra_2	2,319	Rz_2	9,691	Rp_2	4,882
Ra_3	2,548	Rz_3	15,068	Rp_3	5,275
Ra_4	2,305	Rz_4	11,930	Rp_4	4,531

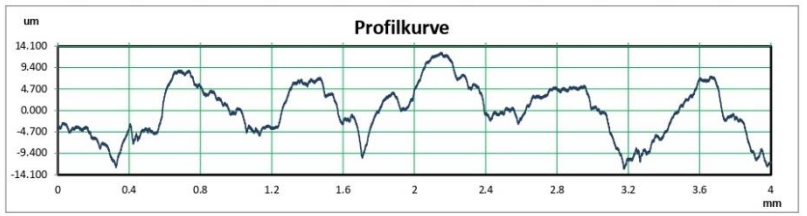

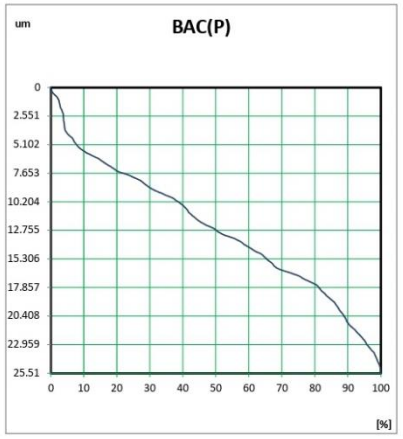

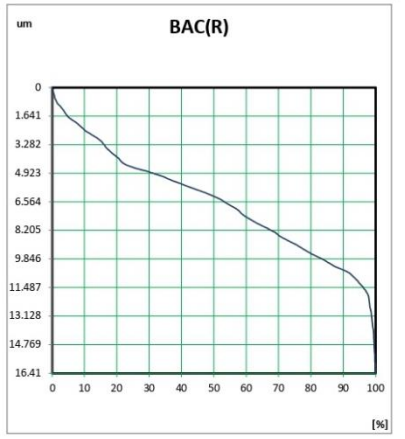

Prüfprotokoll

ACCRETECH

Seriennummer:		Kommentar		Messdatum	30.06.2022
Teilenummer	Planetenträger	Prüfer	Kalhöfer	Messzeit	11:06:36

Messbedingung

Messtyp	Roughness measuremen	Cutoff	0,8mm	λs Filter	2,5um
Berechnungsstandard	ISO1997/2009	Filtermethode	Gaussian	Einheit	mm/um
Auswertelänge	4,00mm	Messbereich	500,0um		
Messgeschwindigkeit	0,30mm/s	Entfernen der Form	Straight		

Messergebnis

Pt	25,086	Ra_5	2,541	Rz_5	16,380
Ra	2,762	Rz	13,613	Rp	6,207
Ra_1	2,468	Rz_1	10,691	Rp_1	4,799
Ra_2	2,895	Rz_2	12,985	Rp_2	5,204
Ra_3	3,055	Rz_3	12,832	Rp_3	5,836
Ra_4	2,851	Rz_4	15,178	Rp_4	7,606

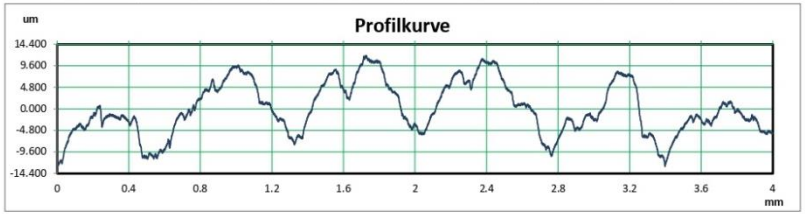

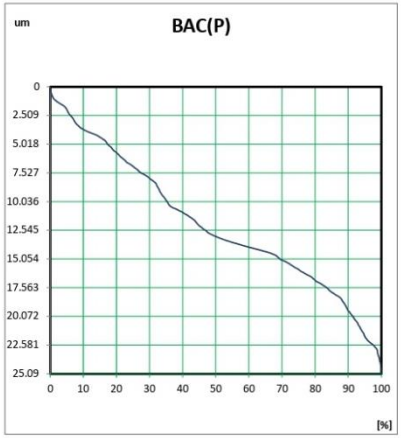

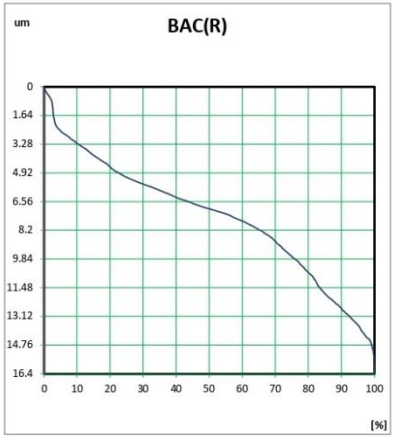

Prüfprotokoll

ACCRETECH

Seriennummer:		Kommentar		Messdatum	30.06.2022
Teilenummer	Planetenträger	Prüfer	Kalhöfer	Messzeit	11:07:26

Messbedingung

Messtyp	Roughness measuremen	Cutoff	0,8mm	λs Filter	2,5um
Berechnungsstandard	ISO1997/2009	Filtermethode	Gaussian	Einheit	mm/um
Auswertelänge	4,00mm	Messbereich	500,0um		
Messgeschwindigkeit	0,30mm/s	Entfernen der Form	Straight		

Messergebnis

Pt	27,476	Ra_5	3,040	Rz_5	15,985
Ra	2,906	Rz	13,791	Rp	5,703
Ra_1	2,975	Rz_1	15,211	Rp_1	4,630
Ra_2	2,555	Rz_2	11,367	Rp_2	5,139
Ra_3	3,250	Rz_3	13,414	Rp_3	5,551
Ra_4	2,711	Rz_4	12,976	Rp_4	5,426

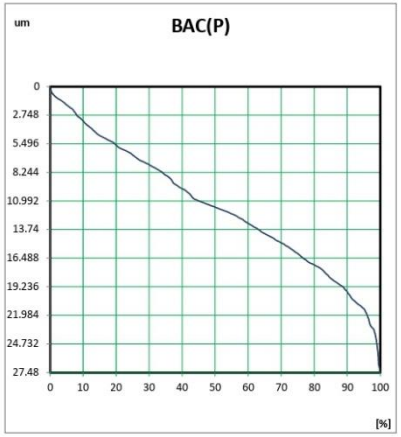

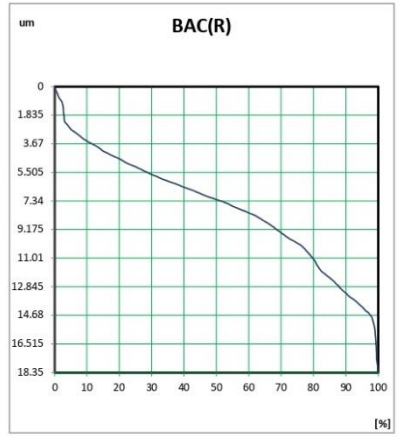

Prüfprotokoll

ACCRETECH

Seriennummer:		Kommentar		Messdatum	30.06.2022
Teilenummer	Planetenträger	Prüfer	Kalhöfer	Messzeit	11:08:20

Messbedingung

Messtyp	Roughness measuremen	Cutoff	0,8mm	λs Filter	2,5um
Berechnungsstandard	ISO1997/2009	Filtermethode	Gaussian	Einheit	mm/um
Auswertelänge	4,00mm	Messbereich	500,0um		
Messgeschwindigkeit	0,30mm/s	Entfernen der Form	Straight		

Messergebnis

Pt	27,573	Ra_5	3,274	Rz_5	15,957
Ra	2,845	Rz	13,980	Rp	5,701
Ra_1	3,241	Rz_1	15,197	Rp_1	4,418
Ra_2	2,609	Rz_2	12,936	Rp_2	5,148
Ra_3	2,876	Rz_3	12,749	Rp_3	5,671
Ra_4	2,225	Rz_4	13,058	Rp_4	5,387

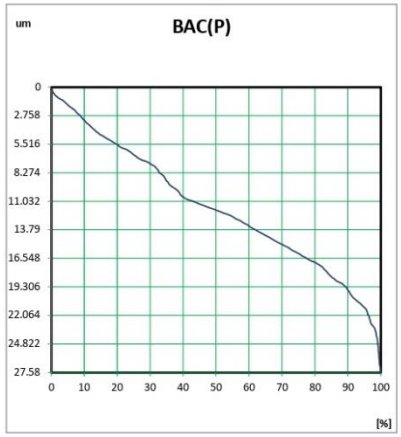

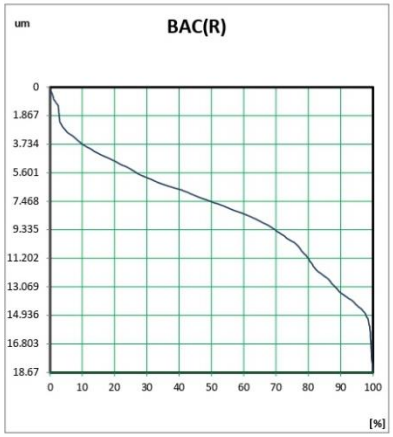

Appendix U – Tri-Hexagon | Top

Prüfprotokoll

Seriennummer:		Kommentar		Messdatum	30.06.2022
Teilenummer	Planetenträger	Prüfer	Kalhöfer	Messzeit	10:00:20
Messbedingung					
Messtyp	Roughness measuremen	Cutoff	0,8mm	λs Filter	2,5um
Berechnungsstandard	ISO1997/2009	Filtermethode	Gaussian	Einheit	mm/um
Auswertelänge	4,00mm	Messbereich	500,0um		
Messgeschwindigkeit	0,30mm/s	Entfernen der Form	Straight		
Messergebnis					
Pt	24,758	Ra_5	0,755	Rz_5	6,003
Ra	1,065	Rz	6,694	Rp	3,610
Ra_1	1,125	Rz_1	6,664	Rp_1	2,834
Ra_2	1,427	Rz_2	8,230	Rp_2	4,219
Ra_3	1,103	Rz_3	6,293	Rp_3	3,959
Ra_4	0,912	Rz_4	6,281	Rp_4	3,876

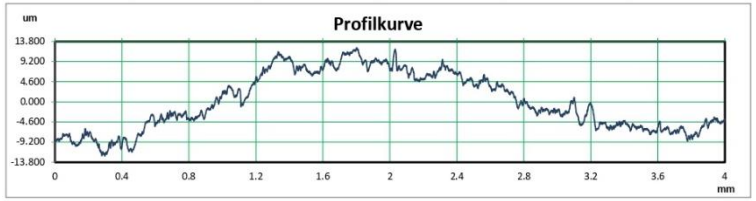

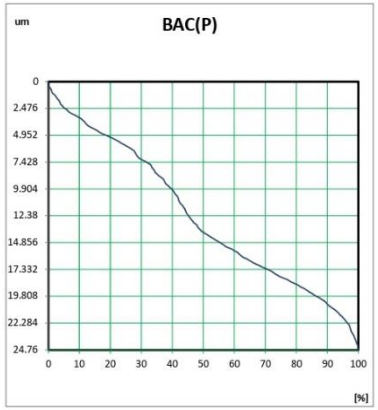

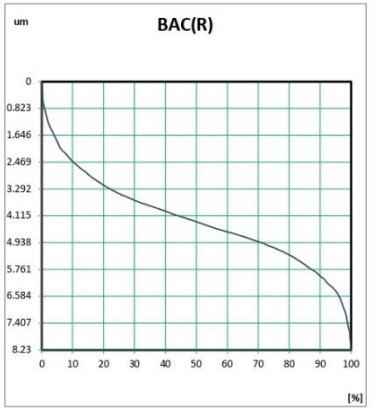

Prüfprotokoll

Seriennummer:		Kommentar		Messdatum	30.06.2022
Teilenummer	Planetenträger	Prüfer	Kalhöfer	Messzeit	10:01:26
Messbedingung					
Messtyp	Roughness measuremen	Cutoff	0,8mm	λs Filter	2,5um
Berechnungsstandard	ISO1997/2009	Filtermethode	Gaussian	Einheit	mm/um
Auswertelänge	4,00mm	Messbereich	500,0um		
Messgeschwindigkeit	0,30mm/s	Entfernen der Form	Straight		
Messergebnis					
Pt	19,483	Ra_5	0,946	Rz_5	6,070
Ra	1,075	Rz	6,941	Rp	3,841
Ra_1	1,072	Rz_1	6,028	Rp_1	3,147
Ra_2	0,887	Rz_2	5,664	Rp_2	2,647
Ra_3	1,283	Rz_3	7,421	Rp_3	4,749
Ra_4	1,189	Rz_4	9,520	Rp_4	5,553

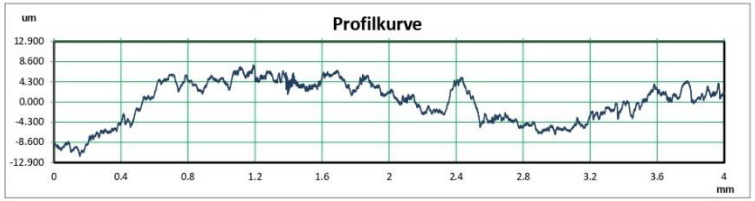

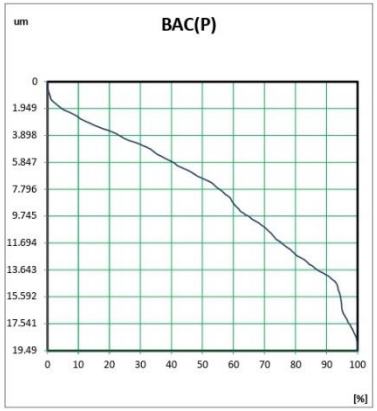

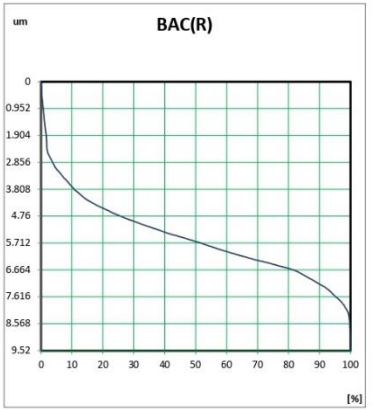

Prüfprotokoll

ACCRETECH

Seriennummer:		Kommentar		Messdatum	30.06.2022
Teilenummer	Planetenträger	Prüfer	Kalhöfer	Messzeit	10:02:21

Messbedingung

Messtyp	Roughness measuremen	Cutoff	0,8mm	λs Filter	2,5um
Berechnungsstandard	ISO1997/2009	Filtermethode	Gaussian	Einheit	mm/um
Auswertelänge	4,00mm	Messbereich	500,0um		
Messgeschwindigkeit	0,30mm/s	Entfernen der Form	Straight		

Messergebnis

Pt	18,900	Ra_5	0,964	Rz_5	5,496
Ra	1,057	Rz	5,975	Rp	3,207
Ra_1	1,002	Rz_1	5,885	Rp_1	3,382
Ra_2	0,939	Rz_2	5,207	Rp_2	2,607
Ra_3	1,661	Rz_3	9,531	Rp_3	5,654
Ra_4	0,719	Rz_4	3,756	Rp_4	1,431

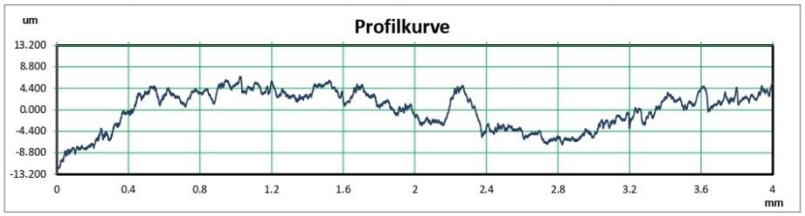

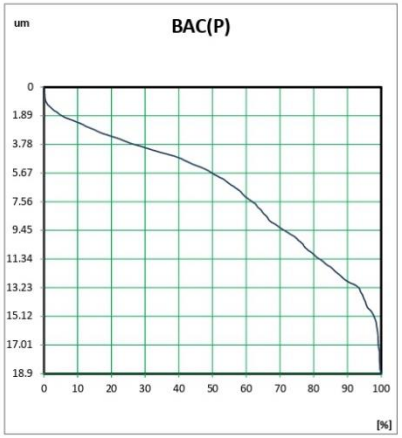

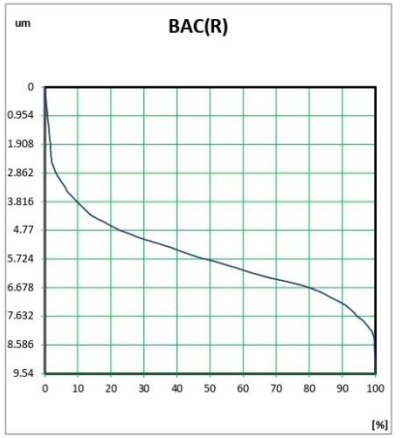

Prüfprotokoll

ACCRETECH

Seriennummer:		Kommentar		Messdatum	30.06.2022
Teilenummer	Planetenträger	Prüfer	Kalhöfer	Messzeit	10:10:22

Messbedingung

Messtyp	Roughness measuremen	Cutoff	0,8mm	λs Filter	2,5um
Berechnungsstandard	ISO1997/2009	Filtermethode	Gaussian	Einheit	mm/um
Auswertelänge	4,00mm	Messbereich	500,0um		
Messgeschwindigkeit	0,30mm/s	Entfernen der Form	Straight		

Messergebnis

Pt	15,555	Ra_5	1,168	Rz_5	7,709
Ra	1,223	Rz	7,461	Rp	3,734
Ra_1	0,980	Rz_1	7,155	Rp_1	3,190
Ra_2	1,348	Rz_2	8,499	Rp_2	4,177
Ra_3	1,309	Rz_3	7,140	Rp_3	3,870
Ra_4	1,310	Rz_4	6,803	Rp_4	2,859

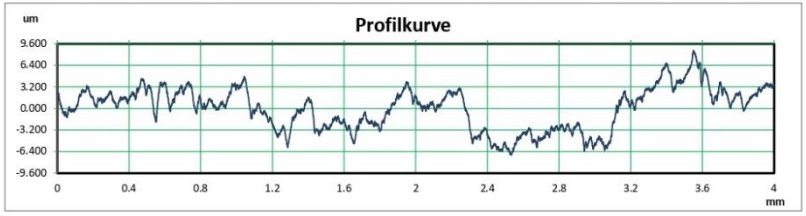

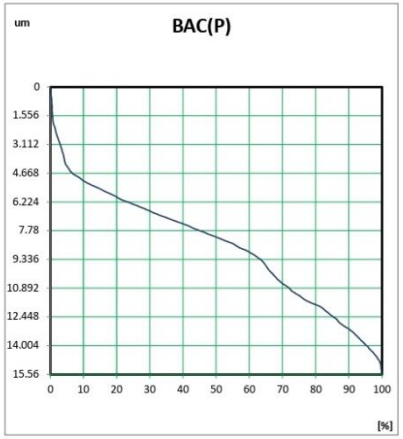

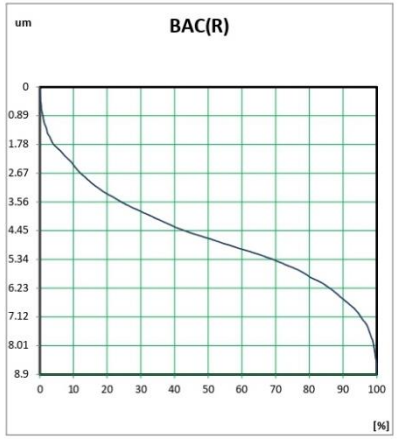

Prüfprotokoll

ACCRETECH

Seriennummer:		Kommentar		Messdatum	30.06.2022
Teilenummer	Planetenträger	Prüfer	Kalhöfer	Messzeit	10:11:51

Messbedingung

Messtyp	Roughness measuremen	Cutoff	0,8mm	λs Filter	2,5um
Berechnungsstandard	ISO1997/2009	Filtermethode	Gaussian	Einheit	mm/um
Auswertelänge	4,00mm	Messbereich	500,0um		
Messgeschwindigkeit	0,30mm/s	Entfernen der Form	Straight		

Messergebnis

Pt	26,056	Ra_5	1,400	Rz_5	8,878
Ra	1,295	Rz	7,794	Rp	4,348
Ra_1	0,916	Rz_1	6,315	Rp_1	3,212
Ra_2	1,259	Rz_2	6,679	Rp_2	3,503
Ra_3	1,939	Rz_3	11,236	Rp_3	5,737
Ra_4	0,964	Rz_4	5,862	Rp_4	3,459

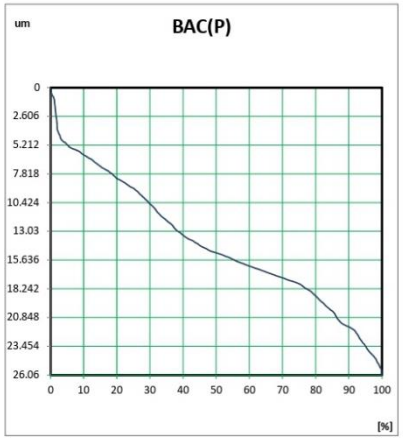

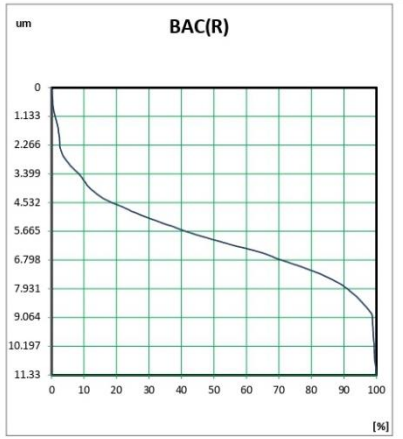

Prüfprotokoll

ACCRETECH

Seriennummer:		Kommentar		Messdatum	30.06.2022
Teilenummer	Planetenträger	Prüfer	Kalhöfer	Messzeit	10:12:56

Messbedingung

Messtyp	Roughness measuremen	Cutoff	0,8mm	λs Filter	2,5um
Berechnungsstandard	ISO1997/2009	Filtermethode	Gaussian	Einheit	mm/um
Auswertelänge	4,00mm	Messbereich	500,0um		
Messgeschwindigkeit	0,30mm/s	Entfernen der Form	Straight		

Messergebnis

Pt	24,263	Ra_5	1,341	Rz_5	8,907
Ra	1,249	Rz	7,652	Rp	4,126
Ra_1	0,796	Rz_1	5,337	Rp_1	2,345
Ra_2	1,518	Rz_2	9,329	Rp_2	3,679
Ra_3	1,630	Rz_3	8,892	Rp_3	5,228
Ra_4	0,962	Rz_4	5,797	Rp_4	3,473

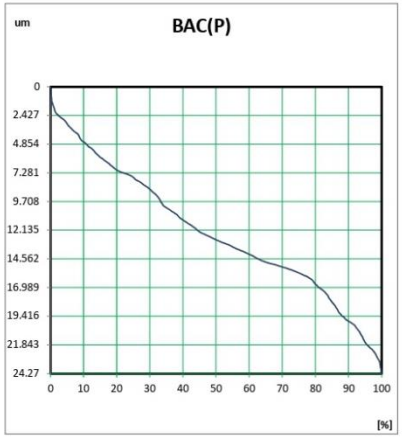

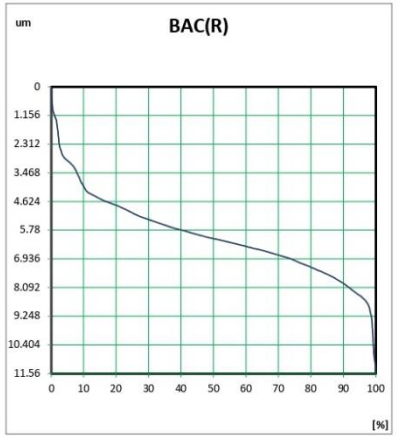

Prüfprotokoll

ACCRETECH

Seriennummer:		Kommentar		Messdatum	30.06.2022
Teilenummer	Planetenträger	Prüfer	Kalhöfer	Messzeit	10:18:28

Messbedingung

Messtyp	Roughness measuremen	Cutoff	0,8mm	λs Filter	2,5um
Berechnungsstandard	ISO1997/2009	Filtermethode	Gaussian	Einheit	mm/um
Auswertelänge	4,00mm	Messbereich	500,0um		
Messgeschwindigkeit	0,30mm/s	Entfernen der Form	Straight		

Messergebnis

Pt	29,012	Ra_5	1,226	Rz_5	6,705
Ra	1,241	Rz	6,633	Rp	3,213
Ra_1	1,044	Rz_1	5,494	Rp_1	2,747
Ra_2	0,991	Rz_2	6,158	Rp_2	3,495
Ra_3	1,003	Rz_3	5,014	Rp_3	2,907
Ra_4	1,940	Rz_4	9,795	Rp_4	4,458

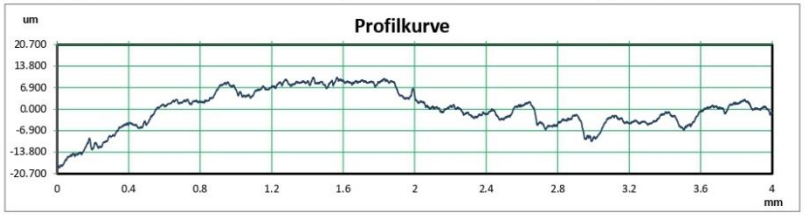

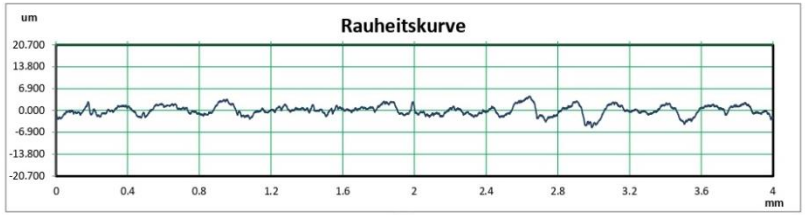

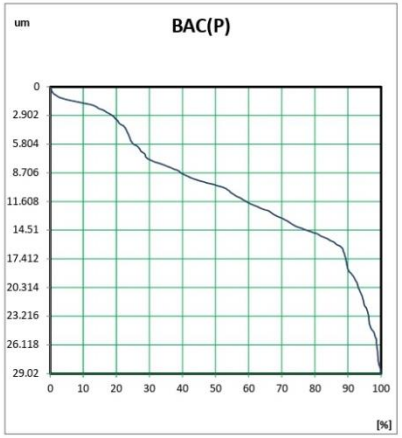

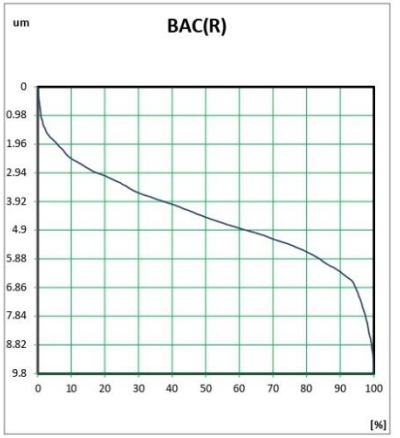

Prüfprotokoll

ACCRETECH

Seriennummer:		Kommentar		Messdatum	30.06.2022
Teilenummer	Planetenträger	Prüfer	Kalhöfer	Messzeit	10:19:46

Messbedingung

Messtyp	Roughness measuremen	Cutoff	0,8mm	λs Filter	2,5um
Berechnungsstandard	ISO1997/2009	Filtermethode	Gaussian	Einheit	mm/um
Auswertelänge	4,00mm	Messbereich	500,0um		
Messgeschwindigkeit	0,30mm/s	Entfernen der Form	Straight		

Messergebnis

Pt	20,927	Ra_5	0,855	Rz_5	5,235
Ra	1,197	Rz	6,545	Rp	3,189
Ra_1	0,983	Rz_1	6,102	Rp_1	3,417
Ra_2	0,975	Rz_2	4,852	Rp_2	2,820
Ra_3	1,926	Rz_3	10,029	Rp_3	4,596
Ra_4	1,246	Rz_4	6,508	Rp_4	2,753

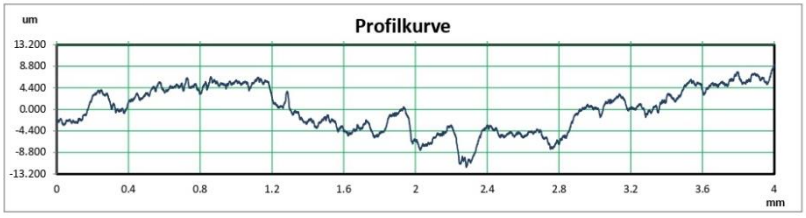

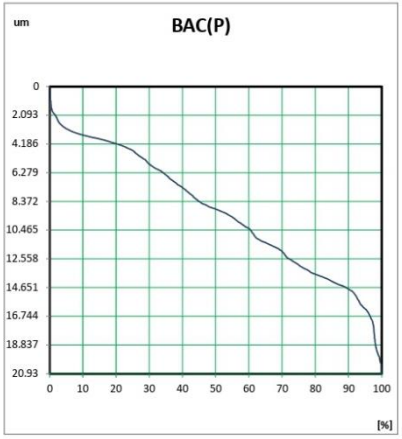

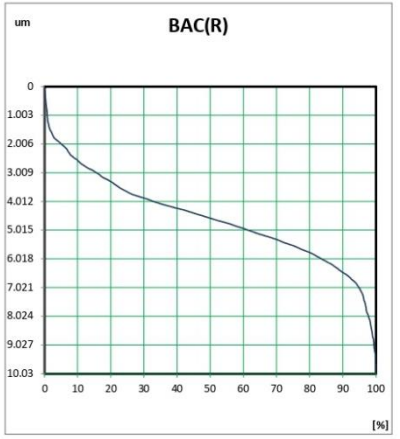

Prüfprotokoll

ACCRETECH

Seriennummer:		Kommentar		Messdatum	30.06.2022
Teilenummer	Planetenträger	Prüfer	Kalhöfer	Messzeit	10:21:20

Messbedingung

Messtyp	Roughness measuremen	Cutoff	0,8mm	λs Filter	2,5um
Berechnungsstandard	ISO1997/2009	Filtermethode	Gaussian	Einheit	mm/um
Auswertelänge	4,00mm	Messbereich	500,0um		
Messgeschwindigkeit	0,30mm/s	Entfernen der Form	Straight		

Messergebnis

Pt	29,252	Ra_5	0,801	Rz_5	4,718
Ra	1,274	Rz	6,617	Rp	3,382
Ra_1	1,185	Rz_1	6,366	Rp_1	3,653
Ra_2	1,111	Rz_2	5,253	Rp_2	2,761
Ra_3	1,935	Rz_3	9,733	Rp_3	5,388
Ra_4	1,338	Rz_4	7,014	Rp_4	3,027

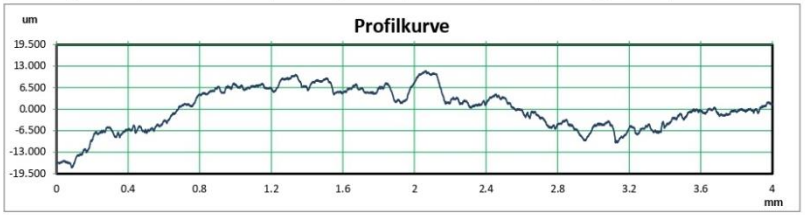

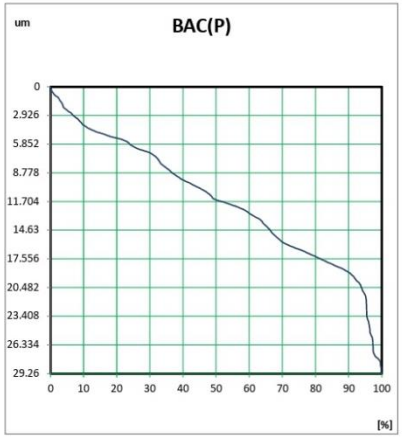

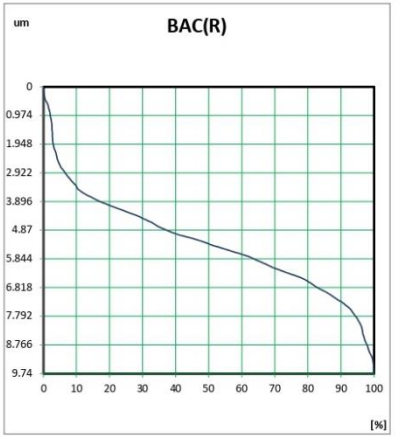

Appendix V – Gyroid | Side

Prüfprotokoll

Seriennummer:		Kommentar		Messdatum	30.06.2022
Teilenummer	Planetenträger	Prüfer	Kalhöfer	Messzeit	10:34:19

Messbedingung

Messtyp	Roughness measuremen	Cutoff	0,8mm	λs Filter	2,5um
Berechnungsstandard	ISO1997/2009	Filtermethode	Gaussian	Einheit	mm/um
Auswertelänge	4,00mm	Messbereich	500,0um		
Messgeschwindigkeit	0,30mm/s	Entfernen der Form	Straight		

Messergebnis

Pt	47,105	Ra_5	3,922	Rz_5	20,143
Ra	4,881	Rz	22,422	Rp	11,399
Ra_1	6,264	Rz_1	23,936	Rp_1	13,224
Ra_2	4,720	Rz_2	27,109	Rp_2	14,410
Ra_3	5,195	Rz_3	21,495	Rp_3	9,781
Ra_4	4,303	Rz_4	19,429	Rp_4	9,644

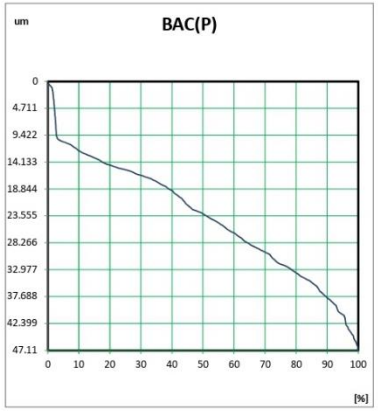

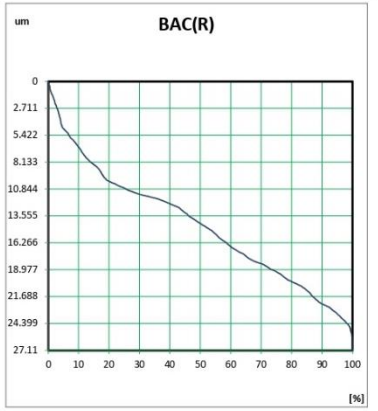

Prüfprotokoll

Seriennummer:		Kommentar		Messdatum	30.06.2022
Teilenummer	Planetenträger	Prüfer	Kalhöfer	Messzeit	10:35:23

Messbedingung

Messtyp	Roughness measuremen	Cutoff	0,8mm	λs Filter	2,5um
Berechnungsstandard	ISO1997/2009	Filtermethode	Gaussian	Einheit	mm/um
Auswertelänge	4,00mm	Messbereich	500,0um		
Messgeschwindigkeit	0,30mm/s	Entfernen der Form	Straight		

Messergebnis

Pt	54,871	Ra_5	4,235	Rz_5	18,627
Ra	4,447	Rz	20,462	Rp	9,207
Ra_1	4,845	Rz_1	26,880	Rp_1	14,381
Ra_2	4,533	Rz_2	17,415	Rp_2	5,944
Ra_3	4,508	Rz_3	19,396	Rp_3	9,604
Ra_4	4,116	Rz_4	19,991	Rp_4	9,714

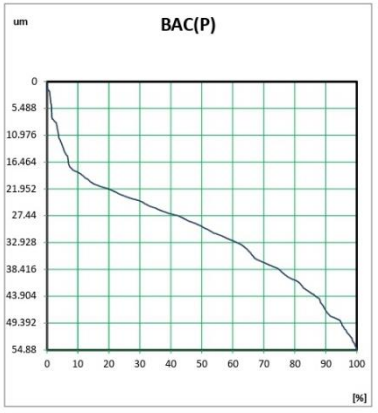

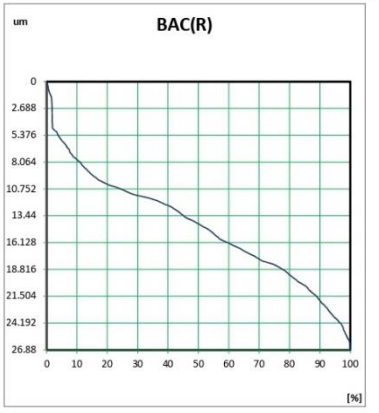

Prüfprotokoll

ACCRETECH

Seriennummer:		Kommentar		Messdatum	30.06.2022
Teilenummer	Planetenträger	Prüfer	Kalhöfer	Messzeit	10:36:32

Messbedingung

Messtyp	Roughness measuremen	Cutoff	0,8mm	λs Filter	2,5um
Berechnungsstandard	ISO1997/2009	Filtermethode	Gaussian	Einheit	mm/um
Auswertelänge	4,00mm	Messbereich	500,0um		
Messgeschwindigkeit	0,30mm/s	Entfernen der Form	Straight		

Messergebnis

Pt	83,575	Ra_5	4,317	Rz_5	18,546
Ra	4,596	Rz	19,343	Rp	9,462
Ra_1	5,389	Rz_1	22,101	Rp_1	9,699
Ra_2	3,948	Rz_2	17,348	Rp_2	9,676
Ra_3	4,511	Rz_3	19,764	Rp_3	9,649
Ra_4	4,813	Rz_4	18,957	Rp_4	6,938

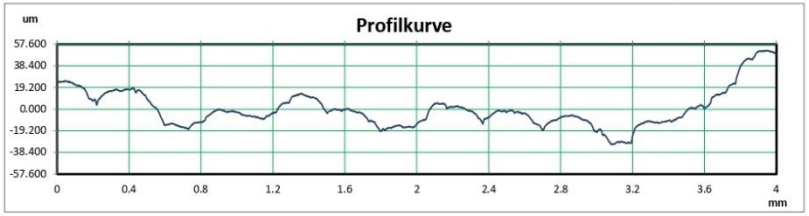

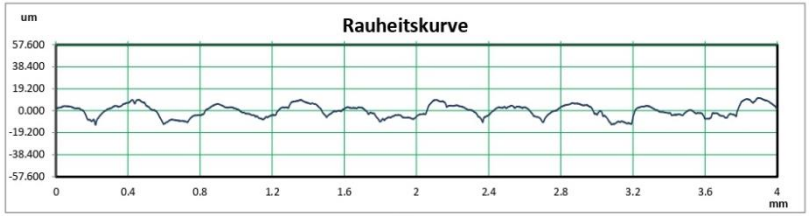

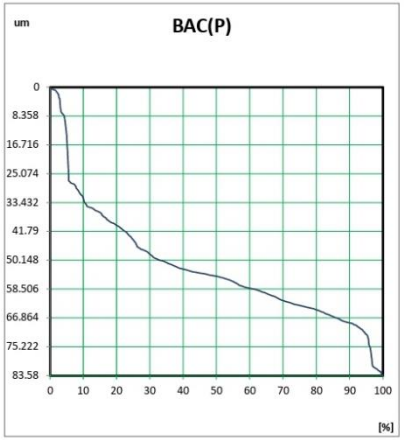

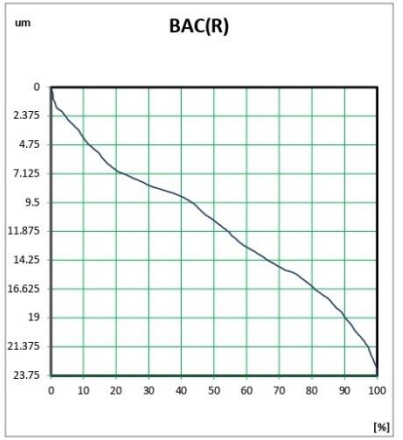

Prüfprotokoll

ACCRETECH

Seriennummer:		Kommentar		Messdatum	30.06.2022
Teilenummer	Planetenträger	Prüfer	Kalhöfer	Messzeit	10:45:51

Messbedingung

Messtyp	Roughness measuremen	Cutoff	0,8mm	λs Filter	2,5um
Berechnungsstandard	ISO1997/2009	Filtermethode	Gaussian	Einheit	mm/um
Auswertelänge	4,00mm	Messbereich	500,0um		
Messgeschwindigkeit	0,30mm/s	Entfernen der Form	Straight		

Messergebnis

Pt	57,198	Ra_5	5,457	Rz_5	25,440
Ra	5,062	Rz	24,760	Rp	9,714
Ra_1	5,578	Rz_1	20,820	Rp_1	7,332
Ra_2	6,971	Rz_2	37,144	Rp_2	14,761
Ra_3	3,025	Rz_3	15,256	Rp_3	8,499
Ra_4	4,278	Rz_4	25,139	Rp_4	9,219

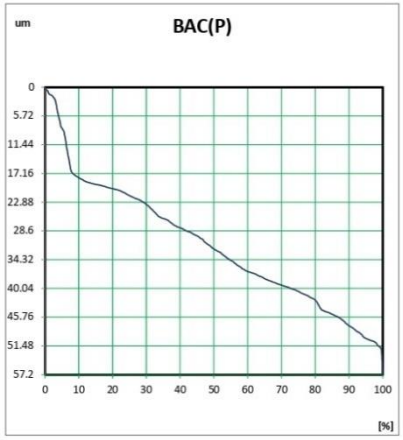

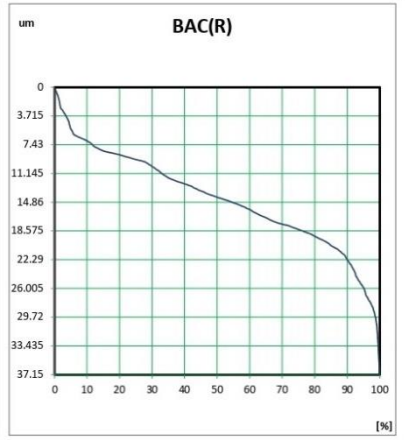

Prüfprotokoll

ACCRETECH

Seriennummer:		Kommentar		Messdatum	30.06.2022
Teilenummer	Planetenträger	Prüfer	Kalhöfer	Messzeit	10:46:50

Messbedingung

Messtyp	Roughness measuremen	Cutoff	0,8mm	λs Filter	2,5um
Berechnungsstandard	ISO1997/2009	Filtermethode	Gaussian	Einheit	mm/um
Auswertelänge	4,00mm	Messbereich	500,0um		
Messgeschwindigkeit	0,30mm/s	Entfernen der Form	Straight		

Messergebnis

Pt	73,860	Ra_5	5,689	Rz_5	26,080
Ra	4,473	Rz	22,060	Rp	9,098
Ra_1	2,884	Rz_1	15,425	Rp_1	8,576
Ra_2	4,425	Rz_2	25,148	Rp_2	9,559
Ra_3	5,620	Rz_3	26,331	Rp_3	9,371
Ra_4	3,747	Rz_4	17,317	Rp_4	5,851

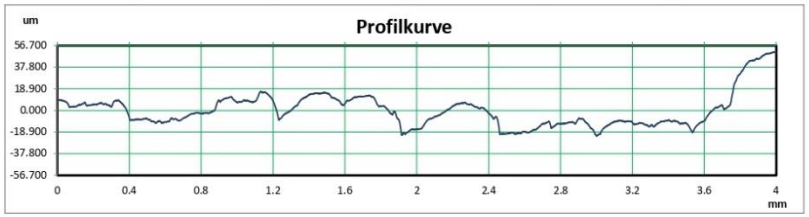

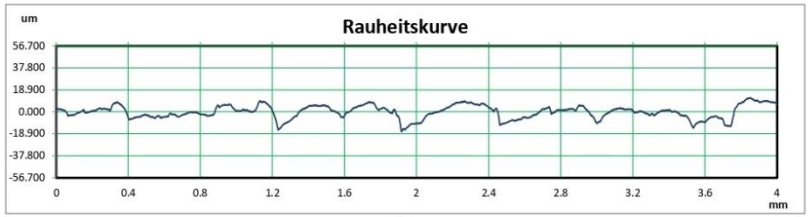

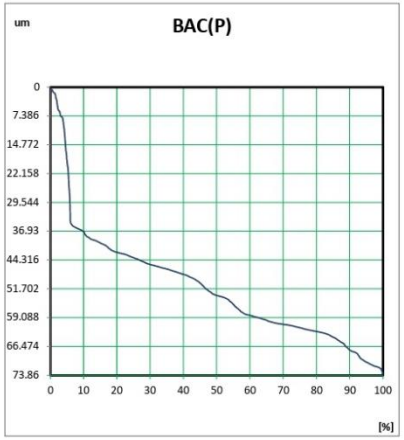

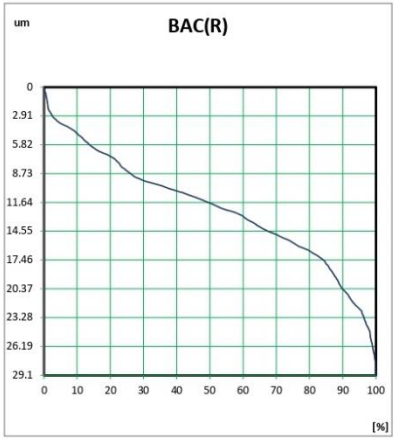

Prüfprotokoll

ACCRETECH

Seriennummer:		Kommentar		Messdatum	30.06.2022
Teilenummer	Planetenträger	Prüfer	Kalhöfer	Messzeit	10:47:57

Messbedingung

Messtyp	Roughness measuremen	Cutoff	0,8mm	λs Filter	2,5um
Berechnungsstandard	ISO1997/2009	Filtermethode	Gaussian	Einheit	mm/um
Auswertelänge	4,00mm	Messbereich	500,0um		
Messgeschwindigkeit	0,30mm/s	Entfernen der Form	Straight		

Messergebnis

Pt	58,448	Ra_5	4,979	Rz_5	25,484
Ra	4,983	Rz	24,365	Rp	9,841
Ra_1	4,938	Rz_1	18,488	Rp_1	7,043
Ra_2	8,436	Rz_2	37,689	Rp_2	15,207
Ra_3	2,606	Rz_3	15,437	Rp_3	8,547
Ra_4	3,957	Rz_4	24,729	Rp_4	9,363

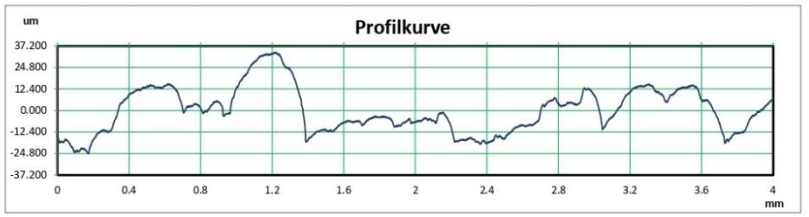

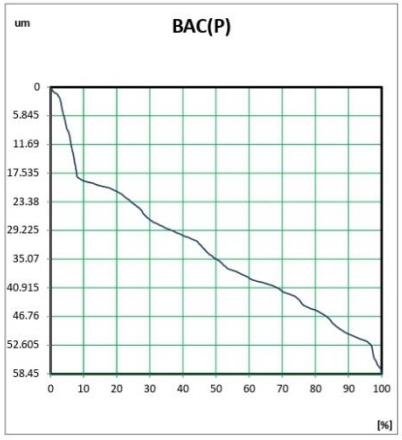

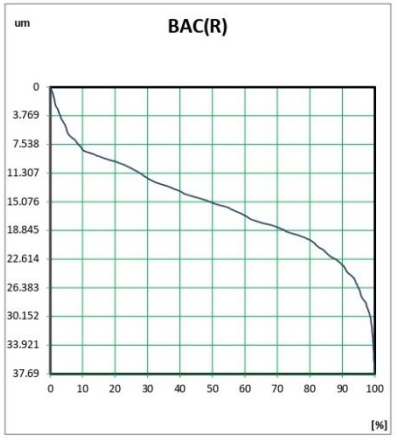

Prüfprotokoll

ACCRETECH

Seriennummer:		Kommentar		Messdatum	30.06.2022
Teilenummer	Planetenträger	Prüfer	Kalhöfer	Messzeit	10:49:40

Messbedingung

Messtyp	Roughness measuremen	Cutoff	0,8mm	λs Filter	2,5um
Berechnungsstandard	ISO1997/2009	Filtermethode	Gaussian	Einheit	mm/um
Auswertelänge	4,00mm	Messbereich	500,0um		
Messgeschwindigkeit	0,30mm/s	Entfernen der Form	Straight		

Messergebnis

Pt	19,581	Ra_5	1,074	Rz_5	6,880
Ra	0,968	Rz	6,354	Rp	3,361
Ra_1	0,668	Rz_1	4,188	Rp_1	2,185
Ra_2	0,984	Rz_2	5,636	Rp_2	3,301
Ra_3	1,060	Rz_3	8,111	Rp_3	4,083
Ra_4	1,053	Rz_4	6,957	Rp_4	4,056

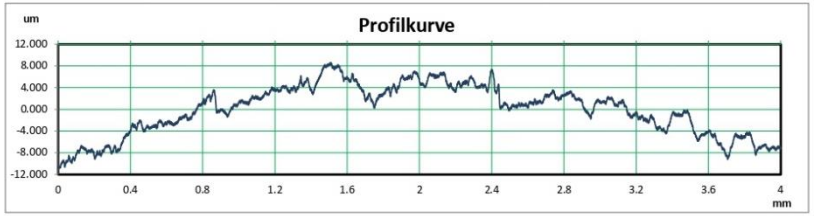

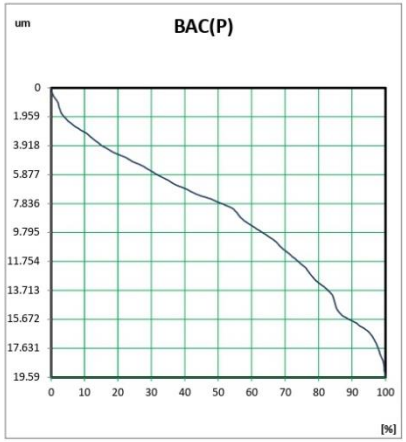

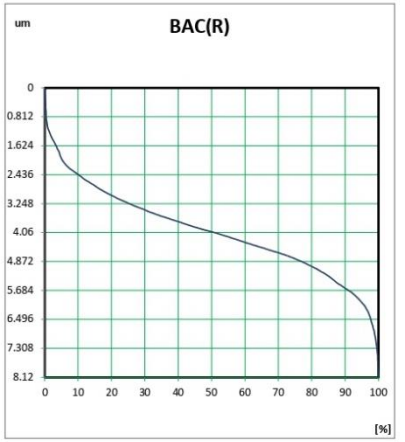

Prüfprotokoll

ACCRETECH

Seriennummer:		Kommentar		Messdatum	30.06.2022
Teilenummer	Planetenträger	Prüfer	Kalhöfer	Messzeit	10:50:41

Messbedingung

Messtyp	Roughness measuremen	Cutoff	0,8mm	λs Filter	2,5um
Berechnungsstandard	ISO1997/2009	Filtermethode	Gaussian	Einheit	mm/um
Auswertelänge	4,00mm	Messbereich	500,0um		
Messgeschwindigkeit	0,30mm/s	Entfernen der Form	Straight		

Messergebnis

Pt	18,823	Ra_5	0,915	Rz_5	6,587
Ra	0,903	Rz	5,565	Rp	2,595
Ra_1	0,651	Rz_1	4,255	Rp_1	2,333
Ra_2	1,047	Rz_2	7,152	Rp_2	3,151
Ra_3	0,937	Rz_3	4,993	Rp_3	2,220
Ra_4	0,967	Rz_4	4,837	Rp_4	2,096

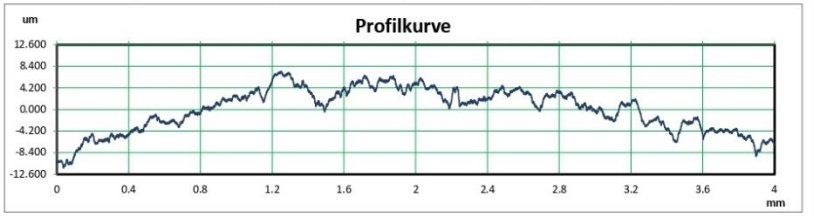

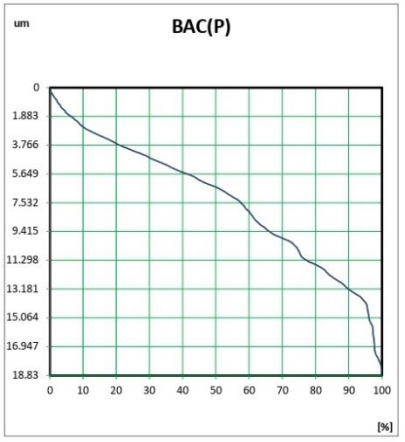

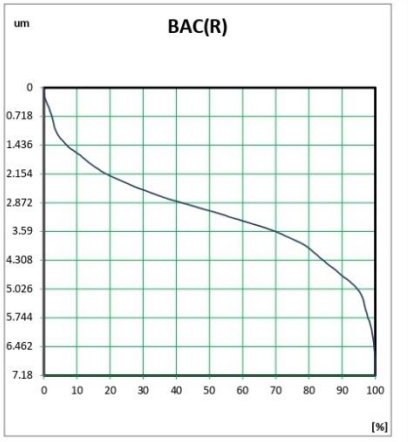

Prüfprotokoll

ACCRETECH

Seriennummer:		Kommentar		Messdatum	30.06.2022
Teilenummer	Planetenträger	Prüfer	Kalhöfer	Messzeit	10:51:37

Messbedingung

Messtyp	Roughness measuremen	Cutoff	0,8mm	λs Filter	2,5um
Berechnungsstandard	ISO1997/2009	Filtermethode	Gaussian	Einheit	mm/um
Auswertelänge	4,00mm	Messbereich	500,0um		
Messgeschwindigkeit	0,30mm/s	Entfernen der Form	Straight		

Messergebnis

Pt	21,412	Ra_5	0,938	Rz_5	5,828
Ra	0,988	Rz	5,641	Rp	2,730
Ra_1	1,328	Rz_1	5,848	Rp_1	3,039
Ra_2	0,699	Rz_2	4,216	Rp_2	2,369
Ra_3	0,859	Rz_3	6,149	Rp_3	3,086
Ra_4	1,116	Rz_4	6,166	Rp_4	2,138

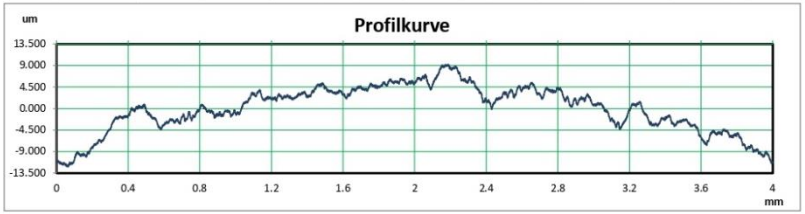

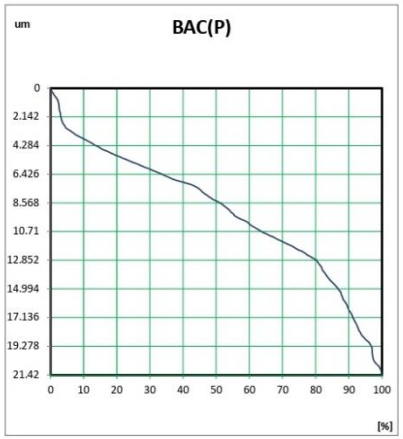

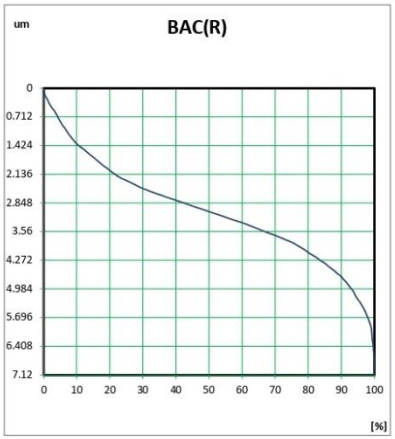

Appendix X – Quarter Cubic | Side

Prüfprotokoll

Seriennummer:		Kommentar		Messdatum	30.06.2022
Teilenummer	Planetenträger	Prüfer	Kalhöfer	Messzeit	10:56:44

Messbedingung

Messtyp	Roughness measuremen	Cutoff	0,8mm	λs Filter	2,5um
Berechnungsstandard	ISO1997/2009	Filtermethode	Gaussian	Einheit	mm/um
Auswertelänge	4,00mm	Messbereich	500,0um		
Messgeschwindigkeit	0,30mm/s	Entfernen der Form	Straight		

Messergebnis

Pt	81,977	Ra_5	7,275	Rz_5	34,525
Ra	5,457	Rz	24,723	Rp	11,066
Ra_1	4,191	Rz_1	20,709	Rp_1	9,145
Ra_2	7,880	Rz_2	32,786	Rp_2	14,991
Ra_3	5,485	Rz_3	24,216	Rp_3	11,879
Ra_4	2,454	Rz_4	11,379	Rp_4	3,405

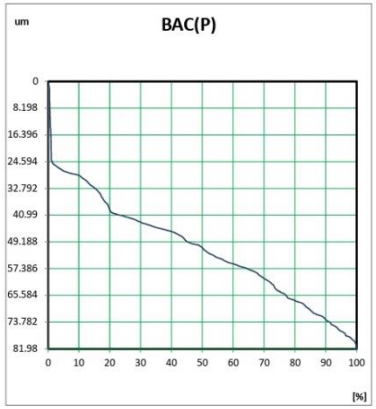

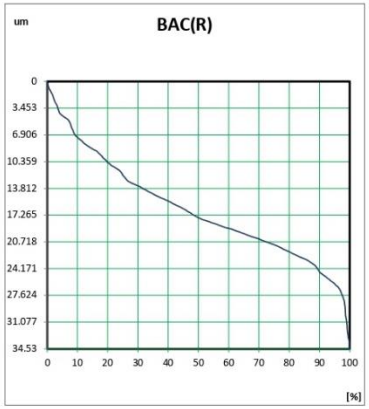

Prüfprotokoll

Seriennummer:		Kommentar		Messdatum	30.06.2022
Teilenummer	Planetenträger	Prüfer	Kalhöfer	Messzeit	10:57:49

Messbedingung

Messtyp	Roughness measuremen	Cutoff	0,8mm	λs Filter	2,5um
Berechnungsstandard	ISO1997/2009	Filtermethode	Gaussian	Einheit	mm/um
Auswertelänge	4,00mm	Messbereich	500,0um		
Messgeschwindigkeit	0,30mm/s	Entfernen der Form	Straight		

Messergebnis

Pt	55,058	Ra_5	5,218	Rz_5	27,332
Ra	5,006	Rz	22,598	Rp	11,023
Ra_1	2,406	Rz_1	9,761	Rp_1	4,090
Ra_2	5,456	Rz_2	20,423	Rp_2	9,110
Ra_3	7,055	Rz_3	32,069	Rp_3	14,146
Ra_4	4,893	Rz_4	23,403	Rp_4	11,817

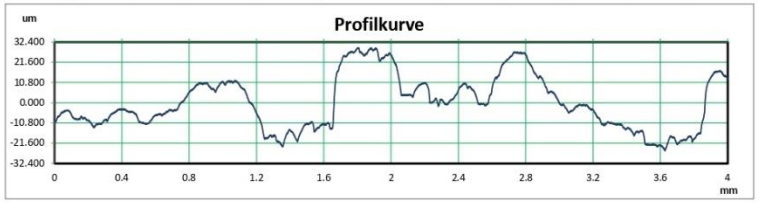

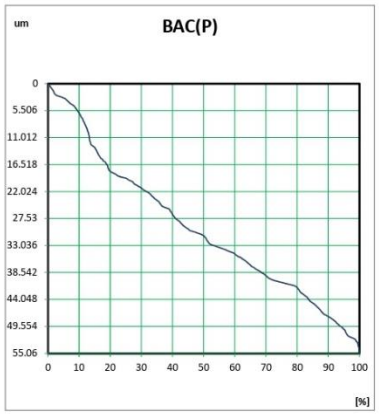

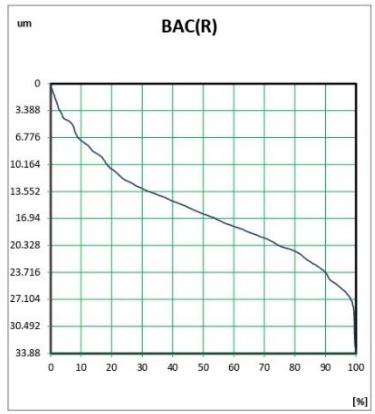

Prüfprotokoll

ACCRETECH

Seriennummer:		Kommentar		Messdatum	30.06.2022
Teilenummer	Planetenträger	Prüfer	Kalhöfer	Messzeit	10:58:38

Messbedingung

Messtyp	Roughness measuremen	Cutoff	0,8mm	λs Filter	2,5um
Berechnungsstandard	ISO1997/2009	Filtermethode	Gaussian	Einheit	mm/um
Auswertelänge	4,00mm	Messbereich	500,0um		
Messgeschwindigkeit	0,30mm/s	Entfernen der Form	Straight		

Messergebnis

Pt	93,794	Ra_5	7,368	Rz_5	35,022
Ra	6,038	Rz	26,542	Rp	13,344
Ra_1	7,494	Rz_1	30,900	Rp_1	13,365
Ra_2	5,372	Rz_2	21,172	Rp_2	9,098
Ra_3	3,762	Rz_3	18,664	Rp_3	12,002
Ra_4	6,194	Rz_4	26,951	Rp_4	15,739

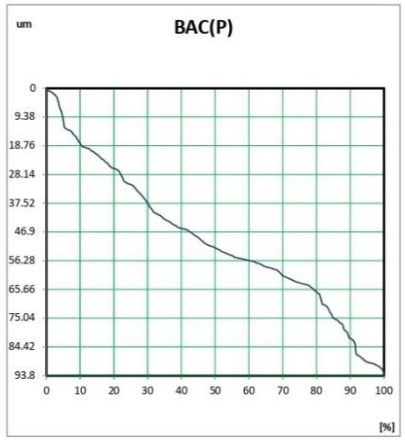

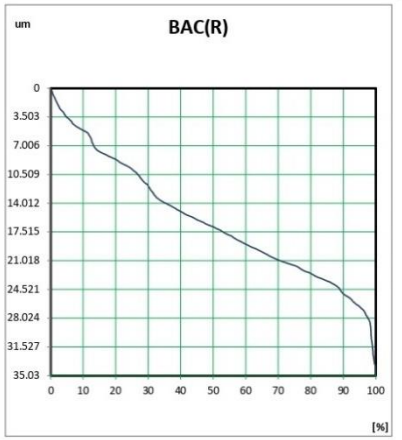

Prüfprotokoll

ACCRETECH

Seriennummer:		Kommentar		Messdatum	30.06.2022
Teilenummer	Planetenträger	Prüfer	Kalhöfer	Messzeit	11:03:14

Messbedingung

Messtyp	Roughness measuremen	Cutoff	0,8mm	λs Filter	2,5um
Berechnungsstandard	ISO1997/2009	Filtermethode	Gaussian	Einheit	mm/um
Auswertelänge	4,00mm	Messbereich	500,0um		
Messgeschwindigkeit	0,30mm/s	Entfernen der Form	Straight		

Messergebnis

Pt	195,286	Ra_5	20,896	Rz_5	101,242
Ra	14,285	Rz	67,594	Rp	26,828
Ra_1	19,568	Rz_1	97,386	Rp_1	41,194
Ra_2	7,376	Rz_2	32,886	Rp_2	11,520
Ra_3	5,088	Rz_3	25,950	Rp_3	10,902
Ra_4	18,496	Rz_4	80,507	Rp_4	34,377

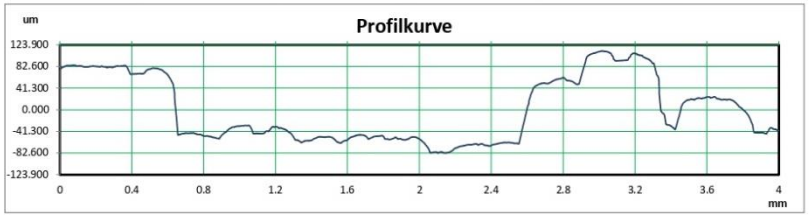

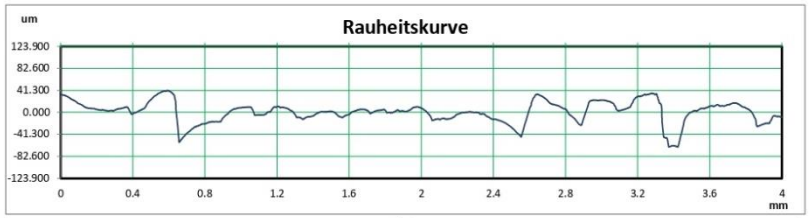

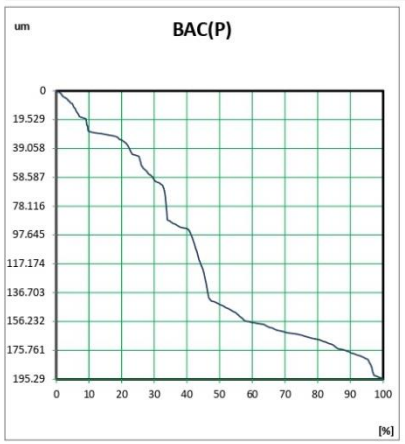

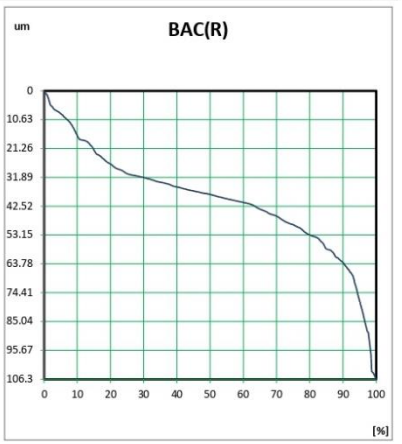

Prüfprotokoll

ACCRETECH

Seriennummer:		Kommentar		Messdatum	30.06.2022
Teilenummer	Planetenträger	Prüfer	Kalhöfer	Messzeit	11:04:18

Messbedingung

Messtyp	Roughness measuremen	Cutoff	0,8mm	λs Filter	2,5um
Berechnungsstandard	ISO1997/2009	Filtermethode	Gaussian	Einheit	mm/um
Auswertelänge	4,00mm	Messbereich	500,0um		
Messgeschwindigkeit	0,30mm/s	Entfernen der Form	Straight		

Messergebnis

Pt	184,830	Ra_5	9,398	Rz_5	44,962
Ra	13,420	Rz	69,410	Rp	28,713
Ra_1	19,478	Rz_1	106,871	Rp_1	45,929
Ra_2	4,550	Rz_2	25,046	Rp_2	11,952
Ra_3	13,544	Rz_3	80,041	Rp_3	34,385
Ra_4	20,133	Rz_4	90,128	Rp_4	33,205

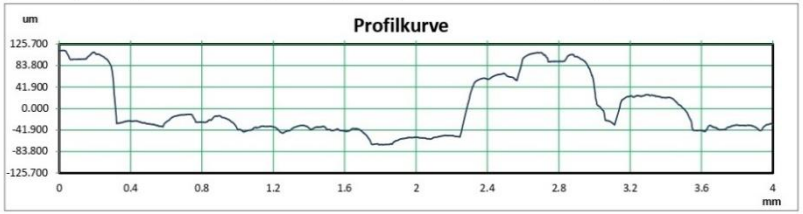

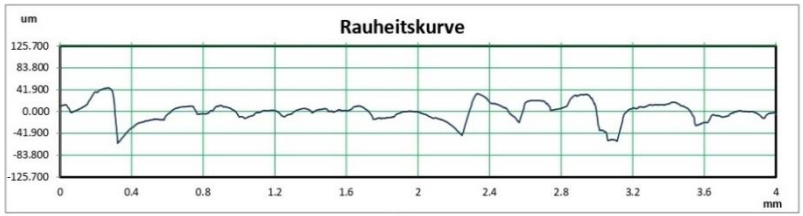

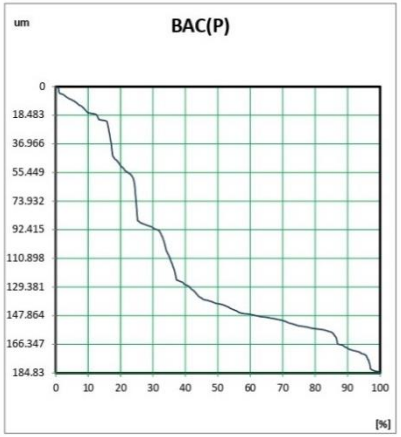

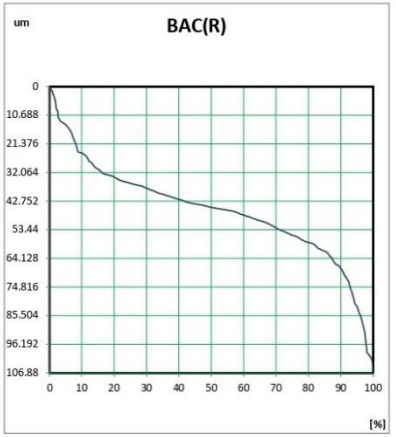

Prüfprotokoll

ACCRETECH

Seriennummer:		Kommentar		Messdatum	30.06.2022
Teilenummer	Planetenträger	Prüfer	Kalhöfer	Messzeit	11:05:21

Messbedingung

Messtyp	Roughness measuremen	Cutoff	0,8mm	λs Filter	2,5um
Berechnungsstandard	ISO1997/2009	Filtermethode	Gaussian	Einheit	mm/um
Auswertelänge	4,00mm	Messbereich	500,0um		
Messgeschwindigkeit	0,30mm/s	Entfernen der Form	Straight		

Messergebnis

Pt	185,915	Ra_5	9,456	Rz_5	44,747
Ra	13,390	Rz	69,628	Rp	28,346
Ra_1	19,186	Rz_1	108,095	Rp_1	44,673
Ra_2	4,554	Rz_2	25,054	Rp_2	11,712
Ra_3	13,446	Rz_3	80,363	Rp_3	34,245
Ra_4	20,307	Rz_4	89,881	Rp_4	33,166

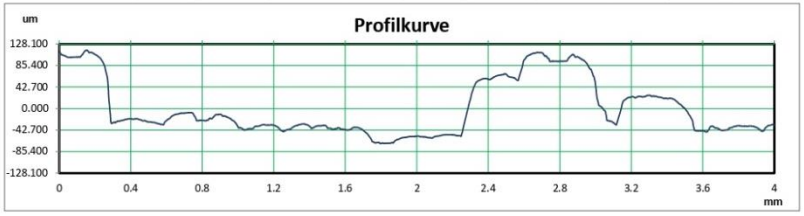

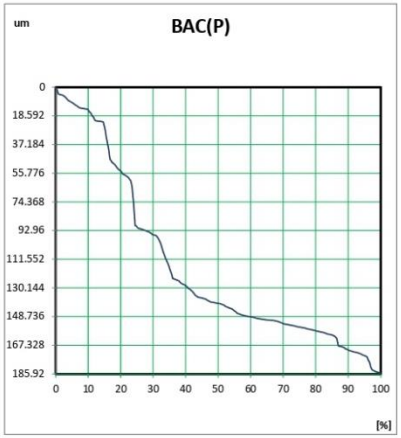

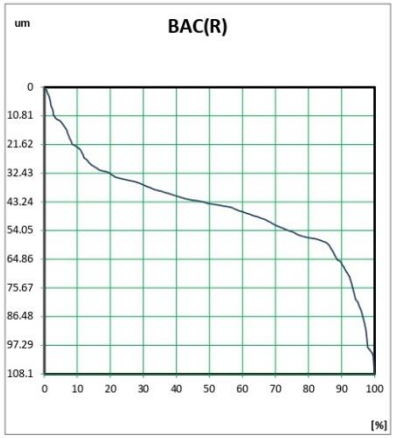

Prüfprotokoll

ACCRETECH

Seriennummer:		Kommentar		Messdatum	30.06.2022
Teilenummer	Planetenträger	Prüfer	Kalhöfer	Messzeit	11:09:45

Messbedingung

Messtyp	Roughness measuremen	Cutoff	0,8mm	λs Filter	2,5um
Berechnungsstandard	ISO1997/2009	Filtermethode	Gaussian	Einheit	mm/um
Auswertelänge	4,00mm	Messbereich	500,0um		
Messgeschwindigkeit	0,30mm/s	Entfernen der Form	Straight		

Messergebnis

Pt	84,332	Ra_5	8,618	Rz_5	37,568
Ra	5,352	Rz	24,730	Rp	11,801
Ra_1	2,598	Rz_1	13,973	Rp_1	6,542
Ra_2	3,586	Rz_2	16,179	Rp_2	6,855
Ra_3	2,551	Rz_3	15,178	Rp_3	6,171
Ra_4	9,407	Rz_4	40,754	Rp_4	21,769

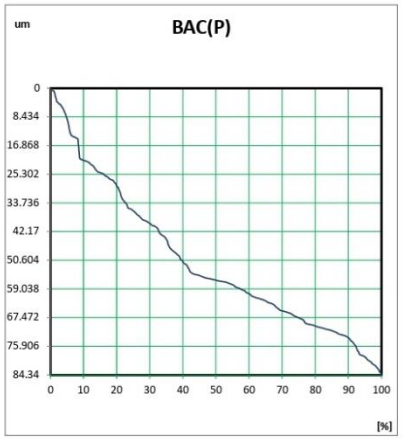

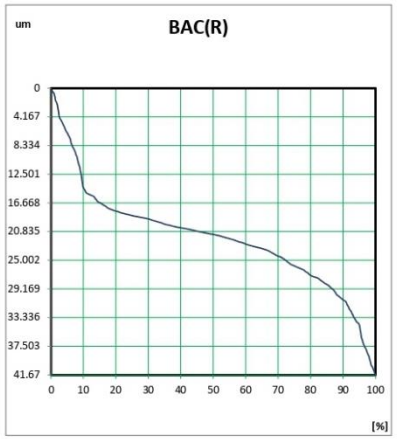

Prüfprotokoll

ACCRETECH

Seriennummer:		Kommentar		Messdatum	30.06.2022
Teilenummer	Planetenträger	Prüfer	Kalhöfer	Messzeit	11:10:56

Messbedingung

Messtyp	Roughness measuremen	Cutoff	0,8mm	λs Filter	2,5um
Berechnungsstandard	ISO1997/2009	Filtermethode	Gaussian	Einheit	mm/um
Auswertelänge	4,00mm	Messbereich	500,0um		
Messgeschwindigkeit	0,30mm/s	Entfernen der Form	Straight		

Messergebnis

Pt	94,980	Ra_5	5,779	Rz_5	26,503
Ra	6,085	Rz	27,375	Rp	13,404
Ra_1	3,961	Rz_1	15,936	Rp_1	6,706
Ra_2	2,663	Rz_2	16,024	Rp_2	4,965
Ra_3	10,120	Rz_3	40,626	Rp_3	21,756
Ra_4	7,899	Rz_4	37,785	Rp_4	17,613

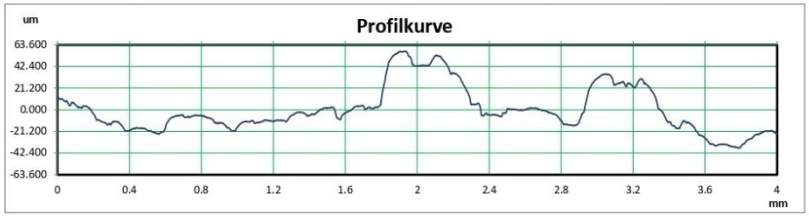

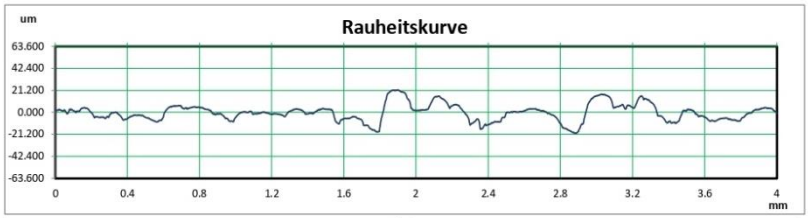

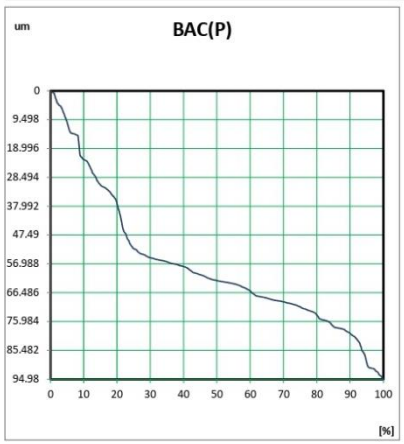

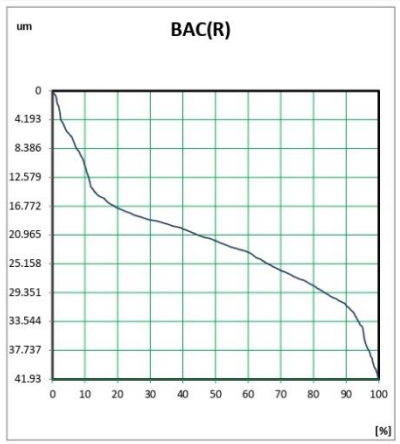

Prüfprotokoll

ACCRETECH

Seriennummer:		Kommentar		Messdatum	30.06.2022
Teilenummer	Planetenträger	Prüfer	Kalhöfer	Messzeit	11:11:50

Messbedingung

Messtyp	Roughness measuremen	Cutoff	0,8mm	λs Filter	2,5um
Berechnungsstandard	ISO1997/2009	Filtermethode	Gaussian	Einheit	mm/um
Auswertelänge	4,00mm	Messbereich	500,0um		
Messgeschwindigkeit	0,30mm/s	Entfernen der Form	Straight		

Messergebnis

Pt	86,205	Ra_5	4,469	Rz_5	20,439
Ra	6,223	Rz	28,008	Rp	14,066
Ra_1	2,458	Rz_1	14,318	Rp_1	5,496
Ra_2	9,765	Rz_2	40,597	Rp_2	21,612
Ra_3	8,397	Rz_3	38,219	Rp_3	17,612
Ra_4	6,025	Rz_4	26,470	Rp_4	15,971